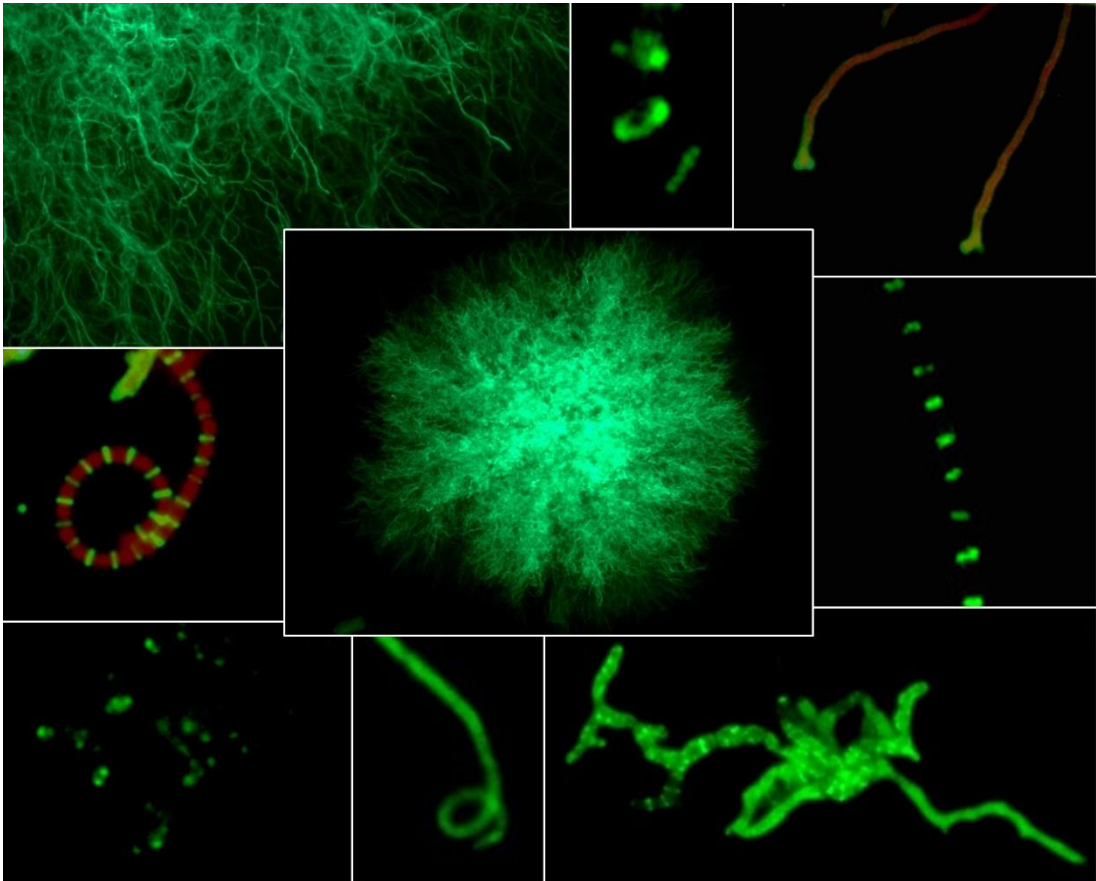


SepF: A link between cell division and polar growth in *Streptomyces coelicolor*



Gemma Louise Cassettari

Doctor of Philosophy (PhD), University of East Anglia, Biological Sciences

February 2022

This copy of the thesis has been supplied on condition that anyone who consults it is understood to recognise that its copyright rests with the author and that use of any information derived therefrom must be in accordance with current UK Copyright Law. In addition, any quotation or extract must include full attribution

COVID-19 Impact Statement

The latter part of the current study including laboratory work and write-up were impacted by the COVID-19 pandemic and subsequent lockdowns.

Research particularly relating to work in Chapter 6 was abruptly stopped in line with the University of East Anglia's lockdown process. It was not possible to recommence the work during the time allowed. The work which was most directly affected is referenced in the text.

The writing period was extended due to the various lockdowns which limited the opportunities to access to my supervisory team.

Abstract

Cell division in bacteria requires the polymerisation of the tubulin homologue, FtsZ, into Z-rings. Homologues of FtsZ are well conserved among bacteria and FtsZ is present even in some archaea. Polymerisation of FtsZ occurs in a GTP-dependent manner with individual subunits treadmilling along the protofilaments and directing the movement of the late divisome proteins involved in peptidoglycan (PG) synthesis during septum formation. Positioning of the Z-ring in *Escherichia coli* and *Bacillus subtilis* is negatively regulated by the synergistic work of the Min system and the nucleoid occlusion system, which prevents the formation of Z-rings at the poles or over the chromosomes. In addition, in *E. coli* the positive regulators, FtsA and ZipA, anchor the Z-ring to the cell membrane whilst in *B. subtilis* in the absence of ZipA, cells rely on FtsA and SepF.

Septum formation in the filamentous bacterium *Streptomyces coelicolor* requires the polymerisation of FtsZ into regularly spaced Z-rings along the multi genomic aerial hyphae. *S. coelicolor* lacks any obvious Min and Nucleoid occlusion systems. However in *S. coelicolor* FtsZ has been shown to be positively regulated by SsgB and three SepF homologues have been identified.

In this work we continued the characterisation of SepF, encoded in the *DCW* gene cluster. First, a thorough analysis of the $\Delta sepF$ phenotype including complementation of the knockout mutant is presented. Using a translational Egfp fusion, the localisation of SepF during sporulation and the dependence of SepF on FtsZ and Scy, involved in controlling polar growth, was tested. Bacterial two-hybrid assays were used to establish possible new interactions between SepF and proteins involved in both cell division and polar growth, and some of these novel interactions were rationalised. Finally, actinorhodin synthesis was compared between the wild-type and *sepF* strains to test the effect of compartmentalisation on antibiotic production.

Access Condition and Agreement

Each deposit in UEA Digital Repository is protected by copyright and other intellectual property rights, and duplication or sale of all or part of any of the Data Collections is not permitted, except that material may be duplicated by you for your research use or for educational purposes in electronic or print form. You must obtain permission from the copyright holder, usually the author, for any other use. Exceptions only apply where a deposit may be explicitly provided under a stated licence, such as a Creative Commons licence or Open Government licence.

Electronic or print copies may not be offered, whether for sale or otherwise to anyone, unless explicitly stated under a Creative Commons or Open Government license. Unauthorised reproduction, editing or reformatting for resale purposes is explicitly prohibited (except where approved by the copyright holder themselves) and UEA reserves the right to take immediate 'take down' action on behalf of the copyright and/or rights holder if this Access condition of the UEA Digital Repository is breached. Any material in this database has been supplied on the understanding that it is copyright material and that no quotation from the material may be published without proper acknowledgement.

List of Contents

COVID-19 Impact Statement.....	2
Abstract.....	3
List of Contents	4
List of Tables	9
List of Figures.....	10
Acknowledgements	15
1.0 Introduction.....	16
1.1 The distinguishing features of the <i>Streptomyces</i> genus.....	16
1.1.1 The complex lifecycle of the <i>Streptomyces</i> genus.....	17
1.2 Septa formation during the development of <i>S. coelicolor</i>	20
1.2.1 Formation of the Z-ring	20
1.2.2 The positive cell division regulator, SepF, in <i>B. subtilis</i>	23
1.2.3 The negative regulators of cell division in <i>E. coli</i> and <i>B.</i> <i>subtilis</i>	26
1.2.3.1 The Min system in <i>E. coli</i>	26
1.2.3.2 The Min system in <i>B. subtilis</i>	28
1.2.3.3 The nucleoid occlusion system in <i>E. coli</i>	30
1.2.3.4 The nucleoid occlusion system in <i>B. subtilis</i>	31
1.2.4 Septa formation in <i>S. coelicolor</i>	32
1.2.4.1 Two distinct types of septa identified during the lifecycle of <i>S. coelicolor</i>	32
1.2.4.2 Z-ring formation in <i>S. coelicolor</i>	34
1.2.4.3 Positive regulators for the polymerisation of FtsZ in Actinobacteria	36
1.3 The Tip organising centre governs polar growth in <i>S. coelicolor</i>	39
1.3.1 Lateral growth in the rod-shaped <i>E. coli</i> and <i>B. subtilis</i>	39
1.3.2 Polar growth in the filamentous bacterium <i>S. coelicolor</i>	40

1.3.2.1 ParAB: The potential link between chromosome segregation and polar growth	42
1.3.2.2 Polar growth and germination	44
1.4 The pigmented antibiotic, actinorhodin	45
1.4.1 The complex regulation of actinorhodin production	46
1.4.2 Actinorhodin biosynthesis	49
1.4.3 The potential functions of actinorhodin.....	53
1.5 The aim of the current study	54
2.0 Materials and Methods	55
2.1 Materials	55
2.1.1 Bacterial strains, cosmids, plasmids, media and antibiotics ...	55
2.1.2 Conditions and primers for the polymerase chain reactions ...	62
2.1.2.1 High-fidelity polymerase chain reactions	63
2.1.2.2 Low-fidelity polymerase chain reactions	64
2.2 Methods	65
2.2.1 General.....	65
2.2.2 Agarose gel electrophoresis.....	65
2.2.3 Ligation for combinate plasmid generation.....	65
2.2.4 Restriction digestions.....	65
2.2.5 Phosphorylation	65
2.2.6 Large scale plasmid preparations	66
2.2.7 Chemical transformation of <i>E. coli</i>	66
2.2.8 Electroporation of <i>E. coli</i>	67
2.2.9 Conjugations into <i>S. coelicolor</i>	67
2.2.10 Replicating of the <i>S. coelicolor</i> exconjugants	68
2.2.11 Glycerol stocks of <i>Streptomyces</i>	68
2.2.12 Macroscopic characterisation of <i>S. coelicolor</i> strains	68
2.2.13 Microscopy	68
2.2.14 Protein expression levels	69
2.2.15 Actinorhodin measurements	70
2.2.16 Bacterial two-hybrid quantification.....	70
2.2.17 Statistical methods and replicate numbers.....	70
3.0 Characterisation and complementation of <i>S. coelicolor</i> ΔsepF.....	72
3.1 Introduction	72

3.2 Results	74
3.2.1 Comparing the SepF homologues in <i>S. coelicolor</i>	74
3.2.2 Generating a <i>S. coelicolor sepF</i> knock-out using Redirect [®] PCR-directed mutagenesis	78
3.2.3 Characterising the $\Delta sepF$ mutant of <i>S. coelicolor</i>	79
3.2.3.1 Macroscopic characterisation of the $\Delta sepF$ mutant .	79
3.2.3.2 Microscopic characterisation of the $\Delta sepF$ mutant...	83
3.2.4 Complementing $\Delta sepF$ using blunt end cloning	87
3.2.5 Characterisation of the $\Delta sepF/pMS82$ -SepF strain	92
3.2.5.1 Macroscopic characterisation of the $\Delta sepF/pMS82$ -SepF strain	92
3.2.5.2 Microscopic characterisation of the novel $\Delta sepF/pMS82$ -SepF strain	94
3.3 Summary.....	97
3.4 Acknowledgements	99
4.0 SepF: A novel link between septa formation and polar growth.....	100
4.1 Introduction	100
4.2 Results	102
4.2.1 The localisation of SepF-Egfp in <i>S. coelicolor</i>	102
4.2.2 Identifying novel SepF binding partners using a bacterial two-hybrid assay.....	105
4.2.2.1 Introducing SepFC-K46A and -F71A into the bacterial two-hybrid assay.....	111
4.2.3 The expression of SepF-Egfp in M145 and Δscy	116
4.2.4 Characterising the localisation of SepF-Egfp in the Δscy mutant	121
4.3 Summary.....	125
4.4 Acknowledgements	128
5.0 Characterising the localisation of DivIVA during the lifecycle of <i>S.</i> <i>coelicolor</i>.....	129
5.1 Introduction	129
5.2 Results	132
5.2.1 Generating constructs for monitoring DivIVA-Egfp	132

5.2.2 Localisation of DivIVA-Egfp in the vegetative hyphae of M145/pMS82-DivIVA-Egfp.....	135
5.2.3 The localisation of DivIVA-Egfp throughout the lifecycle of <i>S. coelicolor</i>	136
5.2.3.1 Characterising the germination of spores from M145/pMS82-2078-DivIVA-Egfp	136
5.2.3.2 Characterising the localisation of DivIVA-Egfp during the aerial growth of M145/pMS82-2078-DivIVA-Egfp	144
5.2.3.3 Characterising the localisation of DivIVA-Egfp during the aerial growth of $\Delta sepF$ /pMS82-2078-DivIVA-Egfp	148
5.2.4 Monitoring the expression levels of DivIVA-Egfp at key stages of the <i>S. coelicolor</i> lifecycle	154
5.3 Summary.....	157
5.4 Acknowledgements	160

6.0 Generation, characterisation and complementation of a novel $\Delta ftsZ$ mutant from <i>S. coelicolor</i>.....	161
6.1 Introduction	161
6.2 Results	163
6.2.1 Generation of a <i>ftsZ</i> knock-out strain using the Redirect [®] PCR-directed mutagenesis approach	163
6.2.2 Isolation of potential $\Delta ftsZ$ strains from <i>S. coelicolor</i>	165
6.2.3 Signs of genetic instability from the colonies of $\Delta ftsZ$	168
6.2.4 Sonication of the $\Delta ftsZ$ mutant	170
6.2.5 Characterising the vegetative and aerial growth of $\Delta ftsZ$	174
6.2.6 Complementation of the novel $\Delta ftsZ$ mutant	177
6.2.6.1 Complementation of the $\Delta ftsZ$ mutant with pMS82-FtsZ-Egfp.....	177
6.2.6.2 Complementation of the $\Delta ftsZ$ mutant with pMS82-FtsZ	180
6.2.7 The localisation of SepF-Egfp during the development of the $\Delta ftsZ$ mutant	186
6.3 Summary.....	188
6.4 Acknowledgements	189

7.0 Investigating the role of compartmentalisation in the spatial and temporal localisation of actinorhodin production	190
7.1 Introduction	190
7.2 Results	193
7.2.1 The level of actinorhodins secreted by the colonies of the wild-type M145 and $\Delta sepF$ strains	193
7.2.2 The temporal and spatial localisation of actinorhodin production in the wild-type M145 and $\Delta sepF$ strains	195
7.2.2.1 Introducing a 5089-Egfp translational fusion into the wild-type M145 and $\Delta sepF$ strains.....	195
7.2.2.2. The level of actinorhodins secreted from the colonies of M145/3G11-5089-Egfp and $\Delta sepF/3G11$ -5089-Egfp	199
7.2.2.3 The localisation of 5089-Egfp in the colonies of M145/3G11-5089-Egfp and $\Delta sepF/3G11$ -5089-Egfp.....	200
7.3 Summary.....	213
7.4 Acknowledgements	216
8.0 Discussion	217
8.1 List of Conclusions	232
8.2 Future Outlook	233
9.0 Appendices	235
10.0 Definitions	249
11.0 References	251

List of Tables

1.0 Introduction

Table 1.1 Names of the actinorhodin gene cluster	46
--	----

2.0 Materials and Methods

Table 2.1 The <i>Escherichia coli</i> K12 strains used throughout the current study	55
---	----

Table 2.2 The <i>S. coelicolor</i> strains used throughout the current study. All strains were incubated at 30°C.	56
--	----

Table 2.3 The cosmids used throughout the current study	56
---	----

Table 2.4 The non-bacterial two-hybrid assay plasmids used throughout the current study	57
---	----

Table 2.5 The bacterial two-hybrid assay plasmids used in the current study	58
---	----

Table 2.6 The media used throughout the current study.	60
---	----

Table 2.7 The antibiotics used throughout the current study	61
---	----

Table 2.8 The primers used throughout the current study	62
---	----

Table 2.9 The cycles for the high-fidelity PCRs completed during the study	63
--	----

Table 2.10 The cycles for the low-fidelity PCRs completed during the study	64
--	----

4.0 SepF: A novel link between septa formation and polar growth

Table 4.1 Summary of the bacterial two-hybrid assay using SepFC	116
---	-----

List of Figures

1.0 Introduction

Figure 1.1 The chromosome of <i>S. coelicolor</i> A3(2)	17
Figure 1.2 The lifecycle of <i>S. coelicolor</i>	18
Figure 1.3 Formation of microtubules	21
Figure 1.4 FtsZ protofilaments in <i>E. coli</i>	22
Figure 1.5 The assembly pathway for the divisome	23
Figure 1.6 SepF in <i>B. subtilis</i>	25
Figure 1.7 The Min system in <i>E. coli</i>	27
Figure 1.8 The Min system in <i>B. subtilis</i>	29
Figure 1.9 The activity of SlmA	30
Figure 1.10 The activity of Noc	31
Figure 1.11 Summary of the <i>whi</i> regulatory network for sporulation in <i>S. coelicolor</i>	33
Figure 1.12 The division and cell wall (DCW) gene cluster of <i>S. coelicolor</i>	34
Figure 1.13 The localisation of SsgA and SsgB in the aerial hyphae of <i>S. coelicolor</i>	37
Figure 1.14 The structure and movement of MreB	39
Figure 1.15 The tip organising centre (TIPOC) at the hyphal tips of <i>S. coelicolor</i>	40
Figure 1.16 Germination in the <i>Streptomyces</i> genus	44
Figure 1.17 The actinorhodin gene cluster	46
Figure 1.18 Regulators of actinorhodin production in <i>S. coelicolor</i>	48
Figure 1.19 Actinorhodin biosynthesis	50
Figure 1.20 The known actinorhodins	52

3.0 Characterisation and complementation of *S. coelicolor* Δ sepF

Figure 3.1 The position of the three <i>sepF</i> genes within the chromosome of <i>S. coelicolor</i>	75
Figure 3.2 Sequence alignment of and domain organisation of SepF homologues from <i>S. coelicolor</i> , <i>B. subtilis</i> , <i>M. smegmatis</i> and <i>M. tuberculosis</i>	76
Figure 3.3 The gene organisation of the division and cell wall clusters from Actinobacteria and <i>B. subtilis</i>	77
Figure 3.4 Generation of the Δ sepF mutant using the Redirect [®] PCR-directed mutagenesis approach	78

Figure 3.5 Comparison of colony development for wild-type M145 and $\Delta sepF$ between 24 and 96 hrs	80
Figure 3.6 Comparison of colonies from wild-type M145 and $\Delta sepF$	82
Figure 3.7 Characterisation of tip morphology and vegetative growth from $\Delta sepF$	84
Figure 3.8 Characterisation of aerial growth from $\Delta sepF$	86
Figure 3.9 The different fragments used to complementation the $\Delta sepF$ mutant	88
Figure 3.10 The integrative pMS82 plasmid	89
Figure 3.11 Generation of the pMS82-SepF plasmid for complementation	90
Figure 3.12 Complementation of the $\Delta sepF$ mutant	93
Figure 3.13 Confirmation of complementation using epi-fluorescence microscopy	95
Figure 3.14 Summary of septa formation and the protein-protein interactions in the wild-type M145 and $\Delta sepF$ strains during cell division and polar growth	98

4.0 SepF: A novel link between septa formation and polar growth

Figure 4.1 Characterisation of FtsZ-Egfp ring formation in the hyphae of M145/pMS82-FtsZ-Egfp using epi-fluorescence microscopy	103
Figure 4.2 Characterisation of SepF-Egfp ring formation in M145/pMS82-SepF-Egfp using epi-fluorescence microscopy	104
Figure 4.3 The mechanism of the bacterial two-hybrid assay	106
Figure 4.4 The interactions of SepFC with known cell division proteins	109
Figure 4.5 The interactions of SepFC with known TIPOC components	110
Figure 4.6 Generation of the SepFC-K46A and SepFC-F71A plasmids for the bacterial two-hybrid assay	112
Figure 4.7 Comparison of SepFC and SepFC-K46A binding partners	114
Figure 4.8 Comparison of SepFC and SepFC-F71A binding partners	115
Figure 4.9 Comparison of A) FtsZ-Egfp and B) SepF-Egfp expression	118
Figure 4.10 Summary of the protein-protein interactions and SepF-Egfp localisation during aerial hyphae development in the wild-type M145 and Δscy strains	120
Figure 4.11 The localisation SepF-Egfp during aerial growth of Δscy /pMS82-SepF-Egfp	123

5.0 Characterising the localisation of DivIVA during the lifecycle of *S. coelicolor*

Figure 5.1 Generation of the DivIVA-Egfp constructs	133
Figure 5.2 Characterisation of vegetative growth from M145/pMS82-DivIVA-Egfp	135
Figure 5.3 Characterisation of spores from M145/pMS82-2078-DivIVA-Egfp	137
Figure 5.4 Germ tube production of the spores from M145/pMS82-2078-DivIVA-Egfp	139
Figure 5.5 Characterisation of the early germination of M145/pMS82-2078-DivIVA-Egfp	141
Figure 5.6 Characterisation of early vegetative growth from M145/pMS82-2078-DivIVA-Egfp	143
Figure 5.7 Characterisation of later vegetative growth from M145/pMS82-2078-DivIVA-Egfp	145
Figure 5.8 Characterisation of aerial growth from M145/pMS82-2078-DivIVA-Egfp on SFM medium	146
Figure 5.9 Characterisation of aerial growth from M145/pMS82-2078-DivIVA-Egfp on MMM medium	147
Figure 5.10 Characterisation of sporulation from M145/pMS82-2078-DivIVA-Egfp	148
Figure 5.11 Characterisation of vegetative growth from $\Delta sepF$ /pMS82-2078-DivIVA-Egfp	150
Figure 5.12 Characterisation of aerial growth from $\Delta sepF$ /pMS82-2078-DivIVA-Egfp on SFM medium	152
Figure 5.13 Characterisation of aerial growth from $\Delta sepF$ /pMS82-2078-DivIVA-Egfp on MMM medium	153
Figure 5.14 The expression of 2078-DivIVA-Egfp in M145/pMS82-2078-DivIVA-Egfp and $\Delta sepF$ /pMS82-2078-DivIVA-Egfp	155
Figure 5.15 Summary of DivIVA-Egfp localisation and protein-protein interactions in wild-type M145 and $\Delta sepF$	159

6.0 Generation, characterisation and complementation of a novel $\Delta ftsZ$ mutant from *S. coelicolor*

Figure 6.1 Generation of the $\Delta ftsZ$ mutant using the Redirect [®] PCR-directed mutagenesis approach	163
---	-----

Figure 6.2 The morphologies of the ex-conjugants during the attempt to generate the \DeltaftsZ knockout strain	164
Figure 6.3 The four classes of potential \DeltaftsZ strains	166
Figure 6.4 Comparison of colony development between the wild-type M145, $\Delta sepF$, and \DeltaftsZ strains	167
Figure 6.5 The colony morphologies of \DeltaftsZ	168
Figure 6.6 The heterogeneity of the \DeltaftsZ strain	169
Figure 6.7 Sonication of hyphal fragments from \DeltaftsZ	172
Figure 6.8 Heterogeneity during the sonicating trials	173
Figure 6.9 Characterisation of vegetative growth from the \DeltaftsZ strain using epi-fluorescent microscopy	174
Figure 6.10 Characterisation of aerial growth from the \DeltaftsZ strain using epi-fluorescent microscopy	176
Figure 6.11 Colony morphology of the complementation using pMS82-FtsZ-Egfp	178
Figure 6.12 Characterisation of the complementation using pMS82-FtsZ-Egfp	179
Figure 6.13 Generation of the pMS82-FtsZ plasmid for complementation	181
Figure 6.14 The colony morphology of the complemented strains	183
Figure 6.15 Confirmation of complementation using epi-fluorescent microscopy	185
Figure 6.16 The localisation of SepF-Egfp in the \DeltaftsZ strain	186
Figure 6.17 Summary of sporulation septa (grey disc) formation and protein-protein interactions in the wild-type M145 and \DeltaftsZ strains.....	187

7.0 Investigating the role of compartmentalisation in the spatial and temporal localisation of actinorhodin production

Figure 7.1 The pigmentation on the surface of the colonies from $\Delta sepF$	190
Figure 7.2 The colony morphology of the $\Delta whiA$ and $\Delta whiB$ strains	192
Figure 7.3 Actinorhodins in the medium of the wild-type M145 and $\Delta sepF$ strains	194
Figure 7.4 Generation of the 5089-Egfp containing strains using the Redirect [®] PCR-directed mutagenesis approach	196
Figure 7.5 Comparison of the 5089-Egfp containing single crossover strains to the wild-type M145 and $\Delta sepF$ strains	198
Figure 7.6 Actinorhodins in the medium of wild-type M145, M145/3G11-5089-Egfp, $\Delta sepF$ and $\Delta sepF$ /3G11-5089-Egfp	200

Figure 7.7 The predicted localisation patterns of 5089-Egfp in the colonies of M145/3G11-5089-Egfp and $\Delta sepF/3G11-5089-Egfp$	201
Figure 7.8 The localisation of 5089-Egfp in the young colonies of M145/3G11-5089-Egfp and $\Delta sepF/3G11-5089-Egfp$	202
Figure 7.9 The localisation of 5089-Egfp in the vegetative colonies of M145/3G11-5089-Egfp and $\Delta sepF/3G11-5089-Egfp$	204
Figure 7.10 The localisation of 5089-Egfp in the maturing colonies of M145/3G11-5089-Egfp and $\Delta sepF/3G11-5089-Egfp$	206
Figure 7.11 Compartmentalisation in the hyphae of M145/3G11-5089-Egfp and $\Delta sepF/3G11-5089-Egfp$	208
Figure 7.12 Fluorescent compartments in the hyphae of M145/3G11-5089-Egfp and $\Delta sepF/3G11-5089-Egfp$	210
Figure 7.13 The localisation of 5089-Egfp in the aerial hyphae of M145/3G11-5089-Egfp and $\Delta sepF/3G11-5089-Egfp$	212
Figure 7.14 Summary of the 5089-Egfp localisation in M145/3G11-5089-Egfp and $\Delta sepF/3G11-5089-Egfp$ and protein-protein interactions in M145 and $\Delta sepF$ during development	215

8.0 Discussion

Figure 8.1 The protein-protein interactions and localisation of key cell division and polar growth proteins during the development of wild-type M145 (top) and $\Delta sepF$ (bottom).....	220
Figure 8.2 The SepF interaction network using STRING (2019).....	221
Figure 8.3 The transition from polar growth to cell division in the sporogenic aerial hyphae of <i>Streptomyces</i>	225
Figure 8.4 The protein-protein interactions and localisation of key cell division and polar growth proteins during the development of wild-type M145 (top) and $\Delta ftsZ$ (bottom).....	228

Acknowledgements

Thank you to all my friends and family who supported me through this marathon of a process.

Special thanks to my parents, whose support has made this all possible and who have been with me every step of the way.

To the BIO technicians, without whose kindness much of the work wouldn't have been possible. To my fellow lab members, past and present, who made this experience so memorable and enjoyable. To my students, whose enthusiasm and hard work has contributed to this thesis. To Gabriella Kelemen and my supervisory team for all their guidance and training as a small summer project turned into a full PhD.

1.0 Introduction

1.1 The distinguishing features of the *Streptomyces* genus

The Actinobacteria phylum contains several clinically relevant bacteria including *Mycobacterium tuberculosis* and *Corynebacterium diphtheriae*, the causative agents for tuberculosis and diphtheria respectively, in addition to the *Streptomyces* genus, well known for the production of secondary metabolites (World Health Organisation). *Streptomyces venezuelae* produces the multi-use antibiotic chloramphenicol, but potentially the most well studied member of the *Streptomyces* genus is the classic model organism, *Streptomyces coelicolor* (Akagawa *et al.*, 1975; Bobek *et al.*, 2017; Hopwood *et al.*, 1970; Jones and Elliot, 2018; Prudence *et al.*, 2020).

Characterisation of *S. coelicolor* focused on the plasmid-free prototrophic derivative, M145, which was one of the first strains in the *Streptomyces* genus to be sequenced (Bentley *et al.*, 2002). Colonies of M145, here considered the wild-type *S. coelicolor*, undergo the fungus-like lifecycle of the *Streptomyces* genus and produce several antibiotics including the pigmented undecylprodigiosin and actinorhodin under laboratory conditions. Sequencing revealed the wild-type M145 strain has a large ~8.67 Mbp linear chromosome, which is almost twice the size of the genomes of the rod-shaped Gram-positive *Bacillus subtilis* and Gram-negative *Escherichia coli* (Blattner *et al.*, 1997; Bentley *et al.*, 2002; Kunst *et al.*, 1997; Figure 1.1). The chromosome of *S. coelicolor* contains ~7,800 predicted genes, including ~31 gene clusters for specialised metabolites, highlighting the complexity and potential utility of the *Streptomyces* genus (Bentley *et al.*, 2002; van Keulen and Dyson, 2014; Zhang *et al.*, 2019).

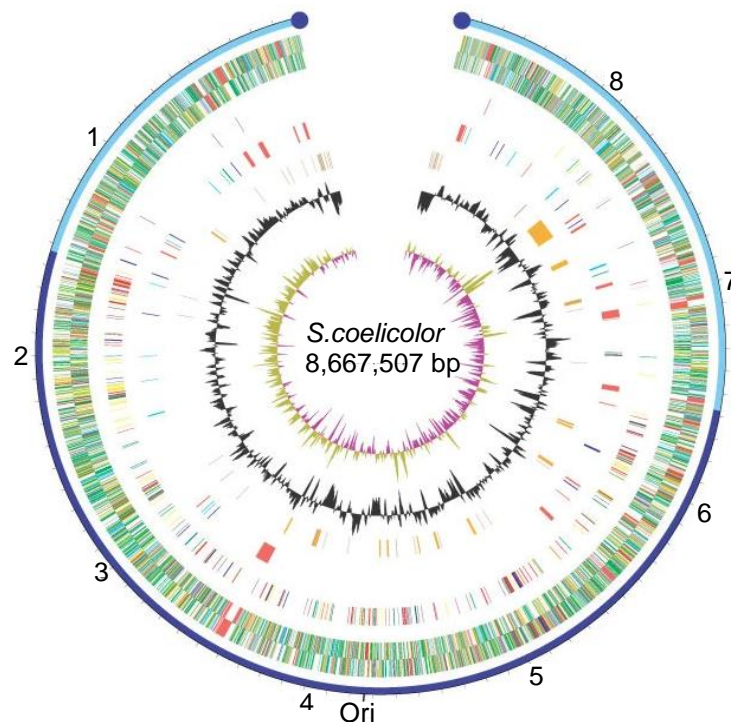


Figure 1.1 The chromosome of *S. coelicolor* A3(2). From the outside inwards: Circle 1 shows the core region (dark blue) and the arm regions (light blue) of the chromosome. Circle 2 and 3 show all genes (reverse and forward strand, respectively) colour-coded by function (black = energy metabolism; red = information transfer and secondary metabolism; dark green = surface associated; cyan = degradation of large molecules; magenta = degradation of small molecules; yellow = central or intermediary metabolism; pale blue = regulators; orange = conserved hypothetical; brown = pseudogenes; pale green = unknown; grey = miscellaneous). Circle 4 highlights the 'essential' gene for cell division, DNA replication, transcription, translation and amino-acid biosynthesis. Circle 5 highlights selected 'contingency' genes (red = secondary metabolism; pale blue = exoenzymes; dark blue = conservon; green = gas vesicle proteins). Circle 6 highlights mobile elements (brown = transposases; orange = putative laterally acquired genes). Circle 7 highlights G + C content and circle 8 highlights GC bias ((G - C/G + C), khaki indicates values >1, purple indicates values <1). The anticlockwise numbers indicate the position in Mb on the chromosome. The origin of replication (Ori) and terminal protein (blue circles) are also indicated (Figure 1 from Bentley *et al.*, 2002).

1.1.1 The complex lifecycle of the *Streptomyces* genus

The classical lifecycle of the *Streptomyces* genus commences when under favourable conditions a spore germinates (Figure 1.2; Flärdh and Buttner, 2009; Jones and Elliot, 2018). Germinating spores produce germ tubes, which grow by polar growth, to form the non-motile vegetative mycelium. The non-motile vegetative mycelium is characterised by vegetative cross-walls and sub-apical branches, due to the phenomenon of apical dominance.

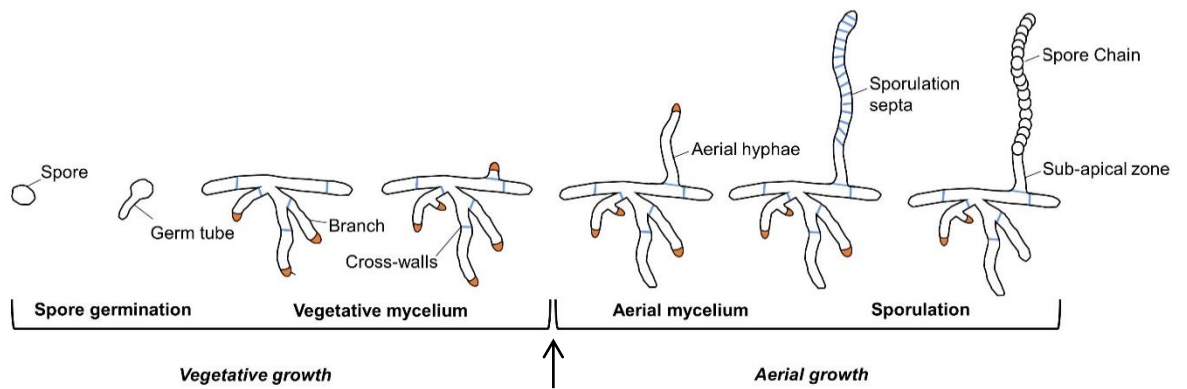


Figure 1.2 The lifecycle of *S. coelicolor*. The lifecycle of *S. coelicolor* has two growth phases, vegetative and aerial (bottom line). The transition between the two growth phases is marked by the production of secondary metabolites (arrow). During the lifecycle, septa formation requires the polymerisation of FtsZ (light blue) into Z-rings and polar growth is governed by the (orange crescents) tip organising centre or TIPOC (Modified from Flårdh and Buttner, 2009).

The majority of *Streptomyces* species live as saprophytes in the soil where the role of the vegetative mycelium is to penetrate the surrounding environment and extract the available nutrients (Chater *et al.*, 2010; Flårdh and Buttner, 2009; Jones and Elliot, 2018). Cellulose, a major component of plant cell walls, is broken down by cellulases and chitin, the second most abundant polysaccharide after cellulose, is broken down by chitinases into the monomer *N*-acetylglucosamine (GlcNAc), which can be used as a carbon and nitrogen source by the colony (Chater *et al.*, 2010; Lim *et al.*, 2016).

Upon depletion of the surrounding nutrients, colonies commence the production of aerial hyphae (McCormick and Flårdh, 2012). Aerial hyphae are covered by a hydrophobic sheath, which enables the aerial hyphae to grow upwards via polar growth and escape the aqueous environment of the vegetative mycelium. The hydrophobic sheath consists of two families of proteins, the chaplins and rodmins, plus in a media dependent manner the protein, SapB (Willey *et al.*, 1991). In *S. coelicolor* the family of chaplins consist of 3 long chaplins (chpA to chpC) and 5 short chaplins (chpD to chpH), which all share a ~40 amino acid hydrophobic chaplin domain (Claessen *et al.*, 2003; Elliot *et al.*, 2003). The short chaplins self-assemble into amyloid-like fibrils at the water-air interface, which are thought to be attached to the cell wall by the long chaplins and lower the water surface tension (Claessen *et al.*, 2003; Dokouhaki *et al.*, 2017). The family of rodmins in *S. coelicolor* consists of the highly similar, RdIA and RdIB (Claessen *et al.*, 2002; Yang *et al.*, 2017a). RdIA has more charged residues near the N-terminal and is unable to form amyloid-like fibrils, unlike RdIB (Yang *et al.*, 2017a). The fibrils of RdIB are long and

potentially more ordered than the fibrils of the chaplins. However in the absence of RdlA and RldB a hydrophobic sheath and aerial hyphae are still formed (Claessen *et al.*, 2002).

With the development of aerial hyphae, some of the vegetative mycelium directly below remain a continuous part of the colony but undergoes programmed cell death (Miguélez *et al.*, 1999). As the aerial hyphae mature, the hyphae do not produce sub-apical branches but develop a distinctive hook-like morphology and sporulate (McCormick and Flärdh, 2012). Sporulation requires the synchronous positioning of multiple sporulation septa which define the uni-genomic spore compartments then spores (Schwedock *et al.*, 1997). Spores can be dispersed via the wind and have more recently been shown to be transported to plant tissues by interacting directly with the flagella of both Gram-positive and Gram-negative bacteria (Muok *et al.*, 2021).

Classically the production of secondary metabolites is thought to coincide with the development of aerial hyphae. In the latter stages of development the antibiotic, actinorhodin, gives the surrounding media a pH sensitive pigmentation, turning blue in alkaline and red in acidic conditions (Abbas and Edwards, 1990; Mak and Nodwell, 2017; Nass *et al.*, 2017). This pigmentation led to the identification of the actinorhodin type II polyketide synthase (PKS) in *S. coelicolor* during the 1970s (Section 1.4.2; Wright and Hopwood, 1976). Despite the early identification of actinorhodin production from colonies of *S. coelicolor*, the localisation of actinorhodin production within the colonies remains unclear.

1.2 Septa formation during the development of *S. coelicolor*

1.2.1 Formation of the Z-ring

Binary fission in the rod-shaped bacteria, *E. coli* and *B. subtilis*, is initiated when the parent cell has elongated to about twice the starting length of the cell and is the process by which two identical daughter cells, containing a complete copy of the genome, are produced (Angert, 2005). For cell division to occur, the macromolecular complex, known as the divisome, must mark the septum site. Integral to the divisome is the Z-ring. The Z-ring is formed by the polymerisation of the structural tubulin homologue, FtsZ (Dyer, 2009).

As a structural homologue, FtsZ shares several characteristics with tubulin. Tubulin protofilaments assemble from α -tubulin and β -tubulin heterodimers, in a head to tail and GTP-dependent manner. Typically 13 protofilaments come together in the same orientation to form a polar microtubule (Figure 1.3). The polar microtubules undergo treadmilling with addition of dimers at the plus end and loss of dimers at the negative end (Cooper, 2000). The microtubules also undergo alternating cycles of growth and shrinkage known as dynamic instability. The dynamic nature of the network of microtubules allows the network to be very responsive to the surrounding environment and perform important structural and transport roles within the eukaryotic cells.

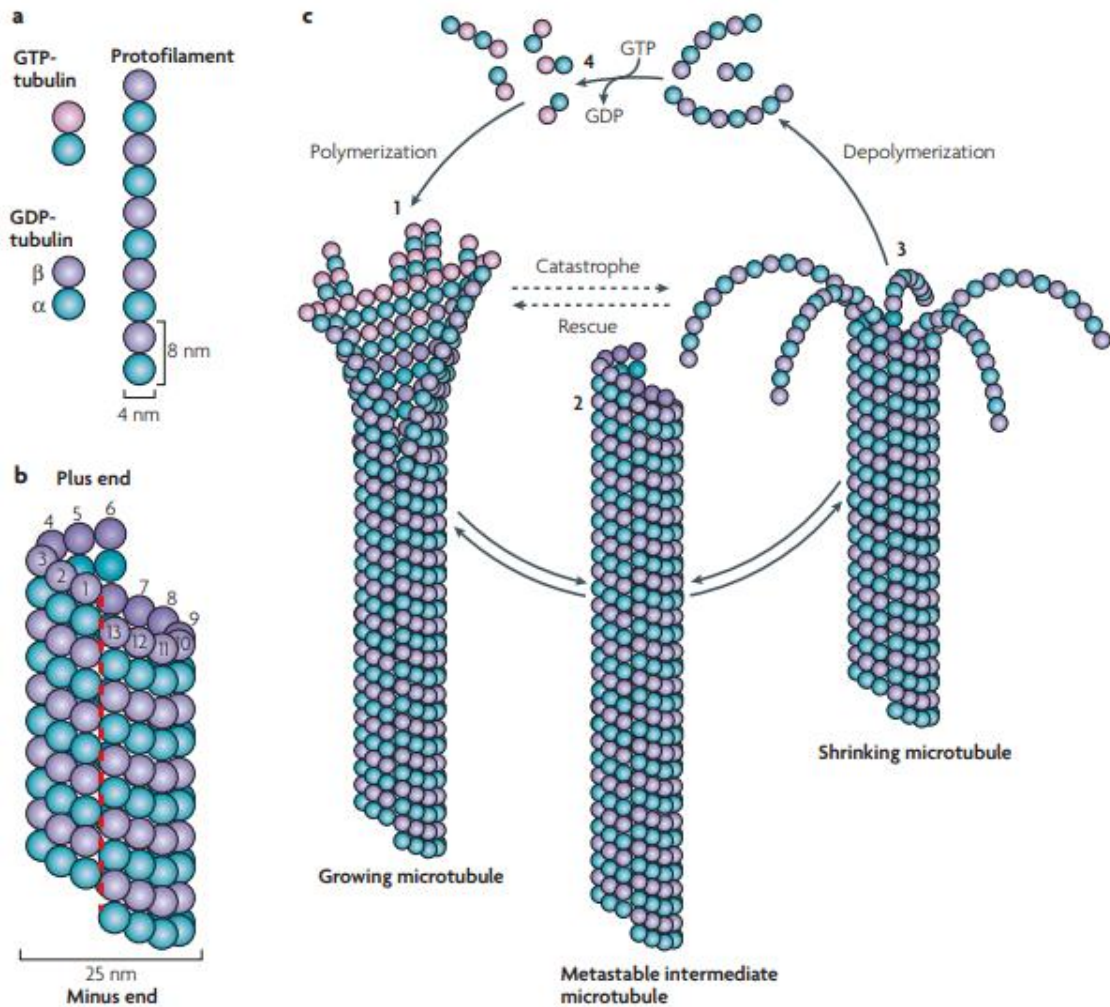


Figure 1.3 Formation of microtubules. a) Stable $\alpha\beta$ -tubulin dimers align in a head-to-tail manner to form protofilaments. b) Typically 13 parallel protofilaments from a cylindrical microtubule. The pitch and repeat of the protofilament generates a lattice seam (red dashed line). c) The assembly and disassembly of microtubules is driven by the GTP bound to the β -tubulin subunit (Box 1 from Akhmanova and Steinmetz, 2008).

Similarly in *E. coli*, FtsZ subunits polymerise in a head to tail manner and undergo treadmilling, dependent on the GTPase activity of the FtsZ subunit (Figure 1.4; Dyer, 2009; Yang *et al.*, 2017b). In an *in vitro* model an artificially membrane-targeted variant of FtsZ polymerises autonomously and potentially forms a helix (Ramirez-Diaz *et al.*, 2018). Mutations disrupting the GTPase activity of FtsZ change the spatial distribution of PG synthesis resulting in slanted, twisted and/or incomplete septum (Yang *et al.*, 2017b).

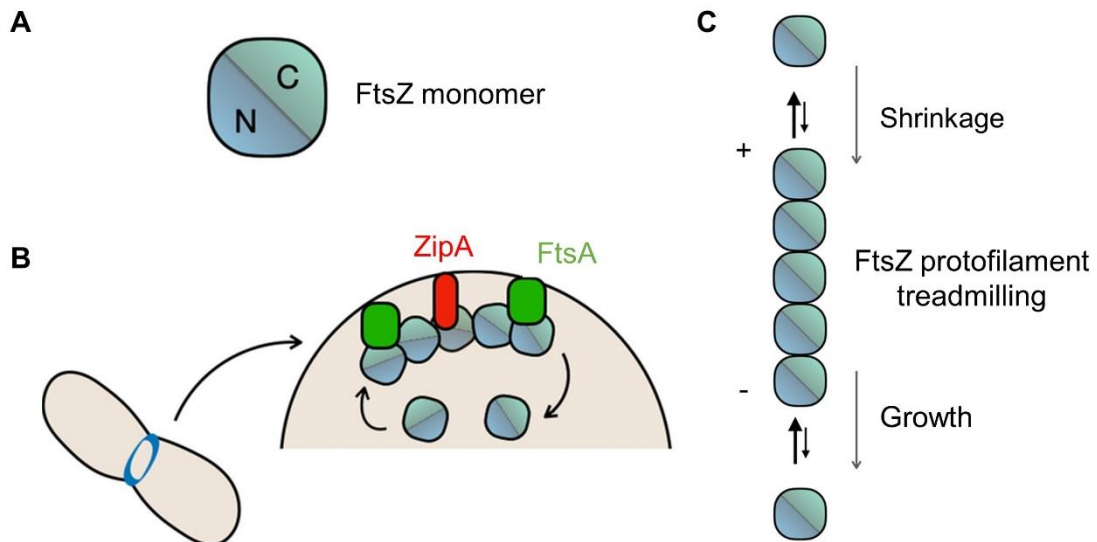


Figure 1.4 FtsZ protofilaments in *E. coli*. A) Schematic of an FtsZ subunit. B) As part of the Z-ring, FtsZ subunits interact with FtsA and ZipA and C) form FtsZ protofilament which undergo treadmill. During treadmilling growth occurs at the -ve end and shrinkage occurs at the +ve end. (Modified from Figure 1 and Figure 2 of Yadu *et al.*, 2021).

In *E. coli* the Z-ring is attached to the cell membrane by the positive regulators, FtsA and ZipA (Hale and de Boer, 1997; Pichoff and Lutkenhaus, 2005). Both FtsA and ZipA contain a membrane binding domain, absent from FtsZ. The C-terminal membrane binding domain of FtsA is inserted into the phospholipid bilayer, promoting rapid hydrolysis of ATP and lipid reorganisation, potentially while FtsZ polymers act as a scaffold and undergo active remodelling (Conti *et al.*, 2018). Individual knock-outs of *zipA* or *ftsA* result in the transient instability of the existing Z-rings, before the restoration and formation of Z-rings in a wild-type manner (Pichoff and Lutkenhaus, 2002). The double knock-out of *zipA* and *ftsA* destabilises the existing Z-rings and prevents Z-ring formation despite the presence of FtsZ foci, suggesting either ZipA or FtsA are sufficient for assembly of the Z-ring. Recently FtsA and ZipA have been shown to directly interact via an exposed helix on FtsA which could enable modification of ZipA and FtsA activity (Vega and Margolin, 2019).

Once formed, the Z-ring together with FtsA and ZipA, recruit additional proteins to the divisome. Over 36 proteins are known components of the divisome in *E. coli* (Du and Lutkenhaus, 2017). These proteins are recruited in a linear, hierarchical manner including the essential or conditionally essential, FtsE, FtsX, FtsK, FtsQ, FtsL, FtsB, FtsW, FtsI and FtsN (Figure 1.5).

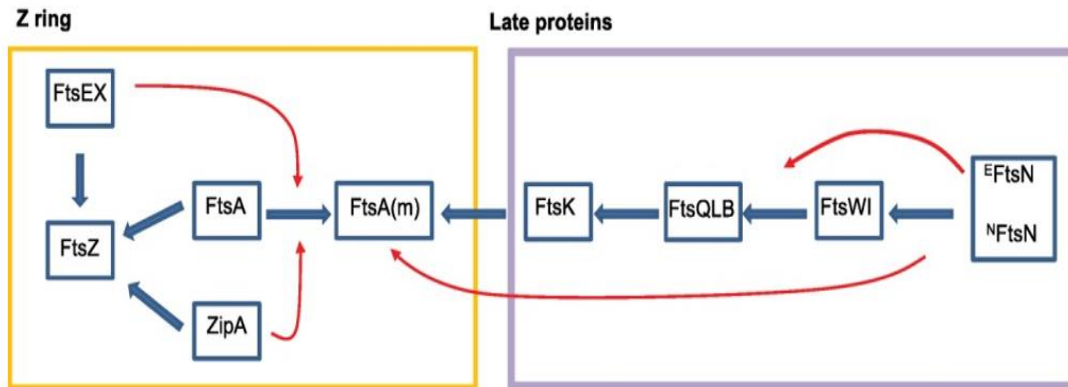


Figure 1.5 The assembly pathway for the divisome in *E. coli*. Polymerisation of FtsZ into Z-rings is aided by ZipA and FtsA. FtsA is converted to a monomer (FtsA(m)) by FtsEX leading to the recruitment of the late divisome proteins. The late divisome proteins complete the septa with the last essential protein, FtsN, triggering constriction (Figure 2A from Du and Lutkenhaus, 2017).

FtsA and ZipA aid the recruitment of FtsK to the Z-ring, which acts as a link between the early and late divisome proteins (Chen and Beckwith, 2008; Hale and de Boer, 1997; Pichoff and Lutkenhaus, 2002; Pichoff and Lutkenhaus, 2005). FtsN is the last essential component of the divisome and triggers cell constriction, which results in the formation of two daughter cells.

1.2.2 The positive cell division regulator, *SepF*, in *B. subtilis*

The positive FtsZ regulator, *SepF*, named due to the role of *SepF* in septa formation, is well conserved in Gram-positive bacteria and has more recently been identified in archaea (Hamoen *et al.*, 2006; Pende *et al.*, 2021). In *B. subtilis* *SepF* is present alongside the positive regulators, FtsA and *EzrA* (Ishikawa *et al.*, 2006). The double $\Delta ftsA/sepF$ knock-out mutant and the double $\Delta ezrA/sepF$ knock-out mutant exhibit synthetic lethality with the cells of $\Delta ftsA/sepF$ exhibiting abnormal Z-ring structures and elongation prior to lethality (Hamoen *et al.*, 2006; Ishikawa *et al.*, 2006). But the $\Delta sepF$ mutant, characterised by slightly longer cells and irregular thick cell septa, is viable in *B. subtilis*.

Overexpression of *SepF* in wild-type *B. subtilis* produced filamentous cells with large membrane invaginations (Gao *et al.*, 2017). The filamentous cells exhibited a cell division block, in the presence of Z-rings and co-localising FtsA. Little is known about the link between early and late divisome proteins in Gram-positive bacteria. But Gao *et al.* (2017) showed that overexpression of *SepF* altered the localisation of the late cell divisome protein, *WalK*, which as part of the *WalRK*

two component system is involved in PG metabolism. Overexpression of SepF in the $\Delta ftsA$ mutant of *B. subtilis*, complements the *ftsA* knock-out, characterised by increased lysis, a 50% reduction in growth rate, ~3x longer vegetative cells and reduced Z-ring formation (Ishikawa *et al.*, 2006). So SepF is expected to have an overlapping role with FtsA in the early divisome and could affect the divisome at multiple stages of development in *B. subtilis*.

SepF recruitment to the divisome is dependent on FtsZ (Hamoen *et al.*, 2006; Ishikawa *et al.*, 2006). Recruitment requires the C-terminal of SepF to recognise the secondary and tertiary structures of FtsZ (Krol *et al.*, 2012). The N-terminal of SepF contains a putative amphipathic helix which could allow the binding of SepF and the Z-ring to the membrane (Duman *et al.*, 2013). SepF functions as a dimer, promoting the assembly and bundling of FtsZ protofilaments, decreasing the critical concentration of FtsZ assembly and suppressing the GTPase activity of FtsZ (Singh *et al.*, 2008). The SepF dimers polymerise via an α -helix, to form ~50 nm ring-like structures (Duman *et al.*, 2013; Gündoğdu *et al.*, 2011). Recently, modification of the diameter of the ring-like structures revealed the diameter corresponds to the diameter of the cross-wall (Wenzel *et al.*, 2021). *In vitro* the ring-like structures have an unusual concave curvature so the current model suggests the ring-like structures of SepF form perpendicular to the protofilaments of FtsZ in *B. subtilis* (Duman *et al.*, 2013; Figure 1.6).

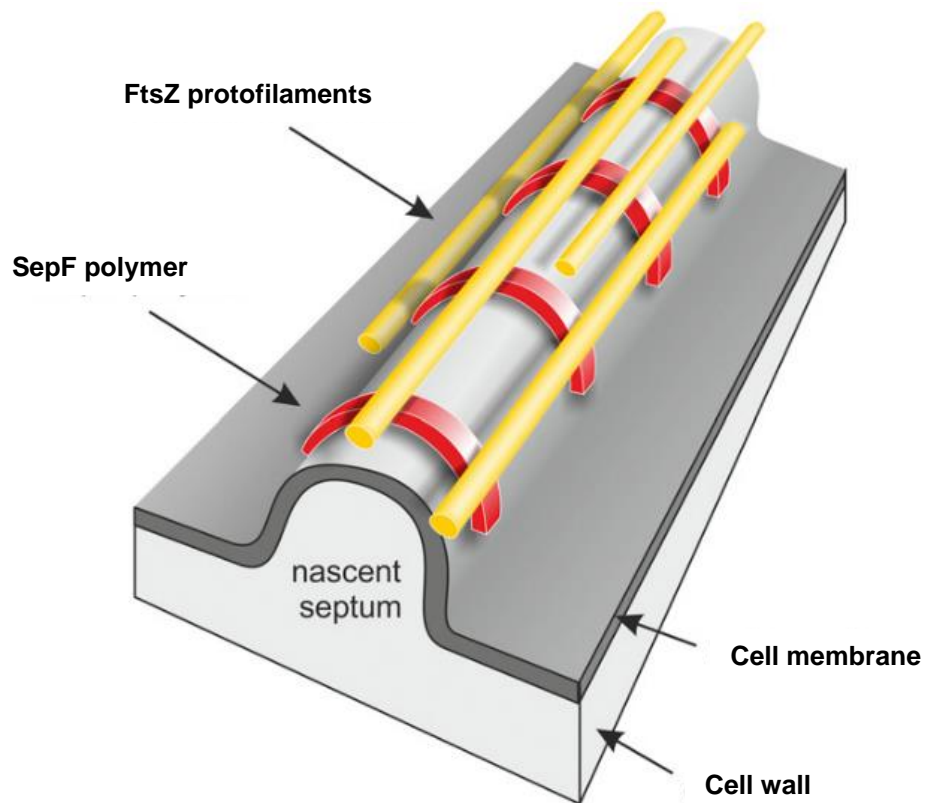


Figure 1.6 SepF in *B. subtilis*. Polymers of SepF (red) bind, as semi-circles, at the convex leading edge of the nascent division septum. The polymers of SepF bundle the protofilaments of (yellow) FtsZ (Figure 10 Duman *et al.*, 2013).

1.2.3 The negative regulators of cell division in *E. coli* and *B. subtilis*

In addition to the positive regulators of FtsZ assembly at the membrane, the positioning of the Z-ring inside the cell is negatively regulated by the synergistic work of the nucleoid occlusion system and the Min system in *E. coli* and *B. subtilis*. The nucleoid occlusion system prevents the formation of the Z-ring near the nucleoid and therefore the guillotining of the chromosome (Wu and Errington, 2011). The Min system prevents the formation of the Z-ring at the poles via the activity of the MinCD complex (Levin *et al.*, 1992; Rowlett and Margolin, 2015). Hence both of these systems are described below.

1.2.3.1 The Min system in *E. coli*

In *E. coli* the Min system consists of three major components: MinC, MinD and MinE (Figure 1.7). MinD, an ATPase, binds to the membrane in an ATP bound form and polymerises, forming MinD clusters (Hu, *et al.*, 2002; Kruse, 2002). Next MinD binds MinC, the dimeric effector protein of the Min system. The C-terminal and N-terminal of MinC contain domains with inhibitory activity against FtsZ polymerisation (LaBreck *et al.*, 2019; Ramm *et al.*, 2019). Importantly the binding of MinC to MinD sequesters MinC to the membrane. The affinity of membrane-bound MinC to FtsZ protofilaments increases when in a copolymer with MinD (Conti *et al.*, 2014; Ghosal *et al.*, 2014).

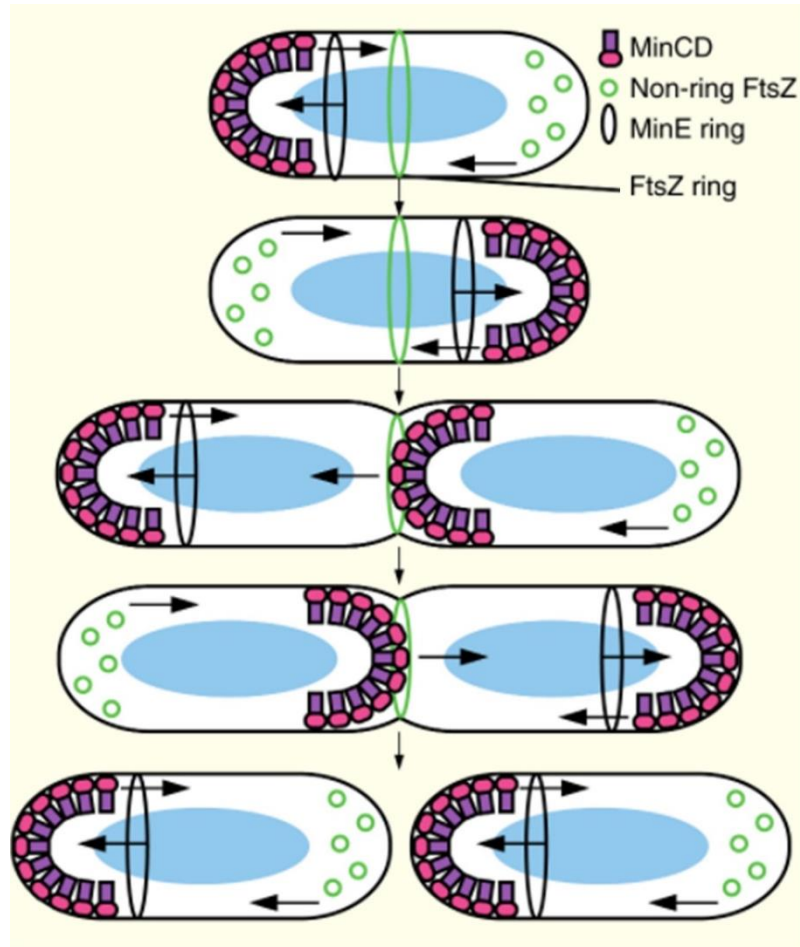


Figure 1.7 The Min system. in *E. coli*. In *E. coli* the Min system oscillates: MinCD complexes are bound to the poles until MinE binds and stimulates the ATPase activity of MinD. Stimulation of the MinD ATPase activity causes MinD and MinC to cycle to the opposite pole with MinE lagging slightly behind. In response to the oscillation of MinC, non-ring FtsZ also oscillates. Prior to division, MinC and MinD pause at the septum before oscillating again in both daughter cells (Figure 2A from Rowlett and Margolin, 2013).

The ATPase-activating protein, MinE acts as a spatial regulator for the MinCD complex and drives the oscillation of MinCD from pole to pole in *E. coli* (Ramm *et al.*, 2019). MinE recognises and binds to MinD, causing the displacement of MinC and triggering the ATPase activity of MinD (Hale *et al.*, 2001; Ramm *et al.*, 2019). Triggering the ATPase activity of MinD causes monomerization and removal of MinD from the membrane. The non-membrane bound MinD undergoes an ADP-ATP exchange to regenerate the ATP bound form of MinD which rebinds to the membrane at a distinct location, usually at the opposite pole (Huang *et al.*, 2003).

MinE also oscillates from pole to pole but lags slightly behind MinD (Loose *et al.*, 2011; Ramm *et al.*, 2019). The lag period enables MinE to remove additional or recently rebounded MinCD complexes from the membrane (Loose *et al.*, 2011). When no MinCD complexes are present at the pole MinE diffuses through the

cytoplasm to the opposite pole, excluding the MinCD complexes from the mid-cell and creating a MinC gradient (Rowlett and Margolin, 2015; Wu and Errington, 2011). Under stress conditions, inducing filamentous growth, the Min system is thought to act like a ruler mechanism, measuring the absolute size of the cell and positioning the Z-ring after every cell length until the stress condition is removed and division can commence again (Wehrens *et al.*, 2018)

1.2.3.2 *The Min system in B. subtilis*

The Min system of *B. subtilis* has homologues of MinC and MinD but not MinE (Figure 1.8; Levin *et al.*, 1992; Rowlett and Margolin, 2015). In the absence of MinE, the Min system of *B. subtilis* uses DivIVA and MinJ to spatially regulate the MinCD complex (Edwards and Errington, 1997). DivIVA acts as a cell-pole targeting protein which potentially senses negativity curving membranes (Jamroškovič *et al.*, 2012; Lenarcic *et al.*, 2009). In turn, DivIVA binds to the adaptor protein, MinJ, which binds to MinD to recruit the MinCD complexes to the cell poles or in the presence of a completed divisome to the mid-cell, potentially preventing the formation of additional Z-rings and minicells (Jamroškovič *et al.*, 2012; Lenarcic *et al.*, 2009; van Baarle and Bramkamp, 2010). Therefore, in *B. subtilis* the MinCD complexes do not oscillate but are located at the poles.

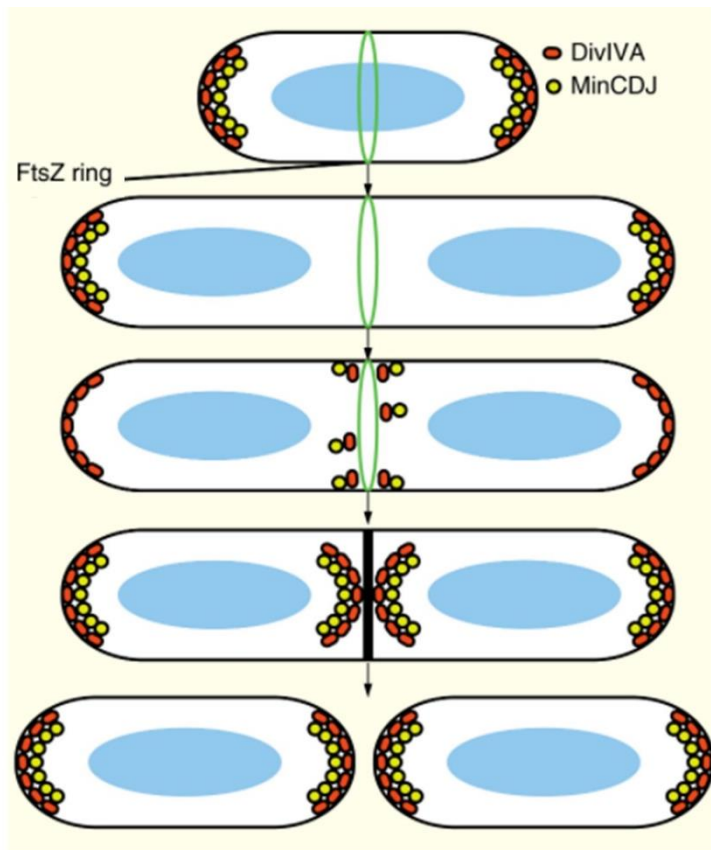


Figure 1.8 The Min system in *B. subtilis*. In *B. subtilis* DivIVA acts as a targeting protein for the Min system. DivIVA binds to MinJ which recruits MinCD complexes to the poles or the mid-cell, prior to division (Figure 2B from Rowlett and Margolin, 2013).

In the sporulating cells of *B. subtilis* DivIVA interacts with the chromosome segregation machinery at the poles, helping to position the *oriC* region, prior to division (Thomaides *et al.*, 2001). The introduction of point mutations into DivIVA affected the vegetative and sporulating cells separately indicating that DivIVA has distinct roles at different phases of development and raising the possibility that DivIVA in *S. coelicolor* could also have multiple functions.

1.2.3.3 The nucleoid occlusion system in *E. coli*

The nucleoid occlusion system prevents Z-ring formation near the nucleoid (Wu and Errington, 2011). In *E. coli* the first known nucleoid occlusion protein, SlmA, binds 24 SlmA binding sites (SBS) dispersed along the chromosome except at the DNA replication terminus binding-site, the Ter region (Bernhardt and de Boer, 2005; Cho *et al.*, 2011; Tonthat *et al.*, 2011; Figure 1.9).

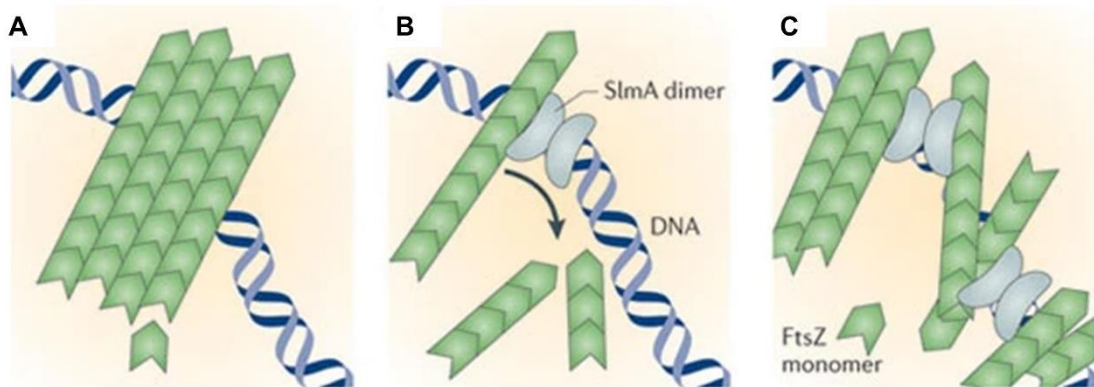


Figure 1.9 The activity of SlmA. A) In the absence of SlmA, FtsZ polymerises into Z-rings. In the presence of SlmA, Z-ring formation is prevented. SlmA binds to chromosomal SlmA-binding sites and either B) disrupts polymers of FtsZ or C) promotes polymerisation of FtsZ in an anti-parallel manner (Figure 2 from Wu and Errington, 2011).

Binding of SlmA to an SBS causes a conformational change which exposes the FtsZ binding site and allows SlmA to simultaneously bind the SBS and FtsZ (Figure 1.9; Schumacher and Zeng, 2016; Tonthat *et al.*, 2011). When SlmA is bound to a SBS and FtsZ, there are two models for the prevention of Z-ring formation: in the first model SlmA disassembles FtsZ protofilaments, but in the second model SlmA forces the FtsZ protofilaments into an anti-parallel arrangement (Cho *et al.*, 2011; Tonthat *et al.*, 2011). Overall, SlmA binding to its target sites in the chromosome blocks FtsZ polymerisation at those locations, leaving the Ter region located at mid-cell and lacking any SlmA binding, free for FtsZ polymerisation. Recently Shen *et al.*, 2020 proposed SlmA has an additional role in altering the frequency and stability of the Min system, described in Section 1.2.3.1, highlighting the complexity and intertwined nature of many bacterial processes, particularly cell division.

1.2.3.4 The nucleoid occlusion system in *B. subtilis*

In *B. Subtilis* the nucleoid occlusion system is thought to be mediated in part by the Noc protein, which has no sequence homology to SlmA (Wu and Errington, 2004). Noc binds to 74 Noc binding sites (NBS), which contain a consensus 5'-ATTCCCGGGAAAT-3' sequence and are dispersed along the chromosome except at the Ter region (Wu *et al.*, 2009). The N-terminal amphipathic helix of Noc has weak membrane targeting activity which requires the formation of nucleoprotein complexes (Adams *et al.*, 2015; Figure 1.10).

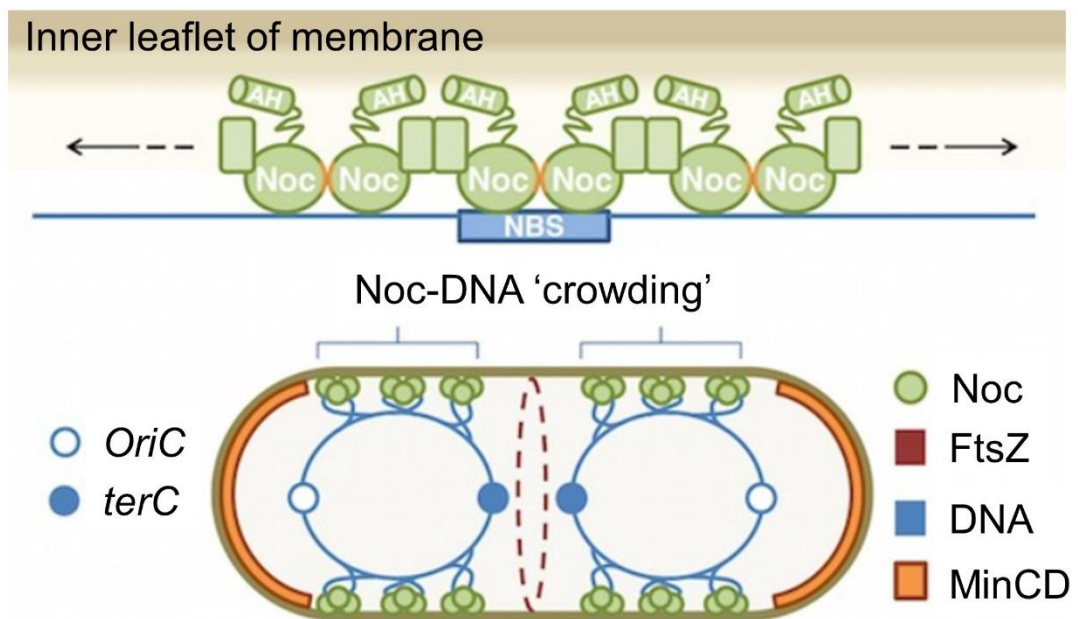


Figure 1.10 The activity of Noc. Noc is a DNA-dependent membrane binding protein. Top) Membrane-associated Noc complexes are distributed asymmetrically by the Noc binding sites (NBS) on the chromosome. Bottom) The crowding at the NBS sites could inhibit division over the nucleoid by physically excluding FtsZ assembly in these areas (Figure 8 and Synopsis from Adams *et al.*, 2015).

The coupling of membrane binding to the formation of nucleoprotein complexes is thought to allow a transient interaction between the chromosome and the membrane plus allow the site-specific, DNA-dependent activation of Noc (Adams *et al.*, 2015; Figure 1.10). In this model the crowding of the active regions of the nucleoid would physically force the division machinery away from the occupied areas and prevent the guillotining of the chromosome.

Alternatively, Yu *et al.*, 2021 used time-lapsed video microscopy of FtsZ to suggest Noc acts to corral FtsZ, preventing protofilaments from moving away from the Z-ring during cytokinesis. In this model the nucleoprotein complexes, described

above, could have a more active role in the nucleoid occlusion system, potentially utilising the suspected inhibitory activity of Noc on FtsZ and relying on other proteins, such as ZapA, to control condensation of FtsZ at the correct position.

1.2.4 Septa formation in *S. coelicolor*

1.2.4.1 Two distinct types of septa identified during the lifecycle of *S. coelicolor*

During the lifecycle of *S. coelicolor* at least two types of septa are formed: vegetative cross-walls and sporulating septa (Figure 1.2). The differences between the two septa types are not fully understood, but the two septa types have distinctive placement, frequency, thickness and roles within the lifecycle of *S. coelicolor* (Jakimowicz and van Wezel, 2012). Vegetative cross-walls are not associated with cell separation and are positioned infrequently within the vegetative hyphae, forming connected compartments in a syncytial network (Jakimowicz and van Wezel, 2012; Sexton and Tocheva, 2020). High resolution images of the vegetative cross-walls show 12 nm wide septal junctions with a 9 nm wide lumen, suggestive of channels for the movement of molecules between compartments (Sexton and Tocheva, 2020). On the other hand, sporulation septa are thicker than vegetative cross-walls and are positioned synchronously at regular ~1-1.2 μm intervals in the aerial hyphae, finally leading to the physical separation of spores (Jakimowicz and van Wezel, 2012; Sexton and Tocheva, 2020).

Sporulation requires several of the *whi* genes, named due to the white or light-grey pigmentation on the surface of the respective knock-out colonies with arrested development at the latter aerial hyphae stages (Flårdh and Buttner, 2009; Flårdh *et al.*, 1999). Briefly, the transcriptional regulator, BldD, limits the activity of WhiG, an RNA polymerase σ factor, prior to sporulation (Figure 1.11; Chater *et al.*, 1989; Elliot *et al.*, 2001; Flårdh and Buttner, 2009; Kelemen *et al.*, 1996). WhiG activates the transcription of *whiH*, *whiI* and *whiA* (Kaiser and Stoddard, 2011). WhiA is a transcriptional regulator with a C-terminal helix-turn-helix domain (Kaiser and Stoddard, 2011). WhiA binds to its own promoter, the *parABp₂* promoter for expression of ParA and ParB and inhibits *whiG* directed transcription, creating a feedback loop. WhiB and WhiA control the expression of several key genes including *ftsZ* and *filP* (Bush *et al.*, 2016). Then during late sporulation WhiH and WhiI become active and spore maturation requires WhiD, WhiE and σ^F .

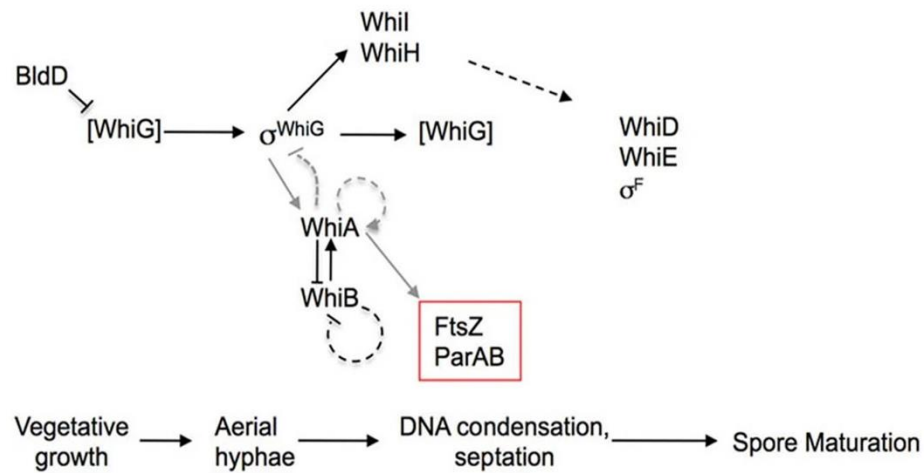


Figure 1.11 Summary of the *whi* regulatory network for sporulation in *S. coelicolor*. BldD prevents the activity of the sigma factor, WhiG, prior to sporulation. WhiG orchestrates the transition to sporulation (σ^{WhiG} = active WhiG and '[WhiG]' = inactive WhiG). σ^{WhiG} directs the transcription of *whiI*, *whiH* and *whiA*. WhiI and WhiH become active in late sporulation. WhiA and WhiB regulate their own and each other's expression. WhiA is required for the sporulation-specific expression of both ParAB and FtsZ and the accumulation of WhiA forms part of a negative feedback loop for WhiG. Subsequent spore maturation requires WhiD, WhiE and σ^F (Figure 1 from Kaiser and Stoddard, 2011).

A possible third type of septum positioned at the base of sporogenic aerial hyphae has been suggested in *S. griseus* (Kwak *et al.*, 2001). The basal septum is hypothesised to be involved in the separation of vegetative hyphae from the aerial hyphae. However the aerial hyphae of the early *whi* (*whiA*, *whiB*, *whiG*, and *whiI*) and *ssgB* knock-out mutants contained similar septa suggesting the basal septa could represent the formation of vegetative cross-walls within the aerial hyphae (Grantcharova *et al.*, 2005; Willemsse *et al.*, 2011). In addition a subapical compartment, spanning between the two septa which separate the spore chain from the non-sporulating hyphal base, has been defined in *S. coelicolor* (Dalton *et al.*, 2007). The subapical compartment expressed NepA-Egfp, a putative small secreted protein.

1.2.4.2 Z-ring formation in *S. coelicolor*

Formation of vegetative cross-walls and sporulation septa requires the polymerisation of FtsZ into Z-rings (McCormick *et al.*, 1994; Santos-Beneit *et al.*, 2017). In *S. coelicolor* the *ftsZ* gene is positioned in the well conserved division and cell wall (DCW) gene cluster. The DCW gene cluster spans SCO2077 to SCO2092 (Figure 1.12).

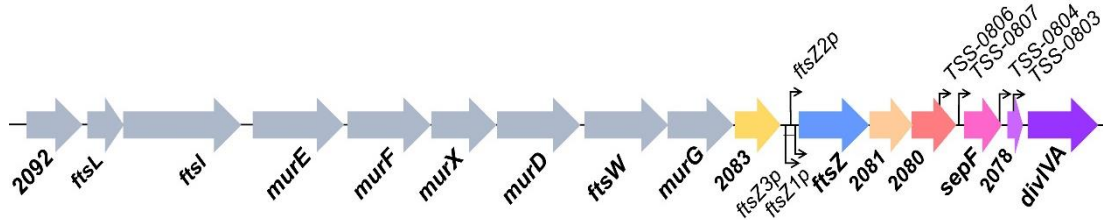


Figure 1.12 The division and cell wall (DCW) gene cluster of *S. coelicolor*. The DCW gene cluster of *S. coelicolor* contains *ftsZ*, *sepF* and *divIVA* in close proximity. The gene names are shown in bold and the promoters for *ftsZ*, *sepF* and *divIVA* are shown in italics. The image was generated using StrepDB (2018) and the promoters were identified by Flårdh *et al.* (2002) and Jeong *et al.* (2016).

Transcribed upstream of FtsZ, the first gene in the DCW gene cluster SCO2092 encodes a S-adenosyl-methyltransferase. Then *ftsL* encodes a small bitopic membrane protein which forms a heterodimer with FtsB, encoded by SCO3095 (McCormick, 2009). An insertion–deletion *ftsL* null mutant affected sporulation in a media dependant manner and FtsL has been suggested to coordinate the symmetrical annular ingrowth of the Z-ring (Bennett *et al.*, 2007). Next *ftsI* encodes a cognate class B high-molecular-weight penicillin-binding protein capable of synthesising PG (Mistry *et al.*, 2008). FtsI is linked to FtsW, a polytopic membrane protein transcribed further downstream, which controls PG synthesis.

The members of the DCW gene cluster, *murE*, *murF*, *murX*, *murD* and *murG* all encode enzymes required for cell wall synthesis (Baum *et al.*, 2007; Gordon *et al.*, 2001; Zhang *et al.*, 2021). Next SCO2083 also known as *ftsQ* encodes a bitopic membrane protein which interacts with FtsL (McCormick, 2009). Knocking out SCO2083 greatly reduces the formation of vegetative cross-walls and sporulation septa and SCO2083 could aid stabilisation of the Z-ring.

Transcribed downstream of *ftsZ*, SCO2081 encodes a putative copper-binding protein and SCO2080 encodes a putative alanine racemase. As a putative alanine racemase, SCO2080 could catalyse the conversion of L-alanine to D-alanine which is essential in the biosynthesis of cell wall PG. Position next to SCO2080 is SCO2079, one of the homologues of SepF which acts as a positive

regulator of FtsZ in *S. coelicolor* (Section 1.2.4.3). Transcribed upstream of *sepF* is SCO2078 or *sepG* is a putative membrane bound protein with multiple transmembrane domains (Kaur, 2018; Zhang *et al.*, 2016). SCO2078 interacts with the sporulation specific divisome component, SsgB (Zhang *et al.*, 2016). The final gene in the DCW gene cluster is *divIVA*. DivIVA is an essential protein in *S. coelicolor* and in contrast to the role of DivIVA in the Min system of *B. subtilis* (Section 1.2.3.2), the *S. coelicolor* DivIVA has a known role in polar growth (Section 1.3.2).

FtsZ is transcribed from three promoters (Figure 1.12; Flårdh *et al.*, 2002). Of the three promoters, *ftsZ2p* is upregulated in sporogenic aerial hyphae when in the presence of the *whi* genes (*whiA*, *whiB*, *whiG*, *whiH*, *whiI* and *whiJ*). In the absence of the *whi* genes, the expression of *ftsZ2p* not sufficiently upregulated, leading to no sporulation septation. Interestingly, the spore production defects of the corresponding Δwhi mutants were overcome by the expression of *ftsZ* under a constitutive promoter (Willemse *et al.*, 2012). The complemented spores were similar to wild-type spores expected for some strain specific variation: spores of the complemented $\Delta whiB$ mutant exhibited a regularly broken sheath and enhanced susceptibility to heat while spores of the complemented $\Delta whiA$ and $\Delta whiG$ mutants exhibited immature DNA compartmentalisation.

In the young aerial hyphae of *S. coelicolor* FtsZ-Egfp first localises diffusely (Grantcharova *et al.*, 2005; Willemse and van Wezel, 2009). Then as the hyphae mature the diffuse fluorescence condenses. Initially FtsZ-Egfp condenses into irregular or spiral-like filaments. Next, Willemse and van Wezel (2009) detected foci aligned at the septa site, before the final localisation of FtsZ-Egfp into rings. The rings of FtsZ-Egfp were positioned at regular intervals, perpendicular to the hyphae wall, forming a ladder-like structure. The role of phosphorylation in the complex localisation pattern of FtsZ is unclear however FtsZ phosphorylated at Ser 319 and Ser 387 have been identified in the aerial hyphae (Manteca *et al.*, 2011; Rioseras *et al.*, 2018).

Unlike in simple rod or spherical bacteria, *ftsZ* is not essential for development in the *Streptomyces* genus (McCormick *et al.*, 1994; Santos-Beneit *et al.*, 2017). In the absence of *ftsZ*, colonies develop aerial hyphae but are unable to produce septa or spores. The $\Delta ftsZ$ mutant from *S. venezuelae* lacks vegetative cross-walls and sporulation septa, resulting in continuous tube-like colonies which exhibit a tendency towards lytic events (Santos-Beneit *et al.*, 2017). Propagation of

the Δ *ftsZ* mutant from *S. venezuelae* was associated with the recovery and regrowth of small hyphae fragments. The small hyphae fragments were often bound by a tip end and a branching end; the former potentially containing DivIVA for future regrowth and the latter potentially having a reduced diameter for resealing (Santos-Beneit *et al.*, 2017).

1.2.4.3 Positive regulators for the polymerisation of FtsZ in Actinobacteria

S. coelicolor does not have an obvious Min system or nucleoid occlusion system, which negatively regulate the positioning of the Z-ring in *E. coli* and *B. subtilis*. However as a sporulating actinomycetes, *S. coelicolor* contains the SsgA-like protein family members, SsgA and SsgB (Noens *et al.*, 2007; Willemse *et al.*, 2011). The colonies of the *ssgA* and *ssgB* knock-out strains produce aerial hyphae with small branching events, and do not undergo regular sporulation, giving the colonies a *whi*-like morphology (Keijser *et al.*, 2003; Noens *et al.*, 2007; van Wezel *et al.*, 2000).

The localisation of SsgA-Egfp and SsgB-Egfp was not significantly altered in the presence or absence of *ftsZ*, suggesting that SsgA and SsgB are not dependent on FtsZ (Figure 1.13; Willemse *et al.*, 2011). Time-lapse imaging and Förster resonance energy transfer (FRET) showed foci of SsgA along the edge or at the tip of sporogenic aerial hyphae prior to a brief co-localisation with SsgB at alternative sides of the hyphae (Noens *et al.*, 2007; Willemse *et al.*, 2011). SsgB localised to the sites of septa formation about 30 min prior to FtsZ. The interaction between FtsZ and SsgB is thought to enable the formation of the FtsZ spiral-like structures, described in Section 1.2.4.2 and the tethering of FtsZ to the membrane, which eventually leads to the formation of the Z-ring (Willemse *et al.*, 2011). Single amino acid substitutions in SsgB result in abnormally positioned septa that sever spores diagonally or along the long axis, perpendicular to the division plane (Xiao *et al.*, 2021). During spore maturation, one focus of SsgA localises to each septa, immediately adjacent to the hyphal wall (Noens *et al.*, 2007). Then in the final mature spore the focus of SsgA are suspected to reorganise into two distinct foci, corresponding to the number of germ tubes produced.

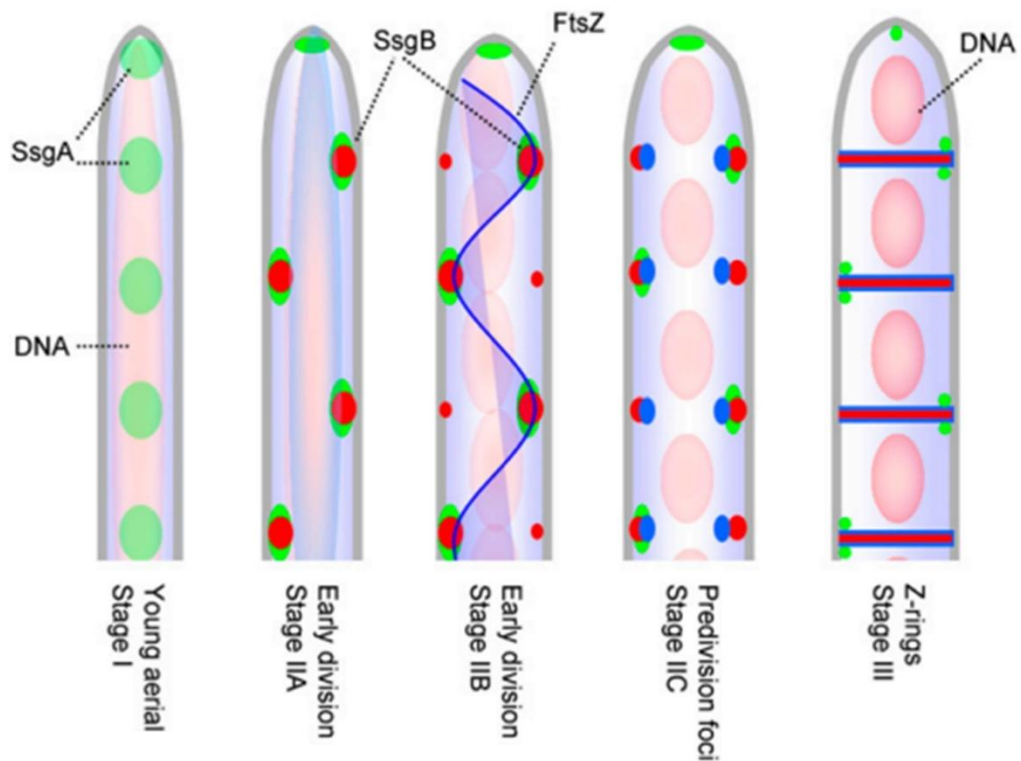


Figure 1.13 The localisation of SsgA and SsgB in the aerial hyphae of *S. coelicolor*. In young aerial hyphae only SsgA forms foci. During early division, SsgA and SsgB briefly colocalise, typically as foci at alternating sides of the hyphae, then FtsZ is hypothesised to attach to the foci of SsgB, forming long spiral-like filaments. The co-localisation of FtsZ and SsgB continues at the pre-division stage, potentially allowing the indirect attachment of FtsZ to the membrane. Next the chromosomes segregate and Z-ring formation leads to the production of sporulation septa. Finally during spore maturation, SsgA localises to either side of the septa, potentially marking the future sites of germ tube emergence (Figure 9 for Willemse *et al.*, 2011).

In addition to SsgB, homologues of SepF have been identified in several Actinobacteria, including *M. smegmatis*, *Corynebacterium glutamicum* and *S. coelicolor* (Gola *et al.*, 2015; Sogues *et al.*, 2020). In *M. smegmatis*, SepF forms ring-like structures as part of the early divisome (Gola *et al.*, 2015). The ring-like structures were formed in a FtsZ-dependent manner due to the interaction of SepF and FtsZ via their C-terminal domains. The interaction between SepF and FtsZ in *M. smegmatis* promoted polymerisation of FtsZ, inducing the bundling of FtsZ filaments, stabilising FtsZ filaments and reducing the GTPase activity of FtsZ (Bhattacharya *et al.*, 2018). The introduction of mutations at residue G51 negatively affected the ability of SepF to stabilise FtsZ filaments, affected the GTPase activity of FtsZ and promotion of FtsZ assembly. Overexpression of SepF in *M. smegmatis* has been showed to cause ~50% longer cells, capable of producing branch-like structures (Gola *et al.*, 2015). Conversely depletion of SepF caused elongated

filamentous cells with branch-like structures in liquid media (Gola *et al.*, 2015; Xiao *et al.*, 2019).

More recently homologues of SepF were identified in the *Corynebacterium* genus (Oliveira Jr *et al.*, 2018; Sogues *et al.*, 2020). In *C. glutamicum* a homologue of SepF is positioned in the DCW cluster (Sogues *et al.*, 2020). Depletion of the *C. glutamicum sepF* caused elongation and branching of cells and depleted cells were unable to form Z-rings or incorporate PG at the mid-cell. The C-terminus of SepF interacted with FtsZ as a homodimer and promoted the polymerisation and bundling of FtsZ. The N-terminal domain of SepF folded into an α -helix upon lipid vesicle interaction, supporting the role of the N-terminal in membrane binding.

There are three homologues of SepF in *S. coelicolor*, SCO1749, SCO2079 and SCO5967. Knocking-out of SCO1749 also referred to as *sepF1* or *SflA* and knocking-out of SCO5967 also referred to as *sepF3* or *SflB* was recently successfully achieved by Zhang *et al.*, 2020. The resulting $\Delta sepF1$ and $\Delta sepF3$ mutants had a fluffier colony edge, produced the grey sporulation pigment and sporulated but developed frequently branching sporogenic aerial hyphae. The current study focuses on SCO2079, encoded in the DCW cluster and transcribed downstream of *ftsZ* (Kaur, 2018). Similarly to FtsZ phosphorylated SCO2079 has been detected in the sporogenic aerial hyphae of *S. coelicolor* (Rioseras *et al.*, 2018). Based on the known homologs of SepF, SCO2079 was expected to be a positive regulator of FtsZ. SCO2079 was considered the primary SepF in the current study and is referred to as SepF from now on. Our study shows SepF is key to cell division and highlights SepF as a potential novel link between cell division and polar growth.

1.3 The Tip organising centre governs polar growth in *S. coelicolor*

1.3.1 Lateral growth in the rod-shaped *E. coli* and *B. subtilis*

During the bacterial lifecycle PG synthesis occurs during septa formation and growth. Bacterial growth is governed by cytoskeletal proteins which direct the cell wall machinery to the desired cellular location. For lateral growth, exhibited by most rod-shaped bacteria including *E. coli* and *B. subtilis*, PG are inserted into the lateral cell wall causing extension at the mid-cell (Höltje, 1998). Lateral growth requires the ATP dependent polymerisation of the actin-like homologue, MreB, into helices or patches (van den Ent *et al.*, 2001; Figure 1.14).

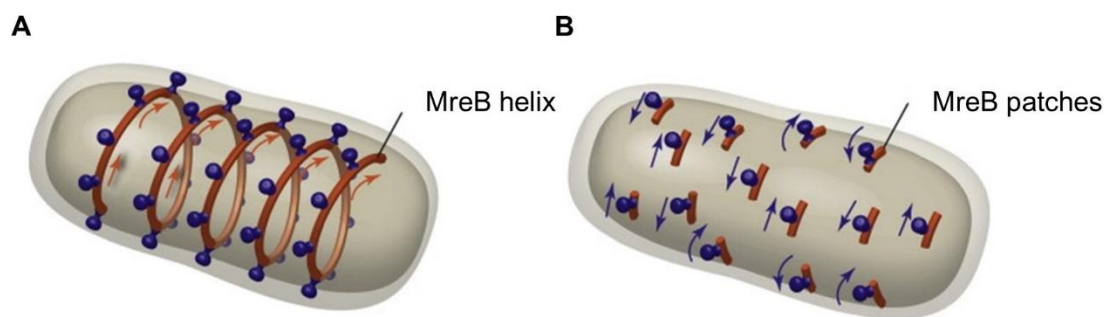


Figure 1.14 The structure and movement of MreB. MreB (burnt orange) binds to the PG elongation machinery (purple). MreB forms either A) a helical structure or B) short patches which move in a bi-directional manner (Modified from Figure 1 of White and Gober, 2012).

MreB is present throughout the cell, except at the poles and associates to the bacterial cytoplasmic membrane at least partially using an N-terminal amphipathic helix (Figure 1.14; Morgenstein *et al.*, 2015; Salje *et al.*, 2011). Movement of MreB is coupled to PG synthesis by the transmembrane protein, RodZ, which interacts with both MreB and either/or PBP2 and RodA (Morgenstein *et al.*, 2015). The interaction between MreB and RodZ regulates the positioning of MreB to curved subcellular regions and the number of MreB helices per cell (Bratton *et al.*, 2018). In addition to the length and pitch of the MreB helix, these factors have been shown to be predictors of cell morphology in *E. coli* (Bratton *et al.*, 2018; Ouzounov *et al.*, 2016).

1.3.2 Polar growth in the filamentous bacterium *S. coelicolor*

Unlike the rod-shaped cells of *E. coli* and *B. subtilis*, the filamentous hyphae of *S. coelicolor* grow by polar growth. Polar growth does not involve MreB but does involve the intermediate filament-like coiled-coil proteins, DivIVA, Scy and FilP (Holmes *et al.*, 2013; Javadi *et al.*, 2019; Oliva *et al.*, 2010). The intermediate-like filaments form the Tip organising centre or TIPOC (Figure 1.15; Flårdh, 2003a; Fuchino *et al.*, 2013; Holmes *et al.*, 2013; Kelemen, 2017). The TIPOC is located at the hyphal tips or at future branching sites for the *de novo* incorporation of PG precursors (Braña *et al.*, 1982; Gray *et al.*, 1990). Recently Sexton and Tochea, 2020, used cryo-electron tomography to show a putative TIPOC as a 6 nm wide layer ~10 nm underneath the cytoplasmic membrane of a vegetative hyphal tip in *S. albus* and that the PG layer at the hyphal tip is 5-20 nm thicker than at the lateral regions.

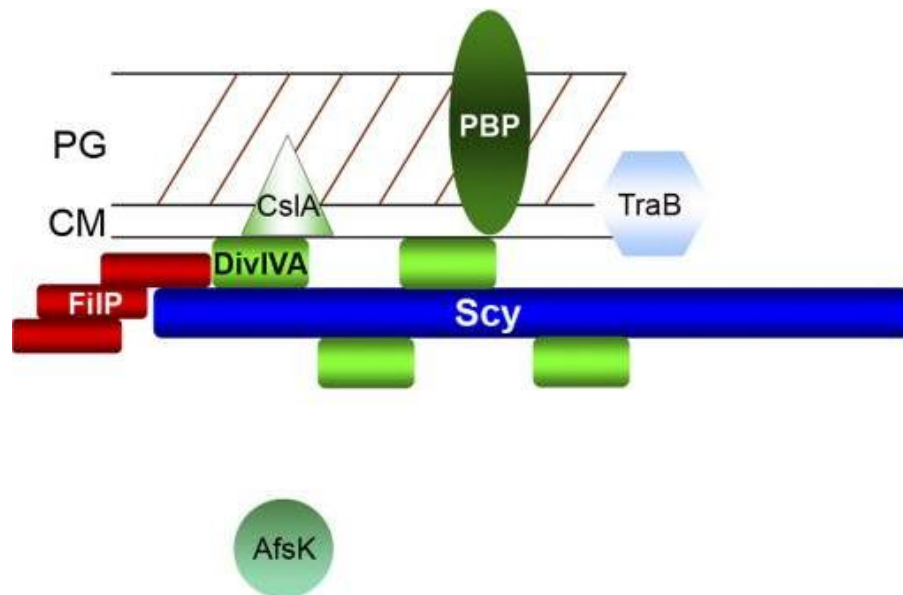


Figure 1.15 The tip organising centre (TIPOC) at the hyphal tips of *S. coelicolor*. The three major components of the TIPOC are the coiled-coil intermediate filament-like proteins, Scy, DivIVA and FilP. Potentially Scy organises the other components of the TIPOC, DivIVA directly interact with the cell wall synthesis machinery and FilP strengthens the hyphae walls (PBP = penicillin-binding protein, CM = cell membrane and PG = peptidoglycan). In addition, other proteins including CslA (cellulose synthase-like protein) TraB (DNA translocase) and AfsK (Ser/Thr protein kinase) localise to the hyphal tip (Modified from Figure 6 of Holmes *et al.*, 2013).

The intermediate filament-like, Scy, interacts with both DivIVA and FilP (Holmes *et al.*, 2013). Both Scy and DivIVA localise to actively growing tips and *de novo* branching sites (Holmes *et al.*, 2013; Flårdh, 2003a). In the absence of *scy*, colonies are able to produce low levels of the grey sporulation pigment and

sporulate, but the hyphae exhibit complex branching patterns and a reduced distance between branching events.

DivIVA is the only essential member of the TIPOC in *S. coelicolor* and has a putative role in organising the cell wall machinery. In *Mycobacterium* the DivIVA family member, Wag31, directly interacts with FtsI (Mukherjee *et al.*, 2009). The interaction between Wag31 and FtsI prevents FtsI heat-induced aggregation and protects FtsI from oxidative stress-induced proteolytic degradation. Potentially one of the methods for regulating hyphal tip extension in *S. coelicolor* is phosphorylation of DivIVA (Rioseras *et al.*, 2018; Hempel *et al.*, 2012; Passot *et al.*, 2021). One of the best known kinases, AfsK, is mentioned below.

FilP is composed of two central coiled-coil domains separated by a short linker and flanked by head and tail domains in *S. coelicolor* (Kelemen, 2017; Javadi *et al.*, 2019; Walshaw *et al.*, 2010). In differing ionic and physiologically mimicking conditions, the polymerisation of FilP, in a head to tail manner, forms various lattices or striated patterns (Alcock, 2019; Javadi *et al.*, 2019). In *S. venezuelae* FilP accumulates in gradient-like zones behind actively growing hyphal tips, which dissipates upon growth arrest (Fröjd and Flärdh, 2019). In the absence of *filP*, the vegetative hyphae of *S. coelicolor* exhibit a meandering morphology suggesting the polymerisation of FilP is important for the strengthening the hyphae cell walls (Alcock, 2019; Bagchi *et al.*, 2008; Fuchino *et al.*, 2013).

In addition to the intermediate filament-like proteins of the TIPOC, several other proteins localise to the tip including TraB, CslA and AfsK (Figure 1.15; Holmes *et al.*, 2013). TraB, a DNA translocase, is required for the transfer of double-stranded DNA in a process distinct from the type IV secretion system (Reuther *et al.*, 2006; Thoma and Muth 2015). The formation of TraB into large oligomeric protein complexes with lipid pore forming activity creates a route for the transfer of DNA and TraB is able to direct plasmid transfer, in an ATP dependent manner, by binding to the *cit* locus on the plasmids (Thoma and Muth 2015). Similar *cit*-chromosomal sequences are distributed across the genome of *S. coelicolor*, potentially allowing the spread and integration of plasmids with the aid of Spd-proteins during conjugation.

CslA, a cellulose synthase-like protein, has cellulose synthases activity in a central cytoplasmic loop (Xu *et al.*, 2008). At the hyphal tip the cytoplasmic loop enables CslA to bind to the cell membrane and DivIVA for the correct positioning and synthesis of β -glucan-containing polysaccharides. β -glucan-containing

polysaccharides are potential associated with the integrity of the hyphal tip: colonies of the *csIA* knock-out strain formed a low number of sporogenic aerial hyphae, had an absence of lamination on the lateral hyphal wall and had irregular spore walls. Interestingly *csIA* is positioned next to *glxA* (Liman *et al.*, 2013). GlxA is required for aerial development during osmotic stress in a medium-dependent manner. In the growing germ tubes GlxA localises to the hyphal tips but in the sporogenic aerial hyphae GlxA mainly localises sub-apically with a preference towards the sporulation septa.

AfsK, a Ser/Thr protein kinase, phosphorylates the C-terminal domain of DivIVA (Hempel *et al.*, 2012). Phosphorylation of DivIVA by AfsK is strongly activated when cell wall synthesis is arrested in a stress response and causes the modulation of DivIVA localisation and hyphal branching. Constitutive activity of AfsK causes the disassembly of DivIVA-containing apical polarisomes, inhibition of growth and the formation of multiple lateral branches (Hempel *et al.*, 2012). Conversely in the absence of *afsK*, colonies exhibit increased distances between branching events. Hence the phosphorylation of DivIVA by AfsK could enable the colonies of *S. coelicolor* to respond to damages during cell wall synthesis. Phosphorylation of DivIVA could also play a role in the latter stages of development as Rioseras *et al.*, 2018 found phosphorylated DivIVA within the sporulating aerial hyphae of *S. coelicolor*.

1.3.2.1 ParAB: The potential link between chromosome segregation and polar growth

In most rod-shaped bacteria chromosome replication then segregation occurs during cell elongation and just prior to cell division (Donczew *et al.*, 2016). Key to chromosome segregation is the ParAB system. The ParAB system consists of cis-acting centromere-like sites known as *parS* sites, a Walker Box ATPase known as ParA and a DNA binding protein known as ParB (Mierzejewska and Jagura-Burdzy, 2012). The *parS* sites are bound by ParB forming the nucleoprotein complex, the segrosome (Pióro and Jakimowicz, 2020). Interaction between ParA and the segrosome stimulates the ATPase activity of ParA. Stimulation of ParA ATPase activity triggers the dissociation of the ParA dimer, the release of ParA from the DNA and the movement of the segrosome.

In *S. coelicolor* the ParAB genes are co-transcribed and expression is directly regulated by two promoters: one active during vegetative growth and one

active during aerial growth (Szafran *et al.*, 2020). During young aerial growth ParA localises to the hyphal tips (Jakimowicz *et al.*, 2007). As the young hyphae elongate, ParA forms a pair of helical filaments in a non-ATP dependent manner. The filaments of ParA promote the formation of ParB complexes and potentially the binding of ParB to *parS* sites. There are 24 *parS* sites on the chromosome of *S. coelicolor* and 20 of the *parS* sites are close to the *oriC* (Jakimowicz *et al.*, 2002). The number of *parS* sites is thought to be driven by the large chromosome size of *S. coelicolor* (Szafran *et al.*, 2020). Binding of ParB to *parS* sites then the binding of ParA to ParB and the activation of the ParA ATPase activity leads to one chromosome per pre-spore compartment in the sporogenic aerial hyphae (Jakimowicz *et al.*, 2007).

Intriguingly, the aerial hyphae stop extending with the accumulation of ParA and the formation of Z-rings (Donczew *et al.*, 2016). Deletion of *parA* in *S. venezuelae* increased the time period for aerial hyphae extension and the rate of tip extension by ~60%, leading to longer sporogenic hyphae. The growth defects of the $\Delta parA$ mutant could be due to a ParA-Scy interaction. The ParA-Scy interaction, initially detected by a bacterial two-hybrid assay, occurs via the C-terminal of Scy (Ditkowski *et al.*, 2013). The interaction enables Scy to transiently recruit ParA to the hyphal tip and negatively regulate the polymerisation of ParA, in addition to potentially altering the higher order structures of Scy. Hence Scy is hypothesised to prevent premature chromosomal segregation and the upregulation of ParA during sporulation is hypothesised to cause the disassembly of Scy from the hyphal tip (Ditkowski *et al.*, 2013; Donczew *et al.*, 2016).

In contrast to the $\Delta parA$ mutant, deletion of *parB* in *S. venezuelae* increased the time period for aerial hyphae extension but decreased the rate of tip extension (Donczew *et al.*, 2016). About 13% of spores from the $\Delta parB$ mutant of *S. coelicolor* had abnormalities including being DNA free and being a highly reduced size (Kim *et al.*, 2000). The growth defects of the $\Delta parB$ mutants could be due to a ParB-DivIVA interaction. The ParB-DivIVA interaction was detected by a bacterial two-hybrid assay using DivIVA from several Actinobacteria, including *S. coelicolor* (Donovan *et al.*, 2012).

1.3.2.2 Polar growth and germination

Dominant spores are transported to their preferred microenvironments before germinating. Muok *et al.*, 2021 showed *Streptomyces* spores utilise structural proteins on the spore coat to directly interact with the flagella of Gram-positive and Gram negative bacteria to enable transportation to plant tissues. In their preferred microenvironment, germinating spores of the *Streptomyces* genus undergo three distinct stages: darkening, swelling and germ tube emergence (Hardisson *et al.*, 1978; Figure 1.16).

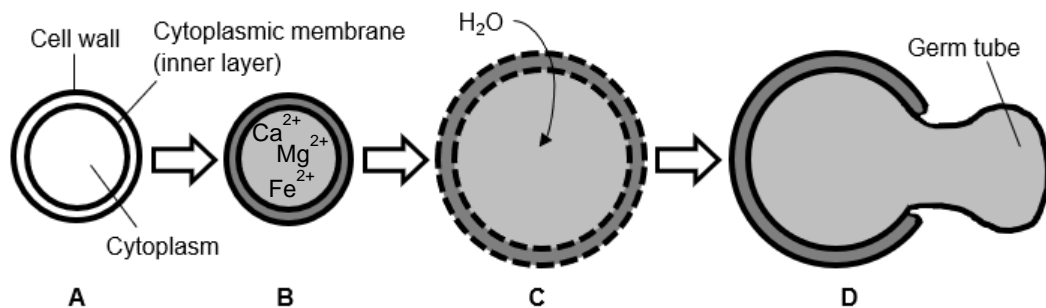


Figure 1.16 Germination in the *Streptomyces* genus. Under suitable conditions A) a spore will commence germination. The three stages of germination are B) darkening, characterised a loss of refractility and use of exogenous Ca²⁺, Mg²⁺ or Fe²⁺ ions, C) swelling, potentially due to the rehydration of the cytoplasm and D) germ tube emergence, governed by the TIPOC (Figure 2 from Harvey, 2019).

Darkening, characterised by a decrease in absorbance and loss of refractility, requires internal reserves and exogenous Ca²⁺, Mg²⁺ or Fe²⁺. During darkening, there is no change in the dry weight of spores from *S. antibioticus*, unlike in other endospores (Figure 1.16; Hardisson *et al.*, 1978; Powell and Strange, 1953). Then spore swelling, potentially from the rehydration of the cytoplasm and the remodelling of the cell wall, requires an exogenous carbon source (Hardisson *et al.*, 1978). Five resuscitation-promoting factors were identified in *S. coelicolor* with some level of PG cleavage, which upon deletion caused a delay in germination (Sexton *et al.*, 2015). Finally during germ tube emergence, the new germ tubes develop using exogenous carbon and nitrogen sources (Hardisson *et al.*, 1978). Germ tube development is governed by polar growth, requiring DivIVA to localise to the sites undergoing active growth (Flårdh, 2003a). Once the germ tube is ~2 µm long the first chromosome is translocated to, and the *oriC* is anchored to, the tip (Szafran *et al.*, 2020). As the germ tube elongates additional sub-apical chromosomes have a more flexible distribution along the hyphal filament.

1.4 The pigmented antibiotic, actinorhodin

Stages of the *S. coelicolor* lifecycle are marked by the production of secondary metabolites: the polyketide antibiotic, actinorhodin, is visible at the time of aerial growth and the grey sporulation pigment is detected during sporulation.

The polyketide grey sporulation pigment is produced by *whiE*, a complex locus of eight genes (Kelemen *et al.*, 1998). The *whiE* gene cluster contains two divergently oriented promoters and transcription is dependent on the early *whi* genes (*whiA*, *whiB*, *whiG*, *whiH*, *whiI* and *whiJ*). Unfortunately, to date attempts to purify the grey sporulation pigment have been unsuccessful, potentially due to the covalent attachment of the pigment to some of the spore wall components (Brian, 1992).

Actinorhodin was the first chromosomally determined antibiotic known to be produced by *S. coelicolor* A3(2) due to the characteristic pigmentation, which turns red in acidic conditions and blue in alkaline conditions (Abbas and Edwards, 1990; Wright and Hopwood, 1976). Actinorhodin with the molecular formula $C_{32}H_{28}O_{14}$ is naturally formed by a type II PKS encoded by the actinorhodin gene cluster, spanning *SCO5071* to *SCO5092* and recently has been synthetically synthesised with a benzdiyne equivalent as a precursor for the pyranonaphoquinone structure (Figure 1.17; Ninomiya *et al.*, 2019; Section 1.4.2). Early genetic studies of the actinorhodin gene cluster revealed seven distinct phenotypic classes; actI, actII, actIII, actIV, actV, actVI, and actVII (Rudd and Hopwood, 1979). Although names based on the phenotypic classes are commonly used in the literature, the genomic numbering is used in the current study (Figure 1.17 and Table 1.1). The early genetic studies also revealed *S. coelicolor* produces a second pigmented antibiotic, the red pigmented, undecylprodigiosin (Rudd and Hopwood, 1980). Collectively, undecylprodigiosin and actinorhodin are referred to as the pigmented antibiotics.

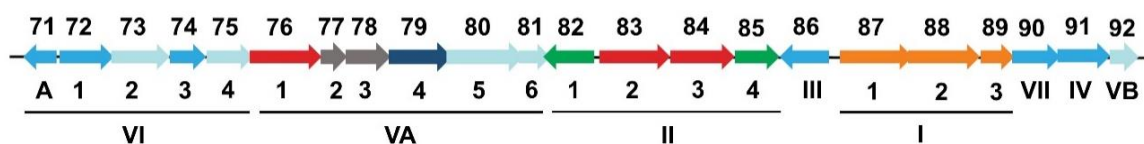


Figure 1.17 The actinorhodin gene cluster. Genes are colour coded based on function: regulators are green, minimal PKS components are orange, membrane pumps are red, tailoring enzymes are blue (sea blue proteins form (S)-DNPA, sky blue proteins form DHK and dark blue proteins dimerise two DHK) and hypothetical proteins are grey. The top line shows the genomic numbering and the bottom two lines show the phenotypic classes of the actinorhodin gene cluster (Modified from Figure 2 in Craney *et al*, 2013).

Table 1.1 Names of the actinorhodin gene cluster. Throughout the current study the genes of actinorhodin gene cluster are referred to using the genomic numbering, not the phenotypic classes.

Genome names (SCO)	Phenotypic names
5071	<i>ActVI-ORFA</i>
5072	<i>ActVI-ORF1</i>
5073	<i>ActVI-ORF2</i>
5074	<i>ActVI-ORF3</i>
5075	<i>ActVI-ORF4</i>
5076	<i>ActVA-ORF1</i>
5077	<i>ActVA-ORF2</i>
5078	<i>ActVA-ORF3</i>
5079	<i>ActVA-ORF4</i>
5080	<i>ActVA-ORF5</i>
5081	<i>ActVA-ORF6</i>
5082	<i>ActII-ORF1</i>
5083	<i>ActII-ORF2</i>
5084	<i>ActII-ORF3</i>
5085	<i>ActII-ORF4</i>
5086	<i>ActIII</i>
5087	<i>ActI-ORF1</i>
5088	<i>ActI-ORF2</i>
5089	<i>ActI-ORF3</i>
5090	<i>ActVII</i>
5091	<i>ActIV</i>
5092	<i>ActVB</i>

1.4.1 The complex regulation of actinorhodin production

In a recent genome wide mutagenesis approach Xu *et al.* (2019) predicted 300+ genes, capable of altering actinorhodin production, including a large number of hypothetical genes. The complex regulation of actinorhodin production will not be discussed in detail. For a more detailed review see Yin *et al.*, 2019 and Xia *et al.*, 2020. Briefly, regulation of actinorhodin production has been linked to primary metabolism by the chitin monomer, GlcNAc and the phosphofructokinase, pfkA2, as well as being more recently linked to homeostasis of cellular components through sulfane sulfur (Borodina *et al.*, 2008; Rigali *et al.*, 2006; Lu *et al.*, 2020; Rigali *et al.*, 2008; Figure 1.18). Regulation of actinorhodin production primarily occurs via the pathway specific activator, SCO5085 (Arias, *et al.*, 1999). SCO5085 was originally thought to bind to the intergenic regions between SCO5071 – SCO5072 and SCO5086 – SCO5087 but no DNA-binding domain has been identified (Arias, *et al.*, 1999; Li *et al.*, 2021). Deletion of SCO5085 causes the differential expression of at least 2 proteins, SCO5071 and SCO5075, encoded within the actinorhodin gene cluster and 14 proteins encoded outside of the actinorhodin gene cluster, suggesting SCO5085 could act as a pleiotropic regulatory factor (Li *et al.*, 2021).

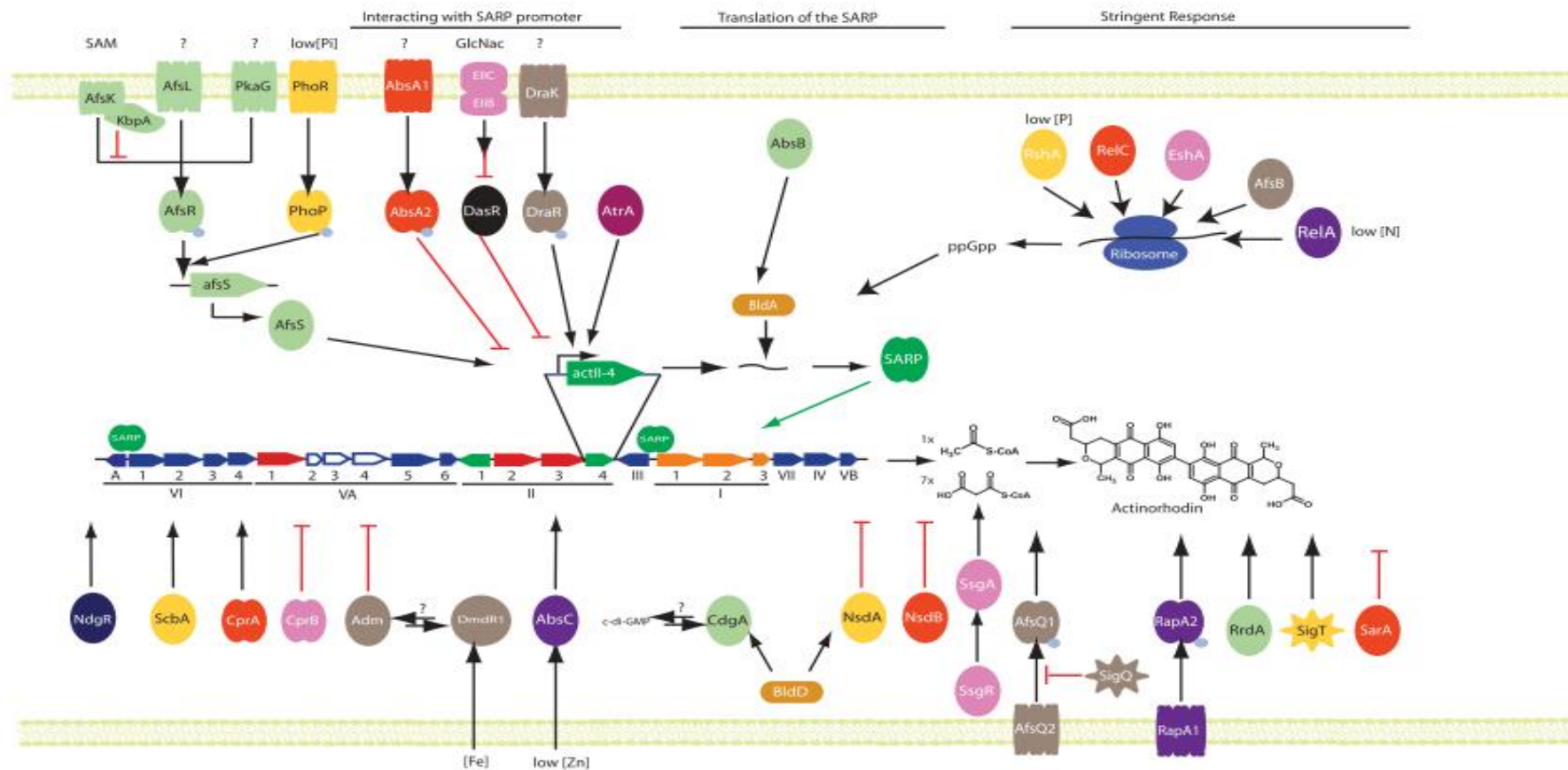


Figure 1.18 Regulators of actinorhodin production in *S. coelicolor*. The *Streptomyces* antibiotic regulatory protein (SARP) for actinorhodin is the pathway specific activator, SCO5085 or ActII-4. The regulators are categorised as ‘interacting with SARP promoter’ if there is experimental evidence for the binding of the promoter region of SARP, ‘translation of the SARP’ if regulators affect translation, and ‘stringent response’ if regulators influence the stringent response. The remaining regulators influence actinorhodin production but the mechanism has yet to be elucidated. The regulatory effect is categorised as repression (red) or activation (black). This Figure is not an exhaustive list of regulators (Figure 4 from Craney *et al.*, 2013).

1.4.2 Actinorhodin biosynthesis

There are at least three types of known bacterial PKSs (Shen, 2003). Type I PKSs are large multifunctional proteins, organised into modules (Shen, 2003; Yu *et al.*, 2012). Modules of iterative type I PKSs complete multiple rounds of polyketide chain elongation and β -keto processing for the formation of metabolites such as cholothricin, maduropeptin and polyketomycin. Modules of non-iterative type I PKSs complete only one round of the polyketide chain elongation and subsequent β -keto processing for the formation of metabolites such as erythromycin and avermectin (Chen and Du, 2016). Type II PKSs are complexes of multiple discrete enzymes, each with a distinct function (Shen, 2003; Yu *et al.*, 2012). Both type I and type II PKSs use acyl carrier proteins (ACP) to activate the acyl CoA substrates and to channel the growing polyketide intermediates (Shen, 2003). Type III PKSs or chalcone synthase-like PKSs are homodimer enzymes with iteratively condensing activity for the formation of metabolites such as RppA for flavolin. Type III PKSs act directly on the acyl CoA substrates, independently of ACP.

Actinorhodin is formed by a type II PKS encoded by the actinorhodin gene cluster. Initially the minimal PKS forms the octaketide backbone of actinorhodin from one acetyl-CoA and seven malonyl-CoA (Orange in Figure 1.19). The minimal PKS consists of a specific ACP, a specific heterodimeric ketosynthase–chain length factor (KS-CLF), and the malonyl-CoA:ACP transacylase (MAT) required for fatty acid biosynthesis (Dreier *et al.*, 1999). Initially malonate is transferred from CoA to the *holo*-ACP with an 18-Å-long phosphopantetheine arm (Beltran-Alvarez *et al.*, 2007). The conversion of the *holo*-ACP to malonyl ACP can be catalysed by MAT or can be self-catalysed. Decarboxylation of malonyl ACP to acetyl ACP is catalysed by the CLF of KS-CLF. The acetyl ACP forms the starter unit for the octaketide backbone and extension using malonyl ACP is catalysed by the iterative cycles of the KS from KS-CLF.

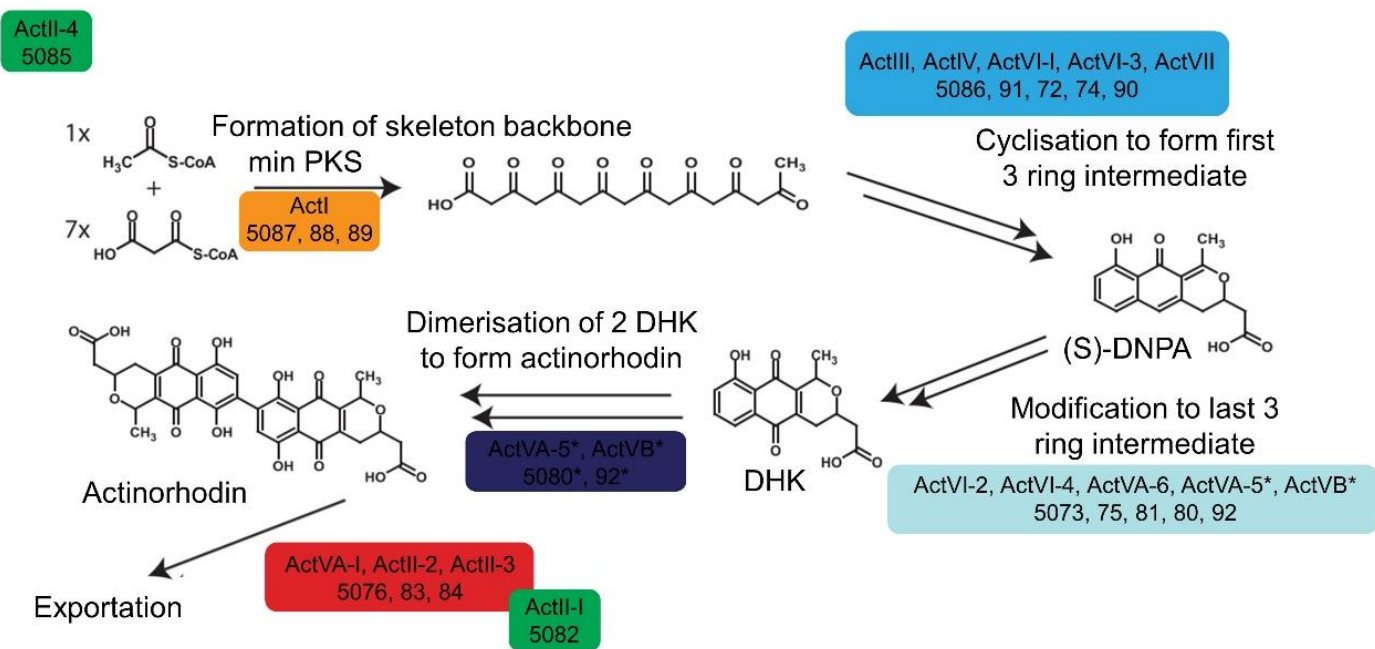


Figure 1.19 Actinorhodin biosynthesis. The pathway specific activator, ActIII-4 /SCO5085 (green), activates actinorhodin biosynthesis. The minimal PKS components (orange) condense 1x acetyl-CoA and 7x malonyl-CoA into an octaketide backbone. The octaketide backbone is converted, by tailoring enzymes, to (S)-DNPA (sea blue) then DHK (sky blue). Two DHK are dimerised to form actinorhodin (dark blue) and actinorhodin is exported by specific pumps (red). Export is partially regulated by the repressor, ActII-I /SCO5082 (green). Genomic names are written without the 'SCO' prefix, colour coding follows Figure 1.16 and the * marks the different suggested positions in the pathway (Modified from Figure 2 in Craney *et al.*, 2013).

The octaketide backbone is cyclised by the KS-CLF and the ACP binds to the first tailoring enzyme, SCO5086, a tetremic ketoreductase, which reduces the carbonyl group at C9 (Hadfield *et al.*, 2004; sea blue in Figure 1.19). Further cyclisation, potentially in the presence of SCO5090 and SCO5091, forms a bicyclic intermediate (Fernández-Moreno *et al.*, 1992). The keto group at C3 of the bicyclic intermediate is reduced to a chiral secondary alcohol by SCO5072, a hydroxyl acyl-CoA dehydrogenase (Taguchi *et al.*, 2000). Then additional cyclisation and dehydration leads to the formation of the first major intermediate, 4-dihydro-9-hydroxy-1-methyl-10-oxo-3-H-naphtho-[2,3c]-pyran-3-(S)-acetic acid, ((S)-DNPA). SCO5071, a hydroxyl acyl-CoA dehydrogenase and/or SCO5071, a dehydratase, could stabilise (S)-DNPA (Hesketh and Chater, 2003; Taguchi *et al.*, 2000). Before SCO5073, an oxidoreductase, primarily causes a stereospecific reduction at C15 of (S)-DNPA to form the second major intermediate 6-deoxy-dihydrokalafungin or DDHK (Taguchi *et al.*, 2000; sky blue in Figure 1.19). DDHK is oxygenated to form dihydrokalafungin (DHK) and finally two DHK are dimerised to form actinorhodin (dark blue in Figure 1.19; Okamoto *et al.*, 2009).

S. coelicolor produces several closely-related compounds to actinorhodin, known collectively as the actinorhodins (Bystrykh *et al.*, 1996; Figure 1.20). One of these actinorhodins, the full lactone form of actinorhodin, γ -actinorhodin, has been chemically synthesised and is distinctive due to its differing solubility profile, instability at pH 10+ and its association with the actinorhodin export system (Bystrykh *et al.*, 1996; Neumeyer and Brückner, 2017). There are three putative export pumps encoded in the actinorhodin gene cluster (red in Figure 1.19). Two of the export pumps, SCO5083 and SCO5084, are co-transcribed and regulated by SCO5082, a TetR-like transcriptional repressor (Tahlan *et al.*, 2007; Xu *et al.*, 2012). In addition, SCO6666 has been recently identified as a putative export pump for actinorhodin, encoded outside the actinorhodin gene cluster (Lee *et al.*, 2020). Efflux of the actinorhodins from the hyphae is thought to be important for the survival of the colony (Xu *et al.*, 2012).

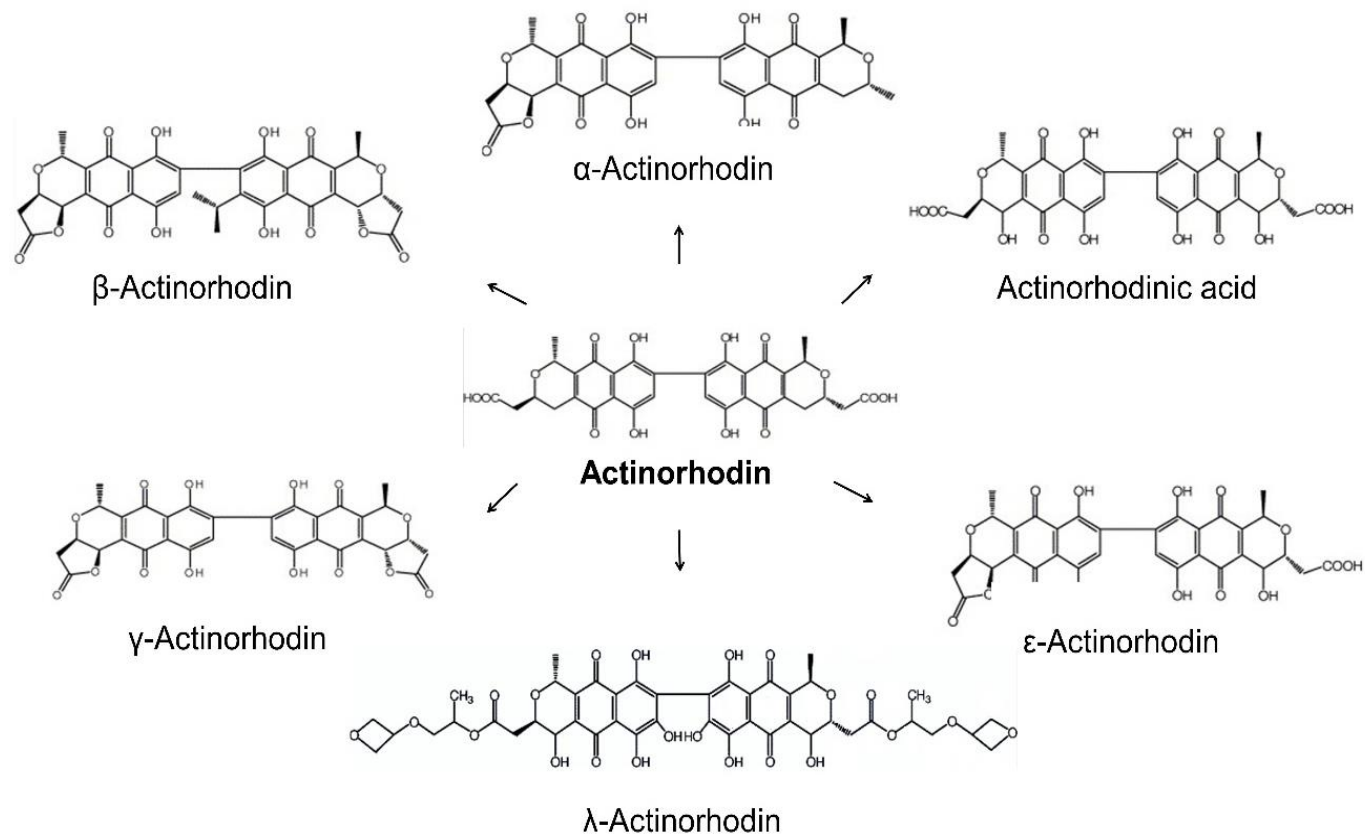


Figure 1.20 The known actinorhodins. (Modified from Figure 1 and 4 of Zhang *et al.*, 2006).

1.4.3 The potential functions of actinorhodin

The high level of actinorhodin production by the colonies of *S. coelicolor* was initially hypothesised to counter the low antibiotic activity of actinorhodin (Wright and Hopwood, 1976). The low antibiotic activity of actinorhodin was detected against *Staphylococcus aureus* using agar plugs. But during a recent reinvestigation into the actinorhodins as an untapped source of antibacterial drugs, the antibiotic activity of purified γ -actinorhodin was >10-fold greater than previously detected. The antibiotic activity of γ -actinorhodin, detected using the broth micro dilution method, included activity against methicillin resistant *S. aureus* and vancomycin intermediate *S. aureus* and was attenuated upon incorporation into agar (Nass *et al.*, 2017).

Furthermore γ -actinorhodin had several characteristics of a potentially useful clinical antibiotic: γ -actinorhodin displayed selective toxicity against Gram-positive bacteria, potentially due to an inability to cross the outer membrane of Gram-negative bacteria (Nass *et al.*, 2017). The proposed mode of action for γ -actinorhodin involves the dissipation of the proton motive force, but unlike the known membrane-active antibacterial agents, γ -actinorhodin did not cause sufficient physical perturbation of the membrane to allow the leakage of K^+ ions. The mode of action for γ -actinorhodin also involves the generation of reactive oxygen species, which together suggests γ -actinorhodin interferes with the electron transport chain (Nass *et al.*, 2017).

Other possible functions have also been attributed to the actinorhodins: in uni- and co-cultures iron competition leading to iron deficiency enhances the production of the blue pigmentation associated with the actinorhodins (Cosine *et al.*, 1999; Lee *et al.*, 2020). Under these conditions γ -actinorhodin is thought to sequester iron due to the structural similarity of γ -actinorhodin to tetracycline (Cosine *et al.*, 1999). The pigmentation of the actinorhodins could also enable γ -actinorhodin to function as a natural dye for the detection of acid production fungi or enable λ -actinorhodin to function as a natural, non-toxic food additive (Manikprabhu and Lingappa, 2013; Zhang *et al.*, 2006).

1.5 The aim of the current study

The aim of the current study was to investigate the potential link between cell division and polar growth then the potential link between cell division and actinorhodin production in *S. coelicolor*. The objectives of the study were to:

- Further characterise the vegetative and aerial hyphae of the $\Delta sepF$ mutant, lacking a key cell division protein in *S. coelicolor*, using fluorescent microscopy. Then confirm the phenotype of the $\Delta sepF$ mutant is due to the lack of *sepF* by complementing the knock-out strain.
- Investigate the mechanism behind the fork-like vegetative tips of the $\Delta sepF$ mutant by identifying the binding partners of SepF involved in cell division and polar growth. A bacterial two-hybrid assay indicated a novel interaction between SepF and the TIPOC component, Scy. Hence we investigated the production and localisation of SepF in the Δscy mutant using the Egfp translational fusion, SepF-Egfp.
- Investigate the localisation of the TIPOC component and Scy binding partner, DivIVA during aerial hyphae development and sporulation using a novel DivIVA-Egfp containing strain and epi-fluorescent microscopy.
- Compare the characteristics of the $\Delta sepF$ mutant to the characteristics of a *ftsZ* knock-out mutant in *S. coelicolor* by generating and complementing a novel *ftsZ* mutant via the Redirect[®] PCR-directed mutagenesis approach.
- Investigate the role of compartmentalisation in the spatial and temporal localisation of actinorhodin production in *S. coelicolor* by monitoring the localisation of the actinorhodin specific, Egfp tagged, ACP with epi-fluorescent microscopy.

2.0 Materials and Methods

2.1 Materials

2.1.1 Bacterial strains, cosmids, plasmids, media and antibiotics

The bacterial strains, cosmids and plasmids, used throughout the current study are summarised in Tables 2.1 to Table 2.5.

Table 2.1 The *Escherichia coli* K12 strains used throughout the current study.

Strains	Descriptions	Standard Growing Temps (°C)	References
BW25113 :pIJ790	<i>Plasmid:</i> λ-RED (gam, bet, exo), cat, araC, rep101 ^{ts} <i>Chromosome:</i> rrnB3 lacZ4787 hsdR514 (araBAD)567 (rhaBAD)568 rph-1	30	Gust <i>et al.</i> , 2003 Grenier <i>et al.</i> , 2014
DH5α	<i>Chromosome:</i> F- endA1 hsdRJ7 (r-, mit) supE44 thi-J ArcA1 gyrA96 relA1 deoR A(lacZYA-argF)- U169 480dlacZAM15	37	Grant <i>et al.</i> , 1990
BTH101	<i>Chromosome:</i> F', cya-99, araD139, galE15, galK16, rpsL1 (<i>StrR</i>), hsdR2, mcrA1, mcrB1, relA1	37	Karimova <i>et al.</i> , 1998
ET12567 :pUZ8002	<i>Plasmid:</i> tra, neo, RP4 <i>Chromosome:</i> dam, dcm, hsdM, hsdS, hsdR, cat, tet	37	MacNeil <i>et al.</i> , 1992 Paget <i>et al.</i> , 1999

Table 2.2 The *S. coelicolor* A3(2) strains used throughout the current study. All strains were incubated at 30°C.

Strains	Descriptions	References
M145	Chromosome: SCP1-, SCP2-	Bentley <i>et al.</i> , 2002
$\Delta sepF$	Chromosome: $\Delta sepF$ (Δ 1-159 amino acid):: <i>apra</i> ^R SCP1-, SCP2-	Kelemen <i>et al.</i> , (unpublished data)
Δscy	Chromosome: Δscy :: <i>apra</i> ^R SCP1-, SCP2-	Holmes <i>et al.</i> , 2013
$\Delta ftsZ$	Chromosome: $\Delta ftsZ$:: <i>apra</i> ^R SCP1-, SCP2-	The current study

Table 2.3 The cosmids used throughout the current study.

Cosmids	Descriptions	References
3GII	Supercomid1: <i>kana</i> ^R Actinorhodin gene cluster	StrepDB, 2018
3G11-5089-Egfp	Supercomid1: <i>kana</i> ^R Actinorhodin gene cluster: 5089- Egfp	Kelemen <i>et al.</i> , (unpublished data)
4A10	Supercomid1: <i>kana</i> ^R Division and cell wall cluster	McCormick <i>et al.</i> , 1994
4A10:: $\Delta ftsZ$:: <i>apra</i> ^R	Supercomid1: <i>kana</i> ^R Division and cell wall cluster: $\Delta ftsZ$:: <i>apra</i> ^R	Kelemen <i>et al.</i> , (unpublished data)
4A10-DivIVA-Egfp	Supercomid1: <i>kana</i> ^R Division and cell wall cluster: DivIVA-Egfp	Kelemen <i>et al.</i> , (unpublished data)

Table 2.4 The non-bacterial two-hybrid assay plasmids used throughout the current study.

Plasmids	Descriptions	References
pMS82	<i>Plasmid: ΦBT1 int/attP, hyg^R</i>	Gregory <i>et al.</i> , 2003
pMS82-SepF	<i>Plasmid: ΦBT1 int/attP, hyg^R, SepF</i>	The current study
pMS82-SepF-Egfp	<i>Plasmid: ΦBT1 int/attP, hyg^R, SepF-Egfp</i>	Kelemen <i>et al.</i> , (unpublished data)
pMS82-FtsZ	<i>Plasmid: ΦBT1 int/attP, hyg^R, FtsZ</i>	The current study
pMS82-FtsZ-Egfp	<i>Plasmid: ΦBT1 int/attP, hyg^R, FtsZ-Egfp</i>	Kelemen <i>et al.</i> , (unpublished data)
pMS82-267-DivIVA-Egfp	<i>Plasmid: ΦBT1 int/attP, hyg^R, 267-DivIVA-Egfp</i>	The current study
pMS82-2078-DivIVA-Egfp	<i>Plasmid: ΦBT1 int/attP, hyg^R, 2078-DivIVA-Egfp</i>	The current study

Table 2.5 The bacterial two-hybrid assay plasmids used in the current study.

Plasmids	Descriptions	References
pUT18C	Generates the T18-protein fusions in the bacterial two-hybrid assay	Euromedex
pUT18	Generates the protein-T18 fusions in the bacterial two-hybrid assay	Euromedex
pKT25	Generates the T25-protein fusions in the bacterial two-hybrid assay	Euromedex
pKNT25	Generates protein-T25 fusions in the bacterial two-hybrid assay	Euromedex
pUT18C-Zip	T18 translational fusion to the leucin zipper of GCN4	Karimova, 1998
pKT25-Zip	T25 translational fusion to the leucin zipper of GCN4	Karimova, 1998
pUT18C-SepFC	Expressing T18-SepFC fusion	Kemelen <i>et al.</i> , (unpublished)
pUT18-SepFC	Expressing SepFC-T18 fusion	Kemelen <i>et al.</i> , (unpublished)
pKT25-SepFC	Expressing T25-SepFC fusion	Kemelen <i>et al.</i> , (unpublished)
pKNT25-SepFC	Expressing SepFC-T25 fusion	Kemelen <i>et al.</i> , (unpublished)
pUT18C-SepFC-K46A	Expressing T18-SepFC K46A fusion	The current study
pUT18-SepFC-K46A	Expressing SepFC-T18 K46A fusion	The current study
pKT25-SepFC-K46A	Expressing T25-SepFC K46A fusion	The current study
pKNT25-SepFC-K46A	Expressing SepFC-T25 K46A fusion	The current study
pUT18C-SepFC-F71A	Expressing T18-SepFC F71A fusion	The current study
pUT18-SepFC-F71A	Expressing SepFC-T18 F71A fusion	The current study

Plasmids	Descriptions	References
pKT25-SepFC-F71A	Expressing T25-SepFC F71A fusion	The current study
pKNT25-SepFC-F71A	Expressing SepFC-T25 F71A fusion	The current study
pUT18C-FtsZC	Expressing T18-FtsZC fusion	Kemelen <i>et al.</i> , (unpublished)
pUT18-FtsZC	Expressing FtsZC-T18 fusion	Kemelen <i>et al.</i> , (unpublished)
pKT25-FtsZC	Expressing T25-FtsZC fusion	Kemelen <i>et al.</i> , (unpublished)
pKNT25-FtsZC	Expressing FtsZC-T25 fusion	Kemelen <i>et al.</i> , (unpublished)
pUT18C-SsgB	Expressing T18-SsgB fusion	Kemelen <i>et al.</i> , (unpublished)
pUT18-SsgB	Expressing SsgB-T18 fusion	Kemelen <i>et al.</i> , (unpublished)
pKT25-SsgB	Expressing T25-SsgB fusion	Kemelen <i>et al.</i> , (unpublished)
pKNT25-SsgB	Expressing SsgB-T25 fusion	Kemelen <i>et al.</i> , (unpublished)
pUT18C-Scy	Expressing T18-Scy fusion	Walshaw, 2010
pKT25-Scy	Expressing T25-Scy fusion	Walshaw, 2010
pUT18C-DivIVA	Expressing T18-DivIVA fusion	Holmes <i>et al.</i> , 2013
pKT25-DivIVA	Expressing T25-DivIVA fusion	Holmes <i>et al.</i> , 2013

The bacterial strains, described above, were grown when appropriate on media containing antibiotics. The media and antibiotics are summarised in Table 2.6 and Table 2.7.

Table 2.6 The media used throughout the current study. Unless stated the media was autoclaved once at 121°C and 15 psi for 15 min.

Media	Descriptions
Soya Flour Mannitol (SFM)	<i>Components:</i> 2% agar, 2% soya flour and 2% mannitol. Dissolved in hard tap water. <i>Autoclaved:</i> Twice. Once for 15 min at 126°C and 15 psi, and once for 15 min at 121°C and 15 psi.
<i>Lysogeny broth (LB) agar</i>	<i>Components:</i> 1% bacto tryptone, 0.5% yeast extract, 0.5% NaCl, 0.1% glucose, 1% agar. Dissolved in dH ₂ O.
<i>LB agar ΔNaCl (LB ΔNaCl)</i>	<i>Components:</i> Same as <i>LB agar</i> expect no NaCl.
<i>LB agar Δglucose (LB Δglucose)</i>	<i>Components:</i> Same as <i>LB agar</i> expect no glucose.
<i>Minimal Media Mannitol (MMM)</i>	<i>Components:</i> 0.5% mannitol, 0.01% FeSO ₄ ·7H ₂ O, 0.02% MgSO ₄ ·7H ₂ O, 0.05% K ₂ HPO ₄ , 0.0569% L-asparagine monohydrate and 1% agar. Dissolved in dH ₂ O. Prior to autoclaving the pH of the media was adjusted to pH 7.2 using orthophosphoric acid.
<i>Super Optimal Broth (SOB)</i>	<i>Components:</i> 2% tryptone, 0.5% yeast extract, 10 mM NaCl, 0.019% KCl, 10 mM MgCl ₂ , 0.6% MgSO ₄ . Dissolved in dH ₂ O.
<i>R5 agar</i>	<i>Components:</i> 10.3% sucrose, 0.025% K ₂ SO ₄ , 1.012% MgCl ₂ ·6H ₂ O, 1% glucose, 0.01% casaminoacids, 0.02 M trace elements (0.3 mM ZnCl ₂ , 0.74 mM FeCl ₃ ·6H ₂ O, 0.06 mM CuCl ₂ ·2H ₂ O, 0.051 mM MnCl ₂ ·4H ₂ O, 0.027 mM Na ₂ B ₄ O ₇ ·10H ₂ O and 0.0083 mM (NH ₄) ₆ Mo ₇ O ₂₄ ·4H ₂ O), 0.5% yeast extract, 0.573% TES buffer and 2.2% agar, Dissolved in dH ₂ O and autoclaved. Then 0.5% KH ₂ PO ₄ , 0.02 M CaCl ₂ ·2H ₂ O, 0.075% L-proline and 0.007 M NaOH was added.

Table 2.7 The antibiotics used throughout the current study.

Antibiotics	Stocks (mg/ml)	SFM media (final concentrations $\mu\text{g/ml}$)	LB media (final concentrations $\mu\text{g/ml}$)
Apramycin	100	50	50
Chloramphenicol	25	25	25
Kanamycin	100	50	50
Arabinose	1 M	N/A	10 mM
Hygromycin	50	25	25
Ampicillin	100	N/A	100
Nalidixic acid	25	25	25
X-gal	20	N/A	40
IPTG	1 M	N/A	0.5 mM

2.1.2 Conditions and primers for the polymerase chain reactions

All PCR reactions were performed using a Bio Rad T100™ Thermal Cycler. The primers used throughout the study are summarised in Table 2.8.

Table 2.8 The primers used throughout the current study.

Primer names	Primer sequences (5' to 3')
SepF 3' end	GCCTTGCCGGGTTGCCACGAGC
SepFP2 XbaBgl FRW	GATCACTCTAGATCTGACCGTGGCCCCGCTCAGCGG
SepF Trunc Xba Nde FRW	GGTCATCTAGAGCATATGTCCGAACGAGAGCCCTACCG
SepF UT REV	GGTCAGAATTCGAGCTCTGGTTGAAGAACCCGCC
SepF UTC REV	GGATCAGAATTCTCTCAGCTCTGGTTGAAGAACCCGC
FtsZ BglProm FRW	GATCACAGATCTGTATACGTGCAGGCCAGCACC
FtsZ EcoRIUTC	GGATCAGAATTCTCTCACTTCAGGAAGTCCGGCACG
FtsZ Trunc Xba Nde FRW	GGTCATCTAGAGCATATGGGGTCCTCGGCCAAGCG
DivIVAP Xba Bgl FRW	GATCACTCTAGATCTTGGACTACGTGTTCCAGTTCG
FP Eco REV	GGATCGAATTCTTACTTGTACAGCTCGTCCATGCCG
2078 Xba Bgl FRW	GATCACTCTAGATCTAACACTTCCGTGAGGGCACTCC
2078 3' End	TCGTTCTCGCGGAGCAGTCGG

2.1.2.1 High-fidelity polymerase chain reactions

The high-fidelity PCRs were completed under the following conditions: Thermofisher Phusion GC buffer x1, 200 μ M of each dNTP, 1.5 mM MgCl₂, 3% DMSO, 1 μ M of each primer and 0.02 U/ μ l Thermofisher Phusion High-Fidelity DNA Polymerase. The cycles for the high-fidelity PCRs are summarised in Table 2.9. For the annealing temperatures, the predicted temperatures from the Thermofisher Tm calculator were increase by 2-3°C to account for the higher concentration of DMSO in the above conditions (<https://www.thermofisher.com/uk/en/home/brands/thermo-scientific/molecular-biology/molecular-biology-learning-center/molecular-biology-resource-library/thermo-scientific-web-tools/tm-calculator.html>). The extension times were calculated as 30 sec per 1 Kbp of the desired PCR product.

Table 2.9 The cycles for the high-fidelity PCRs completed during the study. The base cycle had two standard modifications, X¹ and X². Any additional modifications are stated in 'Add'. The cycles are showed in chapter order: 'comp' stands for complementation, 'SepFC BTH 1' describes the SepFC-K46A-UT/-UTC and F71A-UTC fragment generation, 'SepFC BTH 2' describes the SepFC-F71A-UT fragment generation and 'DivIVA-Egfp' describes the DivIVA blunt end cloning attempts.

Base cycle						
1.	Initial Denaturation	98°C for 120 sec				
2.	Denaturation	98°C for 30 sec				
3.	Primer Annealing	X ¹ for 30 sec				
4.	Extension	72°C for X ²				
5.	Final extension	72°C for 300 sec				
6.	Cool down	20°C for 300 sec				
} 25 cycles						
Specific alterations						
	Δ sepF comp	SepFC BTH		DivIVA-Egfp		Δ ftsZ comp
		1	2	1 promoter	2 promoters	
X ¹	72°C for 60	68°C	63°C	63°C	68°C	65°C
X ²	sec	9 sec	13 sec	66 sec	77 sec	45 sec
Add	3 and 4 are combined	N/A	N/A	N/A	N/A	N/A

2.1.2.2 Low-fidelity polymerase chain reactions

The low-fidelity PCRs were completed under the following conditions: Go Taq polymerase buffer x1, 200 μ M of each dNTP, 2.5 mM MgCl₂, 5% DMSO, 1 μ M of each primer and 0.02 U/ μ l Invitrogen Go Taq DNA polymerase. The cycles used for the low-fidelity PCRs are summarised in Table 2.10. For the annealing temperatures, the predicted temperatures from Snappgene 2016 were increase by 2-3°C to account for the higher concentration of DMSO in the above conditions. The extension times were calculated as 30 sec per 500 bp for the desired PCR product.

Table 2.10 The cycles for the low-fidelity PCRs completed during the study. The base cycle had two standard modifications, X¹ and X². Any additional modifications are stated in 'Add'. The cycles are showed in chapter order: 'comp' stands for complementation, 'BTH' stands for bacterial two-hybrid assay and 'DivIVA-Egfp' describes the DivIVA blunt end cloning attempts.

Base cycles					
1.	Initial Denaturation				96°C for 300 sec
2.	Denaturation				92°C for 60 sec
3.	Primer Annealing				X ¹ for 30 sec
4.	Extension				72°C for X ²
5.	Final extension				72°C for 300 sec
6.	Cool down				20°C for 300 sec
					30 cycles
Specific alterations					
	Δ sepF comp	SepFC BTH	DivIVA-Egfp		Δ ftsZ comp
			1 promoter	2 promoters	
X ¹	63°C	58°C	56°C	58°C	58°C
X ²	72 sec	18 sec	25 sec	47 sec	15 sec
Add	2. at 96°C	N/A	N/A	N/A	N/A

2.2 Methods

2.2.1 General

Unless stated, centrifugations occurred at 4000 rpm, 1878 g for 5 min at 4°C but the centrifugations with phenol and/or chloroform occurred at 13300 rpm, 16300 g for 5 min at RT.

2.2.2 Agarose gel electrophoresis

Agarose gels consisted of 1x TAE buffer (40 mM Tris acetate, 1 mM EDTA, pH 8), 0.5 µg/ml EtBr, and the stated percentage of agarose. Gels were loaded into Bio-Rad Mini-Sub or Sub-cell trays and submerged in 1x TAE buffer. Gels were run at 20 VA or 30 VA respectively for 2 hrs, unless stated. Then the gels were imaged using a Bio-Rad ChemiDoc XRS+ system. Samples were visualised with a loading dye consisting of 5 mM Tris, 5 mM EDTA, 5% glycerol, 0.005% Xylene cyanol and 0.005% Bromophenol Blue at pH 7.4 and compared to λ DNA digested with *EcoRI* and *HindIII*.

2.2.3 Ligation for combinate plasmid generation

An approx.1:3 ratio of vector and insert was mixed in dH₂O for a volume of 11 µl. The mixtures were incubated for 3 min at 65°C, cooled on ice, then 3 µl Invitrogen 5x ligation buffer and 3 µl Invitrogen DNA ligase were added. Finally the ligations were incubated at 4°C overnight.

2.2.4 Restriction digestions

Each restriction digest contained a varying volume of target construct, 10 µl optimum Roche buffer, 1 µl of each Roche restriction enzyme and dH₂O to make up to a final volume of 100 µl. The restriction digests were incubated at 30°C overnight.

2.2.5 Phosphorylation

The phosphorylation reactions contained 25 µl target fragment, 3.5 µl buffer A, 6 µl 10 mM ATP and 1 µl T4 polynucleotide kinase. The phosphorylation reactions were incubated for 1 hr at 37°C then halted by a 10 min incubation at 75°C. Next the reactions were cooled on ice, 15 µl 0.3 M NaOAc was added and

the reactions underwent the Qiagen PCR purification kit with a final elution volume of 25 μ l.

2.2.6 Large scale plasmid preparations

Solution I	50 mM Tris/HCL, pH8:10 mM EDTA
Solution II	200 mM NaOH:1% SDS
Solution III	3 M potassium acetate, pH5.5

Unless stated all stages occurred on ice. For each preparation a 50 ml LB culture with the appropriate antibiotics was incubated at 250 rpm, 3.56 g and 37°C overnight. Then cells were pelleted by centrifuged and the size of the pellet altered the following volumes. Large pellets were washed in 40 ml ice cold solution I, centrifuged, and resuspended in 2 ml of the same solution. Next 4 ml solution II was added for a maximum of 4 min. At 4 min 3 ml ice cold solution III was added, vigorously mixed and incubated for 10 min. Thirdly, samples were centrifuged before and after addition of 2 ml phenol/chloroform. The DNA in the top phase was precipitated by a 20 min incubation in 12 ml ice cold iso-propanol and pelleted by a 15 min centrifugation. The pellet was washed in 500 μ l 70% ethanol before being resuspended in 600 μ l dH₂O. Fourthly the sample was incubated for 1 hr with 1 μ l RNase at 37°C. After the 1 hr incubation the samples underwent another phenol extraction with 500 μ l phenol/chloroform then 600 μ l chloroform. The top phase was separated into two and each half was incubated with 1/10th volume μ l 3 M sodium acetate and 3x volume μ l 100% ethanol for 20 min. The samples were centrifuged for 15 min, washed with 200 μ l 70% ethanol then centrifuged again. Finally the pellets were air dried, resuspended in dH₂O and combined.

2.2.7 Chemical transformation of *E. coli*

To generate the competent *E. coli* cells, a LB culture with the appropriate antibiotics was incubated at 250 rpm, 3.56 g overnight then subcultured under the same conditions for 2 hrs 20 min. From here on, all stages occurred on ice. The cells were pelleted by centrifugation, washed in 20 ml 10 mM NaCl then re-suspended and incubated in 20 ml 30 mM CaCl₂/10 mM RbCl₂ for 1 hr 30 min. After the incubation period, the cells were centrifuged and resuspended in 500 μ l 30 mM CaCl₂/10 mM RbCl₂.

For each chemical transformation, 50 µl competent cells and the desired DNA were incubated together on ice for 30 min. Then the mixture was heat shocked for 1 min at 42°C. Immediately after the heat shock, the cells were suspended in 500 µl ice cold LB and incubated at 37°C for 1 hr 30 min prior to plating. The plating volume and media was transformation specific.

2.2.8 Electroporation of E. coli

To generate the competent *E. coli* cells, a LB culture with the appropriate antibiotics was incubated at 250 rpm, 3.56 g overnight then subcultured under the same conditions for 4 hrs. From here on, all stages occurred on ice. The cells were pelleted by centrifugation, washed twice in 20% glycerol and resuspended in a final volume of 20% glycerol, dependant on the starting volume.

For each electroporation, the desired DNA was introduced into 45 µl competent cells by a BioRad Gene Pulser (200 Ω, 25µ F and 2.5 kV). Immediately after the electroporation, the cells were resuspended in 500 µl ice cold liquid media and incubated for 1 hr 30 min prior to plating. The plating volume and media was transformation specific.

2.2.9 Conjugations into S. coelicolor

The *E. coli* ET12567:pUZ8002 strain containing the construct for conjugation was incubated at 250 rpm, 3.56 g and 37°C overnight in LB with the appropriate antibiotics. From here on, all stages occurred on ice. The *E. coli* cells were pelleted by centrifugation, washed twice in ice-cold LB and resuspended in a final volume of LB, dependant on the number of conjugations.

The *S. coelicolor* material was suspended in 500 µl ice-cold LB. For the sporulating strains, 5 µl spores were heat shocked at 50°C for 10 min then cooled. For the non-sporulating strains a ~15 mm x 15 mm patch was scraped and mechanically broken up. The *E. coli* and *S. coelicolor* material was mixed by gentle tapping then centrifuged at 13300 rpm, 16300 g for 5 min. The pellet was re-suspended in dH₂O and ~90 µl was confluentlly plated thrice onto SFM, excluding 20 mm around the edge of the plates. After 20 hrs of incubation at 30°C the plates were covered by a 500 µl overlay containing sufficient nalidixic acid and any additional appropriate antibiotics to cover a 35 ml plate at the concentrations stated in Table 2.7.

2.2.10 Replicating of the S. coelicolor exconjugants

To replicate the conjugation plates, first each plate was inverted and pressed onto a sterile velvet, covering a wooden block. Then in the same orientation LB+nal+apra and LB+nal+kana plates were in turn pressed into the same velvet. The three plates were incubated until the transferred spores have grown into discernible colonies for the identification of single and double crossovers based on kanamycin resistance. Finally the desired colonies were streaked, as a serial dilution, onto SFM plates containing at least nalidixic acid.

2.2.11 Glycerol stocks of Streptomyces

All stocks were stored at -20°C. The stocks of the sporulating strains were derived from the confluent growth of single colonies on the appropriate SFM plates. The plates were incubated until the production of the grey sporulating pigment. Then the spores were liberated from the colony surfaces by submerging the colonies in 10 ml dH₂O and gently rubbing. Next the spores were collected, pelleted by centrifugation and re-suspended in ~1 ml 20% glycerol.

The stocks of the non-sporulating strains were grown on top of a sterile cellophane and incubated until confluent. Once confluent the hyphae were removed and suspended in ~1 ml storage media (20% glycerol, 1% soya flour).

2.2.12 Macroscopic characterisation of S. coelicolor strains

Plate images were taken with a handheld Canon camera. Colony images were taken using a Zeiss Axiovert Stemi SV 11 microscope, a Jenoptik ProgRes C5 camera (Germany) and version 2.7.6 of the ProgRes software.

2.2.13 Microscopy

Epi-fluorescent microscopy used a Carl Zeiss Axio Scope.A1 microscope, an Axio Cam MRC camera and an X-cite series 120q Wide-Field Fluorescence Microscope Excitation Light Source. Images were analysed using Fiji (2012).

For visualisation of individual hyphae, strains were grown alongside sterile coverslips. The 22 mm x 22 mm sterile coverslips were inserted into 45 ml SFM plates with the appropriate antibiotics at an ~75° angle. The coverslips were inserted into the middle of 30 mm x 10 mm confluent patches, containing 4x10⁷ spores or comparable material. At the stated timepoint, the plates were dried for 20

min and the coverslips were pulled from the plates. The coverslips were either visualised live or fixed and stained. Fixed and stained coverslips were incubated with 400 μ l ice-cold methanol for 1 min, air dried, then incubated with 30 μ l of the stated dye along the growth line for 15 min, under dark conditions. The concentration of the dyes were 50 mg/ml for Wheat Germ Agglutinin Alexa Fluor™ 488 conjugate (WGA-Alexa488 conjugate), 10 mg/ml for propidium iodide (PI) and 25 mg/ml for Wheat Germ Agglutinin Alexa Fluor™ 647 conjugate (WGA-Alexa647 conjugate). Next the coverslips were washed with 300 μ l sterile filtered 1x PBS three times and mounted. All coverslips were mounted by placing the coverslip face down on a slide, in 9 μ l 20% glycerol, and sealing with nail varnish.

For visualisation of individual colonies, strains grown on a sterile cellophanes. Either 2×10^3 spores or comparable material was confluent streaked on cellophanes covering 35 ml SFM plates with the appropriate antibiotics. At the stated timepoints a 15 mm x 15 mm cellophane square was cut and mounted. Cellophane squares were mounted in 9 μ l 20% glycerol between a slide and sterile 22 mm x 22 mm coverslip and sealed with nail varnish.

2.2.14 Protein expression levels

Strains containing an Egfp fusion were grown on sterile cellophanes. Either 3.2×10^7 spores or comparable material was confluent streaked on cellophanes covering 35 ml SFM plates with the appropriate antibiotics. At the stated timepoints the *Streptomyces* material and cellophanes were separated. The cellophanes were discarded. The *Streptomyces* material was combined with 50 μ l ~ 0.1 mm silica beads and 50 mM Tris pH7.6, 2.5 mM $MgCl_2$ buffer then subject to 4 x 30 sec at 7.5 m/s with 300 sec intervals in a BP biomedical FastPrep-24™ RG. Next the samples were centrifuged at 2000 rpm, 300 g for 10 sec, RT and the top layer was centrifuged again at 13300 rpm, 16300 g for 20 min, RT. The final supernatant and pellet were separated and the supernatant was subject to a Bradford assay. For analysis on an 8% native PAGE gel (4.8 ml dH_2O , 2.7 ml 30% acrylamide, 2.5 ml 1.5 M Tris pH8.8, 60 μ l 25% APS, 6 μ l TEMED) 38 mg of total protein for each sample was loaded with a 4% loading dye (200 mM Tris pH 6.8, 40% glycerol, 4% β mercaptoethanol, 4 mg/ml bromophenol blue). Gels were run in a Severn Biotech Ltd Tris Glycine buffer (2.5 mM Tris, 1.92 mM glycine, pH 8.3) at 100 v for 2 hrs 30 min. Then gels were not stained but the excitation of the Egfp in the samples was visualised at 489 nm using a Typhoon Fla 9500 biomolecular imager with a LPB filter.

2.2.15 Actinorhodin measurements

Either 3.2×10^7 spores or comparable material was confluent streaked onto 30 ml R5 agar medium containing the appropriate antibiotics and covered by a sterile cellophane (Moore *et al.*, 2012). Plates were incubated at 30°C for 120 hrs. After 120 hrs of growth the *Streptomyces* material and cellophane were removed from the medium. The *Streptomyces* material was centrifuged at 4000 rpm, 1878 g for 10 min then incubated at 50°C for 72 hrs to determine the dry weight. The cellophanes were discarded. Next the medium was incubated at -20°C for 24 hrs before 30 ml dH₂O was added and the medium was crushed using a 10 ml universal to a liquid consistency. The liquidised plates were sterile filtered through a cotton bud and a 0.2 µm filter. The final filtered volume was 10 ml. Finally 2 ml 6 M KOH was added and the absorbance at OD₆₄₀ was measured using a Jenway 7205 UV/Visible spectrophotometer. The final adjusted measurements were generated by multiplying the absorbance by 2 then dividing the absorbance*2 by the dry weight of the corresponding sample.

2.2.16 Bacterial two-hybrid quantification

For each of the combinations tested in the bacterial two-hybrid, three co-transformants were streaked into LB Δglucose+amp+kana+IPTG+*xgal* plates. Plates were incubated in the dark for 24 hrs, then the blue/white screening was visually interpreted and quantified using Fiji (2012). For quantification, camera images were converted to 16-bit, inverted and three 35 x 35 pixel areas were randomly selected within each streak. Next the image look-up table was changed to the 'fire' RGB values and using the negative controls the background was subtracted. Finally the median signal intensity was measured in each 35 x 35 pixel area and compared to the visual interpretation. The colours of the streaks were classified into three categories: strong positives (actual values: >8000, 1 on Figure 4.4 to Figure 4.5 and Figure 4.7 to Figure 4.8), weak positives (actual values: 1501 to 7999, 0.5 on Figure 4.4 to Figure 4.5 and Figure 4.7 to Figure 4.8) and negative (actual values: <1500, 0.01 on Figure 4.4 to Figure 4.5 and Figure 4.7 to Figure 4.8).

2.2.17 Statistical methods and replicate numbers

Statistical analysis was undertaken using IBM SPSS Statistics 25. To compare colony sizes of the wild-type M145, Δ*sepF*/pMS82-SepF and Δ*sepF* strains first

each dataset was visualised as a histogram then subject to a Kolmogorov-Smirnov test and Shapiro-Wilk test to test for normal distribution (Appendix 1). A Shapiro-Wilk test was used as all three datasets have less than 50 replicates (M145 N=30, $\Delta sepF/pMS82-SepF$ N=45, $\Delta sepF = 45$). Next a Levene's test was done to confirm the homogeneity of variance due to the differences in the sample sizes (Appendix 1). For all tests the null hypothesis was accepted using $p=0.05$ so the assumptions of a parametric test were met. To compare the means from the independent sets of colony size measurements, two independent sample t tests were completed: one to compare the wild-type M145 and $\Delta sepF$ data sets (M145sepf) then one to compare the wild-type M145 and $\Delta sepF/pMS82-SepF$ data sets (M145com). Interpretation of the results is detailed in Section 2.3.2.1 and Section 3.2.5.1.

3.0 Characterisation and complementation of *S. coelicolor* Δ sepF

3.1 Introduction

During the *S. coelicolor* lifecycle two distinct types of septa are formed: vegetative cross-walls and sporulation septa (Figure 1.2). Vegetative cross-walls enable the formation of connected compartments in the syncytial network of the vegetative hyphae and are not associated with cell-cell separation (Jakimowicz and van Wezel, 2012). The sporulation septa are positioned synchronously in the aerial hyphae and lead to the production of unigenomic spores. The differences between these two septa are not fully understood, but both septa require the polymerisation of the tubulin structural homologue FtsZ into the Z-ring as part of the early divisome.

Homologues of FtsZ are widespread among bacteria and some archaea (Osawa and Erickson, 2011; Vaughan *et al.*, 2004). In the Gram-negative *E. coli*, the FtsZ subunits polymerise in a head-to-tail and GTP-dependent manner to form the Z-ring (Dyer, 2009; Guan *et al.*, 2018; Yang *et al.*, 2017b; Chapter 6). In the absence of an FtsZ membrane binding domain, the Z-ring is attached to the cell membrane by either of the positive regulators, FtsA and ZipA (Hale and de Boer, 1997; Pichoff and Lutkenhaus, 2005). Then the Z-ring recruits additional proteins to the divisome. Over 36 proteins are known components of the divisome in *E. coli* (Du and Lutkenhaus, 2017). The divisome proteins are recruited in a linear, hierarchical manner with the last essential component FtsN, triggering cell constriction.

Part of the sporulation-specific divisome in *S. coelicolor* is the positive FtsZ regulator, SsgB (Noens *et al.*, 2007; Willemse *et al.*, 2011). During the very early stages of the divisome, SsgB briefly co-localises with SsgA at alternative sides of the hyphae (Willemse *et al.*, 2011). The SsgB foci are present independently of and prior to FtsZ. Then FtsZ interacts with SsgB, allowing the tethering of FtsZ to the membrane and the formation of FtsZ spiral like structures prior to Z-ring formation (Grantcharova, Lustig and Flårdh, 2005; Willemse and van Wezel, 2009; Willemse *et al.*, 2011). Colonies of the *ssgB* knock-out strain do not undergo sporulation but do produce higher levels of actinorhodin and are significantly larger than the colonies of the wild-type M145 strain (Keijser *et al.*, 2003).

The divisome of the Gram-positive *B. subtilis* contains the positive FtsZ regulator, SepF. Knocking out *sepF* in *B. subtilis* is viable, with knock-out cells exhibiting an increase in cell length and irregular thick cell septa (Hamoen *et al.*,

2006; Ishikawa *et al.*, 2006). Localisation of SepF to the early divisome site is dependent upon FtsZ (Hamoen *et al.*, 2006; Ishikawa *et al.*, 2006). The interaction between SepF and FtsZ occurs via both C-termini and promotes FtsZ polymerisation (Duman *et al.*, 2013; Singh *et al.*, 2008). The N-terminus of SepF has a putative amphipathic helix potentially for the binding of FtsZ to the membrane (Duman *et al.*, 2013). The functional SepF dimer polymerises via an α -helix into ~50 nm ring-like structures, *in vitro*, with an unusual concave curvature (Duman *et al.*, 2013; Gündoğdu *et al.*, 2011). The unusual curvature of the ring-like structure prompted the proposed *in vivo* model, where the SepF rings are positioned perpendicular to the FtsZ protofilaments (Duman *et al.*, 2013; Figure 1.5).

There are three homologues of SepF in *S. coelicolor* (Kaur, 2018; Tan, 2018). Of the three homologues, SCO2079, positioned in the conserved DCW gene cluster, is considered the primary SepF. Previously a $\Delta sepF$ mutant, lacking the first 159 amino acids, was shown to have a severe developmental phenotype, lacking both vegetative cross-walls and sporulation septa (Tan, 2018). The wild-type phenotype was restored by the introduction of a *sepF* fragment, *in trans*, into the $\Delta sepF$ mutant. However, in previous attempts the complementing fragment included a large upstream region, also containing SCO2080, encoding a putative alanine racemase.

The current study aimed to further characterise the $\Delta sepF$ mutant and to complement the $\Delta sepF$ mutant with the smallest DNA fragment carrying only the *sepF* gene. This aim was broken down into several objectives:

- To quantify the colony size of the $\Delta sepF$ and wild-type M145 strains.
- To characterise the formation of vegetative cross-walls and sporulation septa in the hyphae of the $\Delta sepF$ mutant, using epi-fluorescence microscopy.
- To complement the $\Delta sepF$ mutant, with a minimal *sepF* fragment, using blunt end cloning. The minimal SepF fragment contains the two promoters, identified by Jeong *et al.*, (2016).

3.2 Results

3.2.1 Comparing the *SepF* homologues in *S. coelicolor*

The three homologues of *SepF* in *S. coelicolor*, SCO1749 (*SepF1*), SCO2079 (*SepF*), and SCO5967 (*SepF3*) have a high percentage similarity to the *SepF* of *B. subtilis*: *SepF1* has 18.52 percentage identity and 83.33 percentage similarity, *SepF* has 17.84 percentage identity and 70.89 percentage similarity and *SepF3* has 15.57 percentage identity and 71.86 percentage similarity (Stothard, 2000). The genes encoding the three homologues are distributed throughout the chromosome (Figure 3.1). In the core region, which is expected to contain key genes, is *sepF1* and *sepF*, while in the right flanking arm region expected to exhibit greater gene variation, is *sepF3*. More specifically, *sepF1* is positioned next to, in a reverse orientation to SCO1748, a putative transcription regulator, and SCO1750, a putative acyl-CoA dehydrogenase. The *sepF* gene is positioned in the well conserved DCW gene cluster, which contains *divIVA*, essential for polar growth, and *ftsZ* (Figure 1.12). Lastly, *sepF3* is positioned between SCO5966, a putative oxidase, and SCO5968, a putative *bldA*-regulated nucleotide binding protein. Based on the percentage similarity of the *SepF* homologues to the *SepF* of *B. subtilis* and the position of the *SepF* homologues on the chromosome of *S. coelicolor*, the role of *SepF* in cell division was investigated (Kaur 2018).

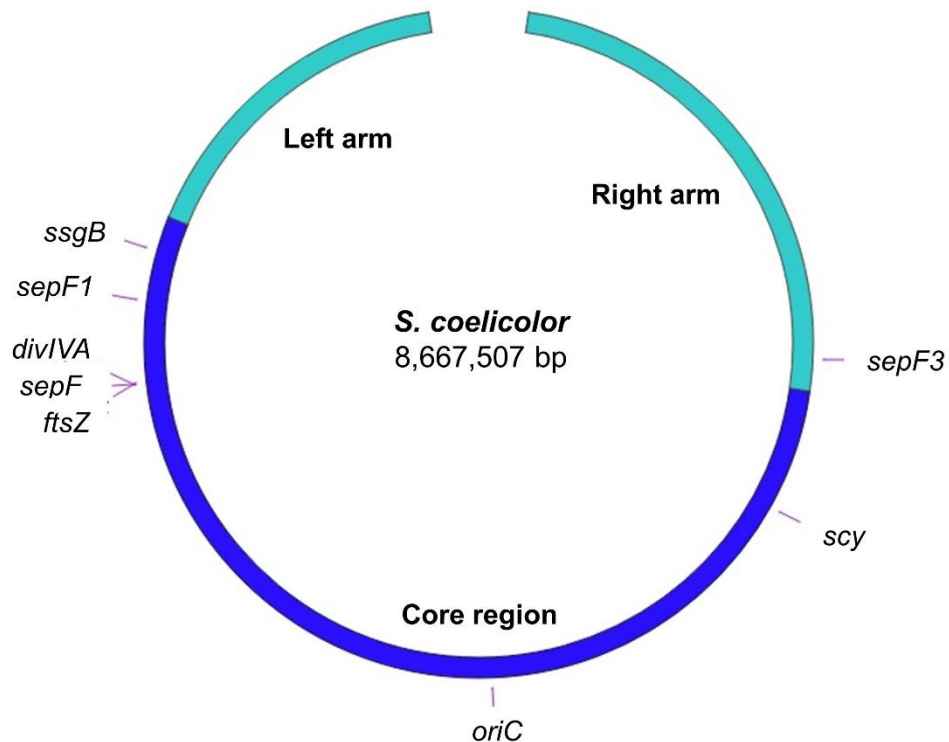


Figure 3.1 The position of the three *sepF* genes within the chromosome of *S. coelicolor*. The position of key developmental genes and *oriC* are also shown (Bentley *et al.*, 2002; SnapGene® 2020).

Next the sequence and domain organisation of the three homologues was compared against the SepF of *B. subtilis*, *M. tuberculosis* and *M. smegmatis* (Figure 3.2). There are three known SepF domains: the N-terminal domain, the central region, and the C-terminal domain. In *B. subtilis* the N-terminal domain is a small amphipathic helix, spanning 10 amino acids, which is implicated in the binding of SepF to the lipid membrane (Duman *et al.*, 2013). Out of the SepF homologues from *S. coelicolor*, the N-terminal domain was detected in both SepF1 and SepF but was missing in SepF3. The central region is the least well conserved, does not have a described function and varies substantially in length. The C-terminal domain governs the FtsZ interactions leading to septa formation in both *B. subtilis* and *M. tuberculosis* (Duman *et al.*, 2013; Gupta *et al.*, 2015). In all the SepF homologues investigated the C-terminus domain was highly conserved, including at residues implicated in the interaction with FtsZ. Therefore the SepFs of *S. coelicolor* are likely to interact with FtsZ and have roles in cell division.

The gene organisation of the DCW cluster from *S. coelicolor* is well conserved amongst the Actinobacteria phylum (Figure 3.3). With the exception of the filamentous *Streptomyces*, all the other representatives of the phylum are rod-shaped. Selected rod-shaped Actinobacteria include *M. tuberculosis*, *Cutibacterium acnes*, the causative agent of acne, the non-pathogenic *Corynebacterium glutamicum*, known for the industrial production of amino acids and *Bifidobacterium longum*, part of the gut microbiota especially in infants.

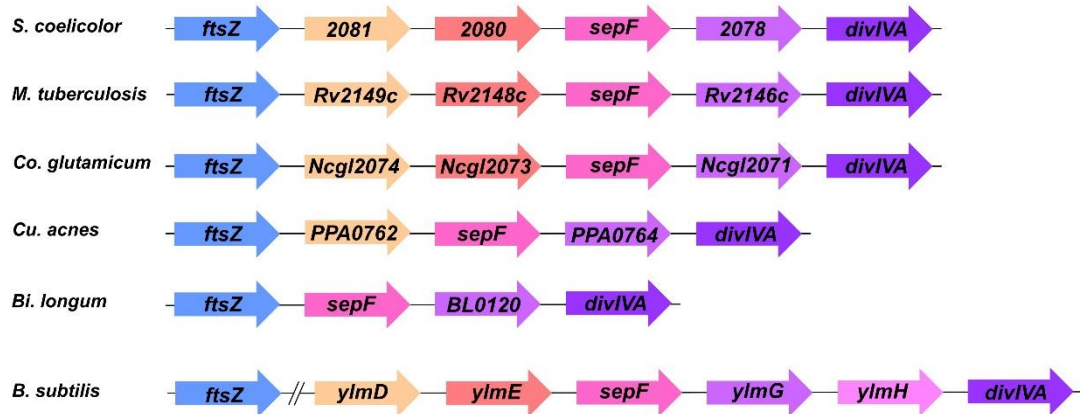


Figure 3.3 The gene organisation of the DCW clusters from Actinobacteria and *B. subtilis*. Sequences are from the Kegg database. The organisms are: *Streptomyces coelicolor* A3(2), *Mycobacterium tuberculosis* H37Rv, *Corynebacterium glutamicum* ATCC 13032 (Kyowa Hakko), *Cutibacterium acnes* KPA171202 formally *Propionibacterium acnes* KPA171202, *Bifidobacterium longum* NCC2705 and *Bacillus subtilis* subsp. *subtilis* 168. Modified from (Tan, 2018).

The genes, *ftsZ* and *sepF*, are separated by two genes *SCO2080* and *SCO2081*, encoding a putative alanine racemase and a putative copper-binding protein in *S. coelicolor* (Figure 3.3). Even in *B. subtilis*, which belongs to the Firmicutes, the homologues of *SCO2080* and *SCO2081*, *YlmE* and *YlmE*, are encoded by genes positioned just upstream of *sepF*, although *ftsZ* is located further upstream. But the absence of the putative alanine racemase and/or the putative copper-binding protein from *Cu. acnes* and *Bi. longum* suggests the alanine racemase and copper-binding protein are unlikely to be essential for the function of the neighbouring proteins.

3.2.2 Generating a *S. coelicolor* *sepF* knock-out using Redirect[®] PCR-directed mutagenesis

The primary *sepF* of *S. coelicolor* was knocked-out using a modified Redirect[®] PCR-directed mutagenesis approach (Gust *et al.*, 2002; Tan, 2018). The first 159 amino acids out of the 213 amino acids for SepF were knocked out to prevent the downstream effects of deleting the putative SCO2078 transcription start site and promoter (Jeong *et al.*, 2016). The $\Delta sepF$ mutant was generated by Tan (2018) but the generation will be briefly discussed below, as the $\Delta sepF$ mutant is key to the current study.

Briefly, the Redirect[®] PCR-directed mutagenesis approach uses PCR to direct homologous recombination of an antibiotic resistant cassette to the desired knock-out site (Figure 3.4).

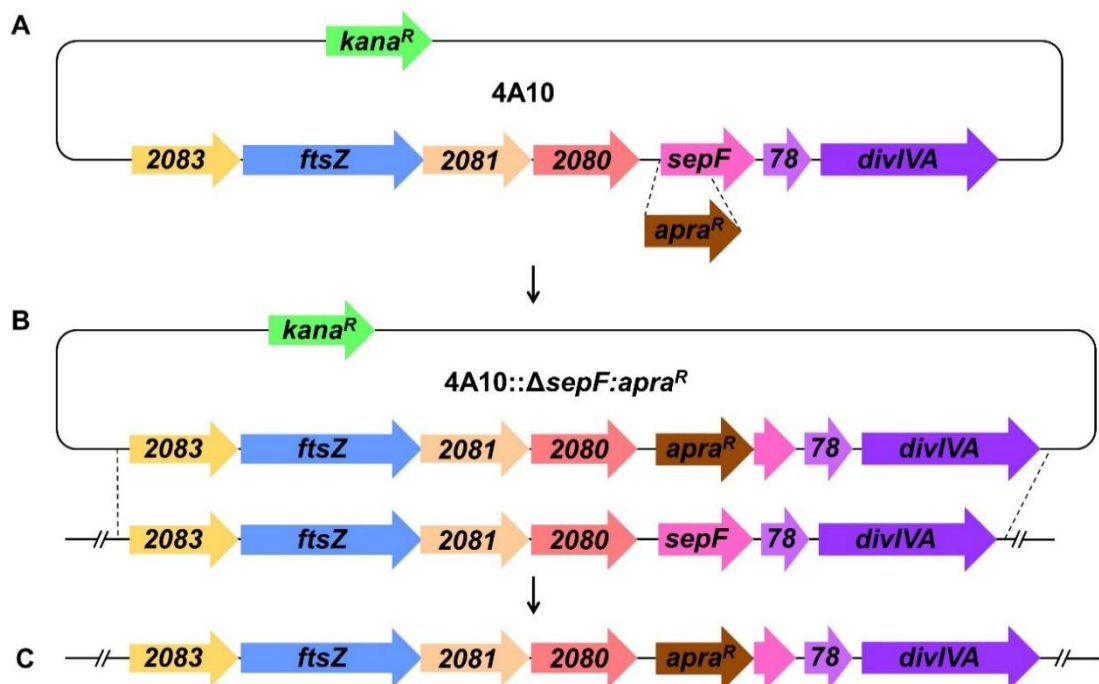


Figure 3.4 Generation of the $\Delta sepF$ mutant using the Redirect[®] PCR-directed mutagenesis approach. A) An extended *apra^R* cassette was introduced, by PCR directed homologous recombination, into 4A10 to generate the 4A10:: $\Delta sepF$:*apra^R* knock-out cosmid. B) The 4A10:: $\Delta sepF$:*apra^R* cosmid was conjugated into wild-type, M145. C) The predicted chromosomal organisation of the $\Delta sepF$ double crossover mutant.

For the $\Delta sepF$ double cross-over mutant, an *apra^R* cassette derived from pIJ774, was extended to contain 40 bp flanking regions, homologous to the flanking regions of the DNA encoding the first 159 amino acids of SepF. Next the extended *apra^R* cassette underwent homologous recombination with 4A10, a cosmid

containing the DCW gene cluster, to generate the 4A10:: $\Delta sepF$: $apra^R$ knock-out cosmid (Figure 3.4A). Then the 4A10:: $\Delta sepF$: $apra^R$ cosmid was electroporated into the methylation-deficient *E. coli* ET12567:pUZ8002 to allow conjugation of 4A10:: $\Delta sepF$: $apra^R$ into *S. coelicolor* wild-type, M145 (Figure 3.4B). Finally the desired $\Delta sepF apra^R$ double crossovers were screened for based on $apra^R$ and $kana^S$ (Figure 3.4C).

3.2.3 Characterising the $\Delta sepF$ mutant of *S. coelicolor*

3.2.3.1 Macroscopic characterisation of the $\Delta sepF$ mutant

Further characterisation of the $\Delta sepF$ mutant, by the current study, confirmed the colonies of $\Delta sepF$ had a distinct phenotype from the colonies of the wild-type strain (Figure 3.5). Colonies of the $\Delta sepF$ mutant were slow to develop and did not produce the grey sporulation pigment, characteristic of the wild-type strain. In the absence of the grey sporulation pigment the white fluffy colonies of the $\Delta sepF$ mutant developed blue pigmentation, which is expected to be actinorhodin, one of the polyketide antibiotics produced by *S. coelicolor*.

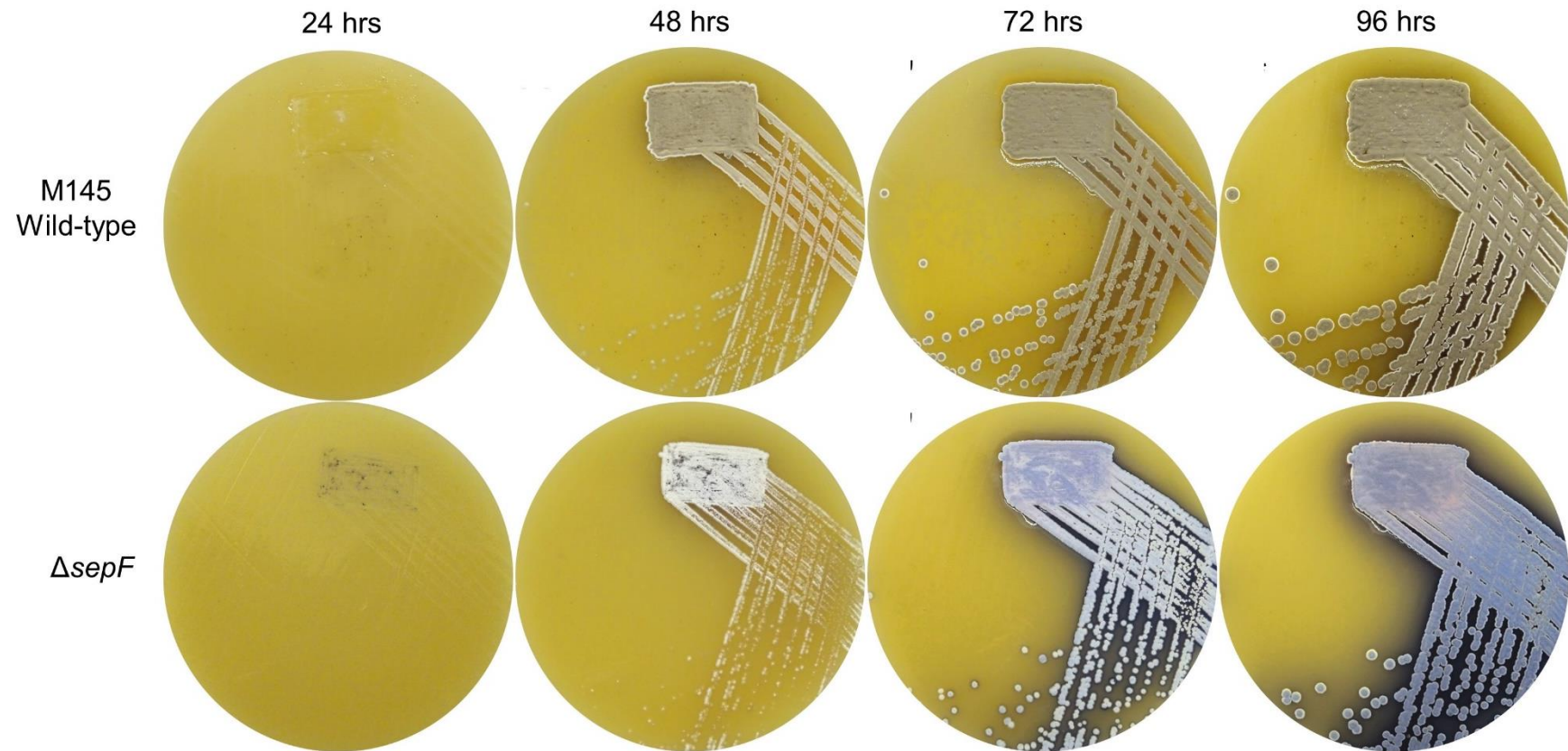


Figure 3.5 Comparison of colony development for wild-type M145 and $\Delta sepF$ between 24 and 96 hrs. The wild-type M145 and $\Delta sepF$ strains were streaked onto SFM medium. Images were taken every 24 hours and processed using Fiji (2012).

Next the size of colonies from the wild-type and $\Delta sepF$ strains were compared by measuring the diameter of the colonies. As colony diameter can be altered by quorum sensing in a density dependent manner, similar colony densities of both strains were streaked onto SFM medium (Figure 3.6A). The streak plates were incubated at 30°C for 96 hrs. At 96 hrs, the diameter of ~45 colonies from both strains was measured using Fiji (2012). The colonies of the wild-type strain with a mean diameter of 3.48 mm \pm 0.05 SE were significantly larger than the colonies of $\Delta sepF$ with a mean diameter of 2.83 mm \pm 0.04 SE ($t=10.407$, $df=73$. $p<0.05$; Appendix 1; Figure 3.6B). Hence knocking-out of *sepF* resulted in a significant reduction in colony size.

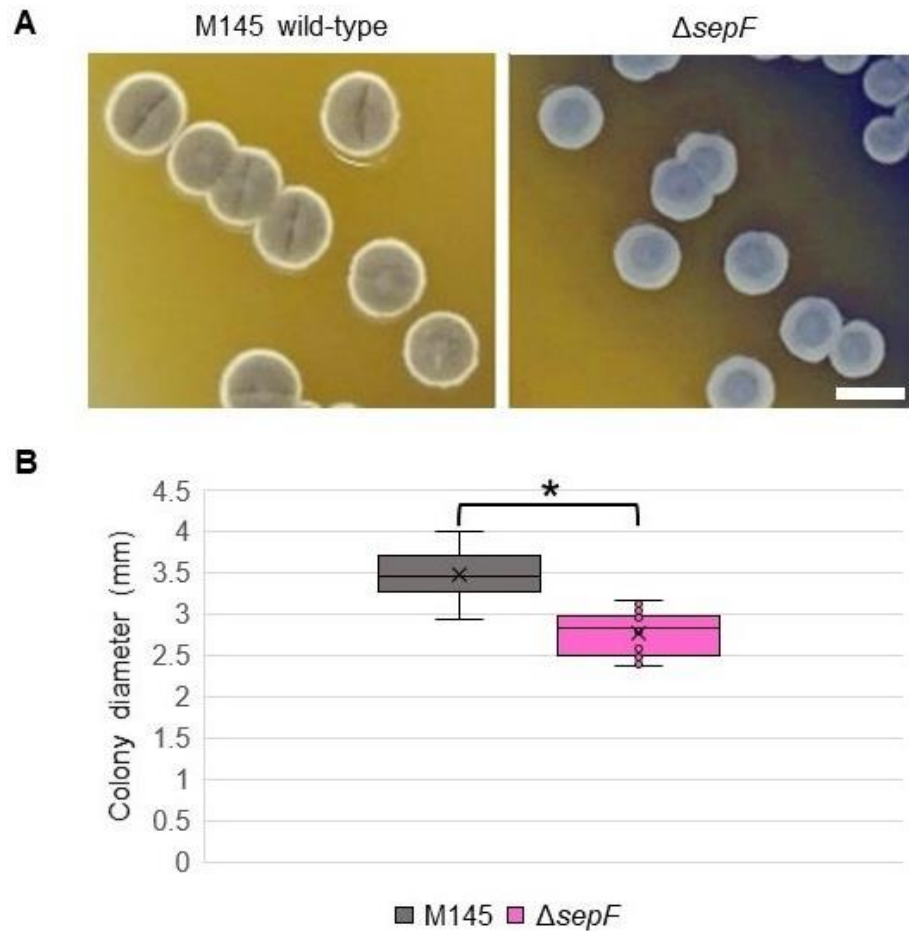


Figure 3.6 Comparison of colonies from wild-type M145 and $\Delta sepF$. The strains, M145 and $\Delta sepF$ were streaked onto SFM to generate single colonies with similar colony densities A) The plates were incubated at 30°C for 96 hrs then close up camera images were taken. The scale bar represents 3 mm. B) The diameter of ~45 colonies for wild-type (grey) and $\Delta sepF$ (pink) were measured using Fiji (2012). The boxes' upper limit denotes the third quartile and the lower limit denotes the first quartile. Inside the boxes, the cross shows the mean and the line shows the median. For wild-type the mean is 3.54 mm \pm 0.05 SE and the median is 3.49 mm. For $\Delta sepF$ the mean is 2.83 mm \pm 0.04 SE and the median is 2.87 mm. The whiskers show the extremes of the data sets. Tests for normal distribution and homogeneity of variance stated the assumptions of a parametric test were met so an independent sample *t* test was completed. The star indicates a statistically significant difference ($p < 0.05$) between wild-type M145 and $\Delta sepF$. See the associated text and appendix 1 for details.

3.2.3.2 Microscopic characterisation of the $\Delta sepF$ mutant

Next the hyphae of the $\Delta sepF$ mutant were characterised using epifluorescence microscopy. To allow visualisation of individual hyphae, samples were grown along sterile coverslips. During plating the sterile coverslips were inserted, at a $\sim 75^\circ$ angle, into the centre of a confluent patch. Then at the stated timepoints the coverslip and the attached hyphae was removed from the plate before being fixed and stained with Wheat Germ Agglutinin Alexa Fluor™ 488 conjugate (WGA-Alexa488 conjugate) and propidium iodide (PI) to allow visualisation of the cell walls and DNA organisation, respectively. Timepoints were taken between 19 and 96 hrs to allow visualisation of vegetative and aerial hyphae from the $\Delta sepF$ and wild-type M145 strains (Figure 3.7 and Figure 3.8).

The majority of vegetative hyphae from the $\Delta sepF$ mutant lacked any signs of vegetative cross-wall formation (Figure 3.7). In the absence of vegetative cross-walls, WGA-Alexa488 conjugate staining was only detected along both sides of the hyphae, forming a long tube (Figure 3.7 second panel). A small number of vegetative hyphae ($\sim 10\%$) showed increased WGA-Alexa488 conjugate staining on either one or both sides of the hyphae wall (Figure 3.7 third panel). The increased staining did not extend across the hyphae and often occurred close to a branch site unlike in the vegetative cross-walls of wild-type M145. The lack of cross-walls in the vegetative hyphae of the $\Delta sepF$ mutant is expected to result in a lack of compartmentalisation.

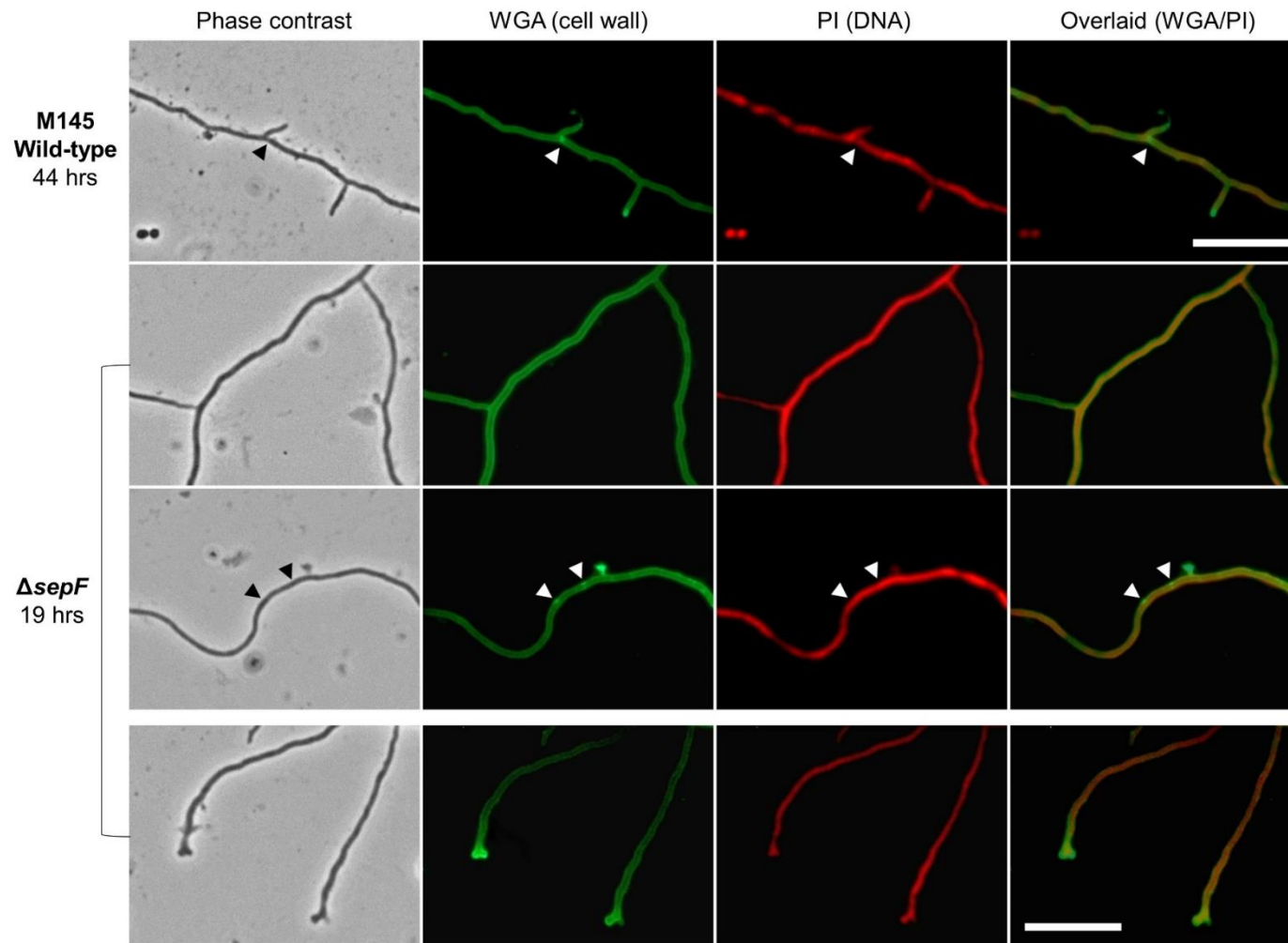


Figure 3.7 Characterisation of tip morphology and vegetative growth from Δ sepF. Both strains, wild-type M145 and Δ sepF, were grown on SFM medium until the timepoints indicated. In addition to the phase contrast image (black/white), strains were fixed and stained with the cell wall stain, WGA-Alexa488 conjugate (green), the DNA stain, PI (red) and the stained images were overlaid (green/red). The arrows indicate the partial cross-wall attempts at the hyphae edge for Δ sepF or complete vegetative cross-walls for wild-type, M145. Images were taken at x100 magnification and 300 ms exposure. The scale bar represents 10 μ m.

The hyphae tips of the $\Delta sepF$ mutant were more prone, at >5% of tips, to an unusual fork-like morphology (Figure 3.7 bottom panel). Compared to the smooth round tips of wild-type M145, the fork-like tips of $\Delta sepF$ were expected to have undergone an additional branching event. Each tip at the fork-like ends were often indistinguishable from one another and similar tips were found in the Δscy mutant, with reduced apical dominance (Holmes *et al.*, 2013). A direct link between the processes of polar growth and septa formation is investigated in Chapter 4.

Similarly to the vegetative hyphae, the aerial hyphae of the $\Delta sepF$ mutant were also unable to produce regular sporulation septa (Figure 3.8). While in the wild-type strain developing sporulation septa can be detected after 48 hours growth on SFM medium, the $\Delta sepF$ mutant failed to show any septation at this time point. After prolonged incubation, after around 68 hours growth, a limited number of aerial hyphae (>15%) produced irregularly spaced often partially formed septa. The irregular sporulation septa were characterised by a tilted or cross shape, potentially representing straight aerial hyphae commencing sporulating at partially formed rings (Figure 3.8 insert). The corresponding spore compartments were previously shown to vary in size between 0.3 and 4.9 μm , compared to the mean spore compartments of 1.2 μm for wild-type M145 (Kaur, 2018). The PI staining in some of the smaller compartments suggests chromosomes were unable to segregate uniformly and patches of high and low chromosome density in the aerial hyphae of the $\Delta sepF$ mutant can be observed. Importantly the irregular septa do not lead to the formation of unigenomic individual spores.

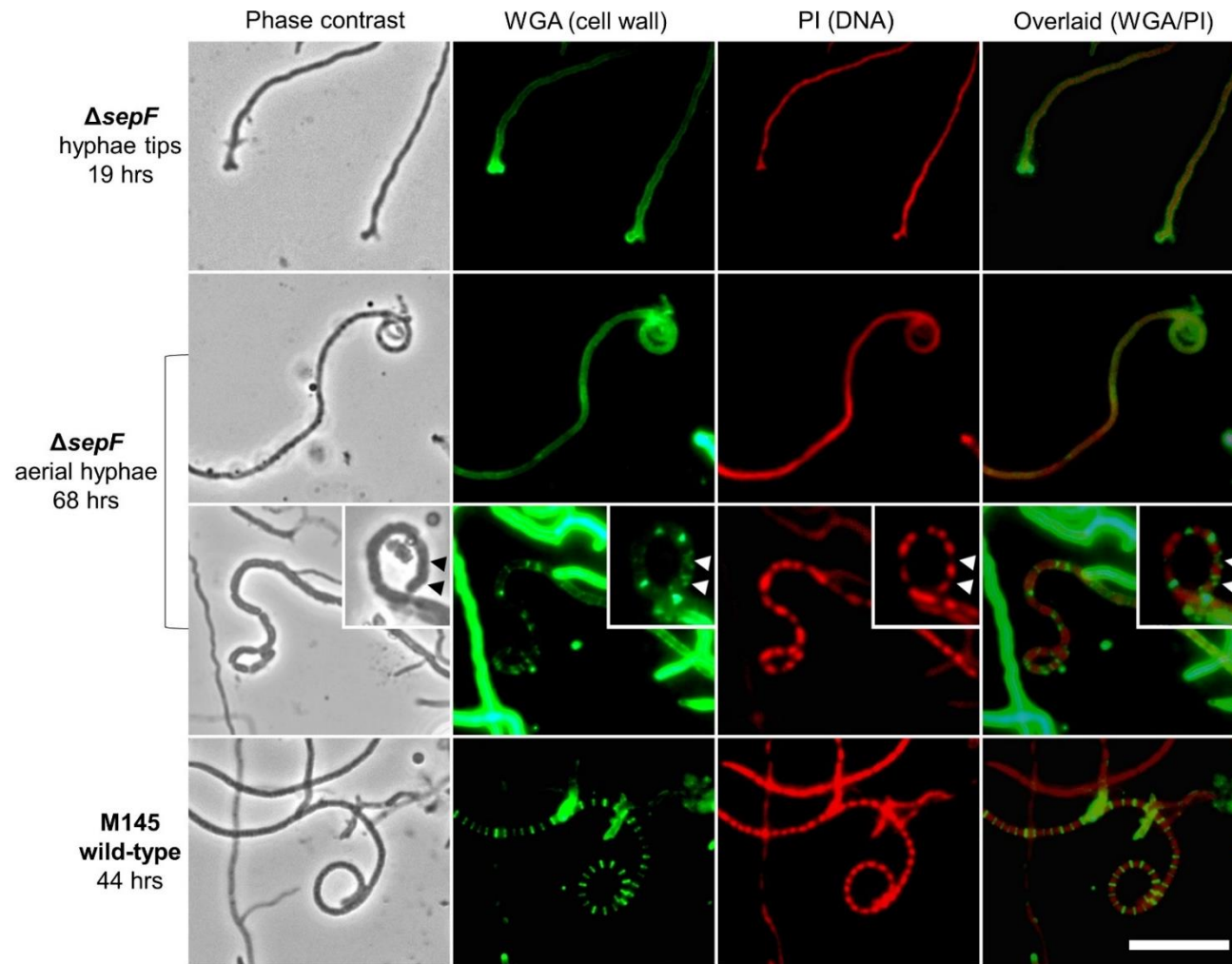


Figure 3.8 Characterisation of aerial growth from *ΔsepF*. Both strains, wild-type M145 and *ΔsepF*, were grown on SFM until the timepoints indicated. In addition to the phase contrast image (black/white), strains were fixed and stained with the cell wall stain, WGA-Alexa488 conjugate (green), the DNA stain, PI (red) and the stained images were overlaid (green/red). The delayed aerial hyphae of *ΔsepF* curled and produce irregular sporulation septa. The white arrows on the insert indicate the cross shaped sporulation septa. Images were taken at x100 magnification and 300 ms exposure. The scale bar represents 10 μm .

In the absence of spores the likely propagating material for the $\Delta sepF$ mutant is small hyphal fragments. The hyphal fragments are predominantly generated mechanically during the plating process and could be associated with the points of increased WGA-Alexa488 conjugate staining. A similar finding was identified in the \DeltaftsZ strain of *S. venezuelae* (Santos-Beneit *et al.*, 2017). After an induced lysis event, the hyphae fragments of the \DeltaftsZ mutant, bound by a tip and branch site were capable of re-growing and forming mature *Streptomyces* colonies. To confirm the phenotype of the $\Delta sepF$ mutant was due to the absence of *sepF* and not downstream polar effects or additional mutations, next the $\Delta sepF$ mutant was complemented.

3.2.4 Complementing $\Delta sepF$ using blunt end cloning

Complementation of the $\Delta sepF$ mutant posed an interesting challenge as the promoters of the DCW cluster are not well characterised. Previously complementation was attempted, prior to the publication of large-scale RNA seq data for identifying the transcription start points in *S. coelicolor* (Jeong *et al.*, 2016). Therefore, the designs of the complementing fragments lacked knowledge on the transcription start sites of *sepF*. Here the previous complementation attempts are summarised, but the data from Jeong *et al.*, (2016) on the positions of the two transcription start sites for *sepF* is included.

The first complementing fragment, ΔP -SepF, included 128 bp upstream of the translational start and contained one of the *sepF* promoters (Figure 3.9A; Tan, 2018). The resulting $\Delta sepF/pMS82-\Delta P$ -SepF strain produced the grey sporulation pigment. But microscopic observations confirmed the aerial hyphae of $\Delta sepF/pMS82-\Delta P$ -SepF did not produce regularly spaced sporulation septa and instead formed very irregular sporulation septation. Hence the introduction of ΔP -SepF with one promoter only resulted in partial complementation of the $\Delta sepF$ mutant.

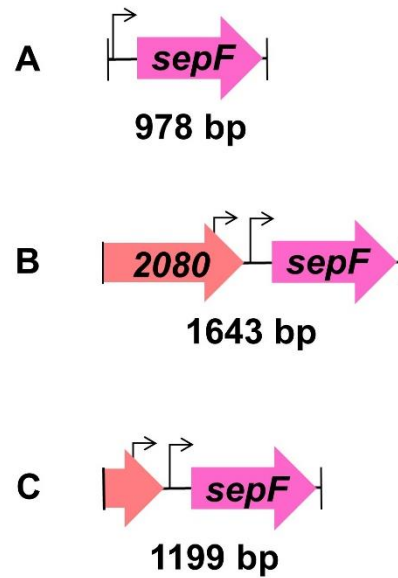


Figure 3.9 The different fragments used to complementation the $\Delta sepF$ mutant. The arrows indicate the putative promoter identified by Jeong *et al.*, 2016. Fragments A and B were introduced into the $\Delta sepF$ mutant by Tan, 2018. Fragment C was introduced into the $\Delta sepF$ mutant in the current chapter. The size of the fragments is positioned below in bold.

The second fragment, 2080-SepF, had a larger 848 bp upstream region containing a promoter-less *SCO2080* and two promoters of *sepF* (Figure 3.9B). The resulting $\Delta sepF/pMS82$ -2080-SepF strain developed the grey sporulation pigment, like the wild-type strain and produced regular sporulation septa with evenly distributed chromosomes. Hence the second fragment successfully completed the $\Delta sepF$ mutant. To exclude the possibility that complementation was affected by an additional copy of *SCO2080* *in trans*, and given the exact location of the promoter sites, the current study attempted to complement $\Delta sepF$ using a fragment which included the two promoters, but did not include an intact *SCO2080* gene (Figure 3.9C).

The integrative pMS82 contains an Φ BT1 integrase (*int*) and an *attP* site as part of a site-specific recombination system (Figure 3.10; Gregory *et al.*, 2003). The site-specific recombination system allows pMS82 to integrate, as a single copy, at the Φ BT1 *attB* site within *SCO4848*. *SCO4848* is a putative integral membrane protein, but disruption of *SCO4848* causes no known phenotype. Integration of pMS82 is maintained under an hygromycin selection due to an *hyg^R* gene on the pMS82 backbone. Hygromycin selection is salt-sensitive so all pMS82 containing strains were grown in the absence of salt.

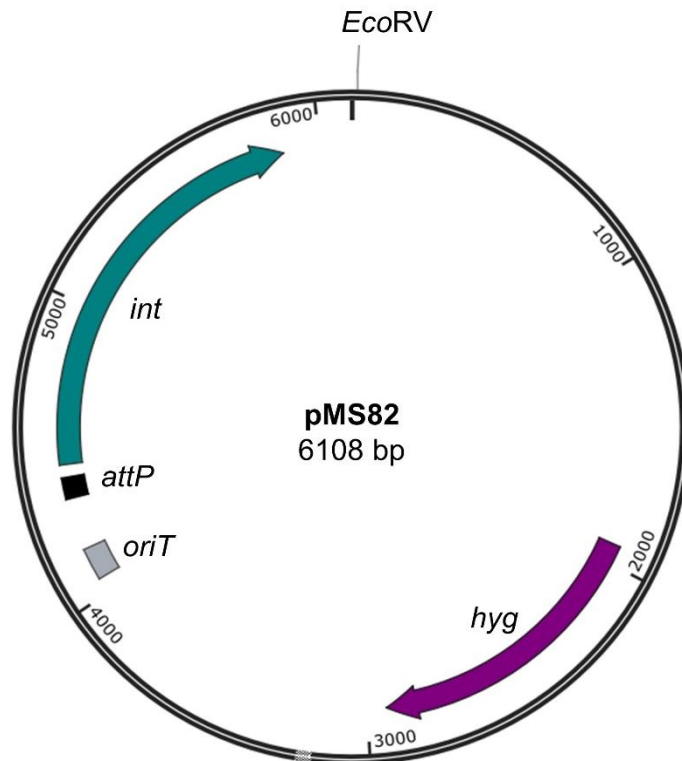


Figure 3.10 The integrative pMS82 plasmid. The pMS82 plasmid integrates at the Φ BT1 *attB* site within *SCO4848*. The plasmid contains an *oriT* (grey), an *attP* site (black), a Φ BT1 integrase (teal), a *hyg^R* gene (purple) and a single *EcoRV* site (top) suitable for blunt end cloning.

To generate the suitable pMS82 vector, initially pMS82 underwent a restriction digest with *EcoRV*. The restriction enzyme, *EcoRV* recognises the palindromic 6-base DNA sequence, 5'-GAT|ATC-3', found once in pMS82 (Figure 3.10). Next the linearised, blunt ended pMS82 was dephosphorylated to prevent re-ligation. The dephosphorylation reaction was incubated at 37°C for 1 hr, then the dephosphorylated, linearised, pMS82-*EcoRV* fragment was analysed on a diagnostic gel (Figure 3.11A). A single band at the expected size of 6108 bp was detected, confirming the dephosphorylated pMS82-*EcoRV* was successfully generated.

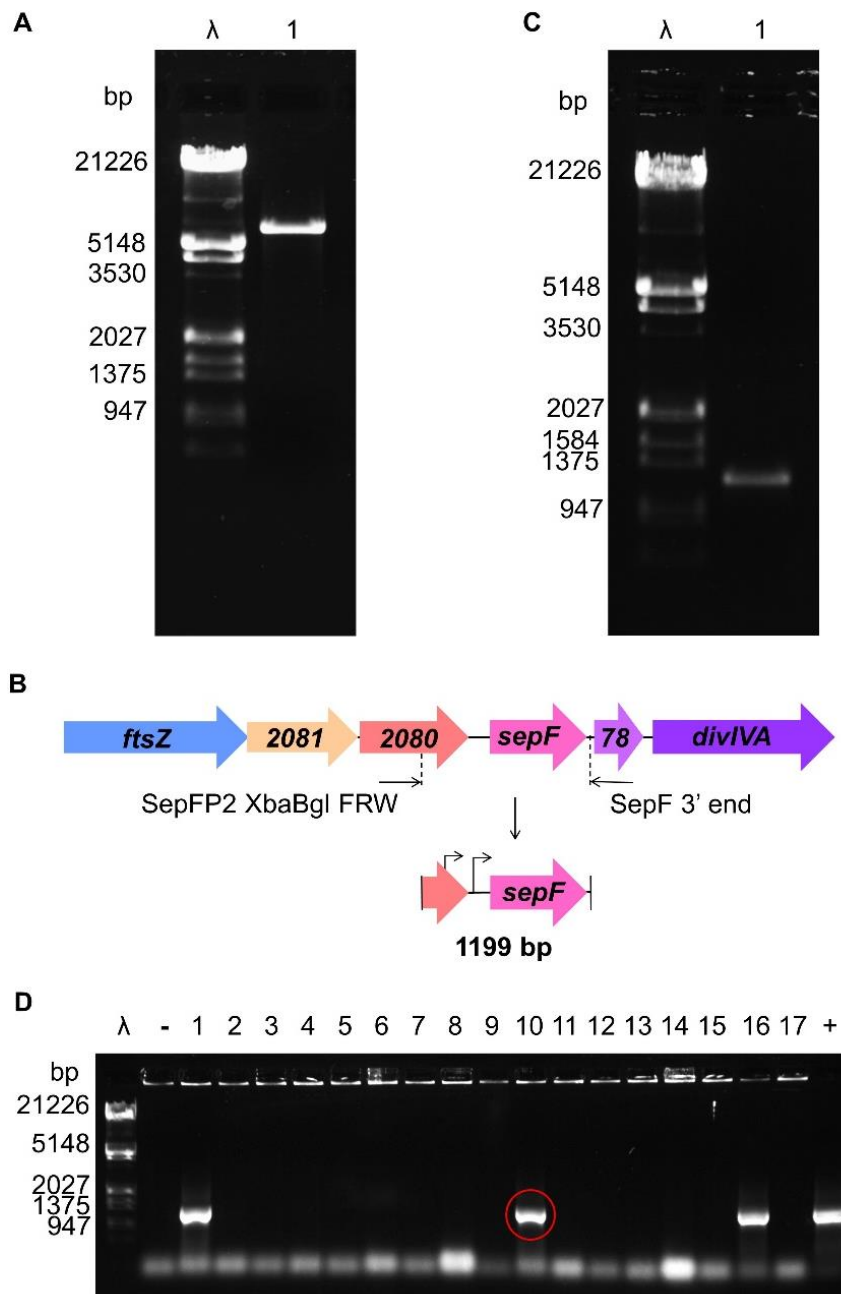


Figure 3.11 Generation of the pMS82-SepF plasmid for complementation. The pMS82 plasmid integrates at the ϕ BT1 *attB* site within *SCO4848* A) pMS82 was digested with *EcoRV*, dephosphorylated, and analysed on a 0.7% agarose gel. Lane λ) λ DNA digested with *EcoRI* and *HindIII*. Lane 1) the dephosphorylated pMS82-*EcoRV* extraction elution. B) The desired 1199 bp SepF fragment, containing the two putative promoters, was amplified using 4A10 as a template and the primers, SepFP2 XbaBgl FRW and SepF 3' end. C) The PCR products were phosphorylated and analysed on a 0.7% agarose gel. Lane λ) λ DNA digested with *EcoRI* and *HindIII*. Lane 1) phosphorylated SepF PCR fragment. The phosphorylated SepF fragment and dephosphorylated pMS82-*EcoRV* were ligated together and transformed into *E. coli* DH5 α . D) A colony PCR, with the same primers as C, was used to analyse the *E. coli* DH5 α transformants. The PCR products were analysed on a 0.7% agarose gel. Lane λ) λ DNA digested with *EcoRI* and *HindIII*, lane -) negative control: PCR using undigested pMS82, lane 1 to 17) potential transformants and lane +) positive control: PCR using 4A10. The colony PCR identified three positive colonies: #1, #10 and #16. Colony #10 was used in future experiments (red circle).

Next the desired 1199 bp *sepF* fragment was PCR amplified using the 4A10 cosmid as a template, the primers, SepFP2 XbaBgl FRW and SepF 3' end and the high-fidelity DNA polymerase, Phusion (Figure 3.11B). Then the 1199 bp PCR product was gel-purified and phosphorylated. Phosphorylation of the PCR product was necessary, as PCR generates non-phosphorylated products and the dephosphorylated pMS82 can only be ligated to a phosphorylated DNA fragment. The phosphorylated SepF fragment was extracted and analysed on an agarose gel (Figure 3.11C). A single band of the expected 1199 bp size, confirmed the phosphorylated *sepF* fragment was successful generated.

After the ligation of the vector and insert fragments together with a control vector only ligation, the mixes were transformed into *E. coli* DH5 α cells, chemically made competent. Under the hygromycin selection pressure transformants were slow to develop, requiring 22 hrs at 37°C before being counted. At 22 hrs the control transformation generated ~10 colonies per 100 μ l. In contrast, the pMS82-SepF transformation generated ~250 colonies per 100 μ l. The increase in the number of transformants suggested the re-ligation of pMS82-*EcoRV* was reduced by dephosphorylation and the likelihood of successful ligations with the desired insert amongst the transformants.

To identify the successful transformants carrying pMS82-SepF, ~20 transformants were streaked onto LB Δ NaCl+hyg and incubated at 37°C for 20 hrs. Streaking the transformants increased the amount of available material and enabled each colony to undergo a two-stage confirmation process, if required. In the first stage, transformants were subject to a low-fidelity colony PCR (Figure 3.11D). The colony PCR aimed to re-amplify the 1199 bp SepF fragment using the DNA released from the transformant as a template and the same primer pairing, used for the generation of the insert. Of the 17 colonies tested three generated a PCR product at the expected 1199 bp size. In the second confirmation stage, these 3 colonies underwent a large-scale plasmid preparation and the resulting plasmids were sequenced with pMS82 specific primers. Sequencing confirmed an unmutated copy of pMS82-SepF in colony #10 (circle in red). Hence only pMS82-SepF #10 was used in further experiments.

To introduce pMS82-SepF into the Δ *sepF* mutant, first pMS82-SepF was passed through the methylation deficient *E. coli* ET12567:pUZ8002 strain. Then the resulting *E. coli* ET12567:pUZ8002/pMS82-SepF strain was used to conjugate pMS82-SepF into Δ *sepF* and circumvent the methylation restriction system of *S. coelicolor*. The conjugation plates were incubated at 30°C for 20 hrs before being

overlaid with nalidixic acid and hygromycin. The overlay aimed to kill any surviving *E. coli* and select for colonies of *S. coelicolor* containing pMS82. The overlaid plates were incubated at 30°C for an additional 7 days. At 7 days, the exconjugants produced the grey sporulation pigment, indicative of sporulation and were highly similar to wild-type. Hence representative exconjugants were streaked onto SFM+nal+hyg medium for single colonies then spore stock generation.

3.2.5 Characterisation of the $\Delta sepF/pMS82$ -SepF strain

3.2.5.1 Macroscopic characterisation of the $\Delta sepF/pMS82$ -SepF strain

To confirm complementation, the $\Delta sepF/pMS82$ -SepF, wild-type M145 and $\Delta sepF$ strains were streaked on SFM medium (Figure 3.12A). The $\Delta sepF/pMS82$ -SepF strain developed very similarity to M145: the grey sporulation pigment developed by 48 hrs and from 72 hrs onwards colonies were smooth and rounded with a white edge (Figure 3.12A).

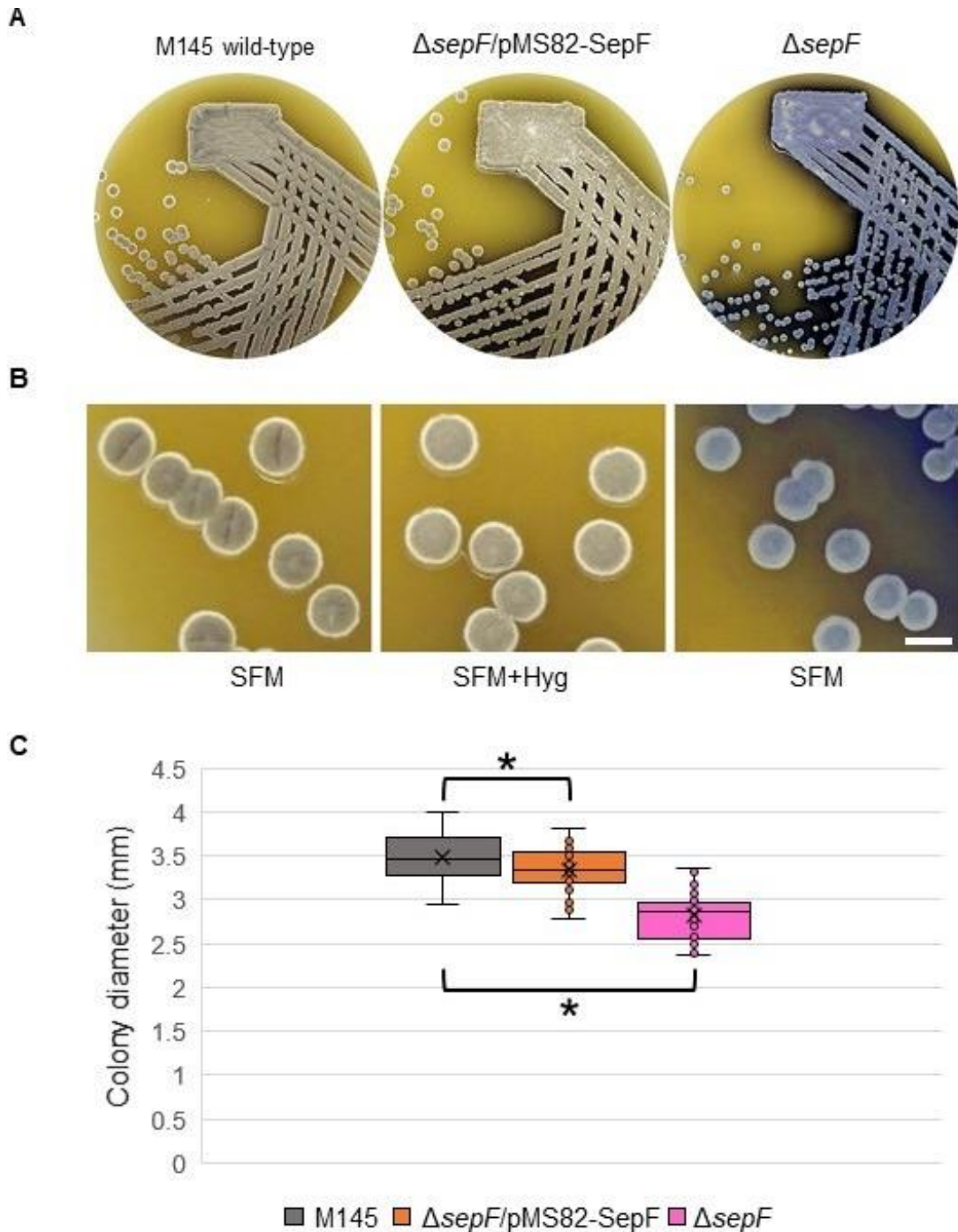


Figure 3.12 Complementation of the $\Delta sepF$ mutant. The three strains, wild-type M145, $\Delta sepF/pMS82-SepF$ and $\Delta sepF$ were streaked onto the indicated media to generate single colonies with similar colony densities A) The plates were incubated at 30°C for 96 hrs B) At 96 hrs close up camera images were taken. The scale bar represents 3 mm. C) The diameter of ~45 colonies for wild-type (grey), $\Delta sepF/pMS82-SepF$ (orange) and $\Delta sepF$ (pink) were measured using Fiji (2012). The boxes' upper limit denotes the third quartile and the lower limit denotes the first quartile. Inside the boxes, the cross shows the mean and the line shows the median. For wild-type the mean is 3.54 mm \pm 0.05 SE and the median is 3.49 mm. For $\Delta sepF/pMS82-SepF$ the mean is 3.33 mm \pm 0.04 SE and the median is 3.34 mm. For $\Delta sepF$ the mean is 2.83 mm \pm 0.04 SE and the median is 2.87 mm. The whiskers show the extremes of the data sets. Tests for normal distribution and homogeneity of variance stated the assumptions of a parametric test were met so two independent sample *t* test were completed. The stars indicate statistically significant differences ($p < 0.05$) between wild-type M145 and both $\Delta sepF$ and $\Delta sepF/pMS82-SepF$. See the associated text and appendix 1 for details.

Next the three strains were streaked at a lower colony density to compare the diameters of the colonies (Figure 3.12B; Section 3.3.3.1). After a 96 hrs incubation period, the complemented colonies of $\Delta sepF/pMS82-SepF$ were measured and subject to an independent t test. With a mean diameter of $3.33 \mu\text{m} \pm 0.04$ SE the complemented colonies were significantly different ($t = 2.447$, $df = 73$, $p < 0.05$) from the colonies of the wild-type (Figure 3.12C). The difference in the diameter of colonies from the $\Delta sepF/pMS82-SepF$ and wild-type strains is likely due to the additional hygromycin selection applied. Next the microscopic characteristics of the $\Delta sepF/pMS82-SepF$ strain were investigated.

3.2.5.2 Microscopic characterisation of the novel $\Delta sepF/pMS82-SepF$ strain

Next the formation of sporulation septa in the aerial hyphae of $\Delta sepF/pMS82-SepF$ was investigated. The aerial hyphae of $\Delta sepF/pMS82-SepF$ were visualised after growth, next to coverslips, for 40 and 44 hrs, using epifluorescence microscopy. Samples were again fixed and stained with WGA-Alexa488 conjugate and PI (Figure 3.13).

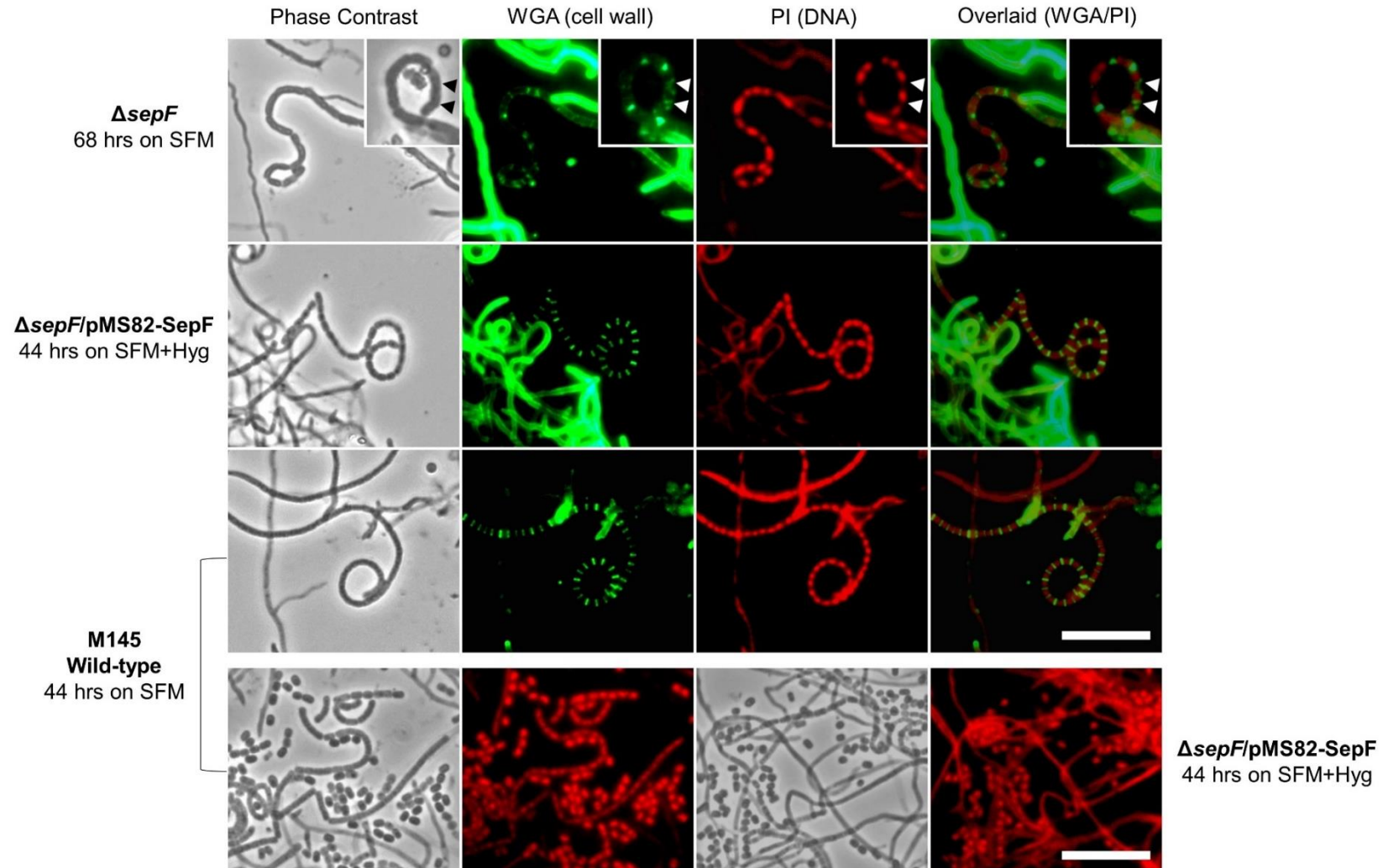


Figure 3.13 Confirmation of complementation using epi-fluorescence microscopy. The three strains, *ΔsepF*; *ΔsepF/pMS82-SepF* and wild-type M145, were grown as stated. In addition to the phase contrast image (black/white), strains were fixed and stained with the cell wall stain, WGA-Alexa488 conjugate (green), the DNA stain, PI (red) and the stained images were overlaid (green/red). The insert shows a close-up of septa produced by *ΔsepF*. The arrows indicate the cross shaped sporulation septa. Images were taken at x100 magnification and 300 ms exposure. The scale bars represent 10 μ m.

The aerial hyphae of $\Delta sepF/pMS82-SepF$ curled and were capable of producing regular sporulation septa (Figure 3.13). Individual sporulation septa spanned across and were positioned perpendicular to the hyphae wall. Together the septa formed long ladder-like structures where each septum represents a 'rung' due to the 2D imaging plane. To compare the ladder structures of wild-type M145 and $\Delta sepF/pMS82-SepF$, the distance between the middle of one rung to the middle of the next rung was measured for using Fiji (2012). The mean compartment size of wild-type, at $1.12 \mu\text{m} \pm 0.01 \text{ SE}$, was highly similar to the mean compartment size of $\Delta sepF/pMS82-SepF$ at $1.10 \mu\text{m} \pm 0.01 \text{ SE}$. The sporulation septa of $\Delta sepF/pMS82-SepF$ lead to the production of individual, rounded spores (Figure 3.13 bottom right panel). The spores of $\Delta sepF/pMS82-SepF$ contained well packaged chromosomes and were indistinguishable from the spores of wild-type. Hence the introduction of pMS82-SepF into the $\Delta sepF$ mutant fully complemented the phenotype of $\Delta sepF$. Full complementation of the $\Delta sepF$ mutant by pMS82-SepF highlights the importance of the second *sepF* promoter and suggests *sepF* is not co-transcribed with other genes in the DCW cluster. But most importantly complementation shows the severe phenotype of $\Delta sepF$ is due to the lack of *sepF* and not downstream polar effects.

3.3 Summary

Bacterial septa formation requires the polymerisation of the tubulin homologue, FtsZ into Z-rings (McCormick *et al.*, 1994; Nogales *et al.*, 1998). In *B. subtilis* the polymerisation of FtsZ is affected by the FtsZ associated proteins, EzrA, FtsA and SepF (Duman *et al.*, 2013). The individual knock-out of SepF in *B. subtilis* leads to viable but slightly longer cells with irregularly thick cell septa (Hamoen *et al.*, 2006; Ishikawa *et al.*, 2006). Including SepF in a double knock-out strain with either EzrA and FtsA is synthetically lethal. In the actinomycetes, *Mycobacterium* and *Streptomyces*, there are no known homologues of FtsA but there are homologues of SepF. Hence SepF is expected to have a key role in cell division of *S. coelicolor*.

Intriguingly *S. coelicolor* has three homologues of SepF (Figure 3.1 to Figure 3.3). Of the three homologues the second encoded by *SCO2079* is positioned in the DCW cluster and is only separated from *ftsZ* by two genes encoding a putative alanine racemase and copper-binding protein. Like the SepF of *B. subtilis*, the SepF of *S. coelicolor* contains a C-terminal domain thought to be involved in the binding and polymerisation of FtsZ plus a N-terminal domain thought to be involved in lipid binding and therefore binding of SepF to the cell membrane (Dunman *et al.*, 2013). *The presence of the N-terminal domain, absent from SepF3, could be key to altering the polymerisation of FtsZ as FtsZ lacks a membrane binding domain and FtsZ has been shown to be position 13 nm underneath the inner membrane at the site of midcell constriction in Caulobacter crescentus* (Hale and de Boer, 1997; McQuillen and Xiao, 2020; Pichoff and Lutkenhaus, 2005). Hence SepF in *S. coelicolor* was expected to have a similar function to the SepF in *B. subtilis*.

Deletion of *sepF* was only previously achieved using CRISPRi (Zhang *et al.*, 2020). The CRISPRi $\Delta sepF$ mutant did not produce vegetative cross-walls and visually overproduced actinorhodin, similar to the $\Delta sepF$ mutant of the current study. The $\Delta sepF$ mutant of the current study, generated by the Redirect[®] PCR-directed mutagenesis approach, revealed further evidence colonies were severely developmentally affected by the absence of SepF: colonies developed slowly, were significantly smaller than wild-type M145 and were covered in a blue pigment, in the absence of the grey sporulation pigment (Figure 3.5 and Figure 3.6). Hyphae of the $\Delta sepF$ mutant did not produce regular vegetative cross-walls or sporulation septa (Figure 3.7, Figure 3.8 and Figure 3.14). With prolonged incubation the aerial hyphae developed partial tilted or cross-shape sporulation septa. In the resulting smaller compartments chromosomal DNA appears to have become trapped

suggesting that the link between chromosome segregation and division is affected. Without prolonged incubation the vegetative hyphae of the $\Delta sepF$ were prone to a fork-like morphology, indicating a slight lack of apical dominance potentially due to altering the integrity of the TIPOC (Figure 3.14). This observation is investigated further in Chapter 4.

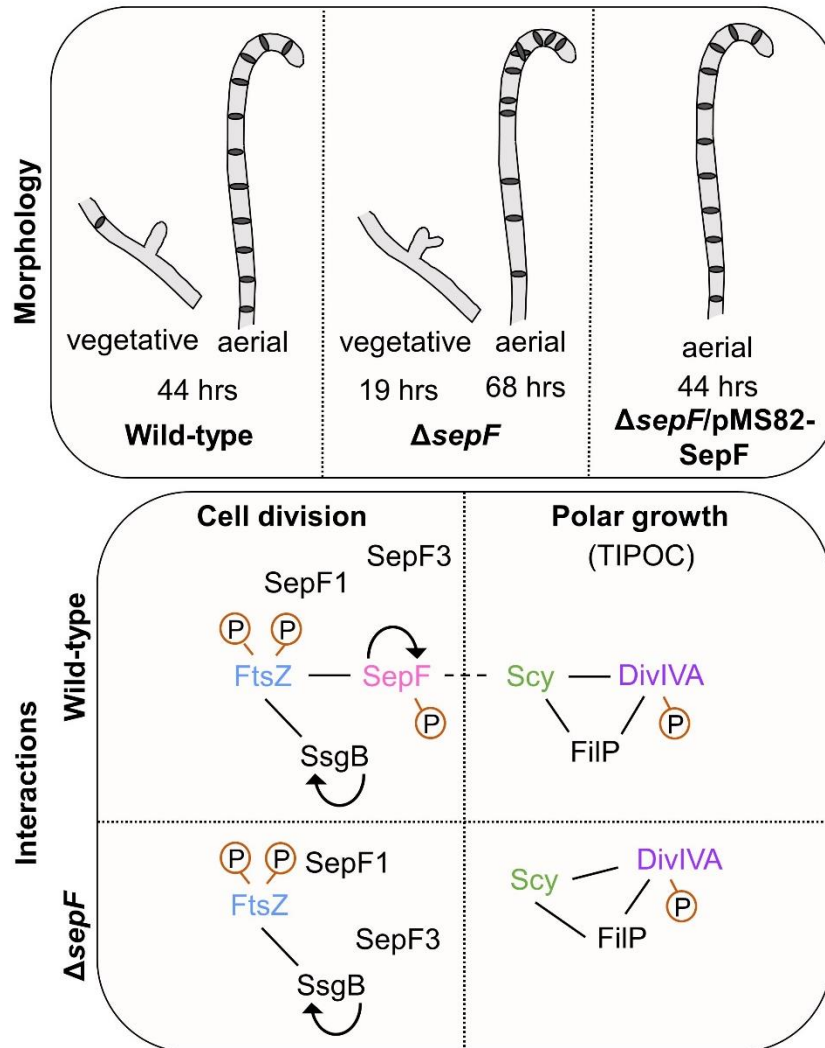


Figure 3.14 Summary of septa formation and the protein-protein interactions in the wild-type M145 and $\Delta sepF$ strains during cell division and polar growth.

'Morphology' (top) shows the position of vegetative cross-walls and sporulation septa (grey discs) in the hyphae of the wild-type M145 (left), $\Delta sepF$ (middle) and $\Delta sepF/pMS82-SepF$ strains. 'Interactions' (bottom) shows the known (solid line) and hypothesis (dashed line) interactions, relevant to Chapter 3, during cell division and polar growth. The cell division components, SepF and SsgB, self-interact and interact with FtsZ (Schlimpert *et al.*, 2017; Willemse *et al.*, 2011). The TIPOC components, Scy, FilP and DivIVA, interact with each other (Fuchino *et al.*, 2013; Holmes *et al.*, 2013; Kelemen, 2017). Due to the fork-like morphology of ~5% of the vegetative hyphae in the $\Delta sepF$ strain a link between cell division and polar growth was hypothesised. Phosphorylation identified by Manteca *et al.*, 2011 and Rioseras *et al.*, 2018 is showed by a circled 'P'.

Generation of a $\Delta sepF$ mutant by the Redirect[®] PCR-directed mutagenesis approach allows the $\Delta sepF$ mutant to be compared to the recently published $\Delta sepF1$ mutant, also known as $\Delta sflA$, and the $\Delta sepF3$ mutant, also known as $\Delta sflB$, (Zhang *et al.*, 2020). The $\Delta sepF1$ and $\Delta sepF3$ mutants had a fluffier colony edge, produced the grey sporulation pigment and sporulated on SFM plates. Frequent branching of the sporogenic aerial hyphae indicated the lack of SflA and SflB affected the integrity of the TIPOC, similar to our observation described above, however SepF and SflA or SflB rarely localised together (Zhang *et al.*, 2020). Therefore in *S. coelicolor* SepF could have a more complex developmental role than previously thought.

Previous attempts to complement the $\Delta sepF$ strain by Tan, 2018 highlighted the importance of including the second promoters upstream of *sepF*. The initial inclusion of the second promoter also resulted the inclusion of a promoter-less *SCO2080* (Figure 3.9). So to exclude the possibility that complementation was affected by the additional copy of *SCO2080*, the current study aimed to complement $\Delta sepF$ with a fragment carrying only the *sepF* gene. Colonies of the complemented $\Delta sepF/pMS82$ -SepF strain produced the grey sporulation pigment and regularly spaced sporulation septa in a wild-type like manner, confirming complementation by the *sepF* gene carrying both of its promoters (Figure 3.12 and Figure 3.13). Hence the severe phenotype of the $\Delta sepF$ mutant is due to the lack of *sepF* and not downstream polar effects.

3.4 Acknowledgements

Throughout the years there were several fellow lab members who contributed to the studies of SepF, including, Alan Lau, Elena Xiao Tan and Sundeep Kaur. Some of their work is clearly referred to in this chapter when it was necessary to the presentation.

4.0 SepF: A novel link between septa formation and polar growth

4.1 Introduction

As a key protein for cell division, SepF has been shown to localise to the developing division septa in the firmicutes *B. subtilis*, the actinomycetes *M. tuberculosis* and in the cyanobacterium, *Synechocystis* (Hamoen *et al.*, 2006; Gola *et al.*, 2015; Marbouty *et al.*, 2009). In addition to co-localisation with FtsZ, bacterial two-hybrid assays have also been used to confirm interaction between SepF and FtsZ (Hamoen *et al.*, 2006; Gola *et al.*, 2015).

In *S. coelicolor*, expression of *ftsZ* is controlled by the regulation of transcription from three promoters, one promoter is constitutive, one is transcribed during vegetative growth and one is transcribed during sporogenic aerial hyphae (Flirardh *et al.*, 2000). The latter promoter enables the upregulation of FtsZ production when the initiation of spores formation in the aerial hyphae requires the formation of potential 100s of FtsZ rings. Despite the importance of correct Z-ring positioning, *S. coelicolor* lacks many of the regulators found in *E. coli* and *B. subtilis* such as the Min system and the Noc system, previously described in the introduction.

However *S. coelicolor* does contain two positive regulators of FtsZ: SsgB and SepF. SsgB, a sporulation-specific positive regulator, has been shown to localise to septum sites prior to FtsZ and promotes polymerisation of FtsZ (Willemse *et al.*, 2011). While in the previous chapter, the $\Delta sepF$ mutant formed significantly smaller colonies and the pigmentation on the surface of the colonies transitioned from white to blue, in the absence of the grey sporulation pigment. The $\Delta sepF$ mutant had a cell division defect, lacking both vegetative cross-walls and sporulation septa. Eventually the aerial hyphae formed partial septa that were tilted or cross-shaped. More intriguingly the hyphal tips of the $\Delta sepF$ mutant were also more prone (>5%) to a fork-like morphology. Two promoters have been identified for *sepF*, but detailed analysis of *sepF* transcription throughout of development is lacking (Jeong *et al.*, 2016).

The fork-like tips of the $\Delta sepF$ mutant suggested knocking-out *sepF* resulted in a polar growth defect. Intriguingly knocking out *scy* resulted in similar defects of polar growth (Holmes *et al.*, 2013). The hyphae of the Δscy mutant often showed tip-splitting, although polar growth of the Δscy mutant is more severely affected

compared to that in the $\Delta sepF$ mutant. The Δscy mutant was further characterised by shorter distances between branching events and barbed wire-like nodes in the vegetative hyphae, leading to the suggested role of Scy in apical dominance. The phenomenon of apical dominance, seen in plants and the hyphae of *Streptomyces*, describes the formation of *de novo* tips only from the lateral cell wall well behind the actively growing tips (Jyothikumar *et al.*, 2008). Scy is one of the three major intermediate-like filaments of the TIPOC. The TIPOC is a multi-protein complex which governs the process of polar growth. During polar growth the *de novo* incorporation of PG precursors occurs at the hyphal tips and branching points (Braña *et al.*, 1982; Gray *et al.*, 1990; Figure 1.2 and Figure 1.15). The other major intermediate-like filaments of the TIPOC, FilP and DivIVA, both interact with Scy (Holmes *et al.*, 2013). FilP, is thought to be involved in strengthening the cell wall of the hyphae, as the vegetative hyphae of the $\Delta filP$ mutant having a meandering morphology (Alcock, personal communication; Bagchi *et al.*, 2008). While DivIVA co-localises with Scy to actively growing tips and *de novo* branching sites, potentially to organise the cell wall machinery (Flårdh, 2010; Hempel *et al.*, 2008; Holmes *et al.*, 2013; Mukherjee *et al.*, 2009).

The current chapter aimed to investigate proteins involved in cell division and in polar growth for possible interactions with SepF *in vivo*, in the heterologous host *E. coli*. In addition the cellular localisation and levels of expression of SepF in *S. coelicolor* was monitored. Hence the aim was broken down into several smaller objectives:

- To characterise the localisation of SepF and FtsZ during the development of the wild-type, M145 strain, using the single copy integrants of pMS82-SepF-Egfp and pMS82-FtsZ-Egfp. Fluorescence from SepF-Egfp and FtsZ-Egfp was visualised with epi-fluorescence microscopy.
- To identify any novel binding partners of SepF, potentially associated with the fork-like tips of the $\Delta sepF$ mutant, using a bacterial two-hybrid assay.
- To compare the expression levels of pMS82-FtsZ-Egfp and pMS82-SepF-Egfp at key developmental stages in *S. coelicolor*.
- To monitor the localisation of SepF-Egfp in the Δscy mutant to test the potential link between SepF and polar growth.

4.2 Results

4.2.1 The localisation of *SepF-Egfp* in *S. coelicolor*

The *sepF* knock-out strain, characterised in Chapter 3, was unable to form regular vegetative cross-walls and sporulation septa. To further establish the role of SepF during cell division the cellular localisation of SepF and FtsZ was monitored during development of the wild-type M145 strain. The SepF-Egfp fusion was delivered into the wild-type strain by the introduction of the pMS82-SepF-Egfp construct, previously generated by Tan (2018). The pMS82-SepF-Egfp construct contains the same DNA fragment, 343 bp upstream of the translational start of *sepF*, required to fully complement the $\Delta sepF$ mutant in Chapter 3. The introduction of pMS82-SepF-Egfp into the $\Delta sepF$ mutant lead to full complementation of the $\Delta sepF$ phenotype, so the SepF-Egfp translational fusion is considered fully functional (Tan, 2018). For comparison, the FtsZ-Egfp fusion was delivered into the wild-type strain by the introduction of the pMS82-FtsZ-Egfp construct, also previously generated by Tan (2018). The pMS82-FtsZ-Egfp construct was derived from pKF51 (Kelemen, personal communication). The DNA insert was moved to pMS82 to enable the introduction of the pMS82-FtsZ-Egfp plasmid into apramycin resistant *Streptomyces* strains.

The M145/pMS82-SepF-Egfp and M145/pMS82-FtsZ-Egfp strains were macroscopically identical to wild-type (data not shown). The localisation of SepF-Egfp and FtsZ-Egfp was investigated using epi-fluorescence microscopy. Both strains were grown next to coverslips until the development of aerial growth, where sporulation septa formation is expected. During aerial growth the mature vegetative hyphae have well formed FtsZ-Egfp and SepF-Egfp rings at expected vegetative cross-wall sites (Figure 4.1 and Figure 4.2).

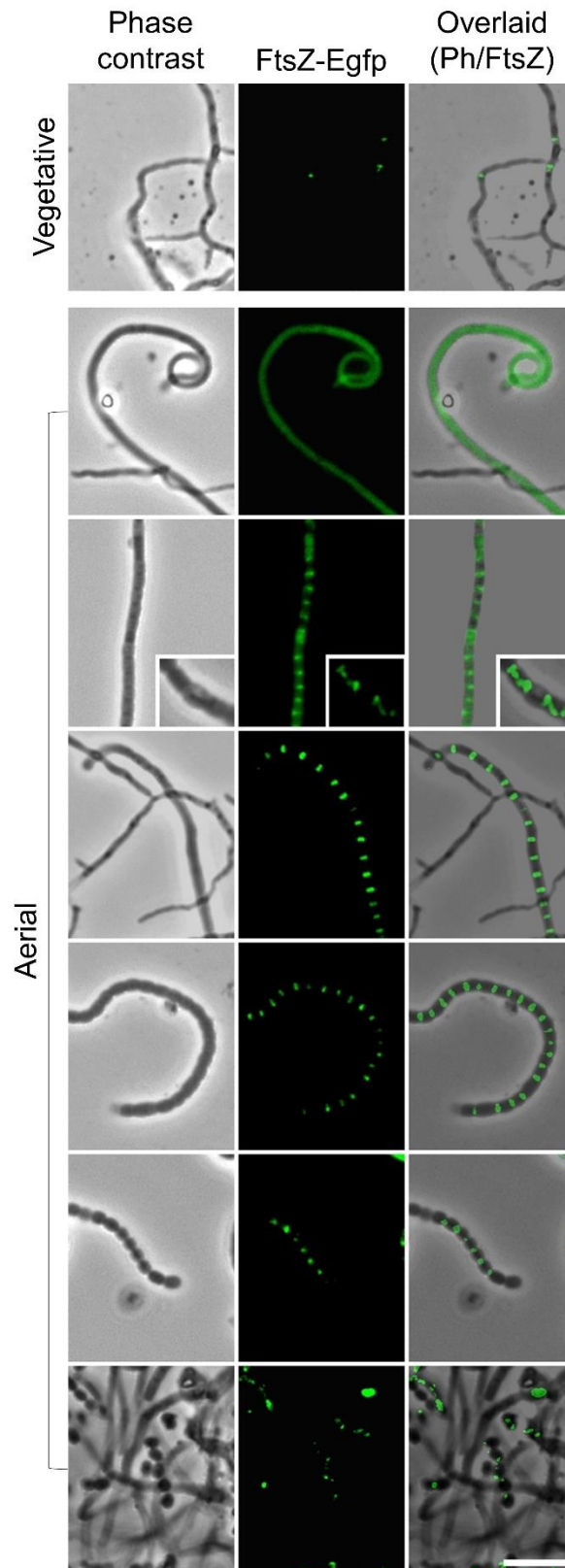


Figure 4.1 Characterisation of FtsZ-Egfp ring formation in the hyphae of M145/pMS82-FtsZ-Egfp using epi-fluorescence microscopy. The M145/pMS82-FtsZ-Egfp strain was grown on SFM+hyg *medium* for 43 hrs. FtsZ-Egfp ring formation is shown in the vegetative hyphae (top panel) and the sporogenic aerial hyphae (bottom panel). The insert shows transient spiral-like fluorescence from FtsZ-Egfp. All images were taken at x100 magnification and 400 ms exposure. The scale bar represents 5 μ m.

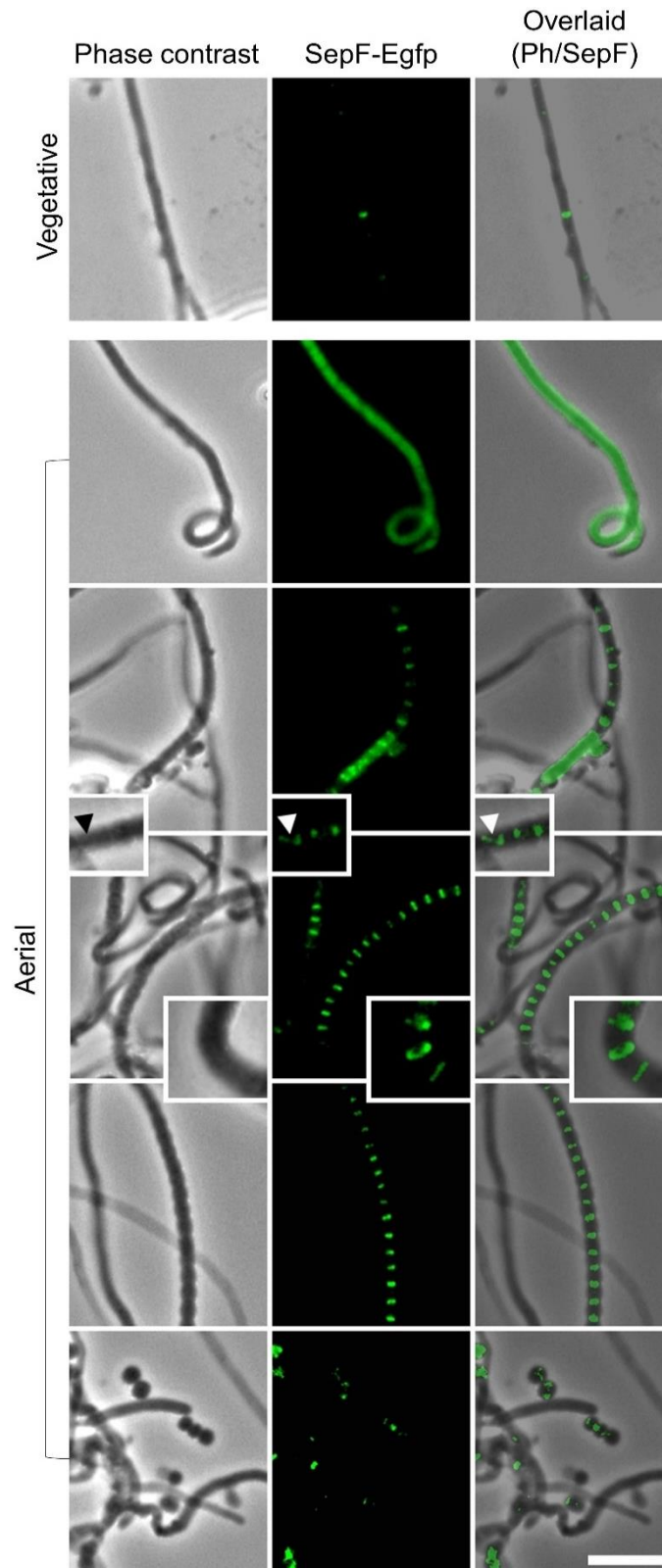


Figure 4.2 Characterisation of SepF-Egfp ring formation in M145/pMS82-SepF-Egfp using epi-fluorescence microscopy. The M145/pMS82-SepF-Egfp strain was grown on SFM+hyg medium for 46 hrs. SepF-Egfp ring formation is shown in the vegetative hyphae (top panel) and the sporogenic aerial hyphae (bottom panel). The arrows on the small insert indicate the transient spiral-like structures of SepF-Egfp. The large insert shows a ring of SepF-Egfp in a bending aerial hyphae. All images were taken at x100 magnification and 400 ms exposure. The scale bar represents 5 μ m.

Young aerial hyphae of M145/pMS82-SepF-Egfp and M145/pMS82-FtsZ-Egfp contained diffuse fluorescence throughout, which were identifiable by a curly hook-like shape. Then as the hyphae matured, the fluorescence condensed. Condensation did not occur uniformly along the hyphae (Figure 4.1 third row and Figure 4.2 third row). Condensation initially lead to the formation of non-uniform spiral-like patterns similar to those detected previously for FtsZ-Egfp (Grantcharova *et al.*, 2005). The spiral-like patterns were transient and transitioned into regular rings of both SepF-Egfp and FtsZ-Egfp. The rings of SepF-Egfp and FtsZ-Egfp were positioned perpendicular to the imaging plane so each ring formed a 'rung' of a 'ladder'. The ladders of SepF-Egfp were highly similar to the ladders of FtsZ-Egfp. Next the rings of SepF-Egfp and FtsZ-Egfp reduce in size indicative of either contraction or re-modelling of the rings as spores mature. Eventually ovoid evenly sized spores of M145/pMS82-SepF-Egfp and M145/pMS82-FtsZ-Egfp were formed. Some of these spores contain fluorescence foci, potentially representing the remnants of sporulation septa or the re-organisation of SepF-Egfp and FtsZ-Egfp. In the absence of co-localisation studies, the current study cannot state that FtsZ and SepF co-localise, but the patterns found are consistent with the co-localisation of FtsZ and SepF. Overall, the localisation of the Egfp translation fusions in the aerial hyphae of M145/pMS82-SepF-Egfp and M145/pMS82-FtsZ-Egfp was highly similar. Together with the lack of normal septation in the $\Delta sepF$ mutant, the similar localisation patterns support the role of SepF as a positive FtsZ regulator.

4.2.2 Identifying novel SepF binding partners using a bacterial two-hybrid assay

The inability of the $\Delta sepF$ mutant to produce regular septa and the similar localisation patterns of SepF-Egfp and FtsZ-Egfp support the expected role of SepF in cell division. However the role of SepF in cell division does not account for the prevalence of fork-like tips in the $\Delta sepF$ mutant. Potential binding partners of SepF were investigated using a bacterial two-hybrid assay *in vivo* in the heterologous host *E. coli* (Figure 4.3).

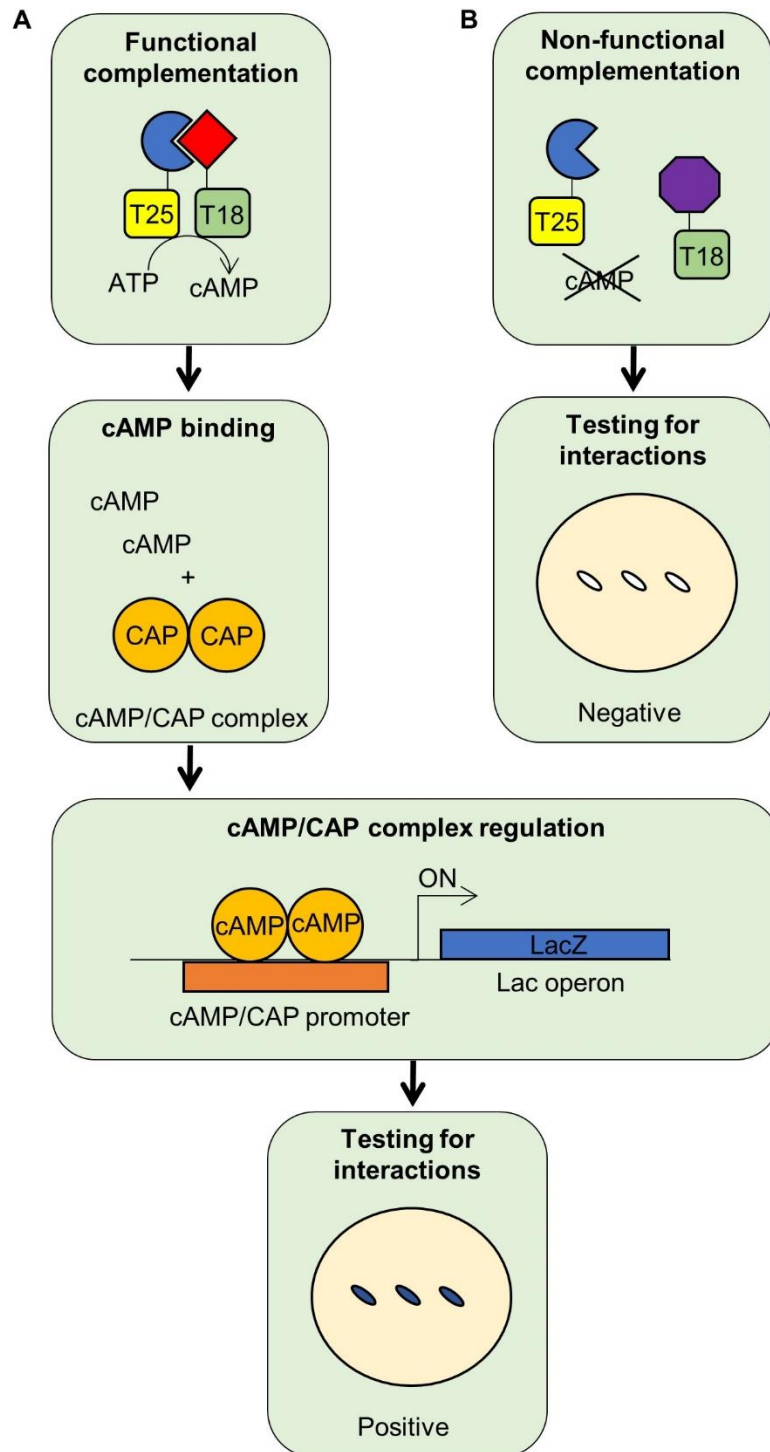


Figure 4.3 The mechanism of the bacterial two-hybrid assay. The catalytic domain of the adenylate cyclase from *Bordetella pertussis*, consists of two complementary fragments, T18 and T25. A) Upon functional complementation the catalytic domain is reconstituted, and cAMP is synthesised. The cAMP/CAP complex is a pleiotropic regulator of the resident lac operon encoding β -galactosidase. In the absence of glucose β -galactosidase breaks down X-gal, giving the colonies a blue pigmentation. B) Upon non-functional complementation colonies remain white (Modified from Euromedex BACTH System Kit – Bacterial Adenylate Cyclase Two-Hybrid System protocol, 2016).

The bacterial two-hybrid assay relies on the two complementary fragments, T18 and T25, of the catalytic domain from the adenylate cyclase of *Bordetella pertussis* (Figure 4.3). The two complementary fragments are not active when physically separated but when the proteins fused to the fragments interact, the adenylate cyclase is reconstituted leading to cAMP synthesis (Figure 4.3A). The small ligand, cAMP binds to the catabolite activator protein, CAP, forming the cAMP/CAP complex. The cAMP/CAP complex acts as an activator for the resident *lac* operon which encodes β -galactosidase. When active, in the absence of glucose, β -galactosidase will break down the chromogenic substrate X-Gal (5-bromo-4-chloro-3-indolyl- β -D-galactopyranoside), leading to the blue pigmentation of the colony. Hence the pairings of protein fusions, which resulted in functional complementation were distinguishable from pairings, which resulted in non-functional complementation, based on a blue/white selection on the appropriate media.

There are four plasmids used in the bacterial two-hybrid assay: pUT18, pUT18C, pKT25 and pKNT25. Each plasmid contains either the T18 or the T25 fragment as the names indicate, a multi-cloning site, an antibiotic resistance gene and an *oriT*. The position of the multi-cloning sites allows the fragment to be fused to either the N-terminal or the C-terminal of the desired protein. The SepFC constructs and all of the described constructs were designed and named to show the T18 and T25 translational fusions at both the N- and the C-terminal ends of the relevant proteins, for example plasmids expressing SepFC-T18, SepFC-T25, T18-SepFC and T25-SepFC were generated previously in the Kelemen lab by Dovile Jonylaite and Lucy Burrows.

Each combination of protein pairs contains a T18 containing plasmid, conferring ampicillin resistance, and a T25 containing plasmid, conferring kanamycin resistance. For each combination, three co-transformants were streaked into LB Δ glucose+amp+kana+IPTG+xgal plates. The plates were incubated in the dark for 24 hrs, then the blue/white screening was visually interpreted and quantified using Fiji (2012). For quantification of the blue/white selection, firstly camera images were taken, converted to 16-bit and inverted. Then three 35 x 35 pixel areas were randomly selected within each streak, the image look-up table was changed to the 'fire' RGB values to allow greater visual separation of the streaks and using the negative controls the background was subtracted. Finally the median signal intensity was measured in each 35 x 35 pixel area and compared to the visual interpretation. The colours of the streaks were classified into three categories: strong positives

(actual values: >8000, represented as 1 on graphs), weak positives (actual values: 1501 to 7999, represented as 0.5 on graphs) and negative (actual values: <1500, represented as 0.01 on graphs). Analysis of the streak classification is described later in the chapter.

The bacterial two-hybrid assay focused on the protein-protein interactions of the C-terminal of SepF. The C-terminal of SepF, SepFC, spans 96 amino acids, from the 118th amino acid to the 213th amino acids (Figure 3.2). SepFC is consistent with the truncated construct used to characterise the interactions of SepF from *B. subtilis* (Duman, *et al.*, 2013). In *B. subtilis* deletion of the 63 amino acid N-terminus of SepF did not affect the interaction between SepF and FtsZ or self-interaction. Therefore the C-terminal of SepF from *B. subtilis* is sufficient to form circular polymers with a ~50 nm diameter. Similarly the Kelemen lab found SepFC formed tubular structures, with a slightly smaller diameter of 34 to 39 nm, which pulled apart to reveal a spiral helical thread (Kelemen, personal communication).

Initially the current study wanted to reproduce the reported interactions between SepF and FtsZ then FtsZ and the *Streptomyces* specific SsgB. The bacterial two-hybrid assay confirmed that the C-terminal of FtsZ, spanning the last 74 amino acids, interacts with SepFC and the sporulation-specific positive regulator, SsgB (Figure 4.4; Appendix 2). Both SepFC and SsgB were also confirmed to self-interact. More intriguingly a novel positive interaction was detected between SepFC and SsgB, which has not been established before. The interaction between SepFC and SsgB raises several potential possibilities: either the early division complex contains all three proteins, SepF, SsgB and FtsZ in the same time, or SepF, SsgB and FtsZ have a complex interaction pattern including potential partner switching prior to septum formation.

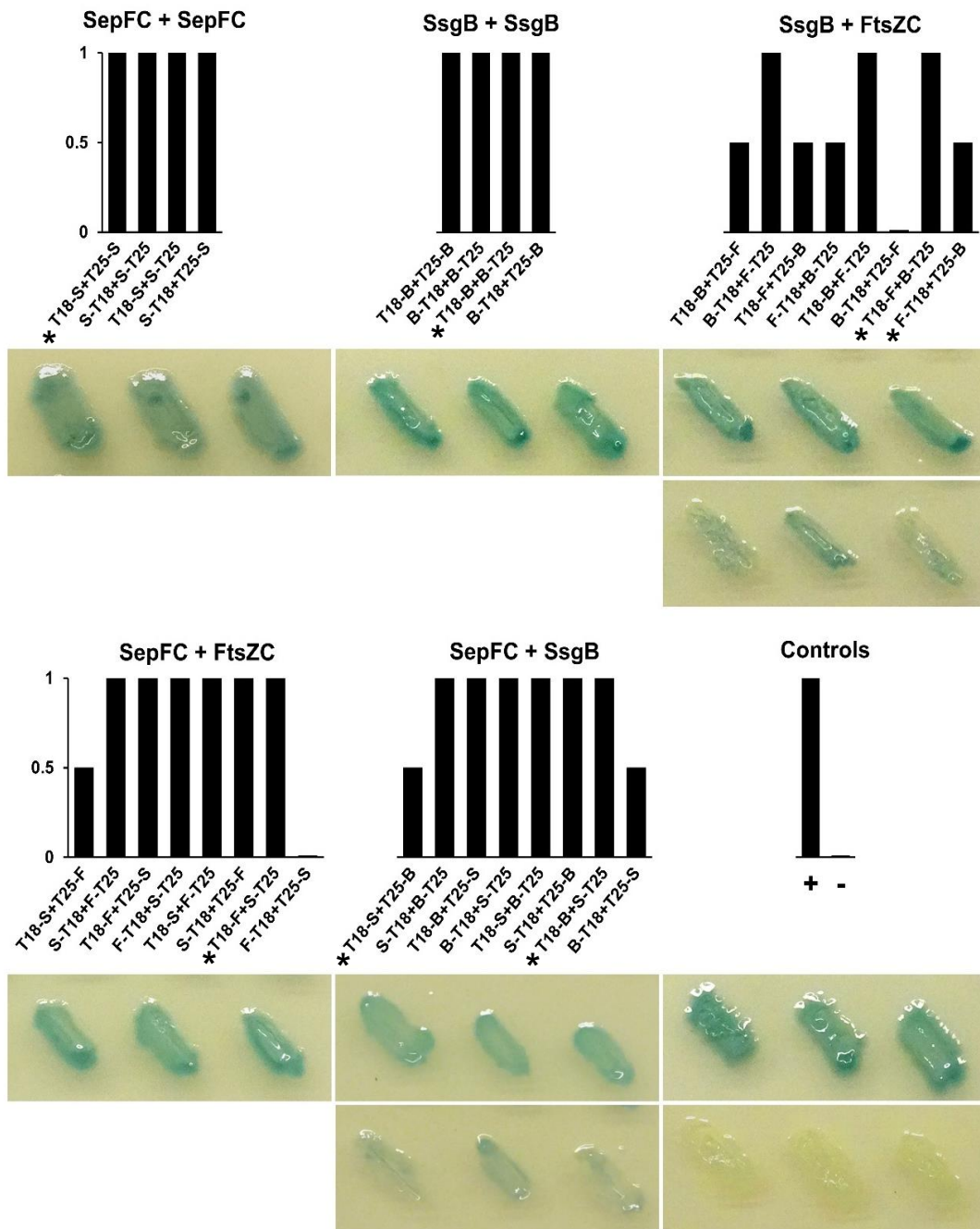


Figure 4.4 The interactions of SepFC with known cell division proteins. Each combination, in the bacterial two-hybrid assay, was visually assessed, quantified and classified into three categories; strong positive, weak positive and negative (graph values: 1, 0.5 and 0.01). The upper plate images show one positive combination in triplet, the lower plate images show one weak positive combination in triplet. The * on the graphs indicate the imaged combinations below. The positive control (top row) contains pUT18C-Zip and pKT25-Zip and the negative control (bottom row) contains an empty pUT18C and pKT25 (Karimova *et al.*, 1998). The combination names (SepFC=S, SsgB=B, FtsZC=F) indicate the position of the T18- and T25- domains.

Next the ability of SepFC to interact with members of the TIPOC, hypothesised to be involved with the fork-like tips of the $\Delta sepF$ mutants, was investigated (Figure 4.5; Appendix 3). The bacterial two-hybrid assay did not detect any positive combination involving DivIVA nor any positive interactions between Scy and either FtsZC or SsgB. But most fascinatingly all combinations tested between SepFC and Scy were positive. The potential interaction between SepFC and Scy supports the earlier observation of similar tip morphologies in the corresponding knock-out strains and gives the first evidence for a direct link between the processes of cell division and polar growth.

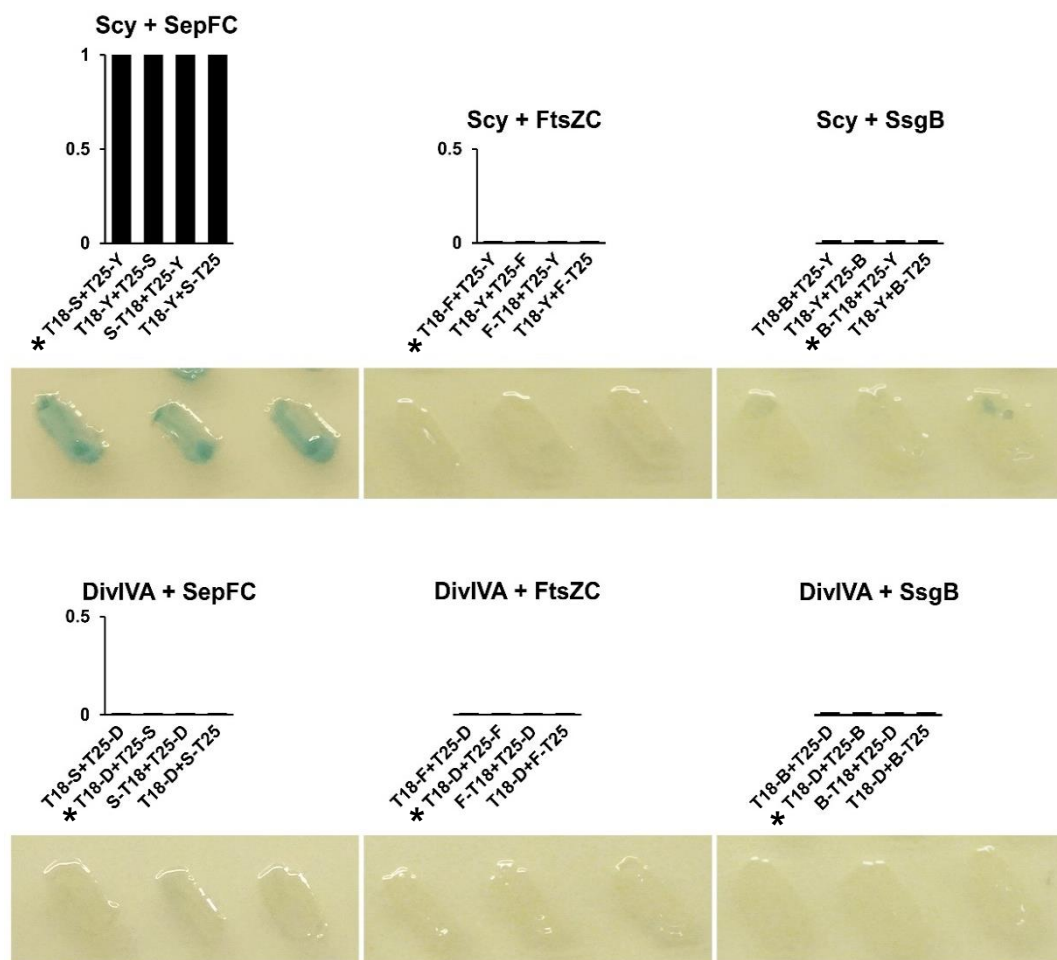


Figure 4.5 The interactions of SepFC with known TIPOC components. Each combination, in the bacterial two-hybrid assay, was visually assessed, quantified and classified into three categories; strong positive, weak positive and negative (graph values: 1, 0.5 and 0.01). The plate images show one representative combination in triplet. The * on the graphs indicate the imaged combinations below. The controls were the same as stated in Figure 4.4. The combination names (SepFC=S, Scy=Y, FtsZC=F, SsgB=B, DivIVA=D) indicate the position of the T18- and T25- domains.

4.2.2.1 Introducing SepFC-K46A and -F71A into the bacterial two-hybrid assay

To further investigate the interactions between SepF and the positive binding partners identified in Section 4.2.2., the effects of two mutations previously shown to affect the interaction between SepF and FtsZ in both *B. subtilis* and *M. tuberculosis* were investigated (Duman *et al.*, 2013; Gupta *et al.*, 2005). For the *Mycobacterium* SepF mutating K190 to alanine did not affect SepF self-interaction but did abolish the SepF-FtsZ interaction (Gupta *et al.*, 2005). While the F215S mutation in the *Mycobacterium* SepF, equivalent to F126S in *B. subtilis*, greatly reduced both the SepF self-interaction and the SepF-FtsZ interaction. The F126S mutation of the *B. subtilis* SepF abolished the interaction with FtsZ but did not affect self-interaction or interaction with wild-type SepF (Duman *et al.*, 2013). According to the Clustal Omega analysis of the SepF sequences (Figure 3.2), residue K101, equivalent to K190 in *Mycobacterium*, and residue F126 of the *B. Subtilis* SepF are well conserved so the equivalent residues were mutated in the SepFC of *S. coelicolor*. The numbers of the mutations, K46A and F71A, relate to the position of these amino acids in the truncated SepFC (Figure 3.2). Residue F71 was mutated to alanine and not serine, as in *Mycobacteria*, to allow consistency between the *S. coelicolor* mutations.

The DNA fragments carrying these mutations were synthesised and cloned into the appropriate plasmids: pKT25, pKNT25, pUT18 and pUT18C. First, the amplification of the *sepFC-K46A* and *sepFC-F71A* inserts was carried out using high fidelity DNA polymerase. For both mutations two inserts were generated. (Figure 4.6A). The inserts were generated using the same forward primer, SepF Trunc Xba Nde FRW, but two different reverse primers, SepF UT REV or SepF UTC REV. The key difference between the reverse primers was the absence or presence of a stop codon allowing T18 and T25 to be fused to either terminal. All four inserts were digested with *EcoRI* and *XbaI* then analysed on a diagnostic 1% agarose gel (Figure 4.6B). For each insert, a PCR product at the expected 291 bp size was detected. Although the *sepFC-K46A-UT* and *sepFC-F71A-UT* inserts were present at lower concentrations, all four inserts were successfully generated.

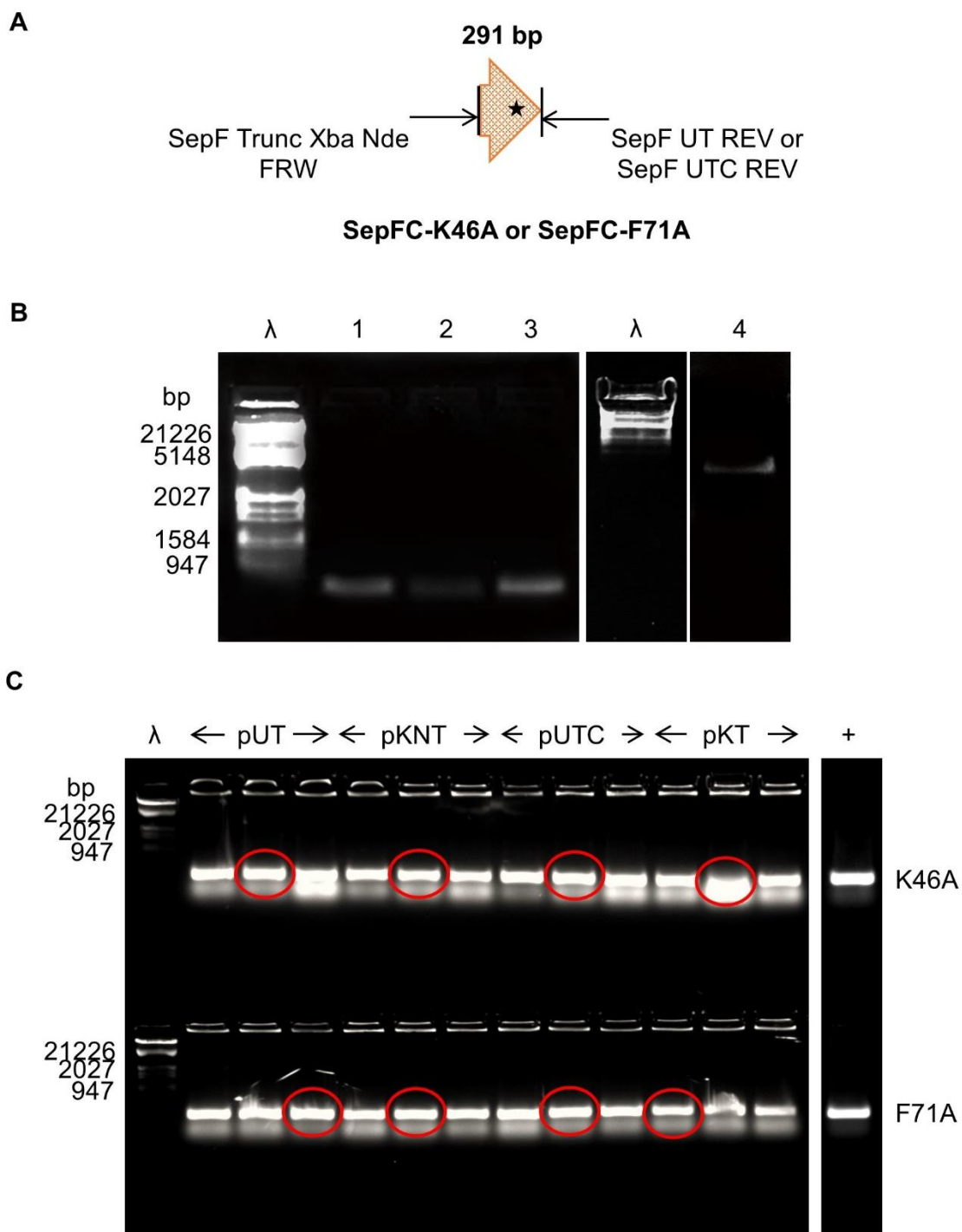


Figure 4.6 Generation of the SepFC-K46A and SepFC-F71A plasmids for the bacterial two-hybrid assay. A) Amplification of the *sepFC-K46A* or *sepFC-F71A* fragments used two synthetic plasmids as the templates and the primers: SepF Trunc Xba Nde FRW and either SepF UT REV or SepF UTC REV. B) The final *sepFC-K46A-UTC*, *-K46A-UT*, *-F71A-UTC* and *-F71A-UT* fragments were digested with *EcoRI* and *XbaI* and analysed on a 1% agarose gel. Lanes λ) λ DNA digested with *EcoRI* and *HindIII*, Lane 1) *sepFC-K46A-UTC*, Lane 2) *sepFC-K46A-UT*, Lane 3) *sepFC-F71A-UTC*, and Lane 4) *sepFC-F71A-UT*. Each fragment was ligated into the suitable bacterial two-hybrid vectors and transformed in *E. coli* DH5α. C) A colony PCR using the primers SepF Trunc Xba Nde FRW and SepF UT REV, analyse three *E. coli* DH5α transformants for each construct on a 1% agarose gel. The colonies used in future experiments are circles in red. Lanes λ) λ DNA digested with *EcoRI* and *HindIII*, Lanes +) the positive 4A10 control.

Each insert was ligated into the suitable pKT25, pKNT25, pUT18 or pUT18C vector digested with *EcoRI* and *XbaI*. Then the ligations were transformed into *E. coli* DH5 α cells, chemically made competent. Successful transformants were selected on media supplemented with kanamycin for pKT25 and pKNT25 constructs or ampicillin for pUT18 and pUT18C constructs.

To identify successful transformants carrying the correct inserts, 3 transformants from each ligation were streaked onto a LB Δ NaCl plate with the appropriate antibiotic and were tested using a low-fidelity colony PCR. The colony PCR used the previous SepF Trunc Xba Nde FRW and SepF UT REV primer pairing as these primers should generate a 291 bp product for all the constructs (Figure 4.6C). For all of the transformants, a PCR product at the desired size was detected, indicating the presence of an insert. For each specific construct one transformant was chosen to undergo a large-scale plasmid preparation (Figure 4.6C, red circles). Sequencing of the large-scale plasmid preparations confirmed the appropriate SepFC-K46A or SepFC-F71A mutations into all four plasmids.

For the bacterial two-hybrid assay, plasmids were co-transformed, in a pair wise manner, into *E. coli* BTH 101 cells, chemically made competent. The plasmid pairs always consisted of an T18 construct, conferring ampicillin resistance and an T25 construct, conferring kanamycin resistance so successful transformants were selected for on LB+amp+kana plates. Then from each pair-wise combination, three successful transformants were re-streaked onto the final LB Δ glucose+amp+kana+IPTG+xgal plates and analysed after 24 hrs of growth at 30°C.

The interactions of SepFC-K46A and SepFC-F71A in all previous combinations which formed a positive interaction with SepFC, were tested (Figure 4.7 and Figure 4.8; Table 4.1; Appendix 4 and Appendix 5). The K46A mutation did not alter the self-interaction of SepFC or the novel SepFC-Scy interaction but the K46A mutation did reduce the SepFC-SsgB interaction and abolished the wild-type SepFC-FtsZC interaction (Figure 4.7). The F71A mutation did not clearly alter the self-interaction of SepFC, but the F71A mutation abolished the SepFC-FtsZC, the SepFC-SsgB and the SepFC-Scy interaction (Figure 4.8).

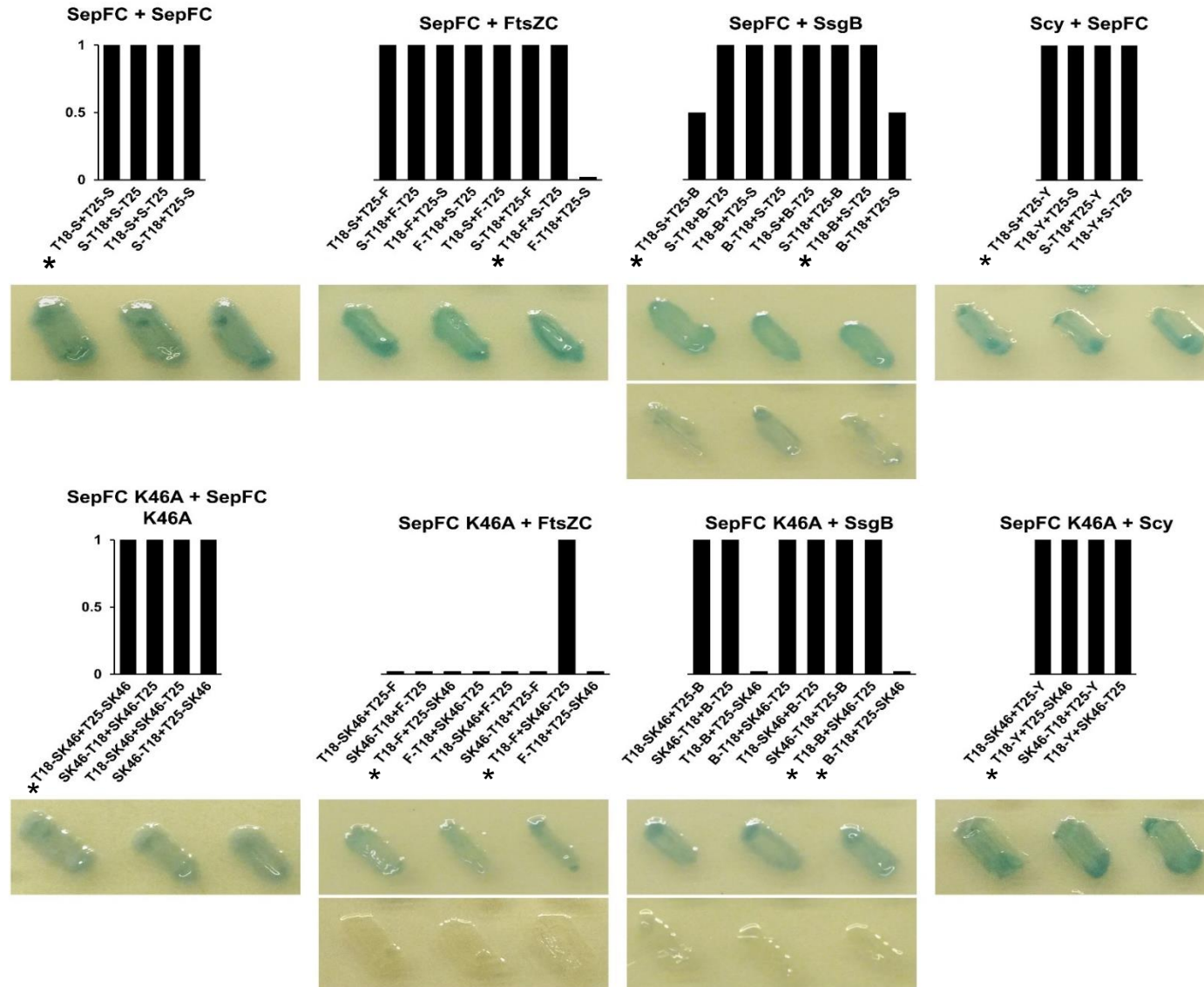


Figure 4.7 Comparison of SepFC and SepFC-K46A binding partners. Each combination, in the bacterial two-hybrid assay, was visually assessed, quantified and classified into three categories; strong positive, weak positive and negative (graph values: 1, 0.5 and 0.01). The upper plate images show one positive combination in triplet, the lower plate images show one weak positive or one negative combination in triplet. The * on the graphs indicate the imaged combinations below. The controls were the same as stated in Figure 4.4. The combination names (SepFC=S, SepFC-K46A=SK46, FtsZC=F, SsgB=B, Scy=Y) indicate the position of the T18- and T25- domains.

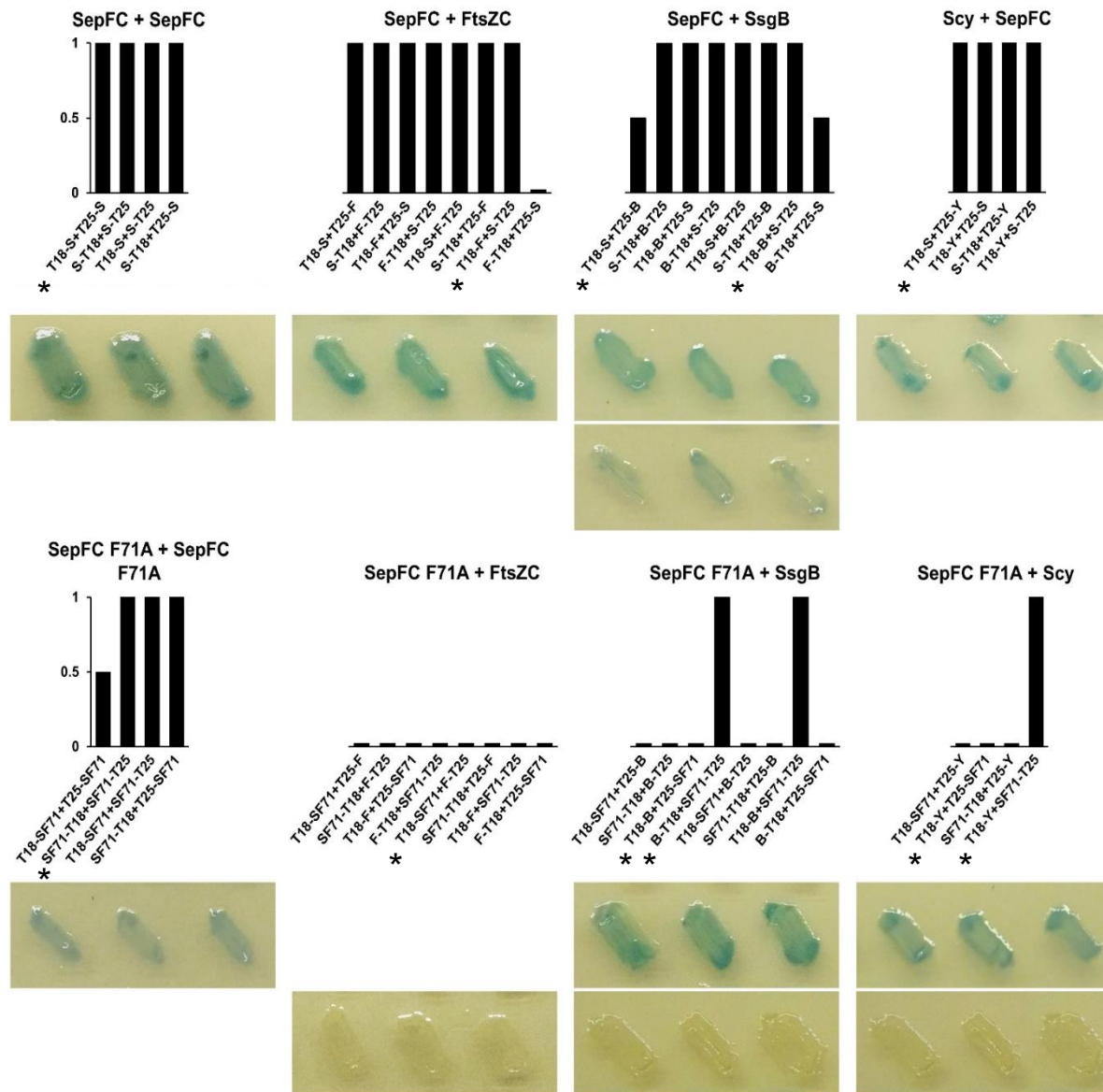


Figure 4.8 Comparison of SepFC and SepFC-F71A binding partners. Each combination, in the bacterial two-hybrid assay, was visually assessed, quantified and classified into three categories; strong positive, weak positive and negative (graph values: 1, 0.5 and 0.01). The upper plate images show one positive combination in triplet, the lower plate images show one weak positive or one negative combination in triplet. The * on the graphs indicate the imaged combinations below. The controls were the same as stated in Figure 4.4. The combination names (SepFC=S, SepFC-F71A=SF71, FtsZC=F, SsgB=B, Scy=Y) indicate the position of the T18- and T25- domains.

Table 4.1 Summary of the bacterial two-hybrid assay using SepFC. The interactions, detailed above, were summarised as strongly positive (+), weakly positive (+/-) or negative (-).

		Potential binding partners			
		SepFC	FtsZC	SsgB	Scy
SepFC derivative	SepFC wild-type	+	+	+	+
	SepFC-K46A	+	-	+/-	+
	SepFC-F71A	+	-	-	-

Interestingly the K46A mutant mirror the K190A mutant in the SepF of *M. tuberculosis* but the F71A mutant more closely mirror the F126S mutant in the SepF of *B. subtilis*. Based on the bacterial two-hybrid assay in the current study both K46 and F71 of SepFC are involved in FtsZ binding and possible SsgB binding but only F71 is involved in the novel SepF-Scy interaction. The implication of one residue in both the FtsZ and Scy interactions, raises the possibility Scy and FtsZ could compete to bind to SepF.

4.2.3 The expression of SepF-Egfp in M145 and Δ scy

To further investigate the importance of the SepFC-Scy interaction, detected by the bacterial two-hybrid assay, the expression of FtsZ-Egfp and SepF-Egfp was monitored at key developmental stages in the *S. coelicolor* wild-type M145 strain and the Δ scy mutant. Previously, expression of FtsZ has been shown to increase in the aerial hyphae prior to sporulation due to the upregulation of the sporulation specific promoter, *ftsZ2p* (Flårdh *et al.*, 2002). Here the current study tested whether SepF expression was also upregulated at the same time as FtsZ. Large scale analysis of transcriptional start points established two promoters for *sepF* (Jeong *et al.*, 2016). Complementation of the Δ sepF mutant confirmed that both promoters are important and suggested readthrough transcription was unlikely to be significant for SepF expression. The fact that *ftsZ* and *sepF* are not co-transcribed raised the possibility that expression of these genes could be regulated independently.

Instead of monitoring transcription of *ftsZ* and *sepF*, a quick method was wanted for assessing gene expression using fluorescence protein fusions expressed from their native promoters. The pMS82-FtsZ-Egfp plasmid and the

pMS82-SepF-Egfp plasmid, carrying the relevant Egfp fusions, were introduced into the wild-type and $\Delta sepF$ or Δscy strains. Each strain was grown on SFM+hyg+cellophane medium to maintain the selection of the plasmid. Hyphae were collected at three developmental stages: matt vegetative growth, early fluffy aerial growth and late sporulating aerial growth, containing spores, where appropriate. When the $\Delta sepF$ mutant was tested, the last sample was collected at a time point comparable to late stages of development. Hyphae from each stage were vigorously broken in a BP biomedical FastPrep-24TM RG and separated into supernatant and pellet fraction after centrifugation. The supernatants were subject to a Bradford assay then equal amounts of total protein was analysed on a native PAGE gel. Native PAGE gels lack SDS. Therefore the movement of proteins in a native PAGE gel is thought to be controlled by size, shape of the proteins or potential association with other proteins forming heterooligomeric complexes and the proteins are expected to stay active during native PAGE. Hence fluorescent protein fusions can be detected from total cell extracts by scanning the gels using a Typhoon Fla 9500 biomolecular imager. The M145/pMS82-SepF-Egfp and M145/pMS82-FtsZ-Egfp strains developed at a similar rate and produced copious amounts of spores, completing the lifecycle in ~2 days. For the $\Delta sepF$ /pMS82-FtsZ-Egfp and Δscy /pMS82-SepF-Egfp strains development was delayed and timepoints were collected after 3-4-days growth.

Unexpectedly, imaging the gels at 480 nm revealed three out of the four strains produced multiple bands, positioned at distinct heights (Figure 4.9). The presence of multiple bands at distinct heights raises several possibilities: the bands represent the different oligomerised forms of the same protein or the complex formations with other proteins or the different phosphorylation states of the proteins.

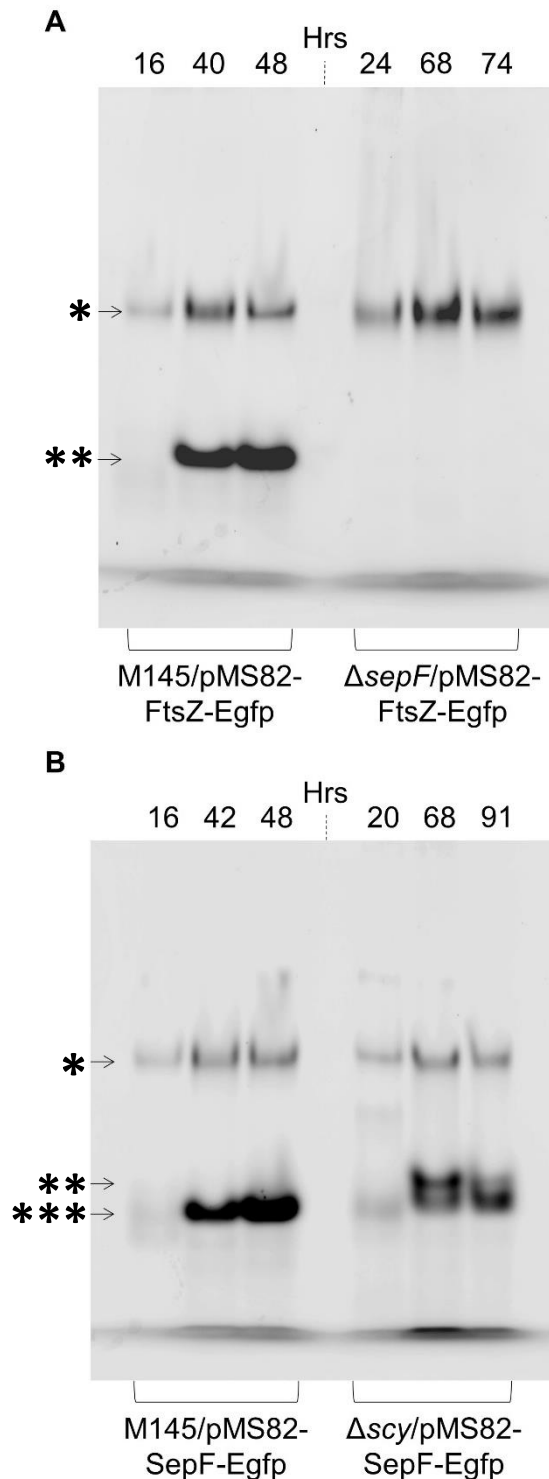


Figure 4.9 Comparison of A) FtsZ-Egfp and B) SepF-Egfp expression. The four strains, M145/pMS82-FtsZ-Egfp, Δ *sepF*/pMS82-FtsZ-Egfp, M145/pMS82-SepF-Egfp and Δ *scy*/pMS82-SepF-Egfp were streaked onto SFM+hyg+cellophane medium. Samples were taken at three distinct stages representing matt vegetative growth, early white fluffy aerial growth and late sporulating aerial growth. A) For M145/pMS82-FtsZ-Egfp, samples were taken at 16 hrs, 40 hrs and 48 hrs. For Δ *sepF*/pMS82-FtsZ-Egfp, samples were taken at 24 hrs, 68 hrs and 74 hrs. B) For M145/pMS82-SepF-Egfp, samples were taken at 16 hrs, 42 hrs and 48 hrs. For Δ *scy*/pMS82-SepF-Egfp, samples were taken at 20 hrs, 68 hrs, 91 hrs. For each sample, a supernatant fraction containing 38 mg of total protein was analysed on an 8% native PAGE gel. The * indicate each banding position described.

In support of the hypothesis that the bands represent different oligomerised forms of the same protein or possible complex formation with other proteins, the bacterial two-hybrid assays showed both SepF and FtsZ are expected to interact with each other and with other proteins, such as SsgB or Scy. Hence different protein assemblies could have been captured using native PAGE. Interestingly, $\Delta sepF/pMS82\text{-FtsZ-Egfp}$ only produced bands at the higher position, denoted as *, which could suggest the lower bands in the M145/pMS82-FtsZ-Egfp samples rely on the presence of SepF potentially in an assembly (Figure 4.9A). The absence of bands, at position **, in the supernatants of $\Delta sepF/pMS82\text{-FtsZ-Egfp}$ suggests the lower set of bands are unlikely to be free Egfp, although the possibility of free Egfp as a product of proteolytic processing cannot be ruled out. Due to the similarity of the upper bands from the M145/pMS82-FtsZ-Egfp and $\Delta sepF/pMS82\text{-FtsZ-Egfp}$ samples, the bands might represent FtsZ polymers, or complex polymers of FtsZ and other proteins.

Following on from the oligomerisation hypothesis stated above, comparison of the bands at position * for M145/pMS82-FtsZ-Egfp and $\Delta sepF/pMS82\text{-FtsZ-Egfp}$ revealed an increase in intensity at the latter two timepoints. The increase in intensity is consistent with the upregulation of FtsZ-Egfp production in the aerial hyphae of both strains. Comparison of the banding pattern from M145/pMS82-SepF-Egfp and $\Delta scy/pMS82\text{-SepF-Egfp}$ revealed a similar pattern (Figure 4.9B). Again the intensity of the bands at position * increased in the latter two timepoints, which could suggest the upregulation of SepF-Egfp in the aerial hyphae of both strains. The supernatant of $\Delta scy/pMS82\text{-SepF-Egfp}$ also contained additional bands at position ** in the latter two timepoints. Hence the native PAGE gel cannot rule out the possibility that in the absence of Scy, binding of SepF-Egfp is altered, which would support a link between the processes of polar growth and septa formation.

Alternatively in support of the hypothesis that the bands represent the different phosphorylation states of the proteins, Rioseras *et al.*, 2018 showed FtsZ and SepF were phosphorylated in the aerial hyphae of *S. coelicolor* after 65 hrs of growth (Figure 4.10). In addition to the phosphorylation at Ser 387 identified by Manteca *et al.*, 2011, Rioseras *et al.*, 2018 identified a novel phosphorylation of FtsZ at Ser 319 which was upregulated after 30 hrs and 65 hrs of growth. Based on this evidence the bands in the M145/pMS82-FtsZ-Egfp and $\Delta sepF/pMS82\text{-FtsZ-Egfp}$ samples, present at position * across the three timepoints could represent a low level of unphosphorylated FtsZ across the lifecycle of *S. coelicolor*. Then in the M145/pMS82-FtsZ-Egfp samples the bands present at position ** in the latter two

timepoints, collected after 30 hrs, could represent FtsZ in a different phosphorylated state. Interestingly the absence of bands at position ** in the $\Delta sepF/pMS82$ -FtsZ-Egfp samples also collected after 30 hrs could suggest the presence of SepF effects the phosphorylation of FtsZ. This observation would suggest SepF aids Z-ring formation by affecting the phosphorylation state of FtsZ monomers.

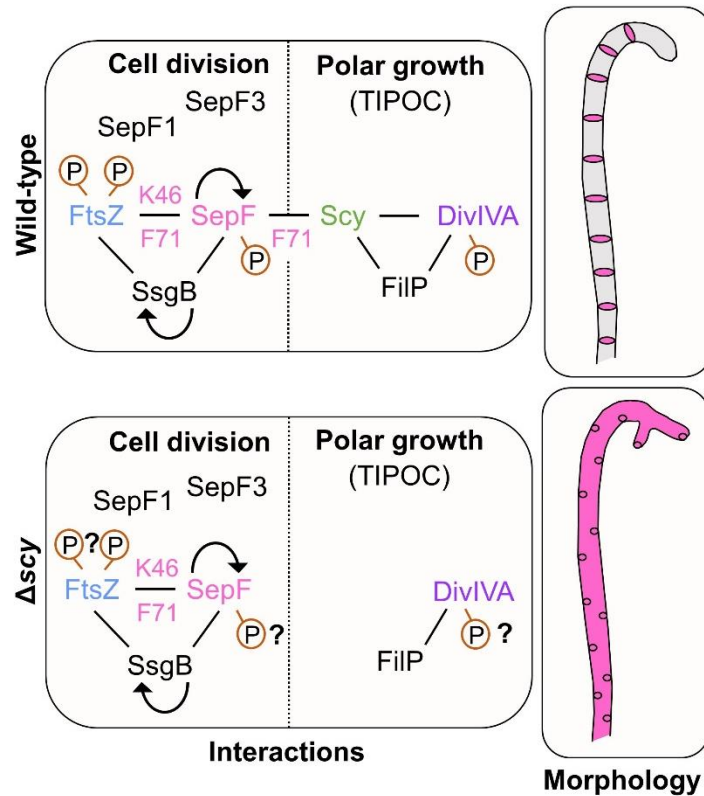


Figure 4.10 Summary of the protein-protein interactions and SepF-Egfp localisation during aerial hyphae development in the wild-type M145 and Δscy strains.

Interactions' (left) shows the known interactions, relevant to Chapter 4, during cell division and polar growth. The cell division components, SepF and SsgB, self-interact and interact with FtsZ (Schlimpert *et al.*, 2017; Willemse *et al.*, 2011). In addition we showed using a bacterial two-hybrid SepF interacts with SsgB and Scy. To our knowledge the SepF-Scy interaction is the first evidence of a direct link between cell division and polar growth. Residues K46 and F71 of the SepF C-terminal affected the SepF-FtsZ interaction and residue F71 affected the SepF-Scy interaction. Scy is known to interact with the TIPOC components DivIVA and FilP (Fuchino *et al.*, 2013; Holmes *et al.*, 2013; Kelemen, 2017). Phosphorylation identified by Manteca *et al.*, 2011 and Rioseras *et al.*, 2018 is shown by a circled 'P'. Speculated alterations to the phosphorylated state of protein are shown by a question mark. 'Morphology' (right) shows the localisation of SepF-Egfp (pink) in aerial hyphae of the wild-type M145 (top) and Δscy (bottom) strains.

Building on from the phosphorylation hypothesis stated above, the consistent presence of a band at position * in the M145/pMS82-SepF-Egfp and

Δ scy/pMS82-SepF-Egfp samples suggests a low level of SepF also present throughout the *S. coelicolor* in a unphosphorylated state (Figure 4.9 and Figure 4.10). Then the bands in the M145/pMS82-SepF-Egfp samples at position *** in the latter timepoints could represent SepF in a phosphorylated state. If this were the case phosphorylation of FtsZ and SepF would occur within a similar timeframe and could be important for Z-ring formation. Therefore the weak band at position *** in the first timepoint and the additional bands at position ** in the latter timepoints of the Δ scy/pMS82-SepF-Egfp samples could suggest in the absence of Scy the phosphorylation state of SepF is altered which would support the SepF-Scy interaction.

Attempts to gel-excise the bands and identify the protein(s) using MALDI-TOF was unfortunately halted due to the Covid-19 pandemic. Without confirming the composition of the different bands, the current study can only speculate at this time whether the different bands represent different assemblies of proteins. Confirmation that none of the bands represent free Egfp, generated via processing the fluorescent protein fusions or via alternative translational start point, is also required. However the reproducibility of the same fluorescent bands means what the bands represents should be investigated further. We could also speculate that although the effect of SepFC-K46A and SepF-F71A on the banding pattern was not investigated, if the banding pattern represents the formation of protein complexes, both mutants would reduce the number of bands present in the M145/pMS82-FtsZ-Egfp, M145/pMS82-SepF-Egfp and Δ scy/pMS82-SepF-Egfp samples due to the absence of at least one binding partner. Furthermore the site of phosphorylation identified by Rioseras *et al.*, 2018 for SepF is unknown therefore the role of residues K46 and F71 in phosphorylation cannot be ruled out.

4.2.4 Characterising the localisation of SepF-Egfp in the Δ scy mutant

To further establish the link between SepF and Scy, the localisation of SepF-Egfp in the Δ scy mutant was monitored (Holmes *et al.*, 2013). The Δ scy mutant has a severe developmental phenotype: colonies are smaller with a light grey pigmentation, corresponding to the production of ~10-fold fewer spores. The vegetative and aerial hyphae of Δ scy had an enhanced prevalence of branching events. Enhanced branching in vegetative hyphae lead to barbed wire-like nodes. The majority of aerial hyphae do not develop into spore chains but in the 10-15% of aerial hyphae that do, enhanced branching leads to irregularly spaced sporulation

septa and the uneven distribution of chromosomes (Holmes *et al.*, 2013). The localisation of FtsZ was also shown to be altered in the Δscy mutant, with FtsZ not forming rings in the non-sporulating aerial hyphae but long filaments parallel with the hyphal axis. The current study investigated whether SepF localised in a similar manner to FtsZ in the Δscy mutant. Characterisation of the localisation of SepF-Egfp in Δscy focused on the $\Delta scy/pMS82-2080-SepF-Egfp$ strain. The $\Delta scy/pMS82-2080-SepF-Egfp$ strain was generated prior to the complementation of $\Delta sepF$, described in Chapter 3, and contains a promoter-less *SCO2080* upstream of *sepF-egfp*. The $\Delta scy/pMS82-2080-SepF-Egfp$ strain was grown on SFM+hyg medium, next to a coverslip, and samples were visualised after >60 hrs of growth to allow the monitoring of SepF-Egfp in the aerial hyphae.

The aerial hyphae of the $\Delta scy/pMS82-2080-SepF-Egfp$ strain predominately lacked the classical curly morphology of the wild-type aerial hyphae (Figure 4.11). Instead the aerial hyphae of the $\Delta scy/pMS82-2080-SepF-Egfp$ tended to be thicker, showed frequent branching, and sometimes more complex forms, as expected in a Δscy mutant.

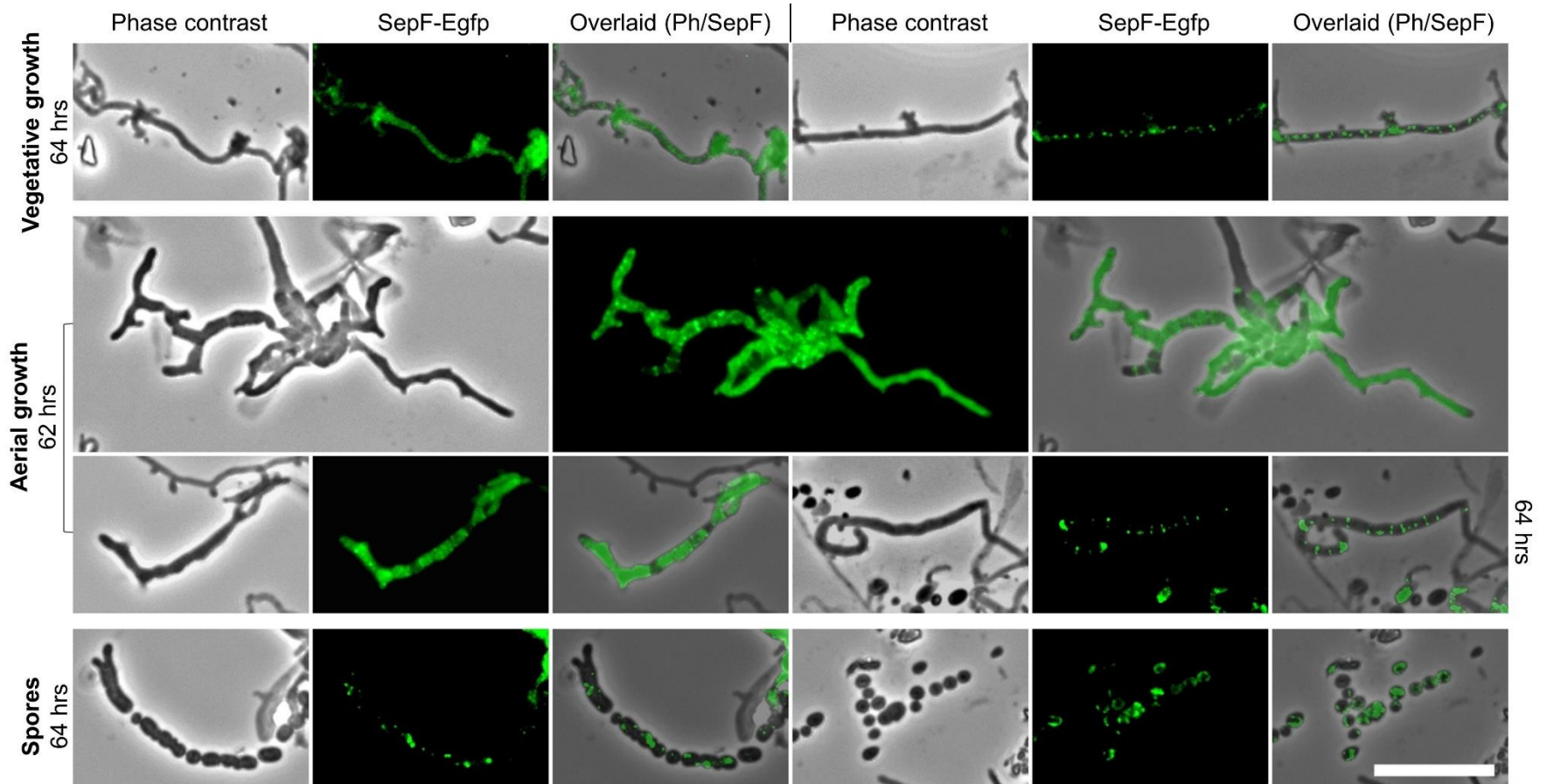


Figure 4.11 The localisation SepF-Egfp during aerial growth of $\Delta scy/pMS82$ -SepF-Egfp. The $\Delta scy/pMS82$ -SepF-Egfp strain was grown on SFM+hyg medium until the stated timepoints. All images were taken at x100 magnification and 400 ms exposure. The scale bar represents 10 μm

Throughout the 14 hr time period investigated ~85% of the aerial hyphae had strong diffuse fluorescence to the hyphal tips (Figure 4.11). In the aerial hyphae where condensation of SepF-Egfp occurred, irregular ladder-like structures were formed. The 'rungs' of the ladder-like structures were positioned very close to the hyphal tips or at unequal distances, leading to production of variably sized spores, characteristic of the Δscy mutant. The spores of the $\Delta scy/pMS82-2080$ -SepF-Egfp strain often contained fluorescent foci and lines, which were not aligned to the ends of the spores. In comparison, in M145/pMS82-SepF-Egfp SepF-Egfp is not detected at the hyphal tips and in the spores SepF-Egfp was predominately positioned perpendicular to the site of septa formation (Figure 4.2)

At the latter timepoints the vegetative hyphae of the $\Delta scy/pMS82-2080$ -SepF-Egfp strain showed similar fluorescence patterns to the aerial hyphae: fluorescence was either diffuse, spanning the width of the hyphae, or condensed into multiple foci, although the localisation of SepF-Egfp to the vegetative hyphae did not result in the formation of regular septa.

Together the localisation of SepF-Egfp in the $\Delta scy/pMS82-2080$ -SepF-Egfp strain suggests the temporal and spatial cues for the localisation of SepF is affected by the absence of Scy and the integrity of the TIPOC is affected, leading to additional branching and the bifurcation of the hyphal tips. Since the end of the current study, Scy-Egfp has been shown to localise to the hyphal tips and at regular intervals away from the tips (Kelemen, personal communication). Potentially, the SepF-FtsZ interaction excludes SepF from the hyphal tip in wild-type M145 and the SepF-Scy interaction occurs at these novel regular intervals. Furthermore, no SepF filaments resembling the FtsZ filaments previously found in the Δscy mutant, were detected, suggesting the FtsZ and SepF localisation is uncoupled in the Δscy mutant.

4.3 Summary

Bacterial cell division is a highly complex process requiring the macromolecular complex, known as the divisome, to mark the septum site. Integral to the divisome is the Z-ring, formed by the polymerisation of FtsZ. Hence, as described in Chapter 1 Introduction, the polymerisation of FtsZ is a tightly regulated process. Recently SepF was identified as a positive regulator of FtsZ in *S. coelicolor*.

Epi-fluorescent microscopy by the current study revealed SepF-Egfp and FtsZ-Egfp localise in a similar manner throughout the maturation of the aerial hyphae to individual spores in wild-type M145 (Figure 4.1 and Figure 4.2). Similar to the previously reported localisation by Grantcharova, Lustig and Flärdh, 2005 and Willemse and van Wezel, 2009, in the young aerial hyphae developing a curled morphology SepF-Egfp and FtsZ-Egfp localised diffusely. Then the aerial hyphae initiated the process of sporulation SepF-Egfp and FtsZ-Egfp condensed initially into irregular filaments then regular rings. We did not detect foci of FtsZ aligned the septa site as previously described by Willemse and van Wezel (2009) potentially due to characterisation in different strains. The rings of SepF-Egfp and FtsZ-Egfp were regularly positioned, perpendicularly to the hyphae wall, forming the 'rungs' of a ladder-like structure.

In *E. coli* the Z-ring marks the place of septum formation and aids the recruitment of late divisome proteins for the synthesis of the new cell wall (Du and Lutkenhaus, 2017; Duman *et al.*, 2015). However, FtsZ is not expected to stay once the septum is formed in *E. coli* and *B. subtilis* (Duman *et al.*, 2013; Söderström *et al.*, 2014). We show in *S. coelicolor* SepF-Egfp and FtsZ-Egfp are detectable at the septum as the spore shape changes from cylindrical to ovoid in maturing spore chains and in individual spores, potentially representing the remnants of the SepF-Egfp or FtsZ-Egfp rings (Figure 4.1 and Figure 4.2). The presence of FtsZ-Egfp and SepF-Egfp after spore maturation either represents a major difference in FtsZ and SepF turnover at the developing septum of *Streptomyces* compared to *E. coli* and *B. subtilis*, or the FtsZ-Egfp and SepF-Egfp fusions alter the turnover of these proteins.

In addition to the cell division defect, the vegetative hyphae of the $\Delta sepF$ mutant were prone (>5%) to fork-like tips. The similarity of the branching tips from the $\Delta sepF$ mutant and the Δscy mutant of Holmes *et al.*, 2013 lead to an investigation into the link between the processes of polar growth and septa

formation using a bacterial two-hybrid assay (Figure 4.10). The bacterial two-hybrid assay detected positive interactions between the C-terminal of SepF and the divisome components, SsgB, FtsZ and SepFC for self-interaction (Figure 4.4). Together with the known interaction between FtsZ and SsgB, these interactions suggest the divisome requires complex protein-protein interactions, either multi-protein assemblies or partner switching.

Fascinatingly, the bacterial two-hybrid assay also detected a positive interaction between SepFC and the TIPOC component, Scy (Figure 4.5). To our knowledge this is the first evidence of a direct link between the processes of polar growth and cell division. Positive interactions were not detected between SepFC and DivIVA or FilP suggesting the link between polar growth and cell division occurring specifically via the SepF-Scy interaction.

Two separate mutations, K46A and F71A, were introduced into SepFC based on known mutations affecting the SepF and FtsZ interaction in *B. subtilis* and *M. tuberculosis* (Duman *et al.*, 2013; Gupta *et al.*, 2005). In *B. subtilis* the F126S mutation abolished the SepF-FtsZ interaction but did not affect self-interaction or interaction with wild-type SepF (Duman *et al.*, 2013). Similarity in *Mycobacterium* the K190A mutation was functional for self-interaction but abolished the SepF-FtsZ interaction (Gupta *et al.*, 2005). While a K215S mutation reduced both the self-interaction and the SepF-FtsZ interaction.

Using the bacterial two-hybrid we showed in *S. coelicolor* the K46A mutation did not alter the self-interaction but did alter the SepF-FtsZ interaction, while the F71A mutation altered the SepFC-FtsZC, the SepFC-SsgB and the SepFC-Scy interaction (Figure 4.7 and Figure 4.8). Therefore the F71 residue of SepFC could be involved in both the SepF-Scy interaction and the SepF-FtsZ interaction, which in turn raises the question as to whether Scy and FtsZ must compete to bind to SepF. Alternatively, the F71A mutation might influence the 3D folding of SepF which in turn would affect all interactions between SepF and SepF binding partners. Overexpression and purification of SepFC-K46A and SepFC-F71A from *E. coli* confirmed neither of the mutations affected the stability of the proteins (Alcock, personal communication).

Next, the expression of SepF-Egfp and FtsZ-Egfp was investigated at the key developmental stages of vegetative growth, young aerial growth and late sporulating aerial growth, by monitoring fluorescence from total cell extracts on native PAGE gels (Figure 4.9). Interpretation of the complex banding patterns was

hampered by Covid-19 so we can only speculate these bands represent either different protein complexes or phosphorylation states.

An advantage of the protein complexes hypothesis is that in the aerial hyphae the transcription of FtsZ is known to be upregulated from the promoter, *ftsZ2p* (Flårdh *et al.*, 2002). Building on this, the increased intensity of the bands in the aerial hyphae timepoints from the M145/pMS82-FtsZ-Egfp and M145/pMS82-SepF-Egfp samples could suggest SepF transcription, like FtsZ transcription, is upregulated at the time of aerial hyphae formation.

An advantage of the phosphorylation hypothesis is two phosphorylation sites, Ser 319 and Ser 387, have already been identified for FtsZ (Manteca *et al.*, 2011; Rioseras *et al.*, 2018). Phosphorylation at Ser 319 was upregulated after 30 hrs and 65 hrs growth which overlaps with the growth periods in the current study. Building on this the bands at position * and ** which increase in intensity over time in the M145/pMS82-FtsZ-Egfp samples could reflect the two phosphorylation states of FtsZ. Therefore the lack of bands at position ** in the $\Delta sepF$ /pMS82-FtsZ-Egfp samples could suggest SepF affects the phosphorylation state of FtsZ.

Rioseras *et al.*, 2018 also detected phosphorylated SepF in the aerial hyphae of *S. coelicolor*. The presence of an unphosphorylated and phosphorylated SepF-Egfp could explain the two distinct banding positions in the M145/pMS82-SepF-Egfp samples. However the banding pattern of Δscy /pMS82-SepF-Egfp continues to be an enigma. Does the absence of Scy affect the phosphorylation of SepF? Does the Scy-SepF interaction prevent SepF from binding with additional binding partners such as the novel SsgB interaction? Future analysis of these samples will be required to establish the exact composition of the bands.

Finally the localisation of SepF was monitored in the Δscy mutant, generated by Holmes *et al.*, 2013. The Δscy mutant has a severe developmental phenotype: the light grey pigmentation of the colony corresponds to the production of ~10-fold fewer spores, the vegetative and aerial hyphae of Δscy exhibit an enhanced prevalence of branching events leading to barbed wire-like nodes and irregularly spaced sporulation septa with the uneven distribution of chromosomes (Holmes *et al.*, 2013). In the Δscy /pMS82-2080-SepF-Egfp strain, containing the pMS82-2080-SepF-Egfp construct used by Tan, 2018 to complement the $\Delta sepF$ mutant, SepF-Egfp did not regularly condense into rings (Figure 4.10 and Figure 4.11). In ~85% of aerial hyphae fluorescence from SepF-Egfp was persistently diffused and in the remaining aerial hyphae SepF-Egfp condensed to form irregular ladders leading to

variably sized spores. Hence the condensation of SepF-Egfp could be key for the production of spores in the $\Delta scy/pMS82-2080$ -SepF-Egfp strain.

Importantly the localisation pattern of SepF was distinct from the previously reported localisation of FtsZ in the Δscy mutant, where loosely curved cables of FtsZ-Egfp, running parallel to the lateral wall was detected in 80% of the aerial hyphae, suggesting that SepF and FtsZ can be de-coupled (Holmes *et al.*, 2013). Since the end of the current study, Scy-Egfp has been shown to localise to the hyphal tips and at regular intervals along the hyphae (Kelemen, personal communication). Potentially, the SepF-FtsZ interaction could exclude SepF from the hyphal tip and Scy can only interact or compete with FtsZ to interact with SepF at the novel regular intervals along the hyphae. Therefore in the Δscy mutant the decoupling on the SepF and FtsZ localisation could suggest Scy is involved the stabilisation of the cytokinetic ring. In conclusion, SepF localisation was severely affected in the Δscy mutant, supporting the novel link between SepF and Scy.

4.4 Acknowledgements

The work in the current chapter coincided but was independent from the overexpression of SepFC, mentioned in Section 4.2.2, by fellow PhD students Lucy Burrows and Emily Alcock. Prior to the current study fellow lab members, Dovile Jonylaite and Lucy Burrows, commenced plasmid generation for the bacterial two-hybrid assay and Neil Homes and Xiao Tan generated the Δscy and $\Delta scy/pMS82-2080$ -SepF-Egfp strains.

5.0 Characterising the localisation of DivIVA during the lifecycle of *S. coelicolor*

5.1 Introduction

The processes of polar growth and cell division are classically thought to be spatially and temporally separated during the lifecycle of *S. coelicolor*. Polar growth occurs at actively growing tips and branching sites. Cell division occurs behind the hyphal tips, either sporadically in the vegetative hyphae or at regular intervals in sporogenic aerial hyphae after the halt of growth. However, the novel interaction between the positive cell division regulator, SepF and the TIPOC component, Scy, detected by a bacterial two-hybrid assay in Chapter 4, indicates the two processes could be linked.

Bacterial growth is governed by cytoskeletal proteins which direct the cell wall machinery to the desired cellular location. Growth of the rod-shaped *B. subtilis* occurs at the mid-cell, by the process of lateral growth, where PG precursors are inserted into the lateral cell walls. Lateral growth is governed by the actin-like homologue, MreB which requires ATP as a co-factor to polymerise and direct the cell wall machinery (Salje *et al.*, 2011; van den Ent *et al.*, 2001). The filamentous *S. coelicolor* undergoes unidirectional tip extension due to the process of polar growth, where PG precursors are inserted at the hyphal tips. Polar growth is governed by the TIPOC. The three major components of the TIPOC, Scy, FilP and DivIVA, are all coiled-coil, intermediate filament-like proteins which do not require any co-factors for their polymerisation (Bagchi *et al.*, 2008; Flärdh 2003a; Fuchino *et al.*, 2013; Holmes *et al.*, 2013; Kelemen, 2017).

DivIVA is encoded by a 1197 bp gene at the end of the DCW cluster, transcribed downstream of *sepF* and *SCO2078*. DivIVA is the only component of the TIPOC that is essential for growth and as a family member of Wag31, DivIVA is thought to organise the PG synthesis machinery during active growth (Hempel *et al.*, 2012). In *Mycobacterium*, Wag31 directly interacts with FtsI, also known as penicillin binding protein 3, preventing heat-induced aggregation of FtsI and protecting FtsI from oxidative stress-induced proteolytic degradation (Mukherjee *et al.*, 2009). In *Streptomyces* DivIVA is found at hyphal tips and also at lateral positions where future tips are formed (Flärdh, 2003a; Hempel *et al.*, 2012).

However, DivIVA localisation studies were restricted to early growth and DivIVA localisation was not characterised throughout the developmental cycle.

Scy acts as a molecular scaffold at hyphal tips where Scy co-localises with DivIVA (Holmes *et al.*, 2013; Kelemen, 2017). The *scy* knockout mutant is severely affected in growth and produces around 10% of spores compared to the wild-type strain. Similarly to DivIVA, Scy localisation was monitored during early growth but there is no information about localisation of Scy during sporulation, where complete cell division takes place. The 10% of aerial hyphae of the *scy* knockout mutant that sporulate, form irregular septa with uneven DNA distribution amongst the spore compartments (Holmes *et al.*, 2013). This observation suggested a link between polar growth and cell division. In the previous chapter, Chapter 4, a direct interaction between SepF and Scy was demonstrated. To further characterise the link between Scy and SepF, in addition to testing the localisation of SepF-Egfp in the Δ *scy* mutant, the reverse characterisation of Scy-Egfp localisation the Δ *sepF* mutant could have been included. However, the previously used Scy-Egfp fusion showed morphological defects when used to study later developmental stages (Holmes *et al.*, 2013; Kelemen, personal communication). Hence the current chapter aimed to monitor the localisation of DivIVA, an integral protein of the TIPOC that co-localised with Scy under all conditions previously tested.

The existing DivIVA-Egfp containing strain, K112, also carries a wild-type copy of *divIVA* (Flårdh, 2003a). The K112 strain produced detectable foci during gemination at the sites of active growth and in the vegetative mycelium at hyphal tips and branching points. But the K112 strain did not readily sporulate under the conditions of the current study, suggesting that this strain is not suitable for studying DivIVA localisation during sporulation (Kelemen, personal communication).

Foci marking future branching sites tended to be positioned on the inside of the outer edge of a curving hyphae, suggesting DivIVA prefers negatively curved surfaces in *S. coelicolor* (Hempel *et al.*, 2008). The ability of DivIVA to bind negatively curved surfaces was also noted in *B. subtilis*, when DivIVA acts as a cell-pole targeting protein in the Min system of the vegetative cells (Jamroškovič *et al.*, 2012; Lenarcic *et al.*, 2009). During cell division, the Min system of *B. subtilis* prevents the formation of Z-rings at the poles by controlling the localisation of the MinCD complexes (Levin *et al.*, 1992; Rowlett and Margolin, 2015). Separately in sporulating cells of *B. subtilis*, DivIVA interacts with the chromosome segregation machinery at the poles to aid the positioning of the *oriC* region, prior to division

(Thomaides *et al.*, 2001). Hence the ability of DivIVA to be involved in two distinct mechanisms during bacterial development is not unprecedented.

The current chapter aimed to monitor the fate of the TIPOC during the transition from growth to cell division and sporulation to address at what spatial location the direct link established between Scy and SepF could possibly take place. As mentioned, polar growth occurs at actively growing hyphal tips and cell division occurs after active growth stops within the aerial hyphae. Therefore the spatial and temporal localisation of the interaction between SepF and Scy was questioned. Instead of monitoring Scy, the current chapter aimed to monitor the localisation of DivIVA throughout development of the wild-type M145 and $\Delta sepF$ strains. This broad aim was broken down into several objectives:

- To generate novel DivIVA-Egfp constructs for the visualisation of DivIVA in the vegetative and aerial hyphae of the wild-type and $\Delta sepF$ strains.
- To characterise the expression of DivIVA-Egfp in the vegetative and aerial hyphae of the wild-type and $\Delta sepF$ strains.

5.2 Results

5.2.1 Generating constructs for monitoring DivIVA-Egfp

The novel link between polar growth and cell division, discussed in Chapter 4, occurred through the interaction of SepF with Scy. As SepF was the focus of Chapter 3, the current chapter focuses on the essential TIPOC member, DivIVA, controlling polar growth. To investigate the localisation of DivIVA in the aerial hyphae and particularly during sporulation the current study generated two novel DivIVA-Egfp constructs that introduce the fluorescent protein fusion into *Streptomyces in trans*.

The DivIVA-Egfp fusion of the previous K112 strain was introduced by a single homologous recombination event at the *divIVA* locus so the K112 strain carries both the *divIVA-egfp* fusion and the native *divIVA*. Generation of the K112 strain utilised the non-replicative plasmid, pKF59, carrying the *divIVA-egfp* fusion and 98 bp upstream of the *divIVA* translation start. When pKF59 integrates at the *divIVA* locus via homologous recombination, expression of the *divIVA-egfp* fusion will take place from the native promoter(s) present within the DCW cluster. Then the native copy of *divIVA* will be transcribed downstream of the *divIVA-egfp* fusion, the associated vector DNA and a 98 bp sequence still positioned upstream of *divIVA*. Large scale RNAseq data identified a promoter for *divIVA* 184 bp upstream of the translational start (Jeong *et al.*, 2016). The position of the promoter suggests the previously used pKF59 derivatives will not express the native *divIVA* from the native promoter(s) and the expression of *divIVA* was likely from the promoter activity of the vector. Under the conditions of the current study, the M145/pKF59 integrant, K112, was unable to undergo regular sporulation (Kelemen, personal communication).

Hence, the current study aimed to generate novel constructs that integrated *in trans*, at the Φ BT1 attB integration site within *SCO4848*, leaving the native site intact for *divIVA* expression (Gregory *et al.*, 2003). Two novel DivIVA-Egfp constructs differing only in the size of the region upstream of *divIVA*, were generated and introduced *in trans*. Similarly to the complementation of the Δ *sepF* mutant, the upstream regions of the two DivIVA-Egfp containing constructs was informed by large-scale RNA seq data which identified either one or two transcription start points for *divIVA* (Jeong *et al.*, 2016; Romero *et al.*, 2014). The smaller pMS82-DivIVA-Egfp construct contained a 267 bp upstream region of the translation start of *divIVA* and one potential transcription start point. The second larger pMS82-2078-DivIVA-Egfp construct contained a 642 bp upstream region of

the translation start of *divIVA*, which included two potential transcription start points and the upstream gene, *SCO2078* (Figure 5.1).

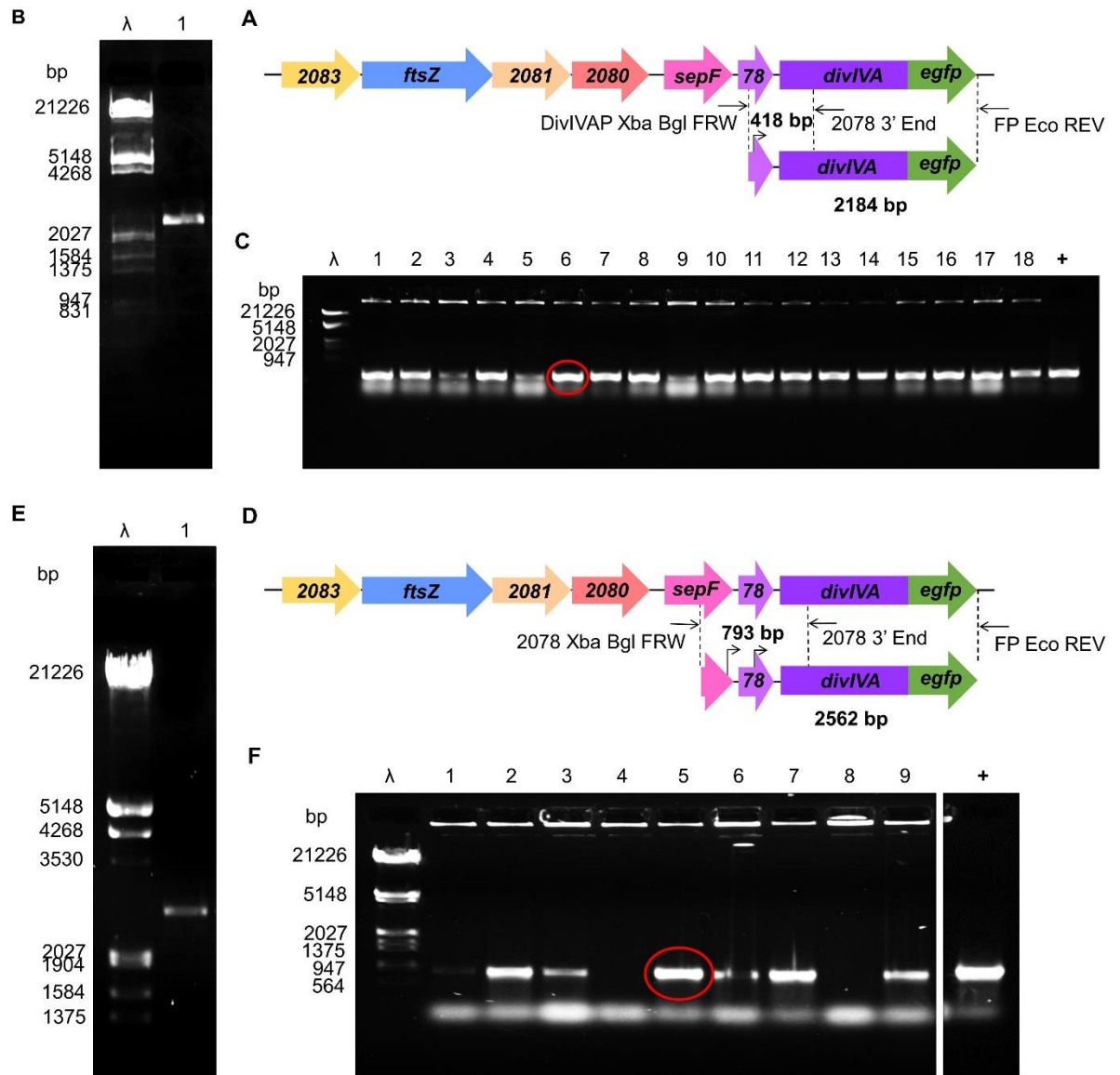


Figure 5.1 Generation of the DivIVA-Egfp constructs. The smaller 2184 bp DivIVA-Egfp fragment (top panel) and the larger 2562 bp 2078-DivIVA-Egfp fragment (bottom panel) contained one or two promoters identified by Jeong *et al.* (2016). A) and D) The fragments were amplified using 4A10-DivIVA-Egfp as a template and the primer, FP Eco REV with either DivIVAP Xba Bgl FRW or 2078 Xba Bgl FRW. B) and E) The PCR products were analysed on 0.7% agarose gels. The fragments were ligated into the pMS82 vector then the ligations were transformed into *E. coli* DH5α. C) and F) Colony PCRs using the primer, 2078 3' end, with either DivIVAP Xba Bgl FRW or 2078 Xba Bgl FRW were used to analyse the *E. coli* DH5α transformants. The PCR products were analysed on a 1% agarose gel. Lanes λ) λ DNA digested with *EcoRI* and *HindIII*. Lane 1 to 18 (C) or Lane 1 to 9 (F) potential transformants and lanes +) the PCR products using 4A10 as a template. The colony PCR for DivIVA-Egfp identified 18 positive colonies and the colony PCR for 2078-DivIVA-Egfp identified 6 positives. Colonies, #6 and #5, were used in future experiments (red circle).

The two DivIVA-Egfp constructs, pMS82-DivIVA-Egfp and pMS82-2078-DivIVA-Egfp, were generated via blunt-end cloning. Initially the two DivIVA-Egfp fragments were amplified using the 4A10-DivIVA-Egfp cosmid as a template and fragment specific primer pairings (Figure 5.1A and Figure 5.1D). The 4A10-DivIVA-Egfp cosmid was previously generated in the Kelemen laboratory using the REDIRECT technology modified for knocking in *egfp* downstream of *divIVA*. The PCR products were gel-purified and phosphorylated. Then the phosphorylated fragments were extracted and analysed on diagnostic agarose gels (Figure 5.1B and Figure 5.1E). For each fragment one band at the expected size was detected, confirming the successfully generated of both fragments.

The two fragments were separately ligated into the dephosphorylated pMS82-*EcoRV* vector, described in Section 3.3.4.1. After the ligation, the mixes were transformed into *E. coli* DH5 α cells, made chemically competent. Successful transformants were selected for using hygromycin then confirmed by low-fidelity colony PCRs (Figure 5.1C and Figure 5.1F). The colony PCRs aimed to amplify the upstream regions of the DivIVA-Egfp fragments, using DNA released from the transformant as a template and fragment specific primer pairings. Of the colonies tested, several produced a PCR product at the expected size and one representative for each construct was picked (#6 and #5 in the red circles). Both colonies underwent a large-scale plasmid preparation and the isolated plasmids were sequenced to confirm the absence of any mutations.

The confirmed pMS82-DivIVA-Egfp #6 and pMS82-2078-DivIVA-Egfp #5 constructs were passed through the methylation deficient *E. coli* ET12567:pUZ8002 strain. Successful *E. coli* ET12567:pUZ8002 transformants allowed the conjugation of pMS82-DivIVA-Egfp #6 and pMS82-2078-DivIVA-Egfp #5 into the wild-type M145 and Δ *sepF* strains. The conjugation plates were overlaid with nalidixic acid and hygromycin to select for colonies of *S. coelicolor* containing the pMS82 derivatives. Exconjugants were streaked for single colonies followed by confluent plating and spore stock generation.

5.2.2 Localisation of *DivIVA-Egfp* in the vegetative hyphae of *M145/pMS82-DivIVA-Egfp*

The introduction of pMS82-*DivIVA-Egfp* and pMS82-2078-*DivIVA-Egfp* into the wild-type M145 strain did not visually affect the morphology of the colonies, suggesting both strains were able to undergo sporulation (data not shown). Epi-fluorescent microscopy of the *DivIVA-Egfp* containing strains, grown along a coverslip, showed the vegetative hyphae of M145/pMS82-*DivIVA-Egfp* had fluorescent foci at the hyphal tip and at multiple sub-apical positions (Figure 5.2 top panel). However the vegetative hyphae of M145/pMS82-*DivIVA-Egfp* were prone to branching events close to the hyphal tip, indicating the presence of only one promoter for *divIVA* was insufficient to maintain the integrity of the TIPOC (Figure 5.2 bottom panel). Therefore the pMS82-2078-*DivIVA-Egfp* containing strains are focused on for the rest of the chapter. In Section 5.2.3 the localisation of *DivIVA-Egfp* throughout the lifecycle of M145/pMS82-2078-*DivIVA-Egfp* was investigated (Figure 5.3 to Figure 5.10) followed by the localisation of *DivIVA-Egfp* in the vegetative and aerial hyphae of $\Delta sepF$ /pMS82-2078-*DivIVA-Egfp* (Figure 5.11 to Figure 5.13).

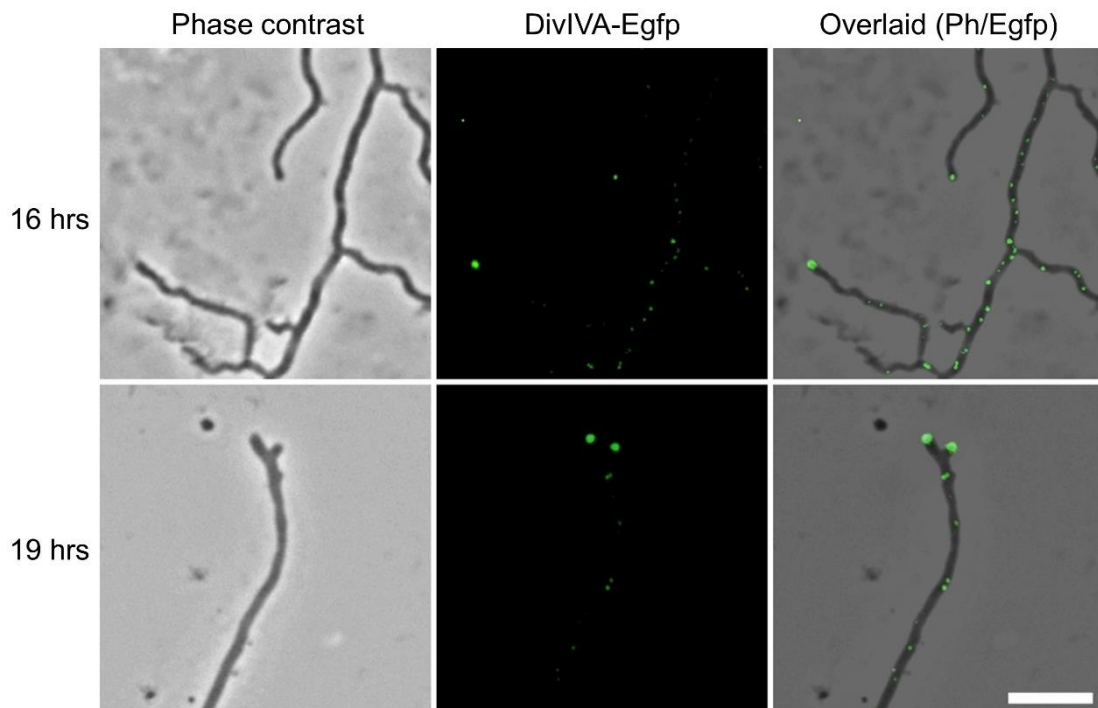


Figure 5.2 Characterisation of vegetative growth from M145/pMS82-*DivIVA-Egfp*. All images were taken under x100 magnification with an exposure of 400 ms. The phase contrast image (left) is shown alongside the fluorescent image (middle) and both images are overlaid (right). The scale bar represents 5 μ m.

5.2.3 The localisation of DivIVA-Egfp throughout the lifecycle of S. coelicolor

5.2.3.1 Characterising the germination of spores from M145/pMS82-2078-DivIVA-Egfp

The spores of the M145/pMS82-2078-DivIVA-Egfp strain had detectable fluorescence prior to swelling. Spores of M145/pMS82-2078-DivIVA-Egfp were plated onto SFM+hyg medium covered with cellophane and incubated, when appropriate at 30°C. At the stated timepoint a square of cellophane was cut from the plate and viewed using epi-fluorescence microscopy. Prior to incubation, at 0 hrs, ~50% of spores had clear fluorescent foci but the percentage of spores containing DivIVA-Egfp could be higher due to the obstructing rapid movement of spores in the 20% glycerol required for slide generation (Figure 5.3). Among the spores with detectable fluorescence, ~50% had one foci, ~35% had two foci and ~5% had either of the rare three foci or four foci. As DivIVA is essential for marking the location of polar growth, the foci were expected to represent the number of germ tubes to be produced during germination.

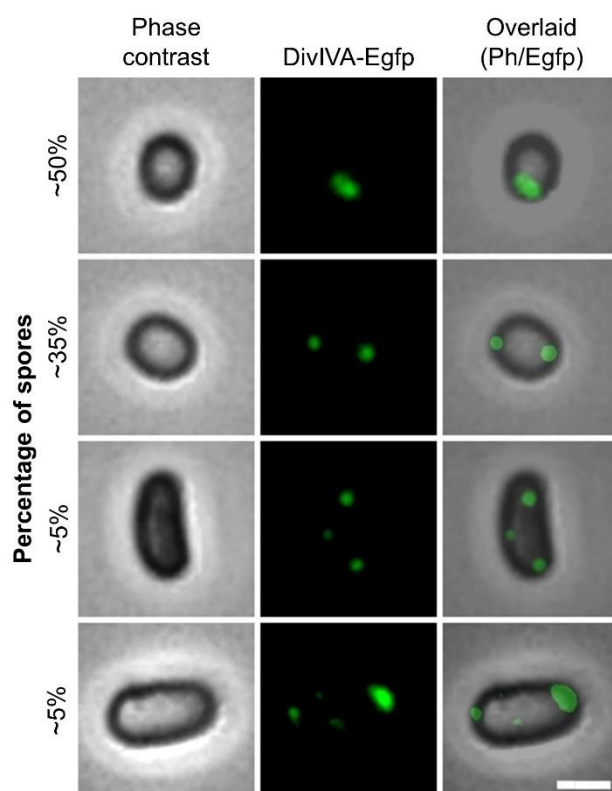


Figure 5.3 Characterisation of spores from M145/pMS82-2078-DivIVA-Egfp. Spores were imaged prior to growth. Top row) spore with one foci representing ~50% of total spores with detectable fluorescence. Second row) spore with two foci representing ~35% of total spores. Third row) spore with three foci. Fourth row) spore with four foci. The third and fourth row represent ~5% of total spores. Images were taken under x100 magnification with an exposure of 400 ms. The phase contrast image (left) is shown alongside the fluorescent image (middle) and both images are overlaid (right). The scale bar represents 1 μ m.

The spores of M145/pMS82-2078-DivIVA-Egfp swelled prior to germ tube emergence. After 0 hrs, 4 hrs and 6 hrs of incubation ~300 spores were visualised and measured along the longitudinal axis and the perpendicular axis, positioned at right angles to one another, using Fiji (2012). Prior to incubation, at 0 hrs, the mean longitudinal length of the spores was $1.22 \mu\text{m} \pm \text{SE } 0.01$ and the mean perpendicular length was $1.03 \mu\text{m} \pm \text{SE } >0.01$. Hence the longitudinal length of spores prior to swelling corresponded closely to the mean reported distance between sporulation septa in the aerial hyphae of the wild-type strain at $1.2 \mu\text{m}$ (Kaur, 2018). After 4 hrs of incubation the mean longitudinal length of spores had increased to $1.33 \mu\text{m} \pm \text{SE } 0.02$ and the mean perpendicular length of spores had increased to $1.13 \mu\text{m} \pm \text{SE } 0.01$. After 6 hrs of incubation the mean longitudinal length of spores had further increased to $1.65 \mu\text{m} \pm \text{SE } 0.01$ and the perpendicular

length of spores had further increased to $1.44 \mu\text{m} \pm \text{SE } 0.01$. At 6 hrs of incubation ~45% of spores had formed germ tubes.

The swollen spores of M145/pMS82-2078-DivIVA-Egfp produced germ tubes in a step wise manner. Every hour between 6 hrs and 10 hrs of incubation ~500 spores were classified into 5 classes: 'no germ tube; pre-swelling', 'no germ tube; post-swelling', 'swollen with 1 germ tube', 'swollen with 2 germ tubes' and 'swollen with 3 germ tubes' (Figure 5.4). Over the 4 hr time period of investigation the number of spores in the first two classes decreased but spores with no identifiable germ tubes were detected throughout. After 10 hrs of growth 14% of spores lacked identifiable germ tubes. Amongst the germinating spores, the class of 'swollen with 1 germ tubes' remained dominant. The classes of 'swollen with 2 germ tubes' and 'swollen with 3 germ tubes' increased throughout the investigation but remained unexpectantly low. These observations suggest germ tubes were produced in a stepwise manner and the emergence of the second germ tube was slow.

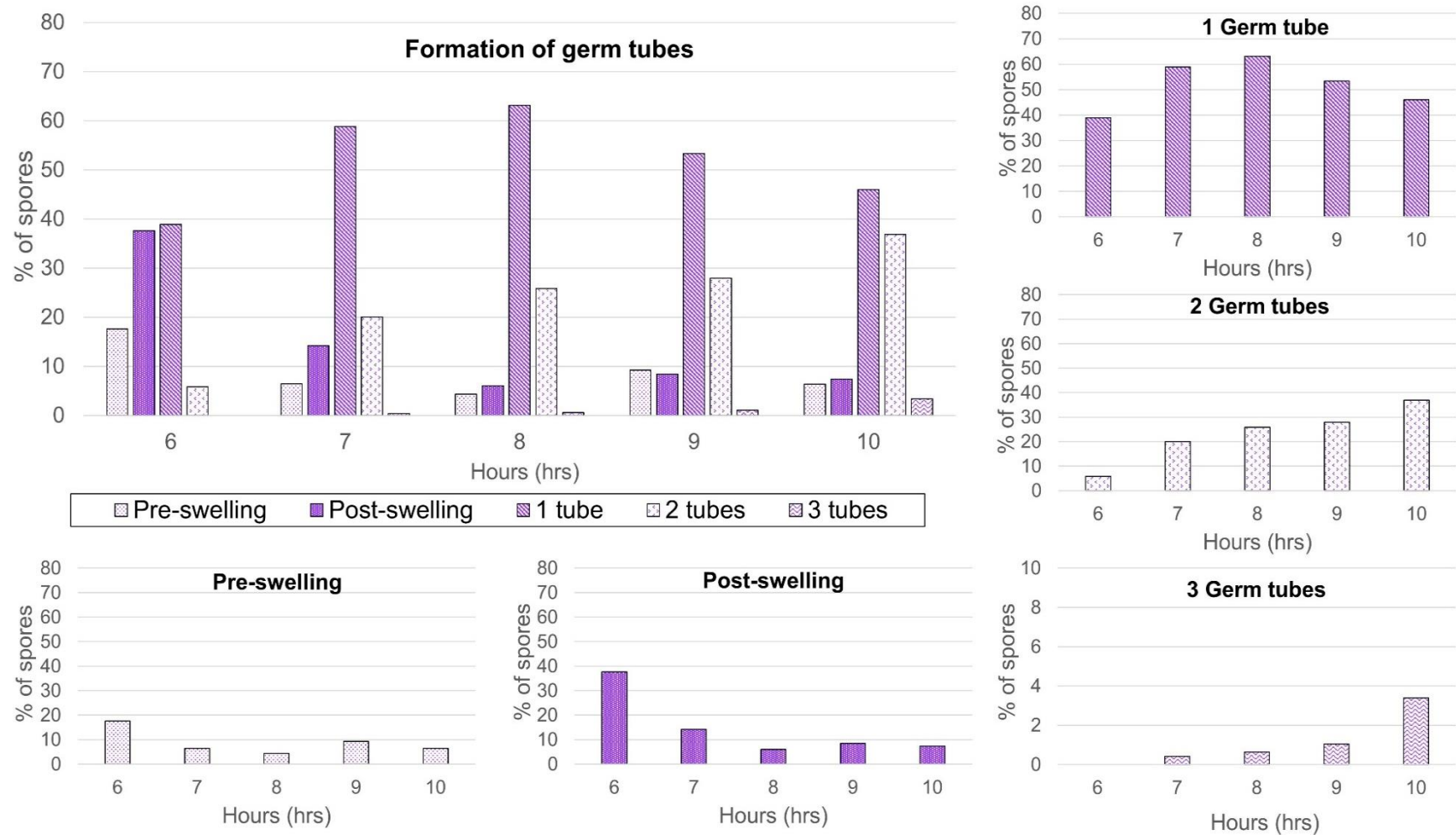


Figure 5.4 Germ tube production of the spores from M145/pMS82-2078-DivIVA-Egfp. Spores were incubated on SFM+hyg medium, covered by a cellophane and were incubated at 30°C until the stated timepoints. At each timepoint ~ 500 spores were visualised at x100 magnification and categorised into 5 classes using Fiji, 2012. The classes were: no germ tube 'Pre-swelling', no germ tube 'Post-swelling' and swollen with '1 Germ tube', '2 Germ tubes' or '3 Germ tubes'. The top left graph shows all the classes combined. The '3 Germ tubes' graph has a smaller scale on the y-axis.

Next the localisation of DivIVA-Egfp was monitored throughout germination, using the same samples. Between 0 hrs, prior to incubation, and 4 hrs, prior to germination the localisation of DivIVA-Egfp in the spores of M145/pMS82-2078-DivIVA-Egfp was highly similar (Figure 5.5). After 5 hrs of incubation, >5% of spores had commenced formation of germ tubes. The young germ tubes had fluorescent foci at the hyphal tips as previously described by Flärdh (2003a). Interestingly, foci at the tip were stronger than additional foci, which were usually positioned on the opposite side of the spore (Arrows on Figure 5.5). This observation suggests that whilst the smaller fluorescent foci marked the sites of germ-tube emergence, once the germ tubes were established, further DivIVA accumulation was required for maintaining polar growth at the tip of the germ-tubes.

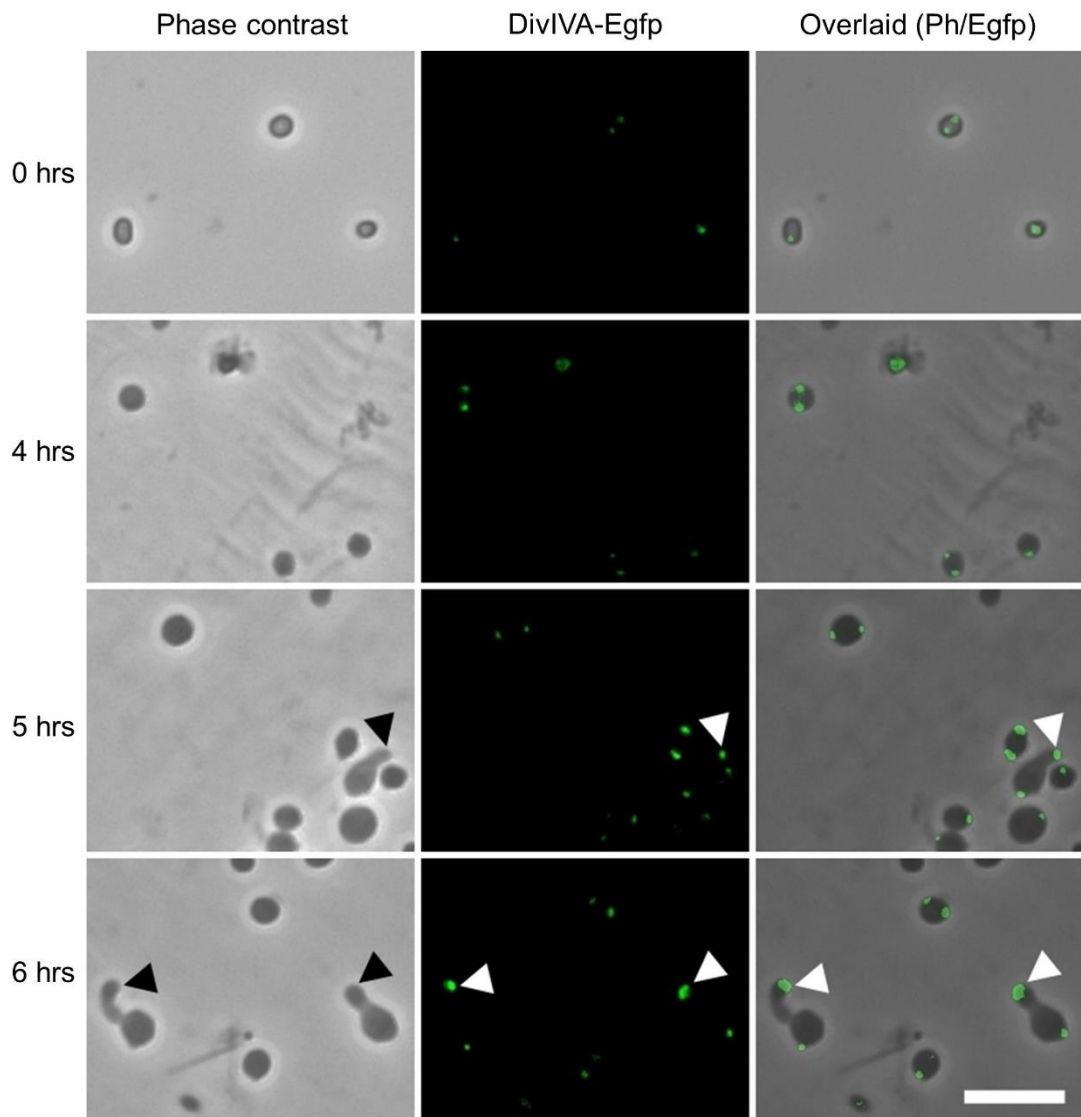


Figure 5.5 Characterisation of the early germination of M145/pMS82-2078-DivIVA-Egfp. Spores were inoculated on SFM+hyg medium, covered by a cellophane and were incubated at 30°C until the timepoints stated. The arrows indicate foci at the tip of germ tubes. All images were taken under x100 magnification with an exposure of 400 ms. The phase contrast image (left) is shown alongside the fluorescent image (middle) and both images are overlaid (right). The scale bar represents 5 μ m.

After 7 hrs of incubation a few of the actively growing germ tubes had individual sub-apical fluorescent foci (Figure 5.6). These sub-apical foci could mark future branching sites as similarly positioned branches were identified from 8 hrs of growth. After 10 hrs of growth the young vegetative hyphae of M145/pMS82-2078-DivIVA-Egfp exhibited one strong focus at the hyphal tip often with multiple sub-apical foci. The latter localisation pattern was similar to the pattern detected in M145/pMS82-DivIVA-Egfp (Figure 5.2 and Figure 5.6). The large number of sub-apical foci has not been previously documented but was observed reproducibly. The function of these multiple DivIVA foci along the vegetative hyphae remains unclear as the number and regular positioning of these foci questions whether they in fact lead to branching events.

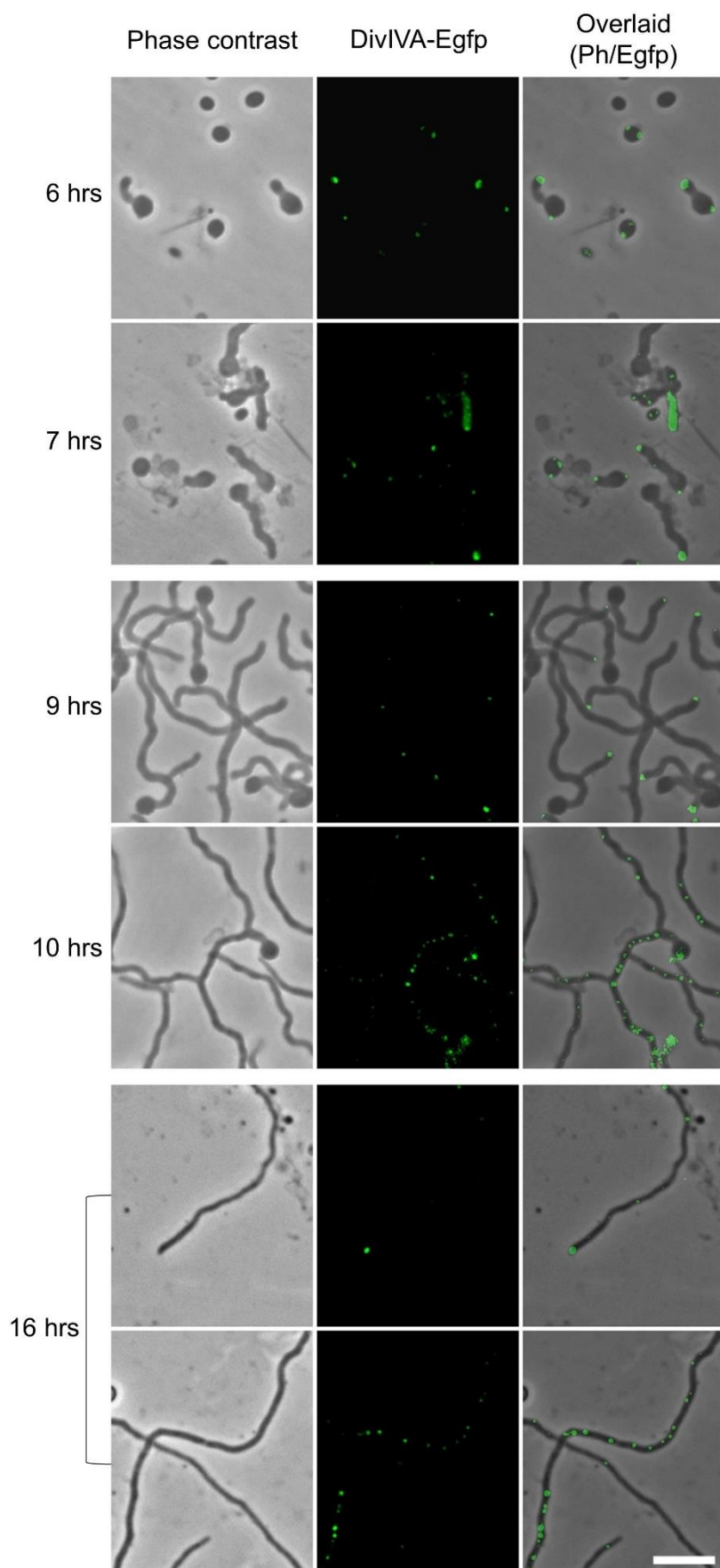


Figure 5.6 Characterisation of early vegetative growth from M145/pMS82-2078-DivIVA-Egfp. Spores were inoculated on SFM+hyg medium, covered by a cellophane and were incubated at 30°C until the timepoints stated. All images were taken under x100 magnification with an exposure of 400 ms. The phase contrast image (left) is shown alongside the fluorescent image (middle) and both images are overlaid (right). The scale bar represents 5 μ m.

5.2.3.2 Characterising the localisation of DivIVA-Egfp during the aerial growth of M145/pMS82-2078-DivIVA-Egfp

The grey sporulation pigment on the surface of colonies from the M145/pMS82-2078-DivIVA-Egfp strain indicated colonies of M145/pMS82-2078-DivIVA-Egfp underwent sporulation. Therefore the localisation of DivIVA-Egfp in the aerial hyphae of M145/pMS82-2078-DivIVA-Egfp, grown along a sterile coverslip, was investigated using epi-fluorescence microscopy.

Fascinatingly, the localisation of DivIVA-Egfp in the aerial hyphae of M145/pMS82-2078-DivIVA-Egfp, grown on SFM and MMM medium, was similar to the localisation of DivIVA-Egfp in the actively growing vegetative hyphae (Figure 5.7 to Figure 5.9). The SFM media is a nutrient rich ill-defined medium while the MMM media is a well-defined nutrient restricted medium, hence growth on the two media occurs under two distinct nutrient conditions.

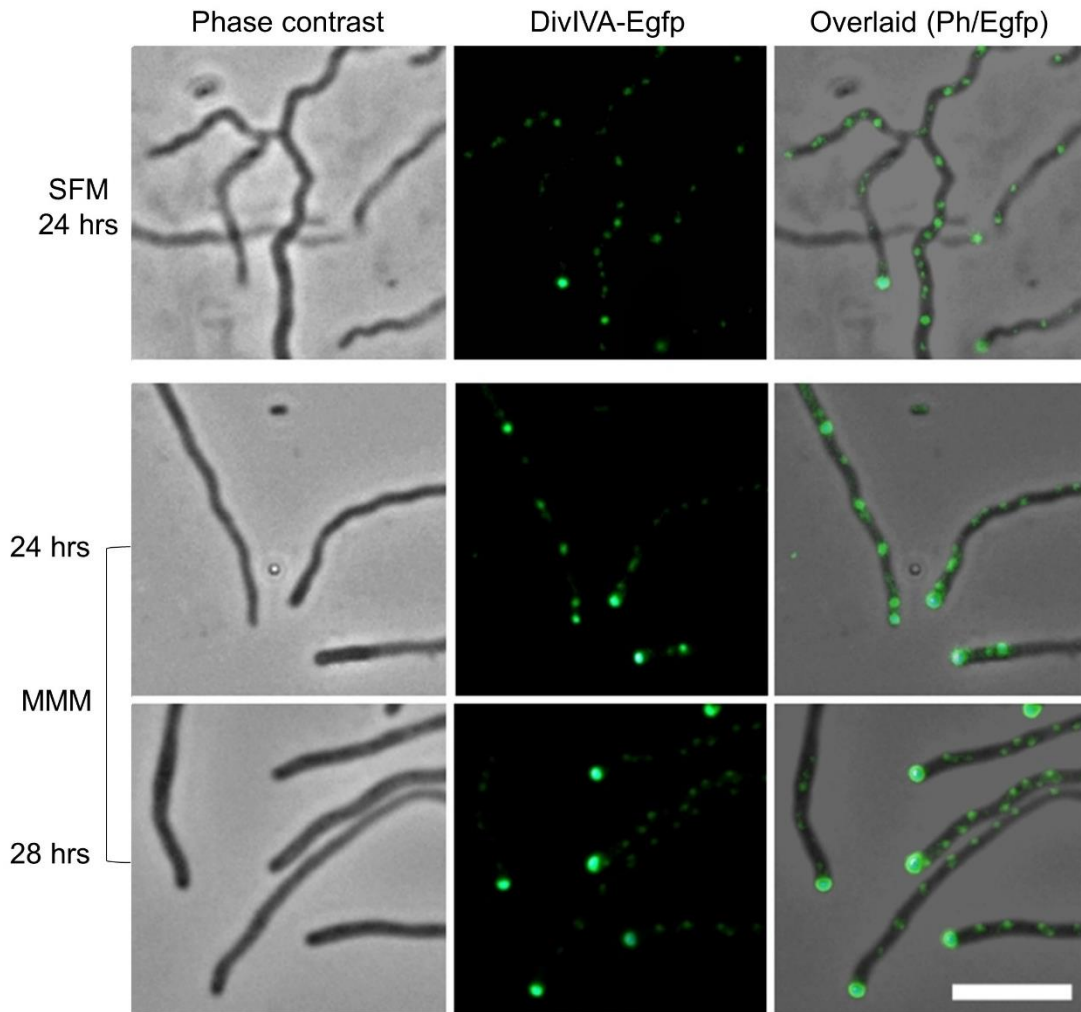


Figure 5.7 Characterisation of later vegetative growth from M145/pMS82-2078-DivIVA-Egfp. Spores were inoculated on medium containing hyg and were incubated at 30°C for the stated timepoints. All images were taken under x100 magnification with an exposure of 400 ms. The phase contrast image (left) is shown alongside the fluorescent image (middle) and both images are overlaid (right). The scale bar represents 2.5 μm .

Initially in the young curved aerial hyphae of M145/pMS82-2078-DivIVA-Egfp, grown on SFM and MMM medium, DivIVA-Egfp localised at the hyphal tip (Figure 5.8). Then as the aerial hyphae matured, additional sub-apical foci were positioned in a regular zig-zag pattern (Figure 5.8 and Figure 5.9). The sub-apical foci did not show a preference for negatively curved surfaces, clearly did not mark future branching sites and were found before any sign of septation.

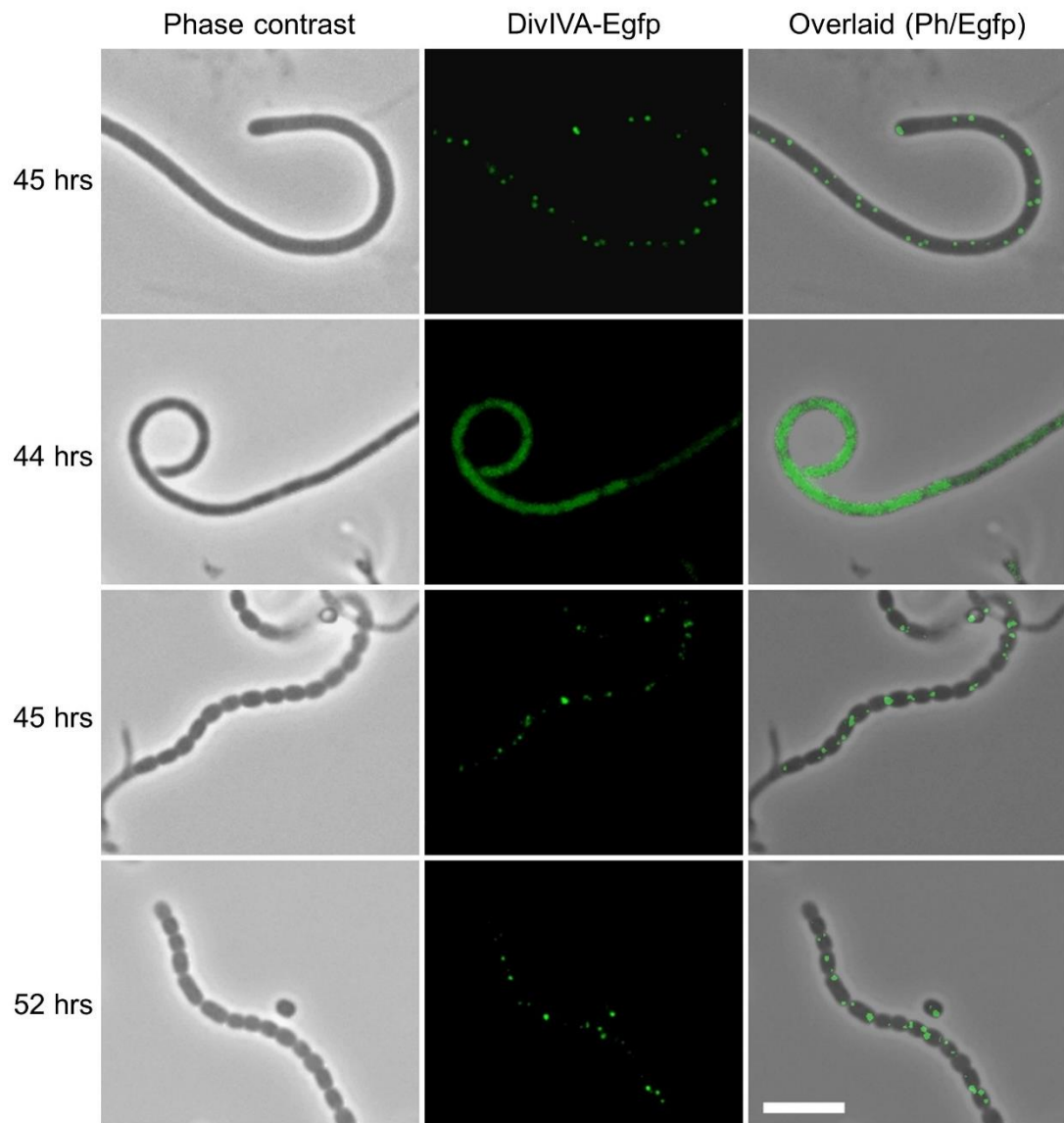


Figure 5.8 Characterisation of aerial growth from M145/pMS82-2078-DivIVA-Egfp on SFM medium. Colonies of M145/pMS82-2078-DivIVA-Egfp were incubated on SFM+hyg medium until the stated timepoints. Images were taken under x100 magnification with an exposure of 400 ms. The phase contrast image (left) is shown alongside the fluorescent image (middle) and both images are overlaid (right). The scale bar represents 5 μ m.

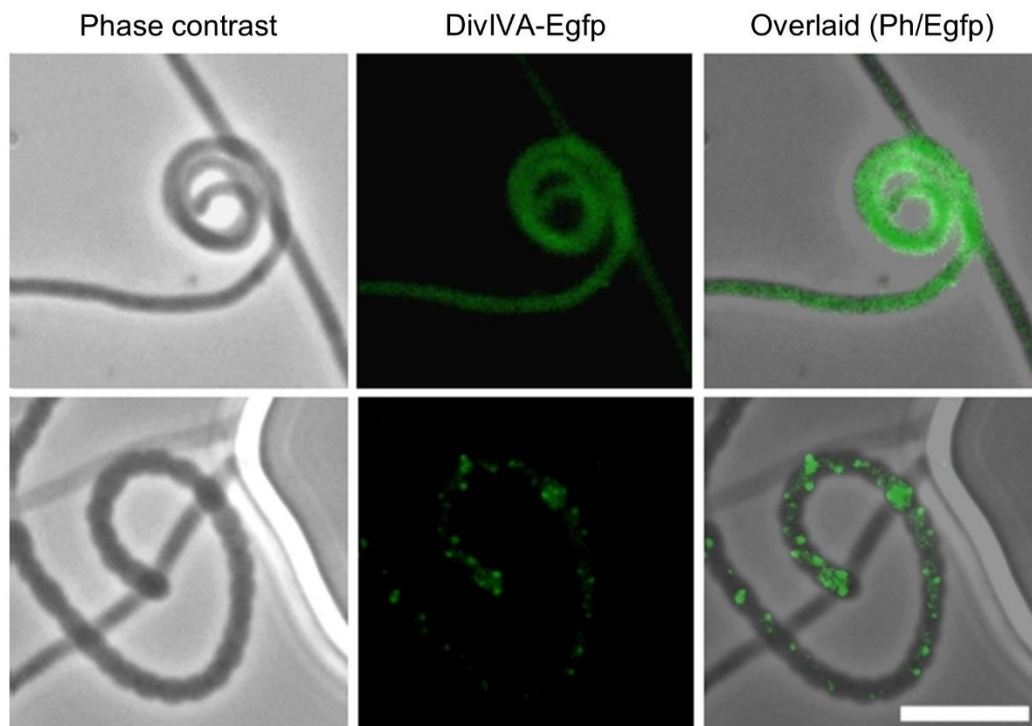


Figure 5.9 Characterisation of aerial growth from M145/pMS82-2078-DivIVA-Egfp on MMM medium. Colonies of M145/pMS82-2078-DivIVA-Egfp were incubated on MMM+hyg medium for 43.5 hrs. Images were taken under x100 magnification with an exposure of 400 ms. The phase contrast image (left) is shown alongside the fluorescent image (middle) and both images are overlaid (right). The scale bar represents 5 μ m.

In several hyphae DivIVA-Egfp localised diffusely in the curling tips, and it is not clear whether this pattern of DivIVA localisation represents an intermediate stage before re-condensing (Figure 5.8 and Figure 5.9). As the cell wall shows signs of pinching after septation, at these sites of cell division DivIVA foci are clearly visible. Often two foci were found slightly off-set from one another on either side of the septum, each spore carrying two fluorescent foci at opposing positions. The two foci in the developing spores resembled the pattern of DivIVA localisation in the spores prior to germination.

To establish if DivIVA is localised at developing septa, the red fluorescent, Wheat Germ Agglutinin Alexa Fluor™ 647 conjugate (WGA-Alexa647 conjugate) which conjugates to stain new cell wall synthesis at the septa was used (Figure 5.10). Again two DivIVA-Egfp foci were detectable slightly off-set from one another on either side of the septum. Therefore the localisation of DivIVA-Egfp in the aerial hyphae of M145/pMS82-2078-DivIVA-Egfp was dynamic and highly complex. Importantly DivIVA-Egfp localised to sites of cell division suggesting the interaction between polar growth and cell division proteins could occur at the developing septum.

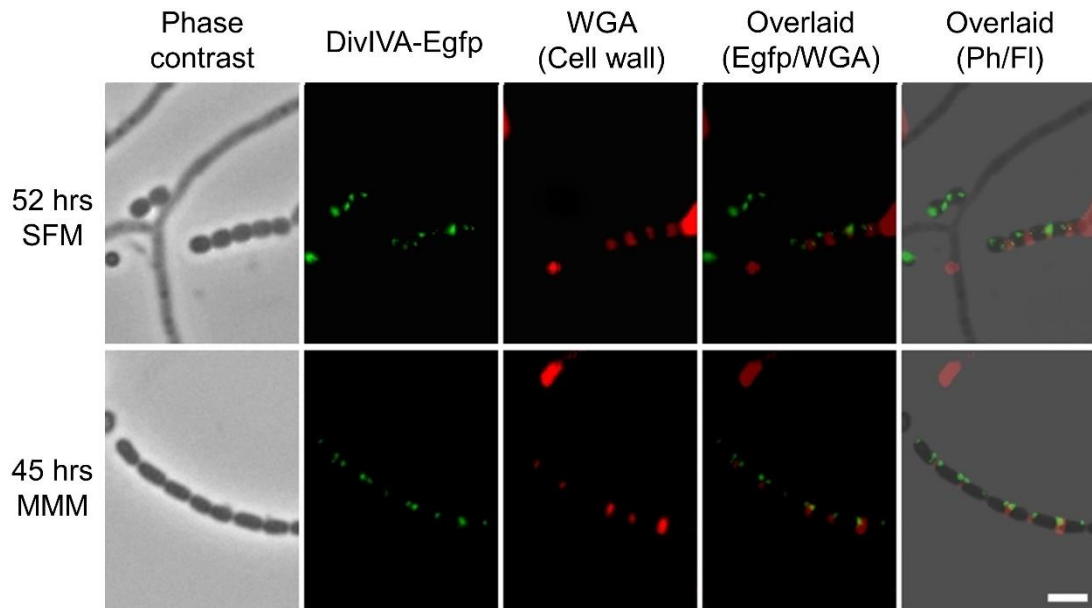


Figure 5.10 Characterisation of sporulation from M145/pMS82-2078-DivIVA-Egfp. Colonies of M145/pMS82-2078-DivIVA-Egfp were incubated on medium containing hygromycin until the stated timepoints. Images were taken under x100 magnification with an exposure of 400 ms. From left to right the image order is: the phase contrast image, the fluorescent DivIVA-Egfp image, the fluorescent WGA-Alexa647 conjugate image, the fluorescent images overlaid, and all three images overlaid. The scale bar represents 2 μm .

5.2.3.3 Characterising the localisation of DivIVA-Egfp during the aerial growth of ΔsepF /pMS82-2078-DivIVA-Egfp

As DivIVA-Egfp localised to sporulation septa in the aerial hyphae of M145/pMS82-2078-DivIVA-Egfp, the localisation of DivIVA-Egfp in the aerial hyphae of ΔsepF was monitored. The ΔsepF mutant is unable to form both regular vegetative cross-walls and sporulation septa. Plus the integrity of the TIPOC in the ΔsepF mutant was thought to be somewhat reduced due to the increased presence of a fork-like morphology in >5% of tips.

The pMS82-2078-DivIVA-Egfp construct was conjugated into ΔsepF for the generation of the ΔsepF /pMS82-2078-DivIVA-Egfp strain, as previously described for the M145/pMS82-2078-DivIVA-Egfp strain. The ΔsepF /pMS82-2078-DivIVA-Egfp strain was indistinguishable from ΔsepF (data not shown). Therefore The ΔsepF /pMS82-2078-DivIVA-Egfp strain was grown on SFM+hyg and MMM+hyg media for characterisation. As mentioned above, the SFM media is a nutrient rich ill-defined medium while the MMM media is a well-defined nutrient restricted medium. Growing the ΔsepF /pMS82-2078-DivIVA-Egfp strain on the two media should allow the characterisation of DivIVA-Egfp localisation under two distinct nutrient conditions

which could alter the formation of fork-like tips as previously observed for the Δscy strain (Kelemen, personal communication). The $\Delta sepF/pMS82-2078-DivIVA-Egfp$ strain was grown along a coverslip and visualised using epi-fluorescent microscopy, as previously completed for the M145/pMS82-2078-DivIVA-Egfp strain.

Similar to M145/pMS82-2078-DivIVA-Egfp, the vegetative hyphae of $\Delta sepF/pMS82-2078-DivIVA-Egfp$ had fluorescent foci at the tips, future branching points, and at regular sub-apical positions (Figure 5.11). Intriguingly at the fork-like over-branching tips, characteristic of a $\Delta sepF$ mutant, multiple fluorescent foci were found (Figure 11 bottom row). This observation suggests that the patches of DivIVA-Egfp at the tip aid the development of extra branching points and split-tips in the $\Delta sepF$ mutant.

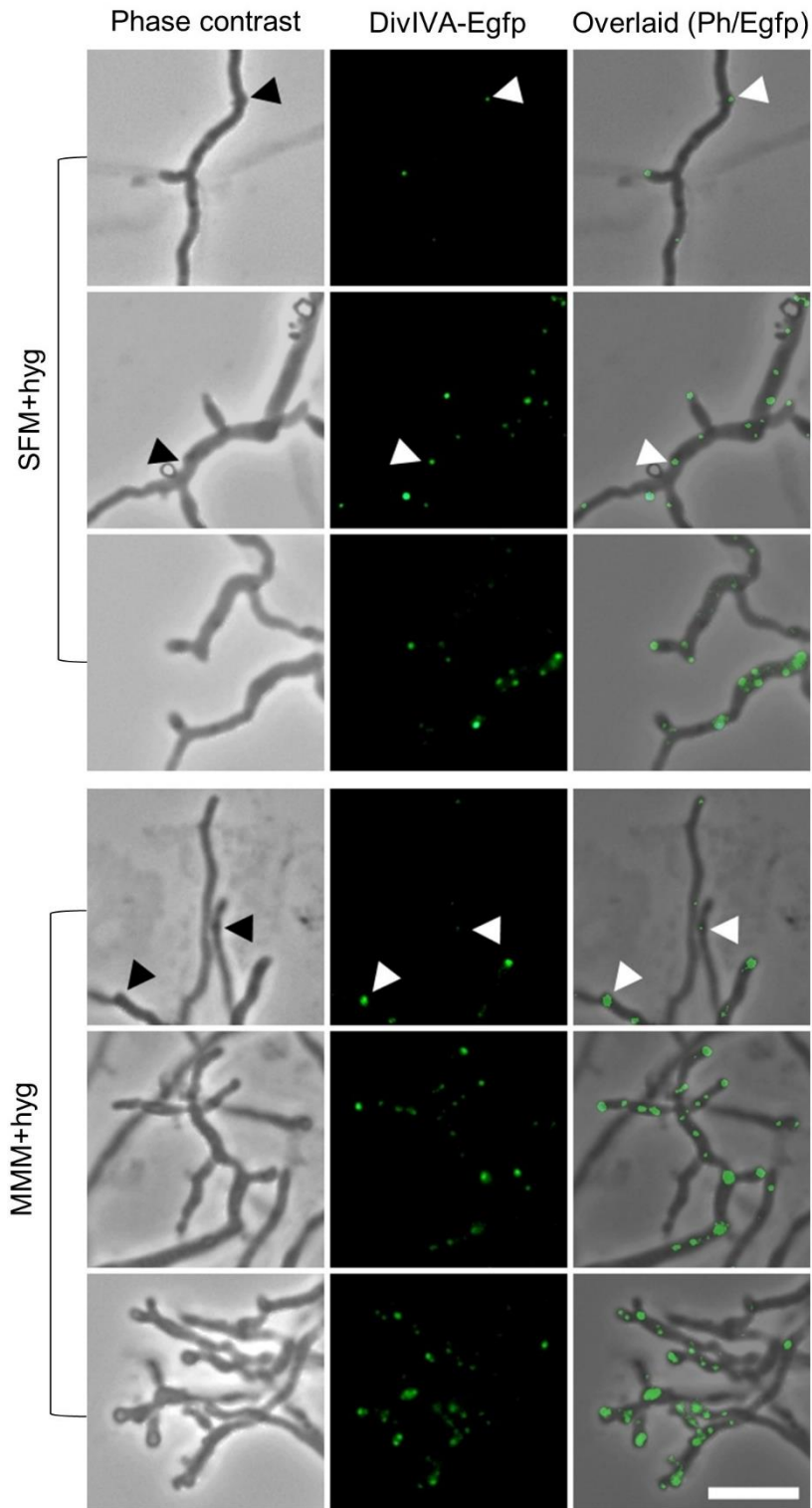


Figure 5.11 Characterisation of vegetative growth from $\Delta sepF/pMS82-2078-DivIVA-Egfp$. Colonies of $\Delta sepF/pMS82-2078-DivIVA-Egfp$ were incubated on the stated media for 77 hrs. The arrows indicate potential branching sites. Images were taken under x100 magnification with an exposure of 400 ms. The phase contrast image (left) is shown alongside the fluorescent image (middle) and both images are overlaid (right). The scale bar represents 5 μm .

The aerial hyphae of the $\Delta sepF/pMS82-2078-DivIVA-Egfp$ strain were less prone to additional branching events than the Δscy strain and as expected for a $\Delta sepF$ mutant, no regular sporulation took place. Despite the inability of the $\Delta sepF/pMS82-2078-DivIVA-Egfp$ strain to form uniform oval spores, fluorescence in the aerial hyphae of $\Delta sepF/pMS82-2078-DivIVA-Egfp$ became diffuse and spanned the curled tips, similar to the aerial hyphae of $M145/pMS82-2078-DivIVA-Egfp$ (Figure 5.12 and Figure 5.13). However the diffuse fluorescence in the aerial hyphae of $\Delta sepF/pMS82-2078-DivIVA-Egfp$ often spatially and/or temporally co-existed with distinct fluorescent foci, unlike in the aerial hyphae of $M145/pMS82-2078-DivIVA-Egfp$, where either diffuse fluorescence or discrete foci were observed (Figure 5.8 and Figure 5.9).

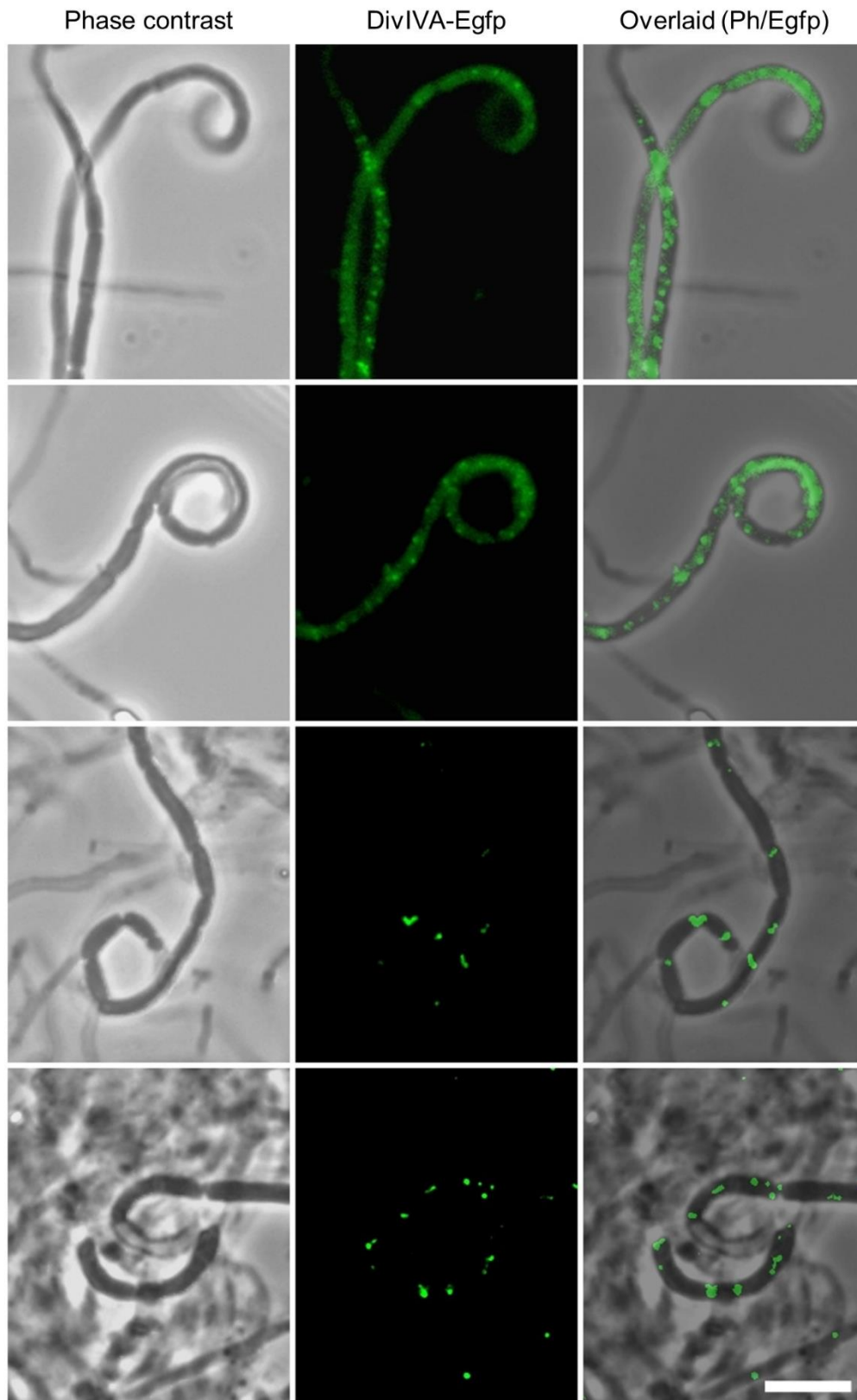


Figure 5.12 Characterisation of aerial growth from $\Delta sepF/pMS82-2078-DivIVA-Egfp$ on SFM medium. Colonies of $\Delta sepF/pMS82-2078-DivIVA-Egfp$ were grown on SFM+hyg medium for 77 hrs. Images were taken under x100 magnification with an exposure of 400 ms. The phase contrast image (left) is shown alongside the fluorescent image (middle) and both images are overlaid (right). The scale bar represents 5 μm .

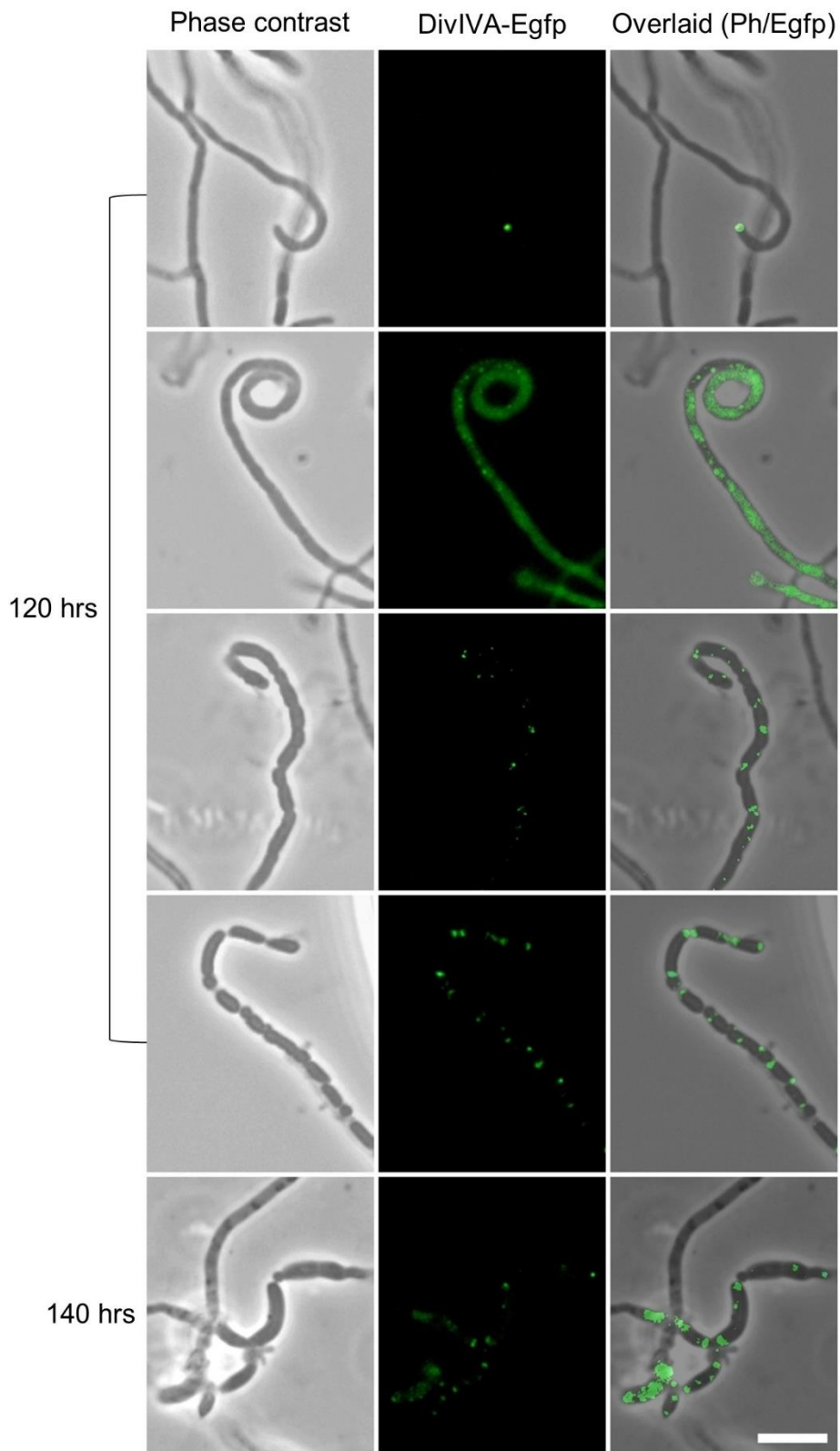


Figure 5.13 Characterisation of aerial growth from $\Delta sepF/pMS82-2078$ -DivIVA-Egfp on MMM medium. Colonies of $\Delta sepF/pMS82-2078$ -DivIVA-Egfp were incubated on MMM+hyg medium until the stated timepoints. Images were taken under x100 magnification with an exposure of 400 ms. The phase contrast image (left) is shown alongside the fluorescent image (middle) and both images are overlaid (right). The scale bar represents 5 μ m.

With extended incubation the aerial hyphae of $\Delta sepF/pMS82-2078-DivIVA-Egfp$ exhibited irregular septation events and fluorescence condensed to the sites of aberrant cell division as either single foci or a line (Figure 5.12 and Figure 5.13). Therefore the localisation patterns of DivIVA-Egfp in the aerial hyphae of $\Delta sepF/pMS82-2078-DivIVA-Egfp$ is similar to the patterns detected in the aerial hyphae of M145/pMS82-2078-DivIVA-Egfp in that DivIVA-Egfp ended up at the developing septum, even in the absence of *sepF*. This suggests that SepF was not required for DivIVA localisation at the developing septa.

5.2.4 Monitoring the expression levels of DivIVA-Egfp at key stages of the S. coelicolor lifecycle

The diffuse localisation of DivIVA-Egfp in the aerial hyphae of M145/pMS82-2078-DivIVA-Egfp and $\Delta sepF/pMS82-2078-DivIVA-Egfp$ suggested that the expression of DivIVA-Egfp could be upregulated in the aerial hyphae, as previously shown for the expression of SepF-Egfp and FtsZ-Egfp (Section 4.3.2). To test this hypothesis, the DivIVA-Egfp expressing strains were grown on SFM+hyg medium, covered by a cellophane membrane, to allow the collection of all cells. Hyphae were collected at three stages, representing vegetative growth, early aerial growth and late sporulating aerial growth, containing spores where appropriate. After cell lysis using a cell disruptor, equal amounts of total protein extracts were analysed on a native PAGE gel using the fluorescence from DivIVA-Egfp.

Similar to the previously described M145/pMS82-SepF-Egfp and M145/pMS82-FtsZ-Egfp samples, the M145/pMS82-2078-DivIVA-Egfp and $\Delta sepF/pMS82-2078-DivIVA-Egfp$ samples produced multiple bands at distinct heights (Figure 5.14). The Covid-19 pandemic prevented the gel excision of the bands and the identification of the protein(s). However in Chapter 4, the absence of additional bands in the $\Delta sepF/pMS82-FtsZ-Egfp$ samples was speculated to suggest the bands below position * are unlikely to be free Egfp (Figure 4.9). Plus two hypothesis for interrupting the gels were suggested: the oligomerisation hypothesis and phosphorylation hypothesis.

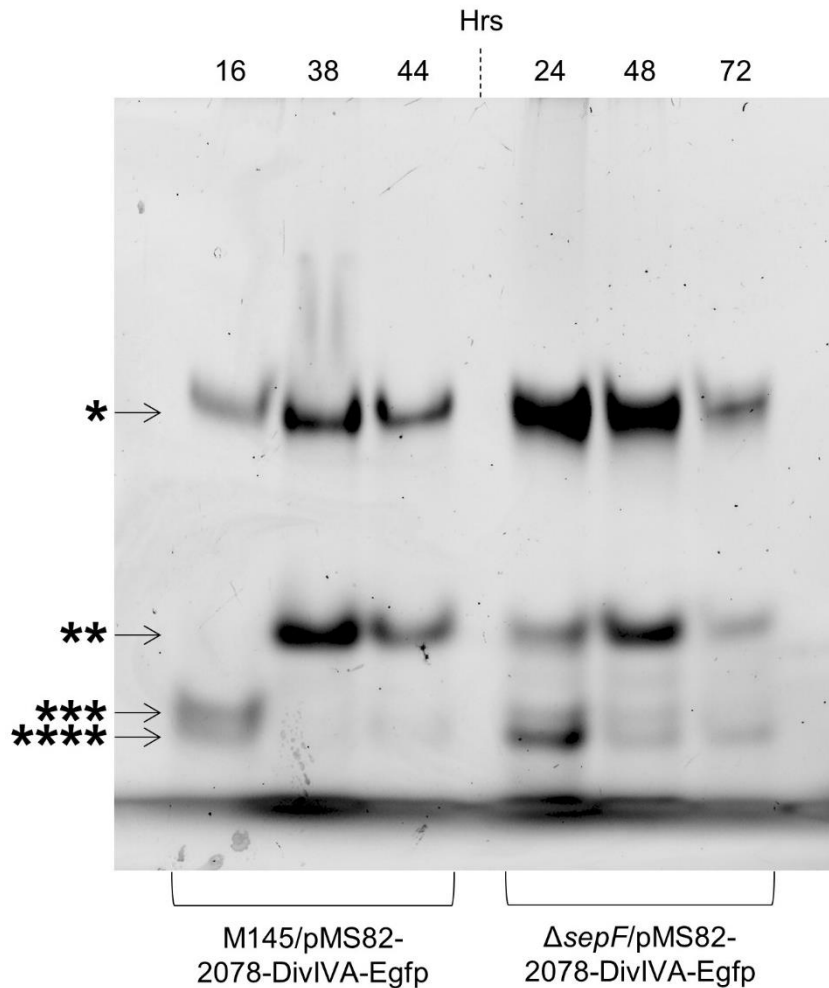


Figure 5.14 The expression of 2078-DivIVA-Egfp in M145/pMS82-2078-DivIVA-Egfp and $\Delta sepF$ /pMS82-2078-DivIVA-Egfp. Both strains were streaked onto SFM +hyg+cellophane plates. Samples were taken at vegetative growth then early and sporulating aerial growth. For M145/pMS82-2078-DivIVA-Egfp, samples were taken at 16 hrs, 38 hrs and 44 hrs. For $\Delta sepF$ /pMS82-2078-DivIVA-Egfp, samples were delayed to 24 hrs, 48 hrs, and 74 hrs. For each sample, a supernatant fraction containing 38 mg of total protein was analysed on an 8% native PAGE gel. The * indicate each banding position described.

Based on the oligomerisation hypothesis the bands at position * and ** are thought to represent the Egfp tagged protein in a polymer or protein complex. Initially the intensity of the bands at position * in the M145/pMS82-2078-DivIVA-Egfp samples increased with the formation of aerial hyphae, which is consistent with the upregulation of DivIVA-Egfp. However the intensity of the bands at position * in the $\Delta sepF$ /pMS82-2078-DivIVA-Egfp samples decreased with the formation of aerial hyphae. Therefore the production of DivIVA-Egfp could be altered in the $\Delta sepF$ /pMS82-2078-DivIVA-Egfp strain.

The bands at position ** from the M145/pMS82-2078-DivIVA-Egfp and $\Delta sepF$ /pMS82-2078-DivIVA-Egfp samples peaked in intensity during young aerial growth for both strains. While bands at position *** and position **** peaked in intensity during vegetative growth and were weakly visible during the aerial growth of $\Delta sepF$ /pMS82-2078-DivIVA-Egfp. Although only speculation, the differences between the M145/pMS82-FtsZ-Egfp and $\Delta sepF$ /pMS82-FtsZ-Egfp samples could potentially represent changes in the production and binding partners of DivIVA-Egfp in the absence of *sepF*. One possibility is DivIVA and SepF compete to bind with Scy so in the absence of SepF additional protein complexes, involving DivIVA and Scy and which localise to the hyphal tip are formed.

The phosphorylation hypothesis is based on the finding by Rioseras *et al.*, 2018 which showed FtsZ, SepF and DivIVA were phosphorylated in the aerial hyphae after 65 hrs of growth. Phosphorylation of DivIVA has been shown to alter the localisation of the polarisome, allowing cell wall synthesis to be arrested in response to stress (Hempel *et al.*, 2012). Based on this evidence the bands at position * were suggested to represent the Egfp tagged protein in an unphosphorylated form while longer bands represent the different phosphorylation states of the Egfp tagged protein. Therefore in the M145/pMS82-2078-DivIVA-Egfp samples the increase in intensity of the bands at position * after the first timepoint could represent the increased presence of DivIVA-Egfp specifically in a non-phosphorylated state. Unlike for FtsZ and SepF the presence of bands at position *** and position **** in the first timepoint of the M145/pMS82-2078-DivIVA-Egfp samples suggests DivIVA could be present in multiple phosphorylation states throughout development of *S. coelicolor*, potentially though the activity of the Ser/Thr protein kinase, AfsK, mentioned in Section 1.3.2. At the latter timepoints for the M145/pMS82-2078-DivIVA-Egfp samples the band at position ** have the highest intensity suggesting these bands represent the dominate phosphorylation state in the hyphae.

In comparison in the $\Delta sepF$ /pMS82-FtsZ-Egfp samples the banding pattern at position * could suggest the presence of larger levels of the non-phosphorylated DivIVA in the vegetative hyphae. Then the consistent presence of bands at position ** and position **** in all three timepoints could indicate the turnover of phosphorylated DivIVA in the absence of *sepF* is altered. Hence the absence of *sepF* could have altered the phosphorylation of DivIVA either directly or indirectly in both the vegetative and aerial hyphae. We further speculate investigating the effect of mutants at residues K46 and F71 of the SepF C-terminus could further support

the direct link between the processes of cell division and polar growth by modifying the banding pattern of DivIVA-Egfp in a similar manner to the absence of *sepF*.

5.3 Summary

In the previous chapter we presented, to our knowledge, the first evidence for a novel link between the processes of polar growth and cell division in *S. coelicolor*. A bacterial two-hybrid assay detected a positive interaction between the FtsZ associated protein, SepF and the TIPOC component, Scy *in vivo*. Scy is a coiled-coil, intermediate filament-like protein which is known to act as a molecular scaffold at hyphal tips where Scy co-localises with DivIVA (Bagchi *et al.*, 2008; Flårdh 2003a; Fuchino *et al.*, 2013; Holmes *et al.*, 2013; Kelemen, 2017). Scy has also been shown to localise at regular intervals away from the tips (Kelemen, personal communication). These subapical positions could be the location of the novel SepF-Scy interaction. Hence we wanted to investigate the localisation of the Scy binding partner and only essential member of the TIPOC, DivIVA, throughout the lifecycle of *S. coelicolor*.

Previously Flårdh, 2003a investigated the localisation of DivIVA-Egfp in the vegetative hyphae of *S. coelicolor* using the K112 strain which utilises a non-replicative plasmid, pKF59, carrying a *divIVA-egfp* fusion and 98 bp upstream of the *divIVA* translation start. However large scale RNAseq data by Jeong *et al.*, 2016 identified a promoter 184 bp upstream of the translational start site of *divIVA*. The importance of the promoter 184 bp upstream of the translational start site of *divIVA* was speculated as under the conditions of the current study, the K112 strain was unable to undergo regular sporulation (Kelemen, personal communication). Therefore we introduced two DivIVA-Egfp expressing constructs with either one or two upstream promoters, informed by large-scale RNA seq data, into *S. coelicolor in trans*. Introduction of the constructs did not alter the colony morphology of wild-type, M145 but microscopy of the M145/pMS82-DivIVA-Egfp strain, containing one upstream promoter revealed an increase in the number of fork-like tips (Figure 5.2). This observation suggests one promoter for DivIVA is insufficient to maintain the integrity of the TIPOC so the M145/pMS82-2078-DivIVA-Egfp strain, containing two promoters was the focus of the current chapter.

Fluorescence from DivIVA-Egfp was present in the spores of M145/pMS82-2078-DivIVA-Egfp prior to swelling and through to germ tube formation, unlike in the previous study using the K112 strain (Figure 5.3 to Figure 5.6; Flårdh, 2003a).

Typically two, rarely three, germ tubes were produced sequentially with each young germ tube containing a fluorescent DivIVA-Egfp foci at the tip. As the germ tubes grew and branched, multiple sub-apical foci formed a zig-zag pattern (Figure 5.6 and Figure 5.7). This localisation pattern of DivIVA has not been previously shown and unlike the other localisation pattern of DivIVA these positions are very unlikely to represent the localisation of the TIPOC leading to branching and polar growth. In the future it will be of special importance to identify the significance of these DivIVA localisation patterns when addressing what determines the localisations of DivIVA.

Importantly the M145/pMS82-2078-DivIVA-Egfp strain was able to undergo sporulation and form regular oval spores (Figure 5.8 to Figure 5.10). As the M145/pMS82-2078-DivIVA-Egfp strain commenced the reproductive stage of the lifecycle and form young aerial hyphae DivIVA-Egfp initially localised to the tip or sub-apically as multiple foci. Then as the aerial hyphae developed the classical curly morphology the localisation of DivIVA-Egfp was diffused, resembling the localisation of SepF-Egfp and FtsZ-Egfp (Figure 5.8 and Figure 5.9). At the sites of cell division prior to spore formation DivIVA formed foci before being detected at both sides of the developing sporulation septa in developing spores (Figure 5.10 and Figure 5.15).

Compellingly, in the absence of *sepF*, DivIVA-Egfp continued to localise to the hyphal tips, including to tips with a fork-like morphology and to the irregular sites of cell division (Figure 5.11 to Figure 5.13 and Figure 5.15). Hence the localisation of DivIVA to the sites of cell division is not dependent on SepF (Figure 5.15). Therefore the localisation study clearly suggests that DivIVA is not only found at actively growing hyphal tips, but also at cell division sites, during sporulation. The localisation of DivIVA-Egfp at regularly spaced sporulation septa supports the finding that Scy localises both apically and sub-apically and supports the Scy-SepF direct interaction, established by a bacterial two-hybrid assay, in the previous chapter (Kelemen, personal communication).

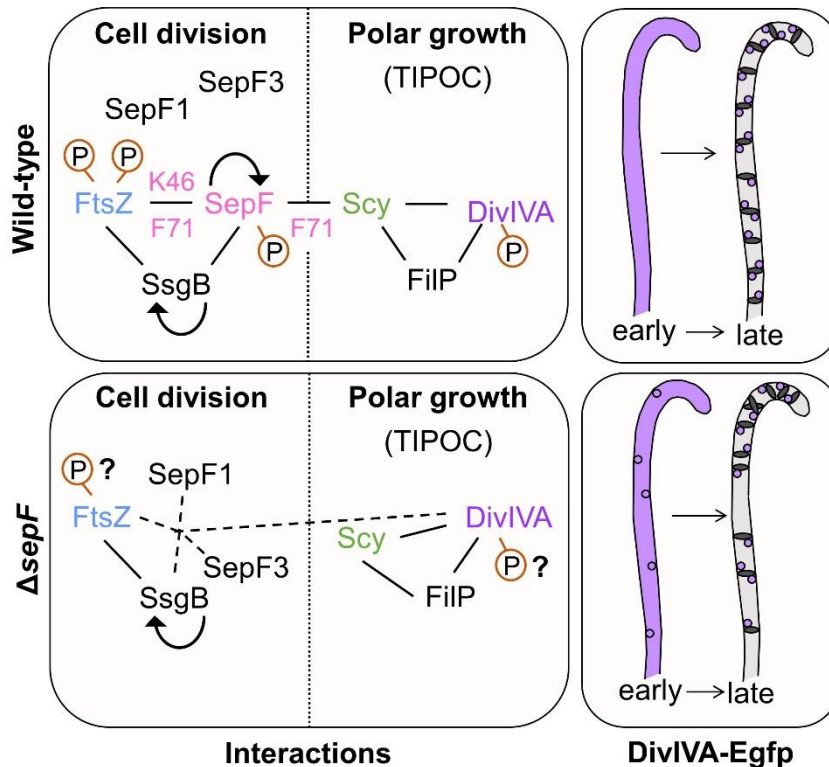


Figure 5.15 Summary of DivIVA-Egfp localisation and protein-protein interactions in wild-type M145 and $\Delta sepF$. ‘Interactions’ (left) shows the known (solid line) and hypothesis (dashed line) interactions, relevant to Chapter 5, during cell division and polar growth. The cell division components, SepF and SsgB, self-interact and interact with FtsZ (Schlimpert *et al.*, 2017; Willemse *et al.*, 2011). In addition in Chapter 4 we showed using a bacterial two-hybrid SepF interacts with SsgB and Scy. To our knowledge the SepF-Scy interaction, identified by the bacterial two-hybrid assay is the first evidence of a direct link between cell division and polar growth. Residues K46 and F71 of the SepF C-terminal affected the SepF-FtsZ interaction and residue F71 affected the SepF-Scy interaction. Scy is known to interact with the TIPOC components DivIVA and FilP (Fuchino *et al.*, 2013; Holmes *et al.*, 2013; Kelemen, 2017). ‘DivIVA-Egfp’ (right) shows the position of DivIVA-Egfp (purple) in the aerial hyphae of the wild-type M145 (top) and $\Delta sepF$ (bottom) strains. DivIVA localises to sites of cell division independently of SepF as foci at either side of the developing sporulation septa (grey disc). We hypothesis DivIVA could interact with other components of the divisome or SepF1 and SepF3. Phosphorylation identified by Manteca *et al.*, 2011 and Rioeras *et al.*, 2018 is shown by a circled ‘P’. Speculated alterations to the phosphorylated state of protein are shown by a question mark.

Interestingly DivIVA was previously thought to be exclusive to polar growth in *Streptomyces*. In *B. subtilis* DivIVA has a very different role, positioning of the MinCD proteins to control FtsZ polymerisation during cell division (Rowlett and Margolin, 2015; Section 1.2.3.2). The opposing roles of DivIVA in *Streptomyces* and *B. subtilis* has always been a puzzle, especially as the genomic localisation of *divIVA* in the DCW cluster is conserved in both bacteria. A secondary role for

DivIVA in the sporulating cells of *B. subtilis* has been suggested with DivIVA interacting with the chromosome segregation machinery at the poles prior to division to help position the oriC region (Thomaides *et al.*, 2001). The current work on the localisation of DivIVA suggests that independently of SepF, DivIVA is able to localise to sites of cell division in *S. coelicolor*. Moreover, regular foci of DivIVA-Egfp were also found in actively growing vegetative hyphae, which raises the question how DivIVA finds these regular positions? Could the positioning of DivIVA involved the other homologues of SepF, SepF1 and SepF3 or other divisome components such as SsgB and FtsZ (Figure 5.15).

Potentially the protein-protein complexes or phosphorylation state of DivIVA involved in these localisations was visualised using on a native PAGE gel (Figure 5.14). Although only speculation the banding pattern of the M145/pMS82-2078-DivIVA-Egfp and $\Delta sepF$ /pMS82-2078-DivIVA-Egfp samples raise the possibility that similar to FtsZ which is upregulated from the sporulation specific promoter, *ftsZ2p*, prior to sporulation, DivIVA is also upregulated in the aerial hyphae (Flårdh *et al.*, 2002). Alternatively the bands could reflect the different phosphorylation states of DivIVA throughout the lifecycle of *S. coelicolor* as Rioseras *et al.*, 2018 showed DivIVA was phosphorylated in the aerial hyphae of *S. coelicolor*. Furthermore the differences between the M145/pMS82-2078-DivIVA-Egfp and $\Delta sepF$ /pMS82-2078-DivIVA-Egfp samples could reflect changes to DivIVA-Egfp in the absence of *sepF*. Future analysis of these samples will be required to establish the exact composition of these bands.

5.4 Acknowledgements

The work in the current chapter utilised the 4A10-DivIVA-Egfp cosmid, generated prior to the current study by fellow student, Benjamin Bone. During the current study the germination experiments were aided by the project student, Jacob Harvey.

6.0 Generation, characterisation and complementation of a novel Δ *ftsZ* mutant from *S. coelicolor*

6.1 Introduction

Cell division in *S. coelicolor* requires the polymerisation of the tubulin homologue, FtsZ, into Z-rings (McCormick *et al.*, 1994; Santos-Beneit *et al.*, 2017). Homologues of FtsZ are well conserved among most bacteria and are present in some archaea (Vaughan *et al.*, 2004). In *E. coli*, the polymerisation of FtsZ occurs in a GTP-dependent manner with individual subunits treadmilling along the protofilaments (Dyer, 2009; Guan *et al.*, 2018; Yang *et al.*, 2017b). The treadmilling of FtsZ subunits directs the movement of the late divisome protein, PBP3, which catalyses the cross-linking of PGs for septa formation (Yang *et al.*, 2017b).

Positioning of the Z-ring in *E. coli* and *B. subtilis* is negatively regulated by the synergistic work of the Min system and the nucleoid occlusion system, which prevents the formation of Z-rings at the poles or over the chromosomes (Ramm *et al.*, 2019; Wu and Errington, 2011). In addition in *E. coli* the positive regulators, FtsA and ZipA, anchor the Z-ring to the cell membrane (Hale and de Boer, 1997; Pichoff and Lutkenhaus, 2005). In *B. subtilis* in the absence of ZipA, cell relies on FtsA, EzrA and SepF. The double knock-out strain of *ftsA* and *sepF* is synthetically lethal but the *sepF* knock-out strain is viable, with slightly longer cells and irregular thick cell septa (Hamoen *et al.*, 2006; Ishikawa *et al.*, 2006). Actinomycetes including *Streptomyces* contain homologues of SepF but lack FtsA and ZipA. Hence SepF is expected to have a central role in controlling FtsZ assembly in *S. coelicolor*.

In *S. coelicolor* *ftsZ* and the three associated promoters are positioned in the conserved DCW cluster and transcribed upstream of *sepF* (Figure 1.12; Flårdh *et al.*, 2002). Of these promoters, upregulation of *ftsZ2p* specifically in the sporogenic aerial hyphae is dependent on the *whi* genes (A, B, G, H, I and J) and provides sufficient FtsZ monomers for the formation of the regular FtsZ rings prior to sporulation. In the aerial hyphae, after the upregulation of the *ftsZ2p* promoter, FtsZ-Egfp localises diffusely before condensing into transient irregular or spiral-like septa then Z-rings (Grantcharova, *et al.*, 2005; Willemse and van Wezel, 2009). Unlike in most bacteria where *ftsZ* is essential, remarkably, *ftsZ* knock-out strains are viable in the *Streptomyces* genus (McCormick *et al.*, 1994; Santos-Beneit *et al.*, 2017). The existing Δ *ftsZ* strain from *S. coelicolor* and *S. venezuelae* form aerial hyphae

but do not form sporulation septa or spores. The lack of septa coincides with a lack of compartmentalisation and large-scale lysis events (Santos-Beneit *et al.*, 2017).

Hence the previously described \DeltaftsZ mutants share several characteristics with the \DeltasepF mutant, characterised in Chapter 3. The \DeltasepF mutant, generated via the Redirect[®] PCR-directed mutagenesis protocol in the Kelemen lab, lacks the DNA encoding the first 159 amino acids out of the 213 amino acids for SepF, causing cell division and branching defects. Colonies of the \DeltasepF mutant were unable to form regular vegetative or sporulation septa, had an increased prevalence of fork-like tips and in the absence of the grey sporulation pigment were covered by blue pigmentation, expected to be actinorhodin.

To compare the \DeltasepF mutant of *S. coelicolor* to an \DeltaftsZ mutant, the current chapter aimed to generate and characterise a *ftsZ* knockout mutant. In the existing *S. coelicolor* \DeltaftsZ strain, the first 277 amino acids of the 400 amino acid long FtsZ was replaced by a neomycin resistance (McCormick *et al.*, 1994). Here, we aimed to use the Redirect[®] PCR-directed mutagenesis approach to generate a \DeltaftsZ mutant, where the entire open reading frame of *ftsZ* is replaced by an apramycin resistance gene (Gust *et al.*, 2002). This aim was broken down into several objectives, outlined below:

- Generate a novel \DeltaftsZ mutant in *S. coelicolor* using the Redirect[®] PCR-directed mutagenesis approach.
- Characterise septa formation in the aerial hyphae of the novel \DeltaftsZ mutant using epi-fluorescent microscopy.
- Complementation of the \DeltaftsZ mutant to confirm the phenotype of the *ftsZ* knock-out mutant is due to the absence of *ftsZ*.
- Characterise the localisation of SepF-Egfp in the \DeltaftsZ mutant using epi-fluorescent microscopy.

6.2 Results

6.2.1 Generation of a *ftsZ* knock-out strain using the Redirect[®] PCR-directed mutagenesis approach

To replace the entire open reading frame of *ftsZ* using the Redirect[®] PCR-directed mutagenesis approach previously used in the Kelemen lab, an *apra^R* cassette was extended to contain 40 bp flanking regions homologous to the flanking regions of the DNA encoding *ftsZ*. Then the extended *apra^R* cassette underwent homologous recombination with the 4A10 cosmid, containing the DCW gene cluster, to generate the 4A10:: Δ *ftsZ*:*apra^R* cosmid, which was later confirmed by sequencing (Figure 6.1A).

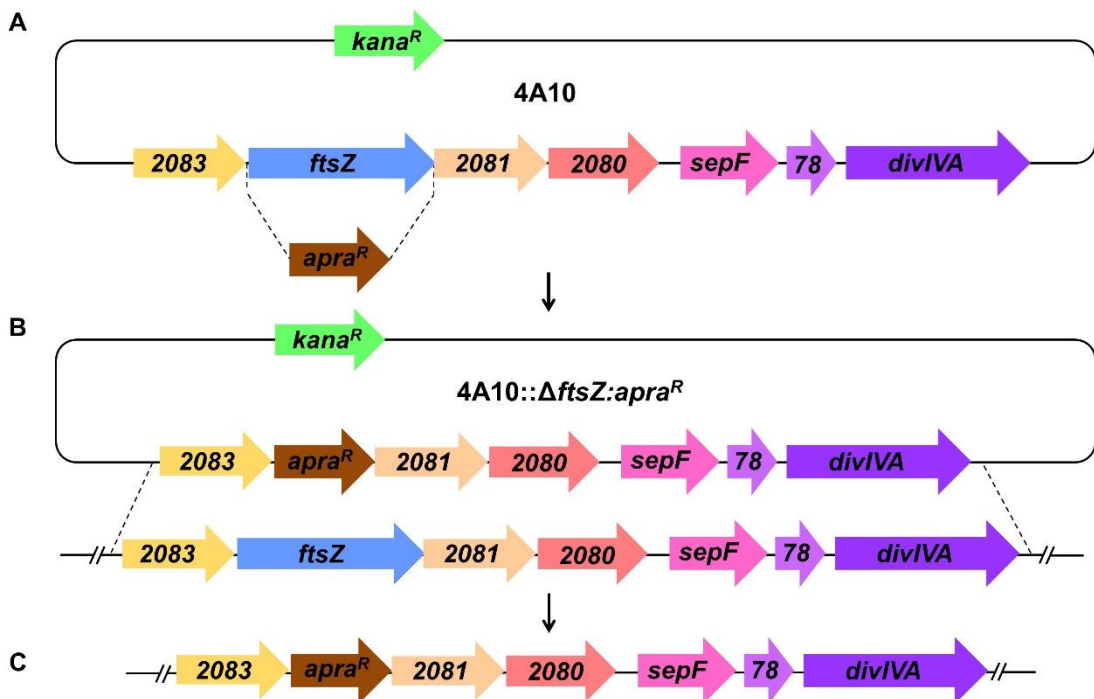


Figure 6.1 Generation of the Δ *ftsZ* mutant using the Redirect[®] PCR-directed mutagenesis approach. A) An extended *apra^R* cassette was introduced, by PCR directed homologous recombination, into the 4A10 cosmid to generate the 4A10:: Δ *ftsZ*:*apra^R* knock-out cosmid. B) The 4A10:: Δ *ftsZ*:*apra^R* cosmid was conjugated into wild-type M145. C) The predicted chromosomal organisation of the Δ *ftsZ* double crossover mutant.

In this work, the 4A10:: Δ *ftsZ*:*apra^R* cosmid was electroporated into the methylation-deficient *E. coli* ET12567:pUZ8002 strain to enable the conjugation of the 4A10:: Δ *ftsZ*:*apra^R* cosmid into wild-type *S. coelicolor* M145 (Figure 6.1B). After the conjugation, exconjugants were selected using apramycin and the desired Δ *ftsZ* *apra^R* double crossover colonies were screened for based on an *apra^R* and *kana^S* genotype (Figure 6.1C).

The conjugation plates were incubated at 30°C for 20 hrs then overlaid with nalidixic acid and apramycin. The overlay aimed to kill the surviving *E. coli* and select for colonies of *S. coelicolor*, containing the *apra^R* cassette. The overlaid plates were incubated at 30°C for 7 days. At 7 days ~140 individual colonies were distinguishable on each plate (Figure 6.2). Most of the large colonies were *apra^R kana^R* single crossovers, when tested by replica plating at 15 days. However, ~100 *apra^R kana^S* colonies representing potential double cross-over *ftsZ* knock-out colonies were observed (Section 6.2.2). About ~20% of the potential double cross-over *ftsZ* knock-out colonies resembled the exconjugates of the Δ *sepF* conjugation and were very small, blue pigmented colonies which did not efficiently replicate due to the size of the colony (Figure 6.2 arrows). In total 23 *apra^R kana^S* colonies were identified and streaked for further investigation.

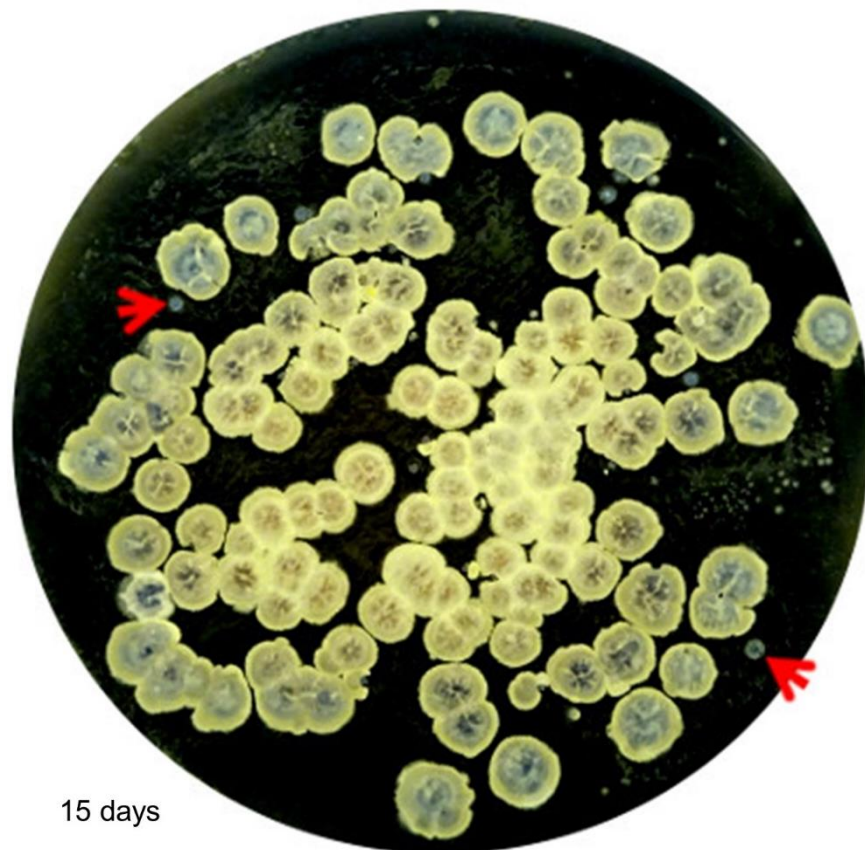


Figure 6.2 The morphologies of the exconjugants during the attempt to generate the Δ *ftsZ* knockout strain. Camera images were taken of the exconjugants after 15 days of growth. The red arrows indicate the 'blue' exconjugants which exhibited an *apra^R kana^S* genotype.

6.2.2 Isolation of potential Δ ftsZ strains from *S. coelicolor*

The streaks of the 23 potential colonies, were incubated on SFM medium supplemented with nalidixic acid and apramycin for 7 days. After 7 days of growth the colonies were classified into four categories (Figure 6.3): colonies in the 'blue' category reached 2 to 3 mm in diameter, were very flat and were covered by a blue pigment. The colonies in the 'blue-pin' category were similar to the colonies in the 'blue' category but had an additional white spot in the middle of the colony. Importantly colonies from both categories were highly similar to the colonies of Δ sepF. Colonies in the 'white' category were distinctive due to the maintenance of a white fluffy colony surface and an increase in colony diameter to 3 to 7 mm. Finally colonies in the 'grey' category were indistinguishable from wild-type in size, pigmentation and growth rate. Out of the 23 colonies there were 9 'blue', 6 'blue-pin', 3 'white' and 5 'grey'.

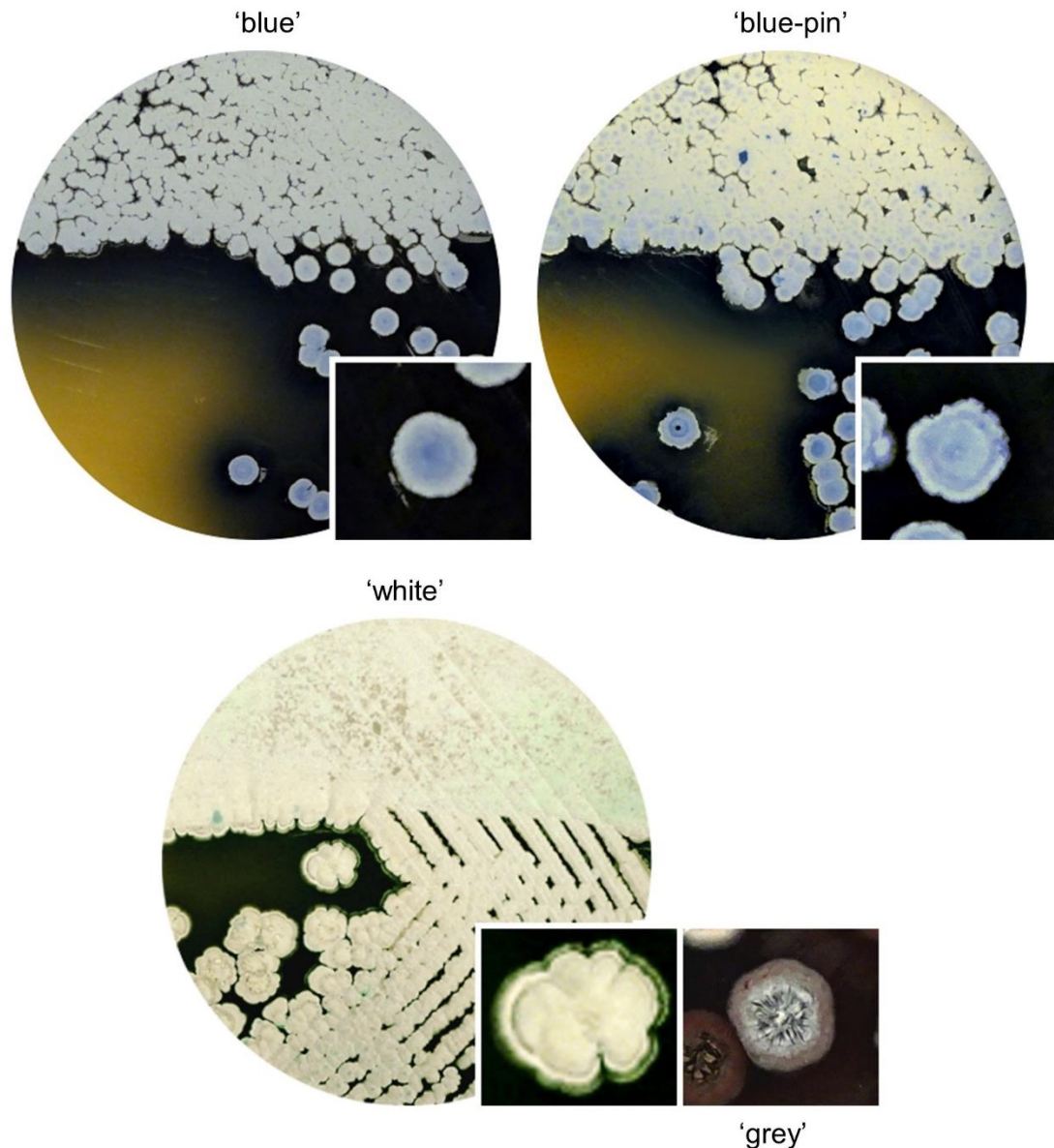


Figure 6.3 The four classes of potential \DeltaftsZ strains. Potential \DeltaftsZ strains were divided into four classes, streaked onto SFM+apra medium and incubated at 30°C. The class is noted in annotation marks (""). Camera images were taken after 13 days. The 'white' plate shows grey pigmented speckling in the confluent area. No 'grey' plate is shown due to the rapid exclusion of these strains from the study.

After a second identical streaking, colonies producing the grey sporulation pigment including colonies of the 'grey' category were not studied further as the \DeltaftsZ strains are known to be non-sporulating. Also, plates containing very heterogenous communities were also excluded. A total of 8 plates were excluded from the screen at this stage. The remaining 15 colonies were re-streaked and grown for an extended 14 day period. The colonies of the 'blue-pin' category exhibited a pigment shift to red in areas of high density, a pigment shift similar to actinorhodin under acidic conditions. The extended incubation period revealed and

excluded an additional 9 strains for the production of the grey sporulation pigment. The 6 remaining strains underwent a final extended re-streaking which excluded the 'blue-pin' and 'white' strains for the production of the sporulation pigment. Only the 'blue' strains remained and these strains were stored for further studies.

After re-streaking the original 23 exconjugants, detailed characterisation of one 'blue' strain was carried out. Only colonies from the 'blue' strain will be discussed further. To assess the macroscopic phenotypes of the \DeltaftsZ mutant, the growth and development of the \DeltaftsZ mutant was monitored on SFM medium together with both the wild-type strain and the \DeltasepF mutant (Figure 6.4).

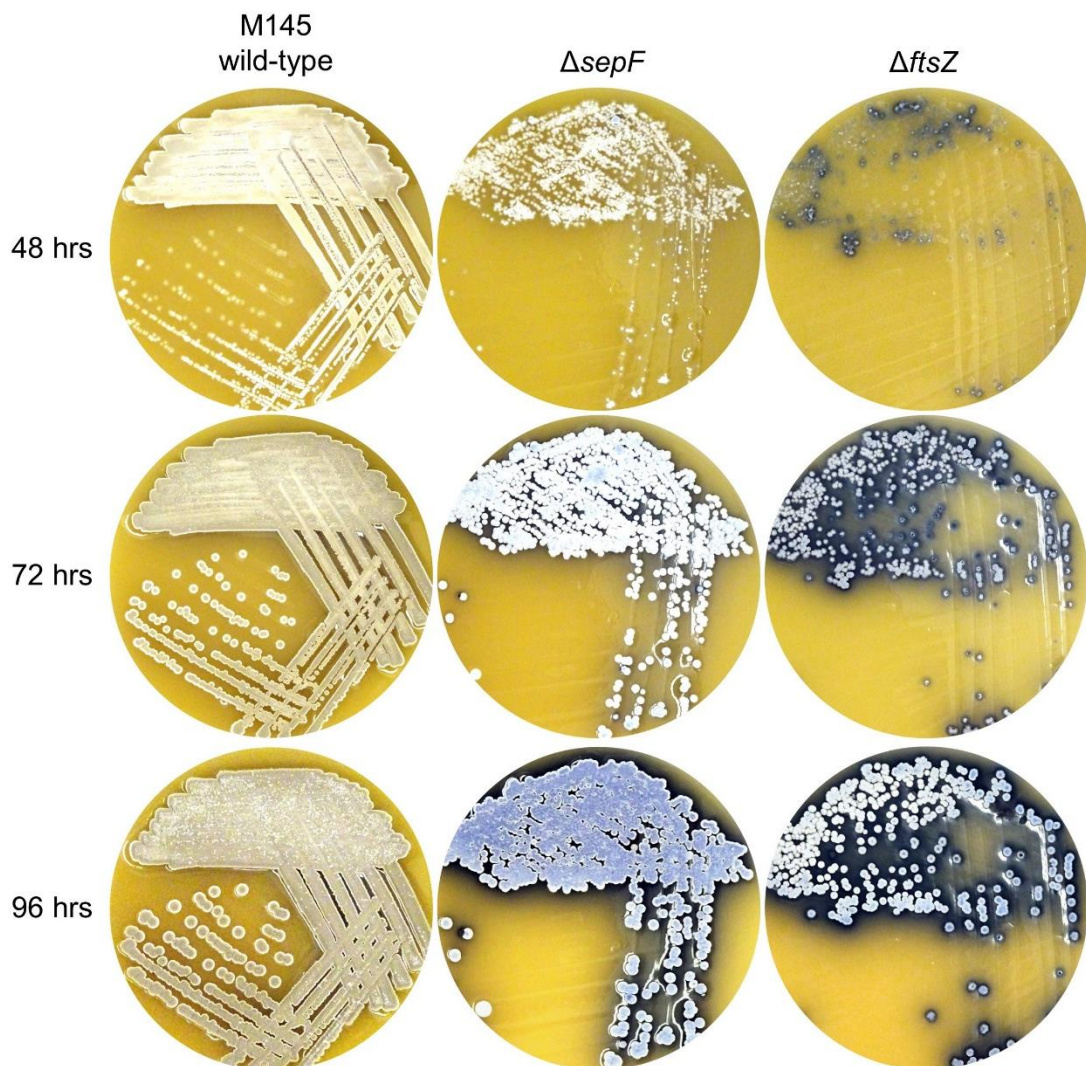


Figure 6.4 Comparison of colony development between the wild-type M145, $\Delta sepF$, and $\Delta ftsZ$ strains. All strains were inoculated onto SFM medium and were monitored every 24 hrs between 48 hrs and 96 hrs.

The colonies of the \DeltaftsZ mutant were macroscopically more similar to the colonies of the \DeltasepF mutant than the wild-type M145 strain. Colonies of both knock-out strains were characterised by a reduced diameter and a blue pigmented surface, expected to be derived from actinorhodin produced in the aerial hyphae (Chapter 7). However, colonies of \DeltaftsZ were slower to develop, smaller in size and were very difficult to confluent plate, compared to the \DeltasepF mutant. Together these observations suggest knocking-out *ftsZ* had a more severe developmental impact than knocking-out *sepF*.

6.2.3 Signs of genetic instability from the colonies of \DeltaftsZ

During the re-streaking of several originally classified “blue” strains, signs of genetic instability were repeatedly found. With each passage of a single colony, only ~60-90% of colonies resembled the original ‘blue’ colony (Figure 6.5).

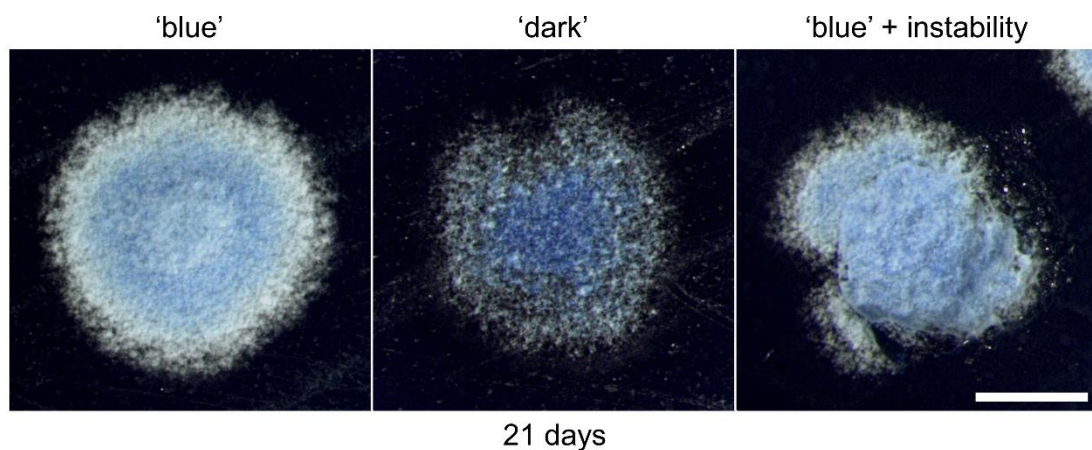


Figure 6.5 The colony morphologies of \DeltaftsZ . The \DeltaftsZ strain was streaked for single colonies on SFM+apra medium. Images were taken using the Zeiss Axiovert microscope and at x8 magnification. The scale bar represents 1 mm.

Some of the colonies had white segments or white spots on the colony surface and the majority of the remaining colonies were categorised as ‘dark’. Colonies in the ‘dark’ category had a further reduced diameter and a flat or concave surface, which was covered by a dark blue almost black pigment. Re-streaking of the ‘dark’ colonies produced very few colonies, all with the same morphology. Hence the ‘dark’ colonies are suspected to contain a secondary mutation, absent in the primary ‘blue’ colonies. The different colony morphologies were more distinct when grown in the presence of cellophane and this phenomenon could merit further investigation (Figure 6.6). One possibility is the involvement of cellulose-like glycans

such as CslA, mentioned in the Introduction, in the differentiation of the colonies grown on the two surfaces.

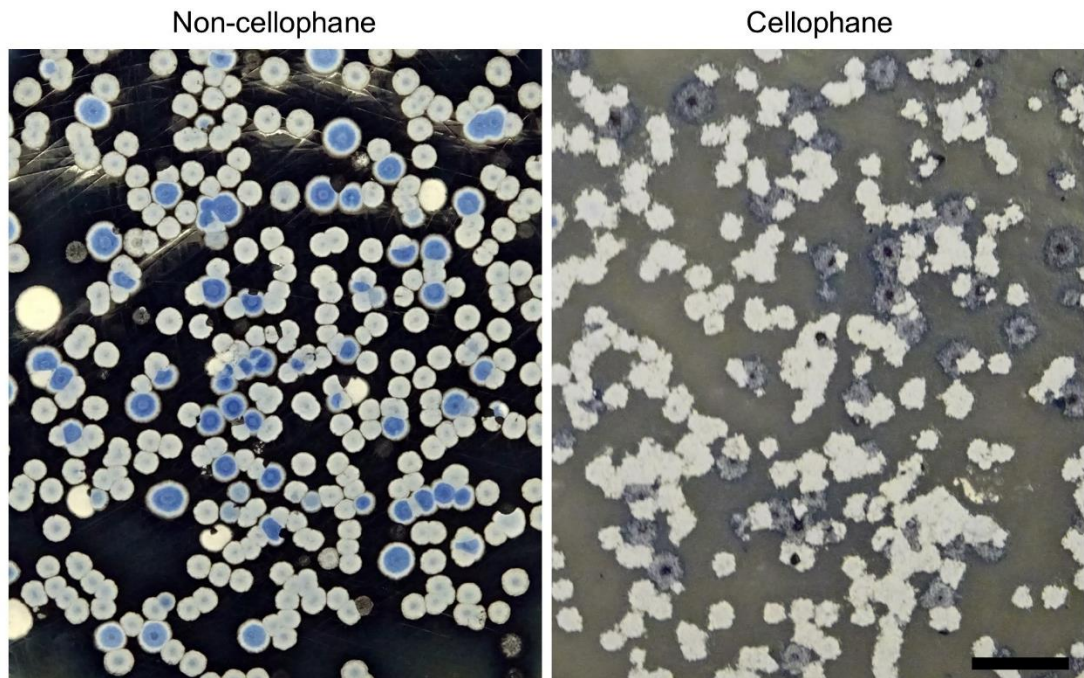


Figure 6.6 The heterogeneity of the \DeltaftsZ strain. The \DeltaftsZ strain was streaked onto SFM medium (left) and SFM medium, covered by a cellophane (right). Camera images were taken after 13 days. The scale bar represents 8 μm .

Intriguingly, the original report of the \DeltaftsZ strain in *S. coelicolor* did not state any instability in the knockout mutant (McCormick *et al.*, 1994). However, generation of the \DeltaftsZ strain in *S. venezuelae* was not straightforward (Santos-Beneit *et al.*, 2017). No double crossover \DeltaftsZ knockouts were found after conjugation, instead a single crossover strain was picked and after repeated re-streaking and screening, a \DeltaftsZ knockout strain was identified. In this work, there is clear indication that the originally classified “blue” knockout strains had a tendency to generate secondary mutations (Figure 6.5 and Figure 6.6). The identification and abundance of colonies with suspected secondary mutations raises several questions. Does the \DeltaftsZ strain require some mutations for viability? Are these secondary mutations predominately positioned in certain genes? Unfortunately characterisation of these strains by full genome sequencing was planned but was not completed due to the Covid-19 pandemic.

6.2.4 Sonication of the Δ ftsZ mutant

To generate chromosomal DNA for the confirmation of the presence of the *ftsZ* knock-out and any additional mutations, an efficient way to propagate the *ftsZ* knockout candidates was needed. During the re-streaking of the Δ ftsZ mutant, generation of an SFM plates with a confluent lawn was almost impossible. This observation is not entirely surprising, as the Δ ftsZ mutant is expected to lack any septation. Therefore a colony of Δ ftsZ is a huge single cell, even though the hyphae carry multiple chromosomes. In order to increase the spreading efficiency, the hyphae of the Δ ftsZ mutant were fragmented using sonication. Previously, *whi* knock-out strains were successfully sonicated, generating short hyphal fragments that increased the “spreadability” of these strains (Kelemen, unpublished).

Propagation of the novel Δ ftsZ strains is suspected to occur via small hyphae fragments, as shown for the Δ ftsZ strain of *S. venezuelae* (Santos-Beneit *et al.*, 2017). The hyphal fragments of Δ ftsZ from *S. venezuelae*, were capable of re-growing when bound by a tip and branch site, due to an expected narrowing of the cell cylinder. In the previous re-streaking attempts, colonies of the putative Δ ftsZ mutant from *S. coelicolor* were mechanically broken up in sterile water until only pipette-able fragments remained. The addition of sonication post the mechanical treatment aimed to increase the efficient generation of small hyphal fragments.

Sonication used either a sonicating waterbath or a sonicating probe that was immersed in the cell suspension. Both technologies were applied to dense cell suspension of the *ftsZ* mutant for different amounts of time before plating onto SFM medium. Sonicated samples were plated alongside a non-sonicated control. After 5 days of incubation the number of colonies was assessed. There was expected to be a significant increase in the number of colonies if the sonication was successful in fragmentation of the Δ ftsZ mutant. Too much sonication might have resulted in no or reduced colony formation due to lysis of the *ftsZ* hyphae. Therefore the aim was to find the optimal sonication conditions for the fragmentation of the *ftsZ* mutant.

Initial sonication experiments using a sonicating waterbath established that 10 min sonication did increase the number of colonies compared to the non-sonicated samples (Figure 6.7). After 15 min sonication the number of colonies decreased, probably due to lysis by sonication. Interestingly even after 25 min sonication, no full lysis was achieved. The lack of full lysis might be because the samples were surrounded by plastic of the Eppendorf tube. Alternatively, the lack of cell death could reflect the tendency of *S. coelicolor* to clump and therefore maintain

the viability of some tightly clumped hyphal fragments during sonication in a water bath. Early attempts using a sonicating probe, with direct contact with the samples, also indicated that sonication can increase the propagating material of the \DeltaftsZ strains (data not shown). However, these trials were shut down due to the Covid-19 pandemic.

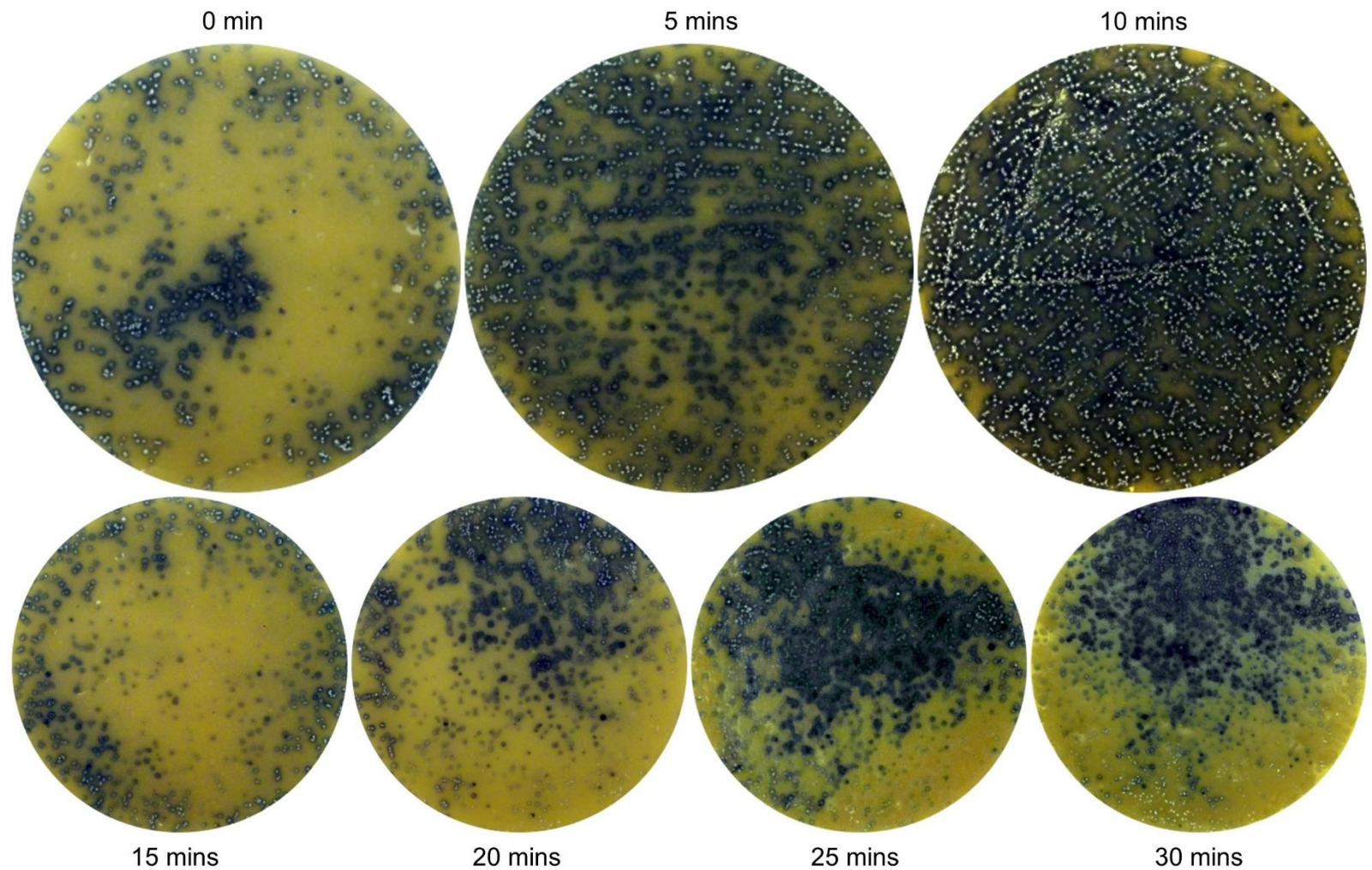


Figure 6.7 Sonication of hyphal fragments from \DeltaftsZ . After the stated amount of sonication in a sonicating waterbath hyphal fragments were plated onto SFM medium (See the associated text for details). Camera images were taken after 120 hrs of incubation at 30°C.

Interestingly, the sonication trials generated some plates where the heterogeneity of colonies seemed to increase with sonication (Figure 6.8). We speculate that when secondary mutations emerge in the multi genomic, complex, hyphal networks with no septation, initially the mutant chromosomes are “hidden”. Only after fragmentation can these mutant chromosomes end up in a short hyphal fragment, and after multiple rounds of replication, generate a segment or a full colony, with a mutant phenotype.

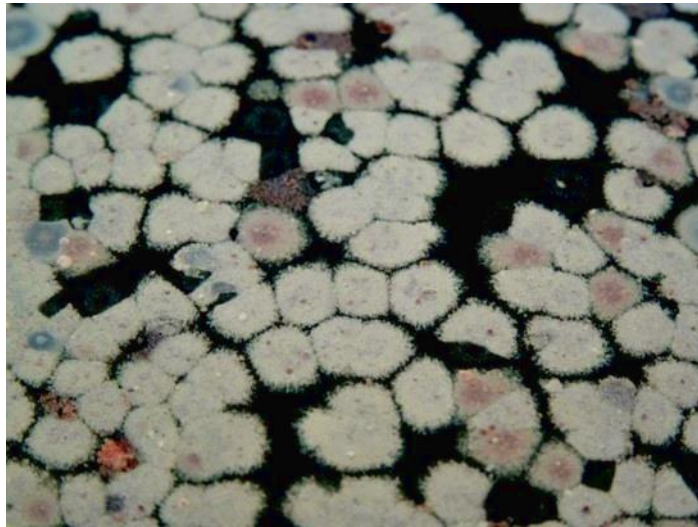


Figure 6.8 Heterogeneity during the sonicating trials. Sonicated samples of \DeltaftsZ were plated onto SFM. Camera images were taken after 21 days.

6.2.5 Characterising the vegetative and aerial growth of \DeltaftsZ

Next the \DeltaftsZ mutant was grown alongside a sterile coverslip in solid SFM medium, stained using PI and WGA-Alexa488 conjugate and visualised with epi-fluorescence microscopy (Figure 6.9).

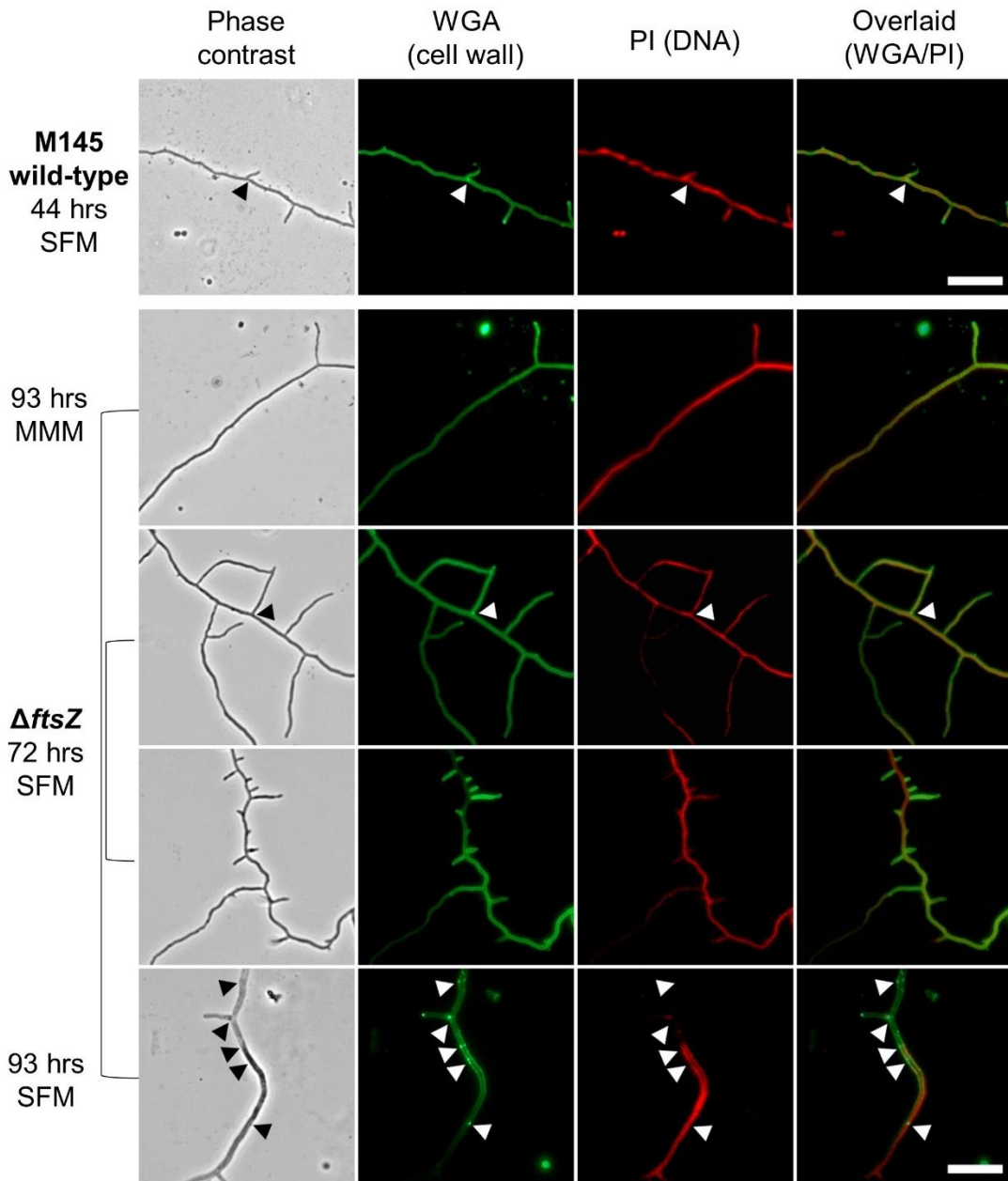


Figure 6.9 Characterisation of vegetative growth from the \DeltaftsZ strain using epi-fluorescent microscopy. The \DeltaftsZ and wild-type M145 strains were grown on the stated media until the stated timepoints. In addition to the phase contrast image (black/white), strains were fixed and stained with the cell wall stain, WGA-Alexa 488 conjugate (green), the DNA stain, PI (red) and the stained images were overlaid (green/red). The arrows indicate the sites of vegetative cross-walls (M145) or increased cell wall staining (\DeltaftsZ). Images were taken at x100 magnification and 400 ms exposure. The scale bars represent 5 μm .

The vegetative hyphae of \DeltaftsZ were unable to form regular vegetative cross-walls (Figure 6.9 second row). Although not a cross-wall, a limited number of hyphae had increased cell wall staining at places often close to branching points (Figure 6.9 third row). The latter observation also coincided with areas containing an increased number of branching events (Figure 6.9 fourth row). Branching points have been suggested to be natural sites for the narrowing of the cell cylinder and could be ideal sites to achieve some compartmentalisation in the absence of septa (Santos-Beneit *et al.*, 2017). In the absence of compartmentalisation, the vegetative and aerial hyphae of \DeltaftsZ exhibited a tendency towards cell lysis, as previously also noted for the \DeltasepF strain and the \DeltaftsZ strain from *S. venezuelae* (Figure 6.9 fifth row; Santos-Beneit *et al.*, 2017).

The aerial hyphae of \DeltaftsZ developed the classical curved hook-like morphology but did not undergo sporulation (Figure 6.10). Unlike the aerial hyphae of \DeltasepF , the aerial hyphae of \DeltaftsZ consistently maintained smooth cell walls with no signs of sporulation septa or spores. Excitingly the fork-like tip morphology from the \DeltasepF mutant was absent in the \DeltaftsZ mutant, which maintained smooth and rounded hyphal tips. Hence the \DeltaftsZ mutant has a more severe cell division phenotype compared to the \DeltasepF mutant.

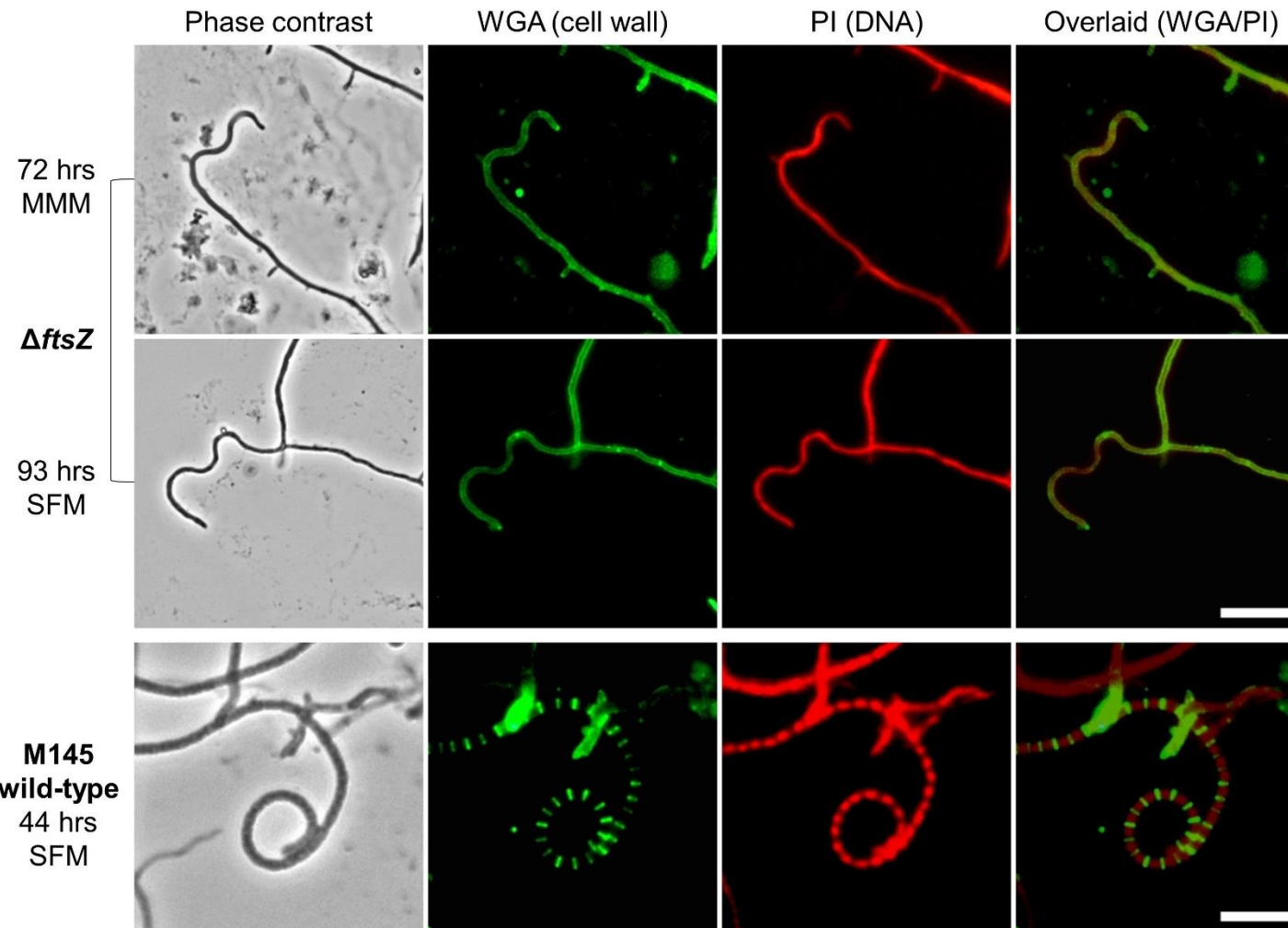


Figure 6.10 Characterisation of aerial growth from the *ΔftsZ* strain using epi-fluorescent microscopy. The *ΔftsZ* and wild-type M145 strains were grown on the stated media until the stated timepoints. In addition to the phase contrast image (black/white), strains were fixed and stained with the cell wall stain, WGA-Alexa 488 conjugate (green), the DNA stain, PI (red) and the stained images were overlaid (green/red). Images were taken at x100 magnification and 400 ms exposure. The scale bars represent 5 μ m.

6.2.6 Complementation of the novel Δ ftsZ mutant

To confirm that the phenotype of the Δ ftsZ mutant was due to the absence of *ftsZ* and not downstream polar effects or other secondary mutations, the Δ ftsZ mutant was complemented. Complementation utilised the integrative pMS82 plasmid, previously described in Chapter 3 to separately introduce *in trans* either an FtsZ-Egfp translational fusion or an untagged FtsZ.

6.2.6.1 Complementation of the Δ ftsZ mutant with pMS82-FtsZ-Egfp

The first complementation attempt utilised the pMS82-FtsZ-Egfp plasmid, used in Section 4.2.1, to monitor the localisation of FtsZ. The FtsZ-Egfp is functional as in the sporulating M145/pMS82-FtsZ-Egfp strain FtsZ-Egfp was readily observed polymerising into protofilaments then rings at future septum sites. The pMS82-FtsZ-Egfp plasmid carries the same *S. coelicolor* DNA fragment as the plasmid published by Flårdh *et al.* (2002). To introduce pMS82-FtsZ-Egfp into the Δ ftsZ mutant, pMS82-FtsZ-Egfp was passed through the methylation deficient *E. coli* ET12567:pUZ8002 strain. Exconjugants were selected using hygromycin and spore stocks made from representative colonies.

Compared to the colonies of Δ ftsZ, the appearance of colonies from the Δ ftsZ/pMS82-FtsZ-Egfp strain showed clear signs of complementation: colonies of Δ ftsZ/pMS82-FtsZ-Egfp were larger, had a smooth rounded edge and were covered by the grey sporulation pigment (Figure 6.11). However, compared to the colonies of wild-type M145, the complemented colonies were slower to develop.

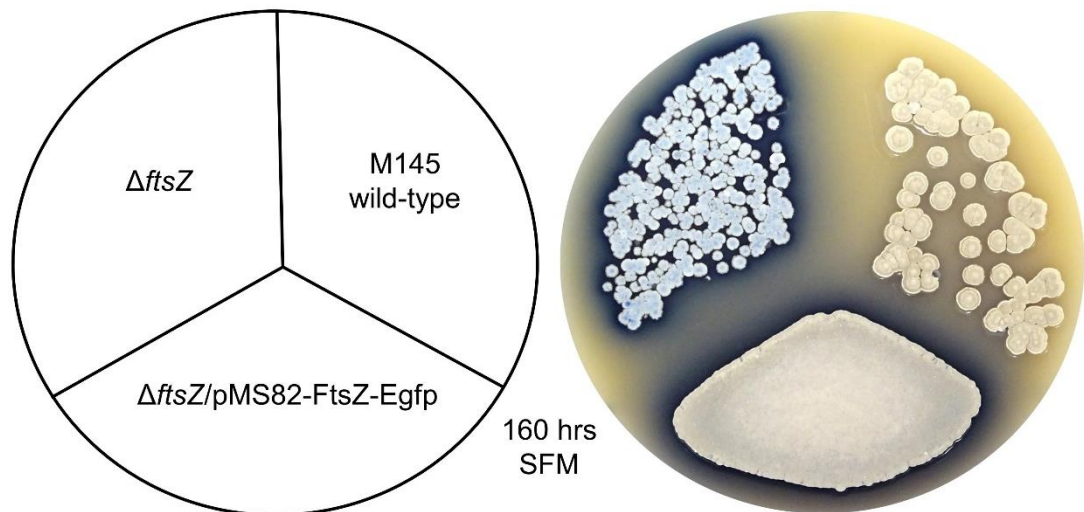


Figure 6.11 Colony morphology of the complementation using pMS82-FtsZ-Egfp. Triangles of the three strains, \DeltaftsZ , $\DeltaftsZ/pMS82-FtsZ-Egfp$ and wild-type M145, were streaked onto SFM medium.

The investigation into septa formation in the colonies of $\DeltaftsZ/pMS82-FtsZ-Egfp$ focused on the aerial hyphae and the process of sporulation. Colonies were grown alongside a sterile coverslip, fixed and stained with PI before visualisation using epi-fluorescent microscopy. Despite a range of timepoints taken between 51 and 93 hrs of growth, only a limited number of FtsZ-Egfp rings were detected (Figure 6.12). The rings of FtsZ-Egfp were organised into ladder-like structures but the ladder-like structures were often irregularly distanced and individual rings did not consistently span the width of the hyphae.

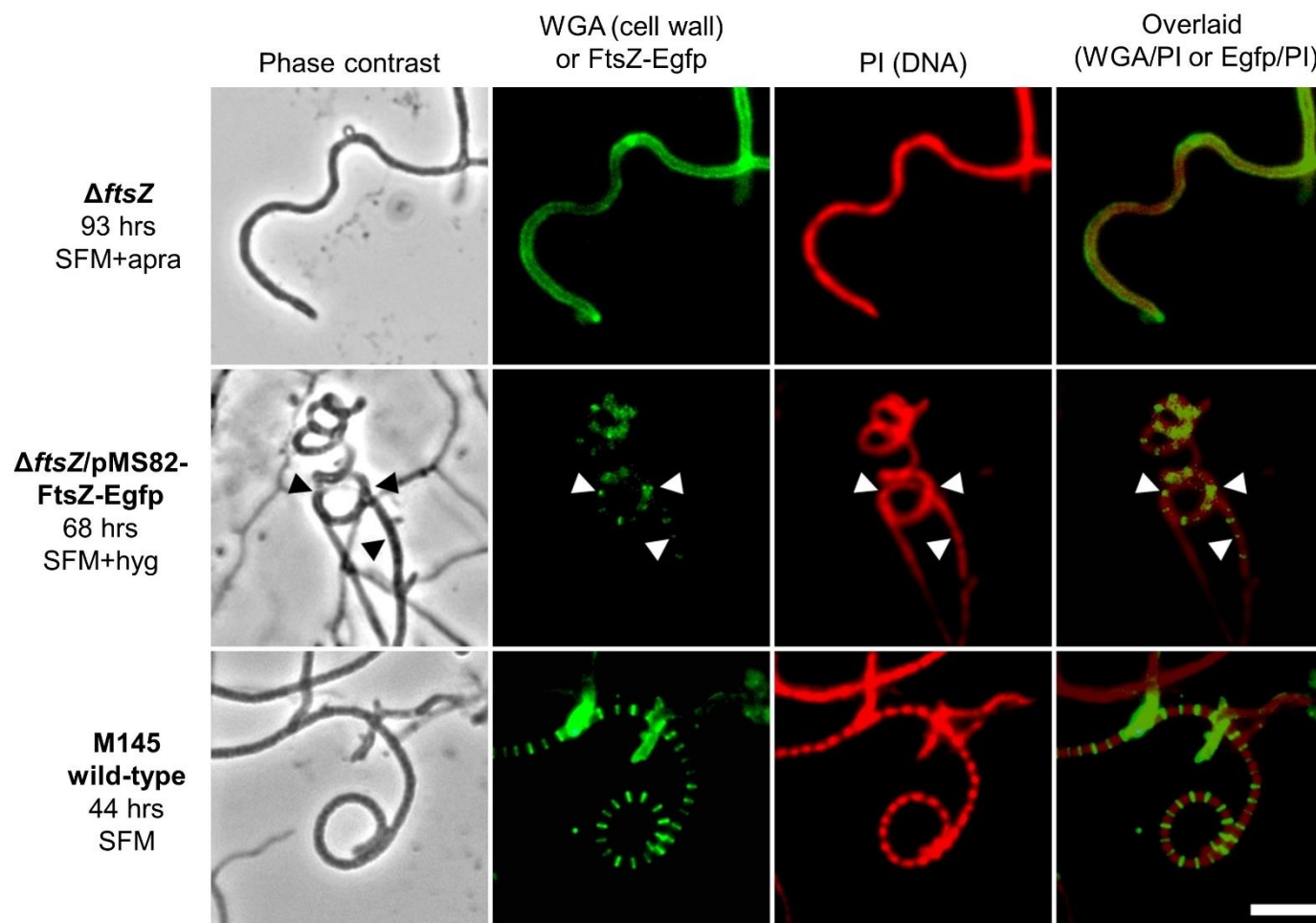


Figure 6.12 Characterisation of the complementation using pMS82-FtsZ-Egfp. The three strains, *ΔftsZ*, *ΔftsZ/pMS82-FtsZ-Egfp* and wild-type M145 were grown on SFM medium and visualised using epi-fluorescent microscopy. In addition to the phase contrast image (black/white), strains were fixed and stained with the cell wall stain, WGA--Alexa 488 conjugate (green), the DNA stain, PI (red) and the stained images were overlaid (green/red). The arrows indicate the partially formed septa in the aerial hyphae of *ΔftsZ/pMS82-FtsZ-Egfp*. Images were taken at x100 magnification and 400 ms exposure. The scale bar represents 5 μ m.

The majority of aerial hyphae from $\Delta ftsZ/pMS82\text{-FtsZ-Egfp}$ developed a curly or hook-like morphology and contained diffuse fluorescence, which is normally detected in young aerial hyphae prior to septa formation. After an extended growth period of 91 hrs, a dense interlocking mycelium was formed from curling smooth hyphae and a low number of round spore-like structures. These observations suggest a low number of aerial hyphae do progress through sporulation but the majority of aerial hyphae from $\Delta ftsZ/pMS82\text{-FtsZ-Egfp}$ are developmentally halted prior to the formation of sporulation septa. Hence the introduction of FtsZ-Egfp into the $\Delta ftsZ$ mutant *in trans* only partially complemented the *ftsZ* knock-out mutant. This observation is not surprising, as FtsZ-Egfp has been widely shown to require a native FtsZ allele for full functionality (Ma *et al.*, 1996).

6.2.6.2 Complementation of the $\Delta ftsZ$ mutant with *pMS82-FtsZ*

Complementation of the $\Delta ftsZ$ mutant with an *egfp* translational fusion resulted in partial complementation. Next the $\Delta ftsZ$ mutant was complemented with an untagged *ftsZ* fragment. To generate the desired *pMS82-FtsZ* plasmid, a 1490 bp *ftsZ* DNA fragment containing *ftsZ* and the complete intergenic region between *ftsZ* and *SCO2073*, including all three *ftsZ* promoters, was amplified using the 4A10 cosmid as a template and the primers, FtsZ BglIProm FRW and FtsZ EcoRIUTC (Figure 6.13A). Then the 1490 bp PCR product was gel-purified, phosphorylated, extracted and analysed on an agarose gel (Figure 6.13B). A single band of the expected 1490 bp size, confirmed the phosphorylated *ftsZ* fragment was successfully generated. The phosphorylated *ftsZ* fragment was ligated into the dephosphorylated *pMS82-EcoRV* vector, described before in Section 3.3.4. Then the ligation mix was transformed into *E. coli* DH5 α cells, chemically made competent. Transformants grew slowly under the hygromycin selection pressure, probably also due to the expression of FtsZ interfering with the physiology of *E. coli*. To exclude any satellite colonies and to increase the available material, transformants were re-streaked onto LB+hyg before being tested by a low-fidelity colony PCR.

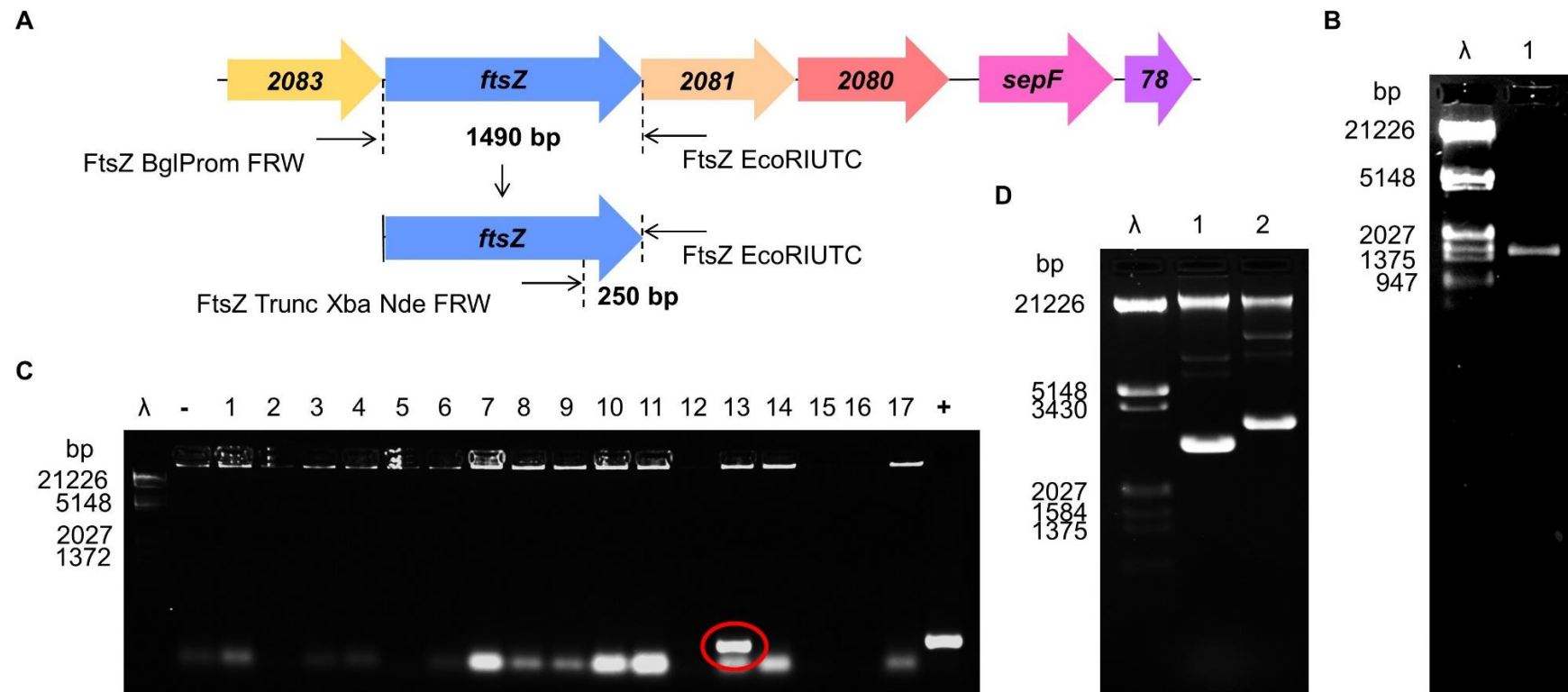


Figure 6.13 Generation of the pMS82-FtsZ plasmid for complementation. A) The 1490 bp *ftsZ* fragment was amplified using 4A10 cosmid as a template and the primers, FtsZ BglIProm FRW and FtsZ EcoRIUTC. B) The *ftsZ* fragment was analysed on a 0.7% agarose gel. Lane λ) λ DNA digested with EcoRI and HindIII, Lane 1) the *ftsZ* fragment. Next the *ftsZ* fragment was phosphorylated and ligated into the dephosphorylated pMS82-*EcoRV* vector, described in Chapter 3. Then the ligation was chemically transformed into *E. coli* DH5 α . C) A colony PCR using the primers, FtsZ Trunc Xba Nde FRW and FtsZ EcoRIUTC, analysed the successful *E. coli* DH5 α transformants. The PCR products were analysed on a 1% agarose gel. Lane λ) λ DNA digested with EcoRI and HindIII, lane 1 to 18) potential transformants and lane +) the positive 4A10 control. The colony PCR identified one positive colony, #14, circled in red. D) Colony #14 underwent a large-scale plasmid preparation and plasmid was analysed on a 1% agarose gel. Lane λ) λ DNA digested with EcoRI and HindIII, Lane 1) the negative undigested pMS82 control, Lane 2) pMS82-FtsZ #14. Complementation of Δ *ftsZ* used pMS82-FtsZ #14.

The colony PCR aimed to identify transformant containing pMS82-FtsZ by amplifying a 250 bp segment of the *ftsZ* insert. The colony PCR used the DNA released from the transformant as a template and the primers, FtsZ BglIProm FRW and FtsZ EcoRIUTC (Figure 6.13A). Of the 72 colonies tested, only one colony was able to generate a band at the desired 250 bp size (Figure 6.13C). The positive transformant underwent a large-scale plasmid preparation to isolate the desired pMS82-FtsZ plasmid. Analysis of the pMS82-FtsZ plasmid on an agarose gel showed a clear size shift compared to the undigested pMS82 plasmid and sequencing confirmed the presence of an unmutated *ftsZ* insert (Figure 6.13D).

The confirmed pMS82-FtsZ plasmid was conjugated into the *S. coelicolor* Δ *ftsZ* and wild-type M145 strains by first passing pMS82-FtsZ through the methylation deficient *E. coli* ET12567:pUZ8002 strain. The conjugation plates were overlaid with nalidixic acid and hygromycin to selection for colonies of *S. coelicolor* containing pMS82 derivatives then incubated at 30°C for 7 days. Colonies of the Δ *ftsZ*/pMS82-FtsZ strain were characterised by a smooth white edge and a grey pigmented surface (Figure 6.14). Unlike the colonies of the Δ *ftsZ*/pMS82-FtsZ-Egfp strain that developed slowly, colonies of the Δ *ftsZ*/pMS82-FtsZ strain produced the grey sporulation pigment at a similar time to the wild-type M145 strain. Hence the colony morphology of the Δ *ftsZ*/pMS82-FtsZ strain suggests the untagged *ftsZ* successfully complemented the Δ *ftsZ* mutant.

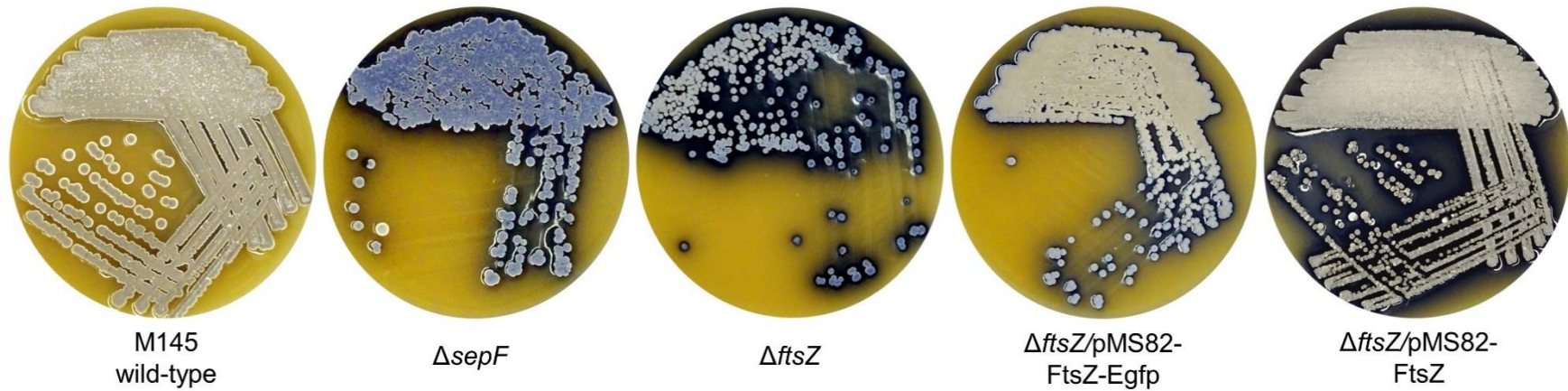


Figure 6.14 The colony morphology of the complemented strains. All five strains, wild-type M145, $\Delta sepF$, $\Delta ftsZ$, $\Delta ftsZ/pMS82-FtsZ-Egfp$ and $\Delta ftsZ/pMS82-FtsZ$, were grown on SFM medium. The strains containing an pMS82 derivative were grown on hygromycin containing medium. Camera images were taken at 96 hrs.

To establish that the sporulation was fully restored after complementation, colonies of $\DeltaftsZ/pMS82-FtsZ$ were grown on SFM+hyg medium, fixed and stained with WGA-Alexa 488 conjugate and PI, then visualised using epi-fluorescent microscopy. To visualise sporulation in the aerial hyphae of $\DeltaftsZ/pMS82-FtsZ$, timepoints were taken between 44 and 50 hrs of growth, which closely matches the timeframe for sporulation in wild-type M145. Unlike for $\DeltaftsZ/pMS82-FtsZ-Egfp$, where fluorescence from FtsZ-Egfp was monitored and detected prior to any septation, for the $\DeltaftsZ/pMS82-FtsZ$ strain samples were stained with WGA-Alexa 488 conjugate to monitor new cell wall synthesis during septation.

The aerial hyphae of $\DeltaftsZ/pMS82-FtsZ$ formed sporulation septa as evenly spaced ladder-like structures (Figure 6.15). Each septa in the ladder extended across the hyphal width and was indistinguishable from the septa formed by wild-type M145. At later timepoints septa formation had led to the formation of copious well-developed spore chains and individual spores. Therefore pMS82-FtsZ was able to fully complement the \DeltaftsZ mutant, which confirms the morphology of the *ftsZ* knockout mutant is primarily due to the lack of *ftsZ*.

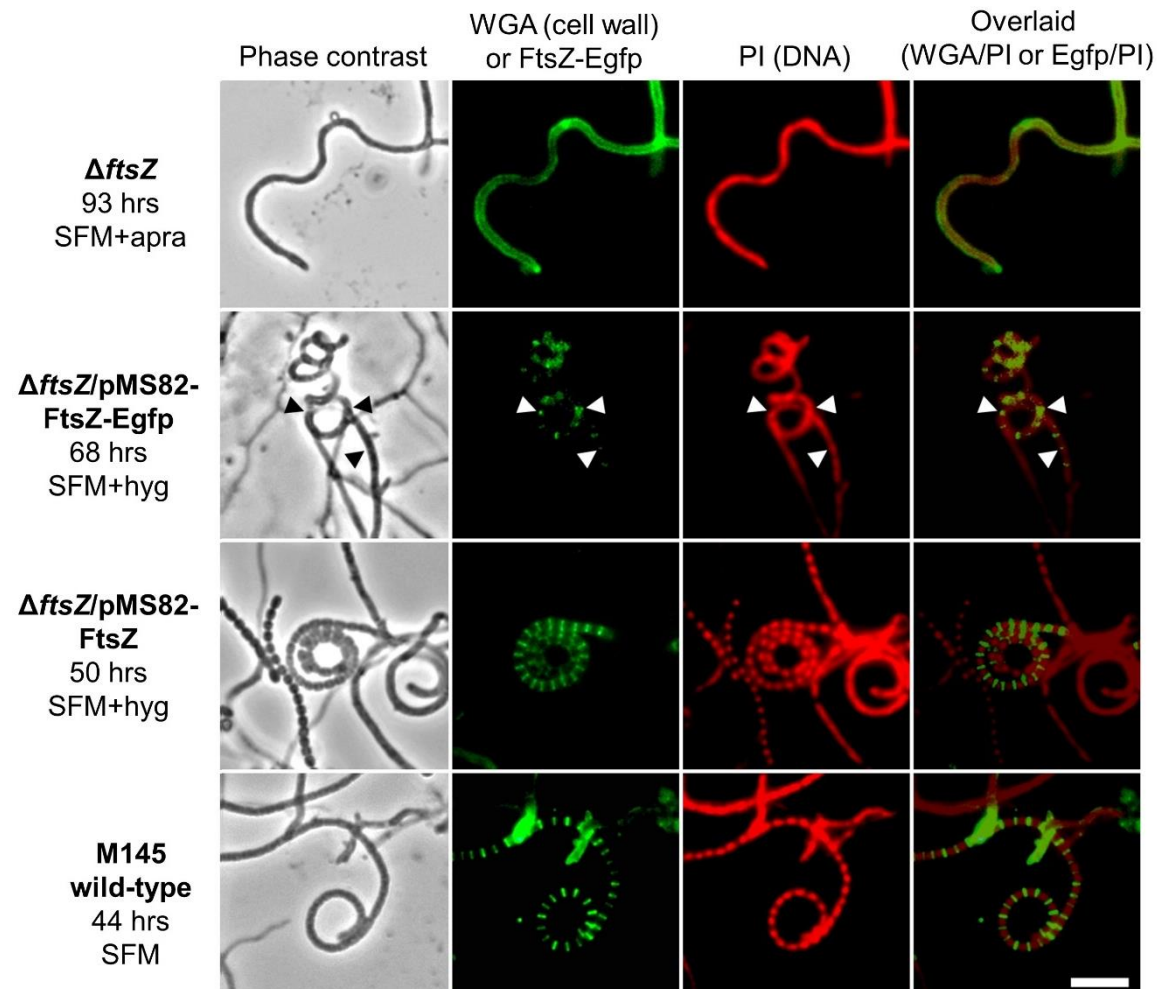


Figure 6.15 Confirmation of complementation using epi-fluorescent microscopy. The four strains, *ΔftsZ*, *ΔftsZ/pMS82-FtsZ-Egfp*, *ΔftsZ/pMS82-FtsZ* and wild-type M145 were grown on SFM medium and visualised using epi-fluorescent microscopy. In addition to the phase contrast image (black/white), when appropriate strains were fixed and stained with the cell wall stain, WGA--Alexa 488 conjugate (green), the DNA stain, PI (red) and the fluorescent images were overlaid (green/red). The arrows indicate the partially formed septa in the aerial hyphae of *ΔftsZ/pMS82-FtsZ-Egfp*. Images were taken at x100 magnification and 400 ms exposure. The scale bar represents 5 μm .

6.2.7 The localisation of SepF-Egfp during the development of the Δ ftsZ mutant

The Kelemen lab has previously shown that FtsZ-Egfp failed to localise into regular rings in the Δ sepF mutant, suggesting the localisation of FtsZ was dependent on sepF (Tan, unpublished). The current section aimed to investigate whether SepF localisation was dependent on ftsZ. Hence the localisation of SepF-Egfp in the Δ ftsZ mutant was monitored. The localisation of SepF to septum sites was previously reported to be dependent on FtsZ in *B. subtilis*, however the current study hypothesised that perhaps in *S. coelicolor*, in the absence of ftsZ, SepF-Egfp could still localise to positions close to the septum due to the SepF-Scy-DivIVA interactions (Hamoen *et al.*, 2005; Ishikawa *et al.*, 2006).

The localisation of SepF-Egfp in the aerial hyphae of wild-type M145 was described in detail in Chapter 4, using pMS82-SepF-Egfp (Figure 4.2). Colonies of the Δ ftsZ/pMS82-SepF-Egfp strain were macroscopically indistinguishable from the colonies of Δ ftsZ, which suggests that an extra copy of SepF cannot compensate for the lack of FtsZ. The Δ ftsZ/pMS82-SepF-Egfp strain was grown alongside a sterile coverslip and visualised using epi-fluorescence microscopy. Numerous SepF-Egfp fluorescent foci were readily observed but no SepF rings were detected in the Δ ftsZ mutant (Figure 6.16).

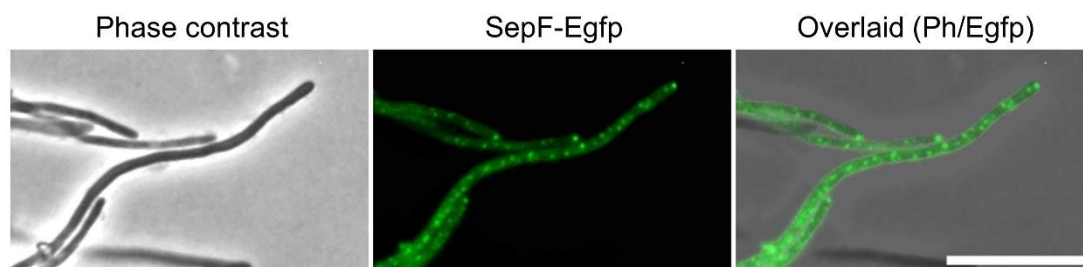


Figure 6.16 The localisation of SepF-Egfp in the Δ ftsZ strain. Colonies of Δ ftsZ/pMS82-SepF-Egfp were incubated on SFM+hyg medium for 96 hrs. Images were taken under x100 magnification with an exposure of 400 ms. The phase contrast image (left) is shown alongside the fluorescent image (middle) and both images are overlaid (right). The scale bar represents 10 μ m

Interestingly, SepF-Egfp was often found at hyphal tips, which was not previously observed in the wild-type strain. This observation could mean that Scy and SepF could not only interact at the developing septa but also at hyphal tips. Although the latter location might be specific to the Δ ftsZ mutant, in which case there might be a competition between Scy and FtsZ to interact with SepF (Figure 6.17). Importantly, neither SepF nor FtsZ localised to regular rings in the absence of

the partner, FtsZ and SepF, respectively. This observation suggests that FtsZ and SepF are interdependent and the cytokinetic ring is composed of both proteins.

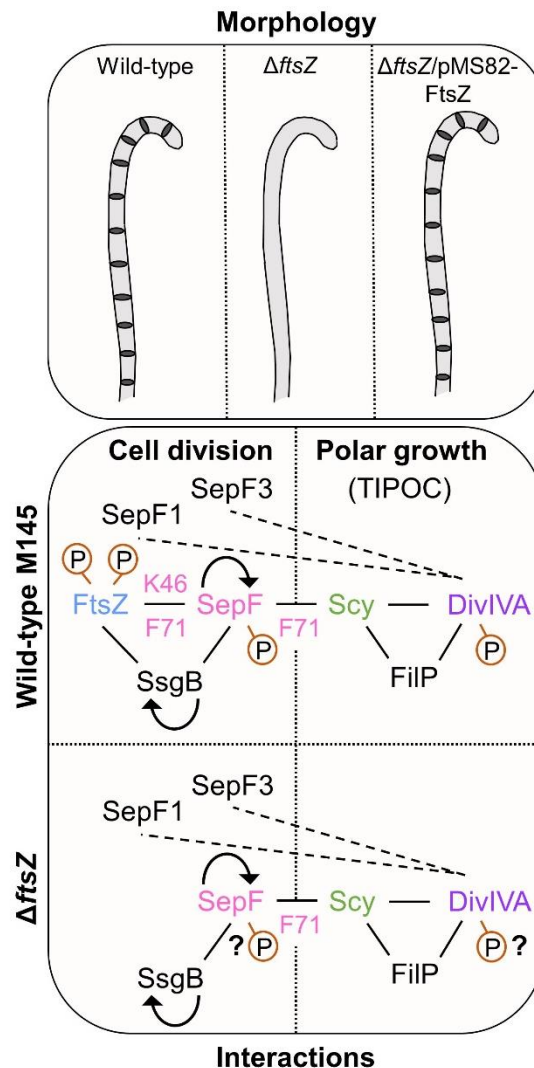


Figure 6.17 Summary of sporulation septa (grey disc) formation and protein-protein interactions in the wild-type M145 and Δ *ftsZ* strains. ‘Morphology’ (top) shows the localisation of sporulation septa in aerial hyphae of the wild-type M145 (left), Δ *ftsZ* (middle) and Δ *ftsZ*/pMS82-FtsZ strains. ‘Interactions’ (bottom) shows the known (solid line) and hypothesis (dashed line) interactions, relevant to Chapter 6, during cell division and polar growth. The cell division components, SepF and SsgB, self-interact and interact with FtsZ (Schlimpert *et al.*, 2017; Willemse *et al.*, 2011). In addition in Chapter 4 we showed using a bacterial two-hybrid SepF interacts with SsgB and Scy. To our knowledge the SepF-Scy interaction, identified is the first evidence of a direct link between cell division and polar growth. Residues K46 and F71 of the SepF C-terminal affected the SepF-FtsZ interaction and residue F71 affected the SepF-Scy interaction. Scy is known to interact with the TIPOC components DivIVA and FilP (Fuchino *et al.*, 2013; Holmes *et al.*, 2013; Kelemen, 2017). DivIVA localises to sites of cell division independently of SepF so we hypothesis DivIVA could interact with other components of the divisome or SepF1 and SepF3. Phosphorylation identified by Manteca *et al.*, 2011 and Rioeras *et al.*, 2018 is showed by a circled ‘P’. Speculated alterations to the phosphorylated state of protein are shown by a question mark.

6.3 Summary

The polymerisation of FtsZ into Z-rings is key to the process of bacterial cell division but intriguingly *ftsZ* knock-outs are viable in the *Streptomyces* genus (McCormick *et al.*, 1994; Santos-Beneit *et al.*, 2017). In the existing *ftsZ* knock-out generated by McCormick *et al.*, 1994 for *S. coelicolor* only the first 277 amino acids of the 400 amino acid long FtsZ was replaced by a neomycin resistance. Hence to directly compare the phenotype of an Δ *ftsZ* mutant from *S. coelicolor* to the phenotype of the Δ *sepF* mutant, described in Chapter 3, the current study generated a novel Δ *ftsZ* mutant, lacking the complete 400 amino acid long FtsZ, using the Redirect[®] PCR-directed mutagenesis approach (Figure 6.17).

Isolation of the potential Δ *ftsZ* double cross-over colonies were not rare but the double cross-over colonies developed much slower than the single crossover exconjugants (Figure 6.2). Numerous colonies were initially picked and after repeated re-streaking any colony producing the grey sporulation pigment was excluded. Screening of the exconjugants lead to the 'blue' colonies being considered the double-crossover Δ *ftsZ* mutant (Figure 5.3).

Compared to the McCormick *et al.*, 1994 Δ *ftsZ* strain, colonies of the current Δ *ftsZ* mutant had a distinctive morphology: both strains lacked vegetative cross-walls and sporulation septa but unlike the McCormick *et al.*, 1994 Δ *ftsZ* strain which still produced the grey sporulation pigment, the current Δ *ftsZ* mutant only produced a blue pigment on the colony surface and in the surrounding media (Figure 6.4 to Figure 6.6, Figure 6.9 to Figure 6.10 and Figure 6.17). Colonies of the current Δ *ftsZ* strain were also prone to producing segments or a secondary morphology, a phenomenon suggestive of genetic instability which has not been previously reported for a Δ *ftsZ* strain (Figure 6.5 and Figure 6.6).

Colonies exhibiting a secondary morphology are suspected to contain additional mutations. Sequencing of the isolated Δ *ftsZ* strains was delayed due to the low efficiency of each passaging event. Attempts to increase the efficiency of a passaging event revealed in the future the addition of sonication prior to streaking could increase the colony forming units and allow the generation of the larger cellular mass that would be required for sequencing (Figure 6.7).

The lack of the grey sporulation pigment and the prevalence of the blue pigment, assumed to be actinorhodin, meant the current Δ *ftsZ* mutant was similar to the Δ *sepF* mutant (Figure 6.4). Compared to the colonies of the Δ *sepF* mutant, the colonies of the Δ *ftsZ* mutant showed a more severe developmental phenotype: the

current \DeltaftsZ mutant had a reduced diameter, grew slower and did not form fork-like tips.

To confirm the \DeltaftsZ mutant, the \DeltaftsZ mutant was complemented *in trans* as previously reported for the \DeltasepF mutant (Chapter 3; Tan, 2018). Colonies of the $\DeltaftsZ/pMS82-FtsZ-Egfp$ strain, containing an FtsZ-Egfp translational fusion, were covered by the grey sporulation pigment (Figure 6.11). However despite the sporulation pigment the majority of the aerial hyphae from $\DeltaftsZ/pMS82-FtsZ-Egfp$ were very slow to develop into any spore chains and did not produce regular FtsZ-Egfp rings (Figure 6.12). Hence the introduction of pMS82-FtsZ-Egfp into the \DeltaftsZ mutant, partially complemented the \DeltaftsZ mutant.

Colonies of the complemented $\DeltaftsZ/pMS82-FtsZ$ strain, containing an untagged *ftsZ*, were also covered by the grey sporulation pigment and were highly similar to wild-type. The aerial hyphae of $\DeltaftsZ/pMS82-FtsZ$ formed regular sporulation septa (Figure 6.14 to Figure 6.15 and Figure 6.17). which lead to copious evenly sized spores. Hence the introduction of the pMS82-FtsZ into the \DeltaftsZ mutant, fully complemented the \DeltaftsZ mutant and showed the phenotype of the \DeltaftsZ mutant was due to lack of *ftsZ* and not polar effects. We are aware of other laboratories attempting to generate a \DeltaftsZ knockout strain in *S. coelicolor* without success. We are confident that our novel strain will be very useful in the future for further studies about the link between cell division and polar growth.

Previously Tan, 2018 found FtsZ did not form rings in the absence of *sepF*. Hence we investigated the localisation of SepF in the colonies of the \DeltaftsZ mutant. Epi-fluorescence showed in the \DeltaftsZ mutant SepF-Egfp localised as fluorescent spots but no SepF rings were ever detected (Figure 6.16). These observations suggest that SepF was unable to polymerise into a ring in the absence of FtsZ. Hence we established that SepF and FtsZ are interdependent.

6.4 Acknowledgements

The work in the current chapter utilised the 4A10:: $\DeltaftsZ:apra^R$ cosmid, generated by Eve Maunders, and the pMS82-FtsZ-Egfp and pMS82-SepF-Egfp plasmids, generated by Xiao Tan. The cosmid and plasmids were generated by previous lab members prior to and independently of the current study.

7.0 Investigating the role of compartmentalisation in the spatial and temporal localisation of actinorhodin production

7.1 Introduction

In the previous chapters SepF was shown to be an important positive regulator of the key early divisome component, FtsZ. In the absence of *sepF*, colonies of *S. coelicolor* are unable to form regular vegetative cross-walls and sporulation septa (Chapter 3). After an extended 68 hrs period, partial, often twisted sporulation septa form but these septa do not lead to the formation of spores or production of the grey sporulation pigment. Instead, the pigmentation on the surface of the $\Delta sepF$ colonies exhibited a litmus-like colour transition from blue to reddish pink (Figure 7.1). The colour transition is characteristic of the pH sensitive antibiotic, actinorhodin, known to be produced by *S. coelicolor* which is pink in acid and blue in alkaline conditions (Abbas and Edwards, 1990).

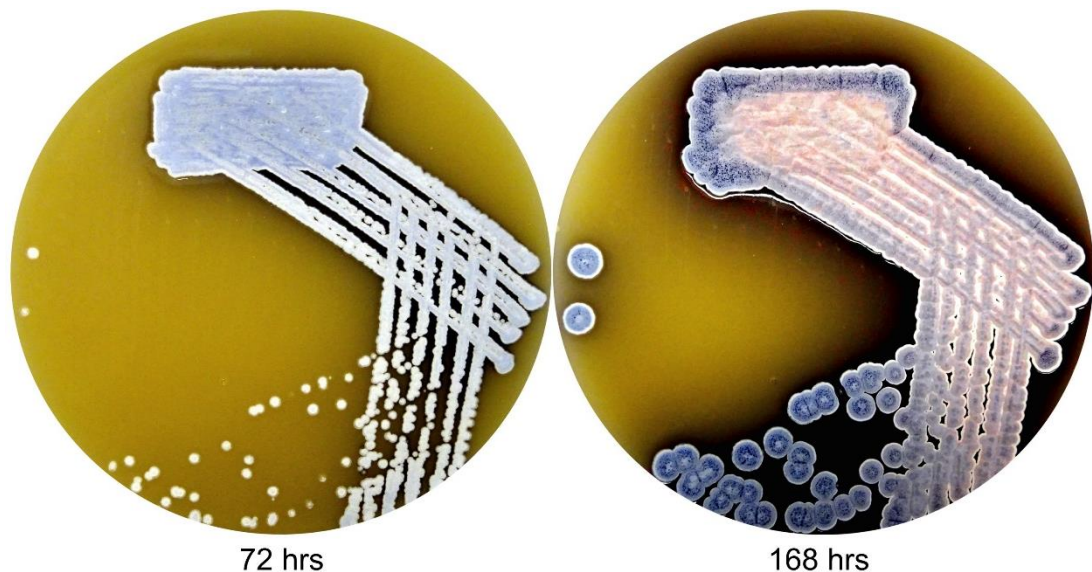


Figure 7.1 The pigmentation on the surface of the colonies from $\Delta sepF$. The $\Delta sepF$ mutant was streaked onto SFM+apra medium and incubated at 30°C until the stated timepoints.

Actinorhodin is formed by a type II PKS encoded by the actinorhodin gene cluster, spanning genes *SCO5071* to *SCO5092* (Figure 1.17, Figure 1.20 and Table 1.1; Craney *et al.*, 2013). Initially the octaketide backbone of actinorhodin is formed by the minimal PKS (Dreier *et al.*, 1999). The minimal PKS consists of a heterodimeric KS-CLF encoded by *SCO5087* and *SCO5088*, an ACP encoded by

SCO5089 and the MAT from fatty acid biosynthesis. The *holo*-ACP, formed by the addition of an 18-Å-long phosphopantetheine arm to a conserved Asp-Ser-Leu motif, is responsible for the repeated transfer of malonyl units from MAT to KS-CLF for the extension of the growing chain (Beltran-Alvarez *et al.*, 2007; Keatinge-Clay *et al.*, 2004). The decarboxylation of malonyl ACP to acetyl ACP is catalysed by the CLF of KS-CLF then the extension of the growing chain from the acetyl ACP starter unit is catalysed by the iterative cycles of the KS from KS-CLF. A total of eight cycles is required to form the octaketide backbone. Once formed the octaketide backbone is cyclised by KS-CLF and the ACP affects the initial tailoring step by binding to SCO5086, a tetrameric ketoreductase, which reduces the carbonyl group at C9 (Hadfield *et al.*, 2004). Additional modification by other tailoring enzymes, leading to the step-wise generation of the intermediates, (S)-DNPA, DDHK and DHK before DHK is dimerised to form actinorhodin (Figure 1.20; Okamoto *et al.*, 2009; Taguchi *et al.*, 2000).

In addition to actinorhodin, *S. coelicolor* produces a class of closely related compounds, together referred to as the actinorhodins (Bystrykh *et al.*, 1996). One of the actinorhodins is the full lactone form of actinorhodin, γ -actinorhodin. γ -actinorhodin is distinguishable from actinorhodin due to their opposing solubility in chloroform and methanol plus their opposing cellular localisation as γ -actinorhodin is secreted by the export pumps and found extracellularly. Interestingly γ -actinorhodin was recently shown to have selective bactericidal activity against Gram positive bacteria, a key property for potentially useful antibacterial drugs (Nass *et al.*, 2017).

The function and ecological importance of antibiotic production remains unclear. The classical theory for antibiotic production suggests antibiotics are produced as inter-microbial weapons, in a similar function to that seen in a clinical setting, in response to an external stimulus (Romero *et al.*, 2012; Wang *et al.*, 2010). The alternative theory for antibiotic production suggests antibiotics, at sub-inhibitory concentration, coordinate a range of social behaviours, such as quorum-sensing, expression of virulence genes and biofilm formation. One behaviour specific to *Streptomyces* could be the programmed cell death of vegetative hyphae to support the formation of aerial hyphae (Miguélez *et al.*, 1999). In this model antibiotics could act as a signalling molecule in response to an internal stimulus, such as cell density.

Importantly γ -actinorhodin is readily secreted to the medium when most *S. coelicolor* derivatives are grown on solid medium. However, the blue pigment is not observed on the surface of the colonies of the wild-type strain suggesting that actinorhodin is produced in the vegetative mycelium, but not in the aerial mycelium and spores. Previously, blue pigment on the surface of solid grown cultures were documented for some of the *whi* mutants that lack septum formation, such as *whiA*, *whiB*, *whiH*, *whiG*. When the $\Delta whiA$ and $\Delta whiB$ strains were grown on solid SFM medium the $\Delta whiA$ strain developed a blue pigmentation, albeit less than the $\Delta sepF$ strain, whilst the $\Delta whiB$ strain stayed white (Figure 7.2).

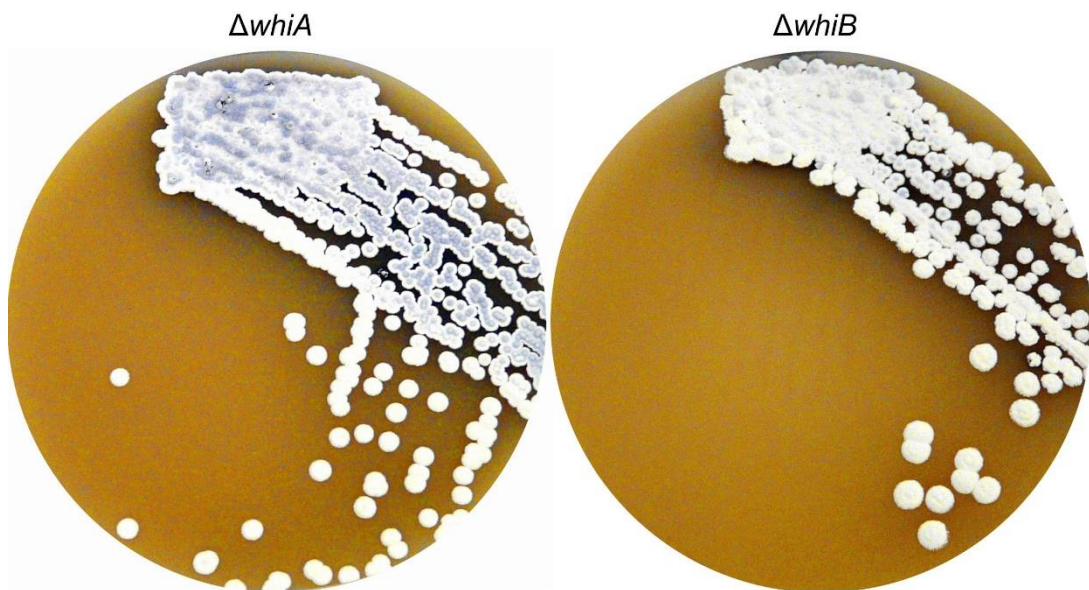


Figure 7.2 The colony morphology of the $\Delta whiA$ and $\Delta whiB$ strains. Both strains, $\Delta whiA$ and $\Delta whiB$ were streaked onto SFM and incubated at 30°C. Camera images were taken after 120 hrs.

The current chapter aimed to investigate the pigmentation on the surface and in the surrounding media of the $\Delta sepF$ mutants. Due to the transition of the pigment from blue to pink, the pigment was expected to be from the actinorhodins. As actinorhodins are not observed on the surface of wild-type colonies, the pigmentation on the colonies of the $\Delta sepF$ mutants was hypothesised to be due to the over-production of the actinorhodins and the localisation of production to the aerial hyphae, in the absence of regular septa and the grey sporulation pigment. To test the hypothesis, the current chapter aimed to:

- Characterise the level of actinorhodins produced by the wild-type and $\Delta sepF$ strains.
- Isolate M145 and $\Delta sepF$ strains containing a SCO5089-Egfp translational fusion, using the Redirect[®] PCR-directed mutagenesis approach. As

mentioned above, SCO5089 or ActI-ORF3 is the actinorhodin biosynthesis specific ACP, which as part of the minimal PKS produces the initial octaketide backbone for actinorhodin (Dreier *et al.*, 1999).

- Characterise the spatial and temporal localisation of 5089-Egfp in M145/3G11-5089-Egfp and $\Delta sepF$ /3G11-5089-Egfp, using epi-fluorescent microscopy.

7.2 Results

7.2.1 The level of actinorhodins secreted by the colonies of the wild-type M145 and $\Delta sepF$ strains

The localisation of actinorhodins in the media used to grow wild-type *S. coelicolor* was noted during the early identification process of actinorhodin (Abbas and Edwards, 1990). In the current study the pigmentation surrounding and on the surface of $\Delta sepF$ colonies indicated the production of the actinorhodins was enhanced in the *sepF* knock-out mutant. Unfortunately attempts to compare the intracellular levels of actinorhodins in the hyphae of $\Delta sepF$ and wild-type using HPLC and mass spectrometry were unsuccessful. These attempts were potentially hampered by the characteristic low solubility and different solubility of the actinorhodins in chloroform and methanol, mentioned in the Introduction.

Comparison of the extracellular levels of actinorhodins, exported from the hyphae of the wild-type M145 or $\Delta sepF$ strains into the media revealed increased levels of actinorhodins secreted from the colonies of the $\Delta sepF$ mutant. Both strains were grown on R5 agar medium containing the appropriate antibiotics and covered by a sterile cellophane for 120 hrs. At 120 hrs the absorbance of the liquidised plate at OD₆₄₀ was measured and then divided by the dry weight of the removed *Streptomyces* material. All of the strains subjected to this method grow well in the presence of cellophane. There was greater variation than expected between the dry weights of the replicates, potentially due to the softness of the media hindering the removal of the *Streptomyces* material. Exclusion of the replicates considered outliers reduced the number of replicates to below three preventing statistical analysis. However the visual comparison of the pigmentation in the medium closely matched the trends shown by the normalised absorbances and, as shown in Section 7.2.2.2 and Section 7.2.2.3, all of the strains subjected to this method grow well in the presence of cellophane.

The samples from wild-type M145 remained clear and had a ~2-fold lower absorbance than the blue pigmented samples from $\Delta sepF$ (Figure 7.3). Therefore colonies of $\Delta sepF$ secreted more actinorhodins, which leads to the blue halo in the surrounding media. This observation would suggest that actinorhodin production is elevated in the colonies of $\Delta sepF$.

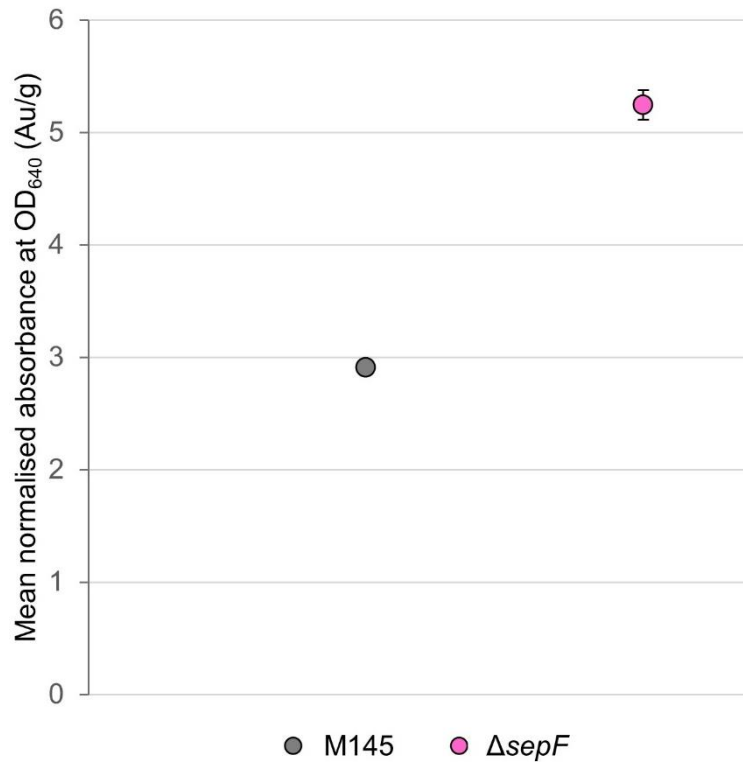


Figure 7.3 Actinorhodins in the medium of the wild-type M145 and $\Delta sepF$ strains. Each strain was confluent streaked onto R5 medium covered with cellophane, then grown at 30°C for 120 hrs. At 120 hrs the absorbance of the liquidised medium, at OD_{640 nm}, was measure and divided by the dry mass of the *Streptomyces* material. The replicate number for M145 was two and the replicate number for $\Delta sepF$ was three. For the $\Delta sepF$ samples standard error error bars are shown. Due to the lack of replicates no statistical analysis was completed.

7.2.2 The temporal and spatial localisation of actinorhodin production in the wild-type M145 and $\Delta sepF$ strains

7.2.2.1 Introducing a 5089-Egfp translational fusion into the wild-type M145 and $\Delta sepF$ strains

Next the temporal and spatial localisation of actinorhodin production was investigated, using a SCO5089-Egfp translational fusion. The SCO5089-Egfp translational fusion is referred to as 5089-Egfp from now on. The 3G11-5089-Egfp cosmid, containing 5089-Egfp, was generated and introduced into wild-type M145 and $\Delta sepF$ strains via the Redirect[®] PCR-directed mutagenesis approach (Gust *et al.*, 2002).

Briefly the Redirect[®] PCR-directed mutagenesis approach utilised an *egfp-apra^R* cassette with a four amino acid long linker, consisting of proline, valine, alanine and threonine to allow independent folding of both the protein of interest and Egfp. The *egfp-apra^R* cassette was extended to contain 40 bp flanking regions, homologous to the 40 bp flanking regions of the STOP codon of SCO5089. Next in *E. coli* BW25113/pIJ790 carrying the λ RED recombinase, the extended *egfp-apra^R* cassette underwent homologous recombination with the 3G11 cosmid, which contains the actinorhodin gene cluster, to generate the 3G11-5089-Egfp cosmid (Figure 7.4A and Figure 7.4B). The 3G11-5089-Egfp cosmid was electroporated into the methylation deficient *E. coli* ET12567:pUZ8002 strain to allow conjugation of 3G11-5089-Egfp into the wild-type M145 strain and the $\Delta sepF$ mutant (Figure 7.4C). Introduction of 3G11-5089-Egfp into the unmarked wild-type strain allowed the screening and identification of *apra^R kana^S* colonies and *apra^R kana^R* colonies, which had undergone either double or single crossover events, respectively (Figure 7.4D). After introduction of 3G11-5089-Egfp into the *apra^R* marked $\Delta sepF$ mutant, only kanamycin selection was used on the exconjugants. Selection allowed the identification of *apra^R kana^R* colonies, which had undergone single crossover events. In theory, from the single crossover recombinants double crossovers could have been produced and screened for, not by replica plating but by PCRs focusing on the Egfp fusion.

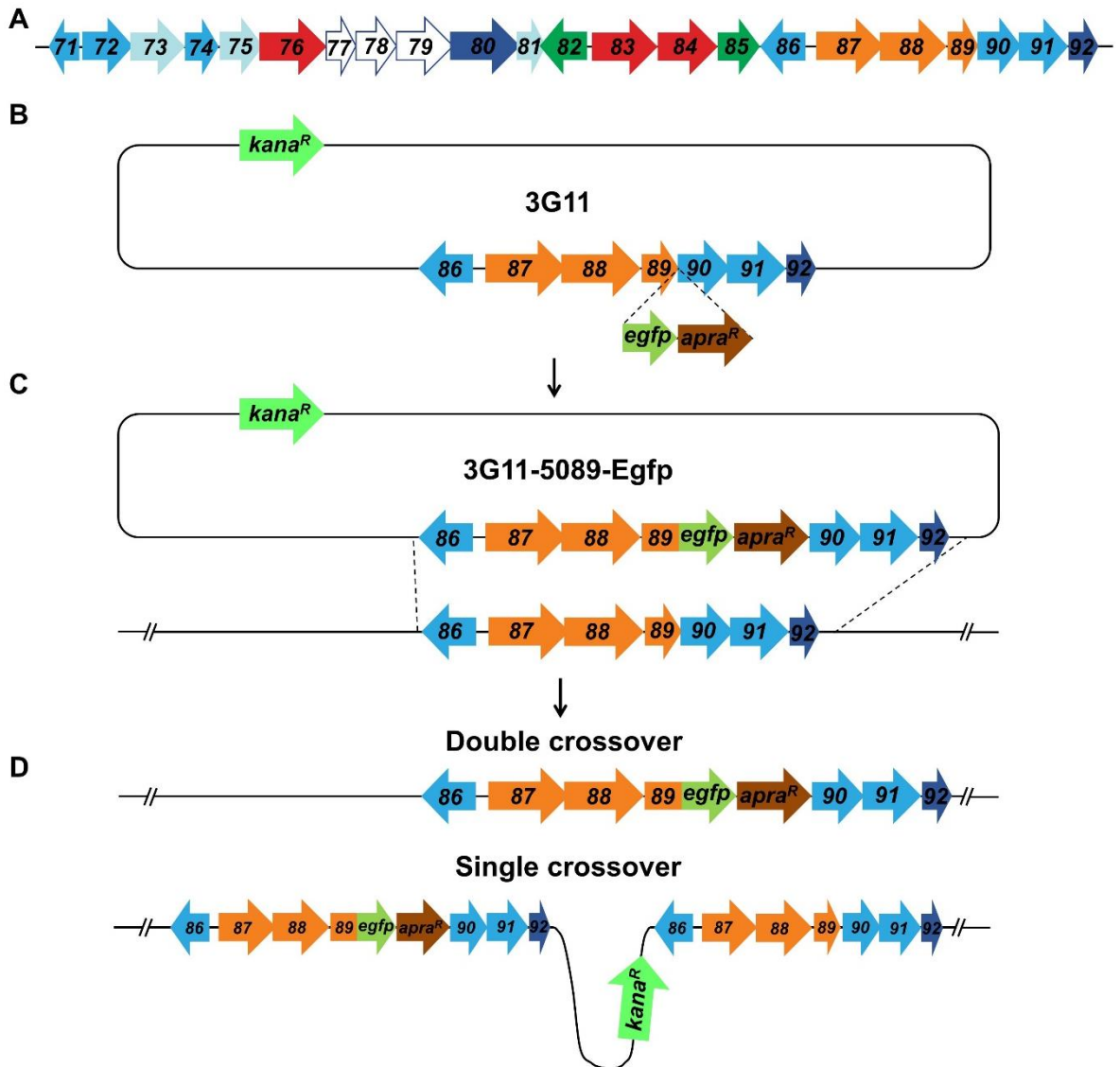


Figure 7.4 Generation of the 5089-Egfp containing strains using the Redirect[®] PCR-directed mutagenesis approach. A) The actinorhodin gene cluster spanning SCO5071 to SCO5092.. The 3G11 cosmid contains the complete actinorhodin gene cluster. SCO5088 to SCO5092 are shown in detail in B to D. B) An extended *egfp-apra^R* cassette was introduced by PCR directed homologous recombination, into 3G11 to generate the 3G11-5089-Egfp cosmid. C) The 3G11-5089-Egfp cosmid was conjugated into the wild-type M145 and $\Delta sepF$ strains. D) The predicted chromosomal organisation of the successful single and double crossover strains. The single crossover strains contain the complete 3G11-5089-Egfp cosmid.

Unlike the *apra*^R *kana*^S colonies which have undergone a double crossover event and contain a single copy of the actinorhodin gene cluster including the 5089-Egfp translational fusion, the *apra*^R *kana*^R colonies which have undergone a single crossover event contain two copies of the actinorhodin gene cluster and a copy of the other genes within the 3G11 cosmid DNA. Characterisation of the exconjugants derived from the unmarked wild-type strain showed single and double crossover events resulted in distinct colony morphologies. The double crossover colonies were characterised by the presence of the grey sporulation pigment but the absence of the blue pigmentation from the actinorhodins (Figure 7.5). The absence of the blue pigmentation could be explained by downstream polar effects caused by the replacement of *SCO5089* by the 5089-Egfp translational fusion, followed by the apramycin resistant cassette. The introduction of the Egfp fusion could have prevented the expression of the later genes in the biosynthetic pathway and the export of the actinorhodins. Most of the exconjugants were single crossovers, which were characterised by enhanced blue pigmentation in the surrounding media and a reduction in colony diameter (Figure 7.5). Passaging the blue single crossover sporadically produced 'white' colonies characterised by little if any blue pigmentation and the restoration of the colony diameter. The white single crossover colonies were reproducibly found but how the white colonies are produced remains unknown. These white single crossover colonies are expected to contain a secondary mutation.

Similarly, exconjugants derived from the Δ *sepF* mutant had the distinctive 'blue' and 'white' colony morphologies of the single crossovers (Figure 7.5). The exconjugants of the Δ *sepF* mutant were distinctive from the wild-type exconjugants as in the absence of the grey sporulation pigment, the blue single crossovers from Δ *sepF* had a blue pigmented colony surface and the white single crossovers had a white pigmented colony surface.

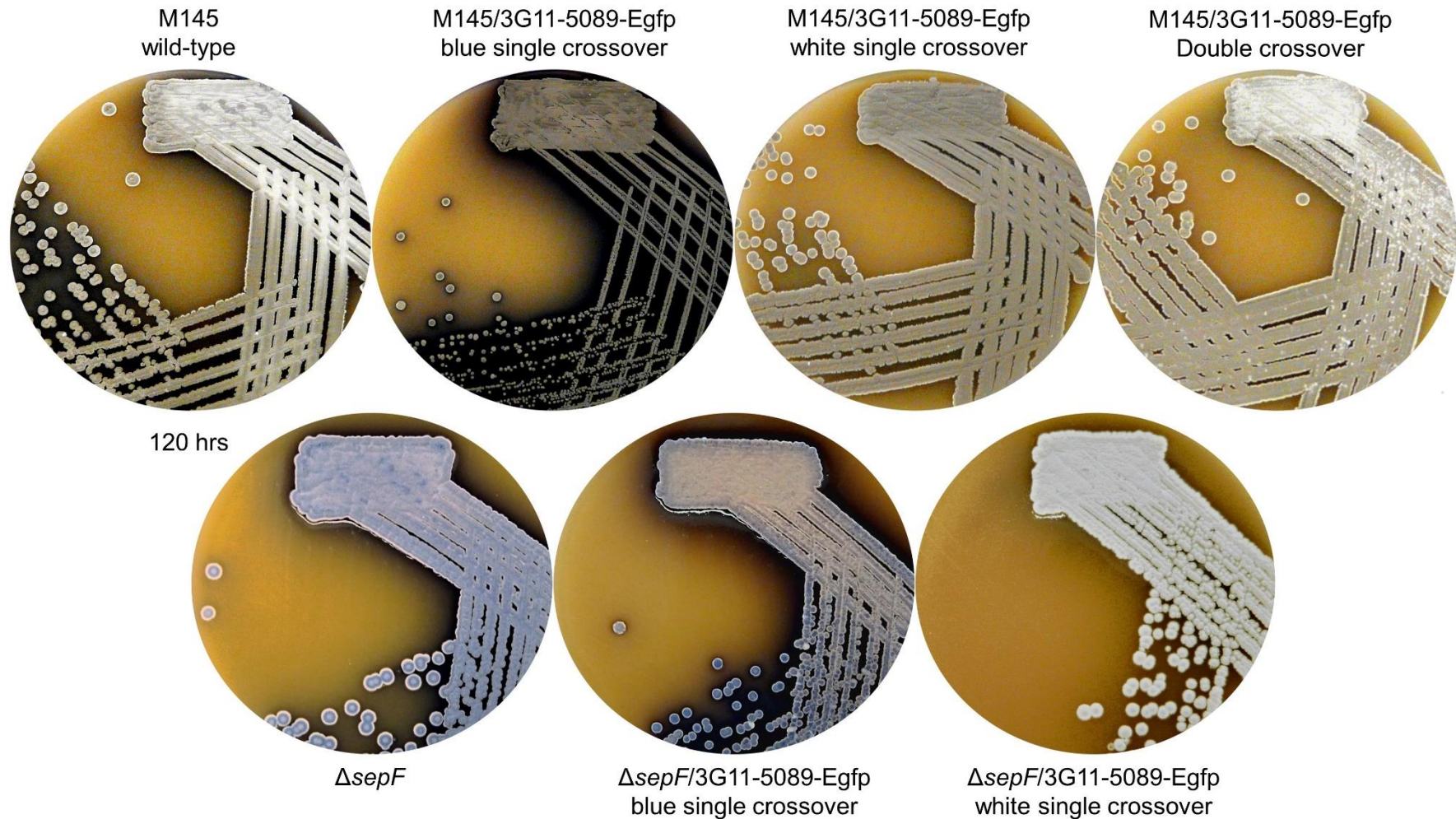


Figure 7.5 Comparison of the 5089-Egfp containing single crossover strains to the wild-type M145 and $\Delta sepF$ strains. All strains were grown on SFM medium at 30°C for 120 hrs. The single crossover strains were grown in the presence of kanamycin.

The microscopic analysis of the wild-type derivatives which have undergone a double cross-over event and expected polar effects, indicated the absence of the blue pigmentation corresponded to an absence of detectable fluorescence from 5089-Egfp (data not shown). So, the current study focused on characterising the spatial and temporal localisation of actinorhodin production in the blue single crossover strains.

7.2.2.2. The level of actinorhodins secreted from the colonies of M145/3G11-5089-Egfp and $\Delta sepF/3G11-5089-Egfp$

The blue single crossover strains, now referred to as M145/3G11-5089-Egfp and $\Delta sepF/3G11-5089-Egfp$, contain two copy of the actinorhodin gene cluster and are characterised by an enlarged blue pigmented halo in the media (Figure 7.5). Therefore the level of actinorhodins in the medium used to grow the M145/3G11-5089-Egfp and $\Delta sepF/3G11-5089-Egfp$ strains was expected to be higher and were measured and compared to the levels detected for the wild-type M145 and $\Delta sepF$ strains, in Section 7.2.1.

Interestingly the M145/3G11-5089-Egfp samples had ~17.5-fold higher absorbance than the M145 samples and the $\Delta sepF/3G11-5089-Egfp$ samples had ~4 fold higher absorbance than the $\Delta sepF$ samples (Figure 7.6). When the M145/3G11-5089-Egfp and $\Delta sepF/3G11-5089-Egfp$ samples were directly compared there was ~2-fold higher absorbance from the M145/3G11-5089-Egfp samples. Hence the presence of the second actinorhodin gene cluster in the single crossover strains is thought to enhance the production of the actinorhodins and therefore enhance the secretion of the actinorhodins into the surrounding media.

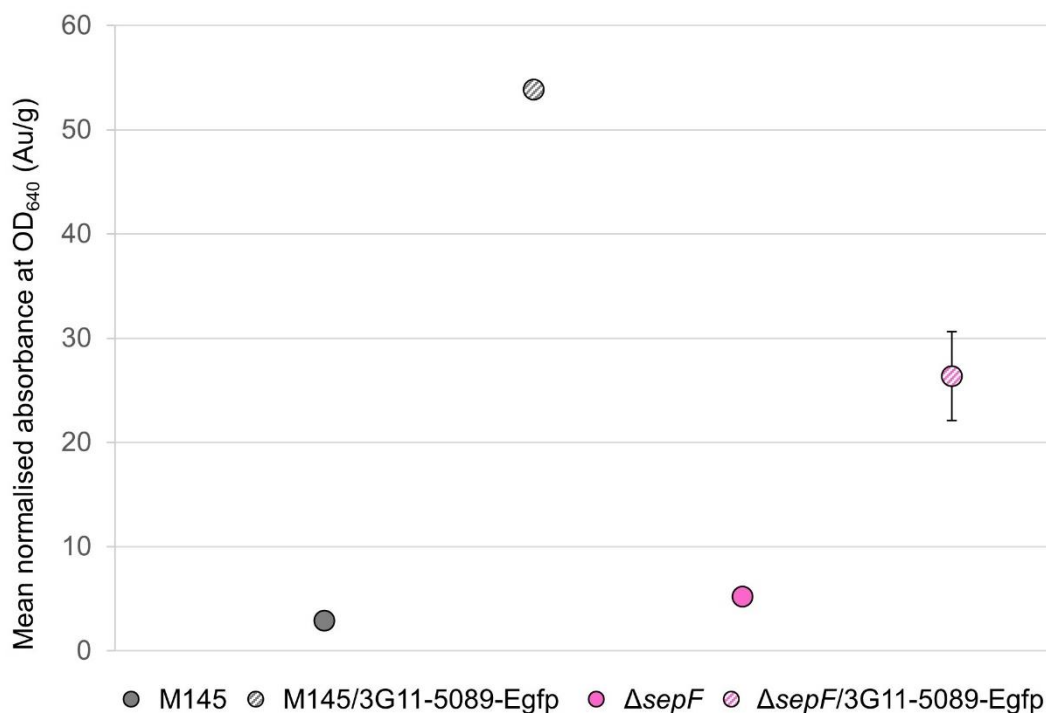


Figure 7.6 Actinorhodins in the medium of wild-type M145, M145/3G11-5089-Egfp, $\Delta sepF$ and $\Delta sepF/3G11-5089-Egfp$. Each strain was confluent streaked onto R5 medium covered with cellophane, then grown at 30°C for 120 hrs. At 120 hrs the absorbance of the liquidised medium, at OD_{640 nm}, was divided by the dry mass of the *Streptomyces* material. The replicate number for M145 and M145/3G11-5089-Egfp was two and the replicate number for $\Delta sepF$ and $\Delta sepF/3G11-5089-Egfp$ was three. For data sets with three replicates standard error error bars are shown. Due to the lack of replicates no statistical analysis was completed.

7.2.2.3 The localisation of 5089-Egfp in the colonies of M145/3G11-5089-Egfp and $\Delta sepF/3G11-5089-Egfp$

Initially to investigate the localisation of 5089-Egfp in the colonies of M145/3G11-5089-Egfp and $\Delta sepF/3G11-5089-Egfp$, whole colonies grown on SFM+kana medium, covered by a cellophane, were visualised using epi-fluorescent microscopy. Cellophane allows nutrients to pass between the media and the hyphae but prevents the hyphae from penetrating the media. Hence the whole colony can be lifted from the medium and visualised. At 4 hrs intervals between 16 hrs and 48 hrs of incubation, a 15 mm x 15 mm square of cellophane, covered by dispersed *Streptomyces* colonies, was removed from the medium and sealed between a coverslip and slide. At a colony level, the fluorescence from 5089-Egfp was predicted to either commence at the periphery of the colony and move inwards or commence at the centre of the colony and move outwards, based on the classical and alternative theory for antibiotic production (Figure 7.7; Raaijmakers and Mazzola, 2012; Section 7.1).

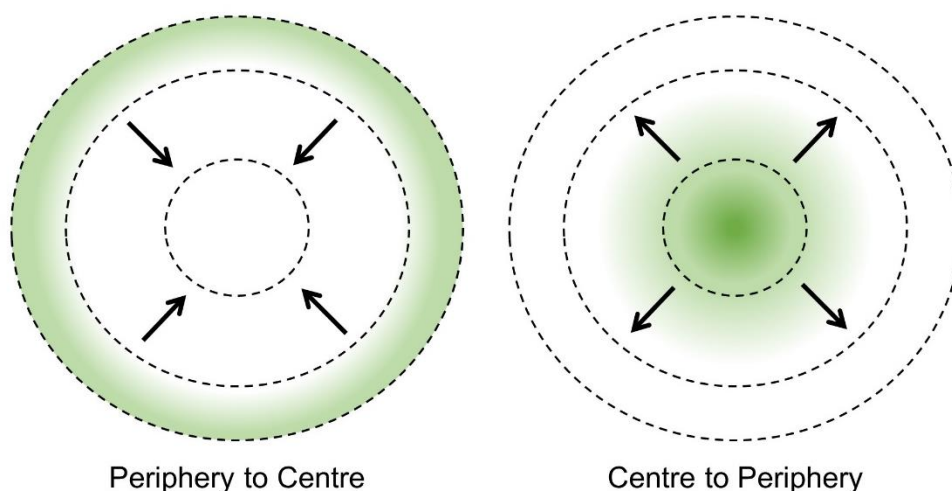


Figure 7.7 The predicted localisation patterns of 5089-Egfp in the colonies of M145/3G11-5089-Egfp and $\Delta sepF/3G11-5089-Egfp$. The localisation of 5089-Egfp was predicted to commence either at the periphery or at the centre of the colonies, based on the classical and alternative theories for antibiotic production (Raaijmakers and Mazzola, 2012; Section 7.1).

In the first part of the investigation, between 16 hrs and 24 hrs of incubation, fluorescence commenced from the centre of the colonies (Figure 7.8). After 16 hrs of growth, colonies from M145/3G11-5089-Egfp and $\Delta sepF/3G11-5089-Egfp$ were a loose network of vegetative hyphae which lacked any fluorescence. Over the next 4 hrs colonies increased in the size and density. By 20 hrs of growth, the denser central regions of the colonies from both strains contained fluorescence in discrete areas of the hyphae, despite the presumed absence of cross-walls in the $\Delta sepF/3G11-5089-Egfp$ strain. By 24 hrs of growth, the number of colonies containing fluorescence and the amount of fluorescent, positioned sporadically in the middle of each colony had increased. Interestingly the colonies of $\Delta sepF/3G11-5089-Egfp$ were only distinguished from the colonies of M145/3G11-5089-Egfp by a subtle increase in the spread of fluorescence or a subtle off-setting of the fluorescence from the centre of the colony.

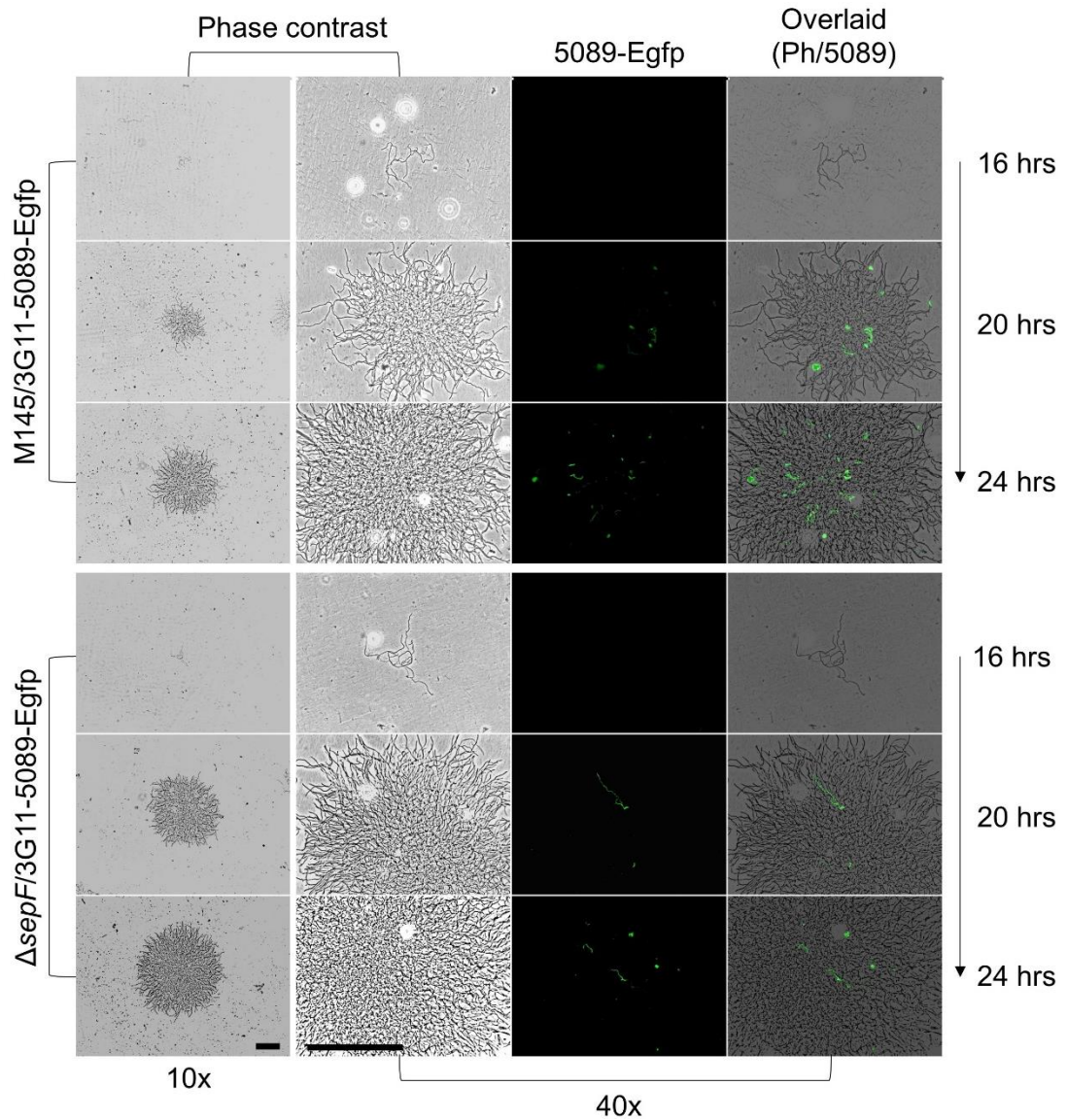


Figure 7.8 The localisation of 5089-Egfp in the young colonies of *M145/3G11-5089-Egfp* and Δ *sepF/3G11-5089-Egfp*. Colonies were visualised, at the stated timepoints, under 10x and 40x magnification. The phase contrast image (left) is shown alongside the fluorescent image, taken with 200 ms exposure (middle) then both images were overlaid (right). The scale bars represent 50 μ m.

Between 28 hrs and 36 hrs of incubation, fluorescence increased and extended from the centre of the colony to the periphery (Figure 7.9). In both strains, by 28 hrs of growth, the fluorescence increased to form a 'fluorescent core'. The fluorescent cores increased in circumference and density but did not fully reach the periphery by 36 hrs of growth. The spread of fluorescence was preceded by an increase in hyphal density and was characterised by extensive change in detectable fluorescence between 32 hrs and 36 hrs, particularly in the colonies of $\Delta sepF/3G11-5089-Egfp$. At the periphery there was strain specific variation in the percentage of hyphae with fluorescent tips; only ~5-10% of hyphal tips from M145/3G11-5089-Egfp had detectable fluorescence but ~15-80% of hyphal tips from $\Delta sepF/3G11-5089-Egfp$ had detectable fluorescence. Although the cause of this variation remains unclear, one possibility is that fluorescence is absent from actively growing hyphal tips

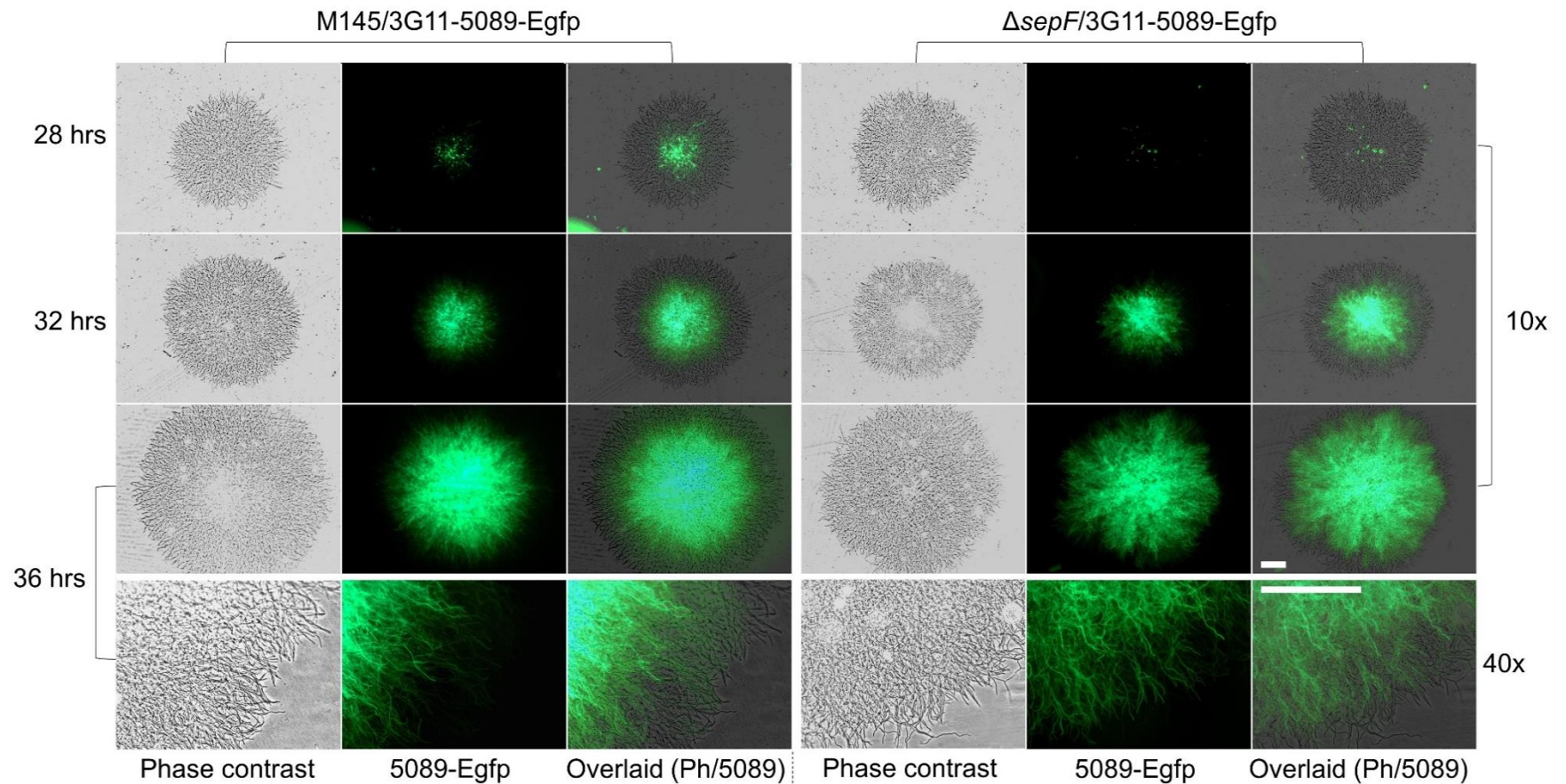


Figure 7.9 The localisation of 5089-Egfp in the vegetative colonies of M145/3G11-5089-Egfp and $\Delta sepF/3G11-5089-Egfp$. Colonies were visualised at the stated time points, under 10x and 40x magnification. For each panel the phase contrast image (left) is shown alongside the fluorescent image, taken with 200 ms exposure (middle) then both images were overlaid (right). The scale bars represent 50 μ m.

Between 40 hrs to 48 hrs of incubation, the spatial localisation of 5089-Egfp across the whole colony was maintained (Figure 7.10). This time period coincides with sporulation in the wild-type M145 strain and the time when actinorhodins are detectable in the media. The fluorescence pattern of 5089-Egfp did not really change between 40 hrs and 48 hrs, suggesting that once SCO5089 is produced, SCO5089 remains present within the colonies. Alternatively, the Egfp fusion could have altered the stability of SCO5089. Overall the localisation of 5089-Egfp in the colonies of M145/3G11-5089-Egfp and $\Delta sepF$ /3G11-5089-Egfp was highly similar with fluorescence initially detectable in the centre of the colonies then expanding outwards to the periphery.

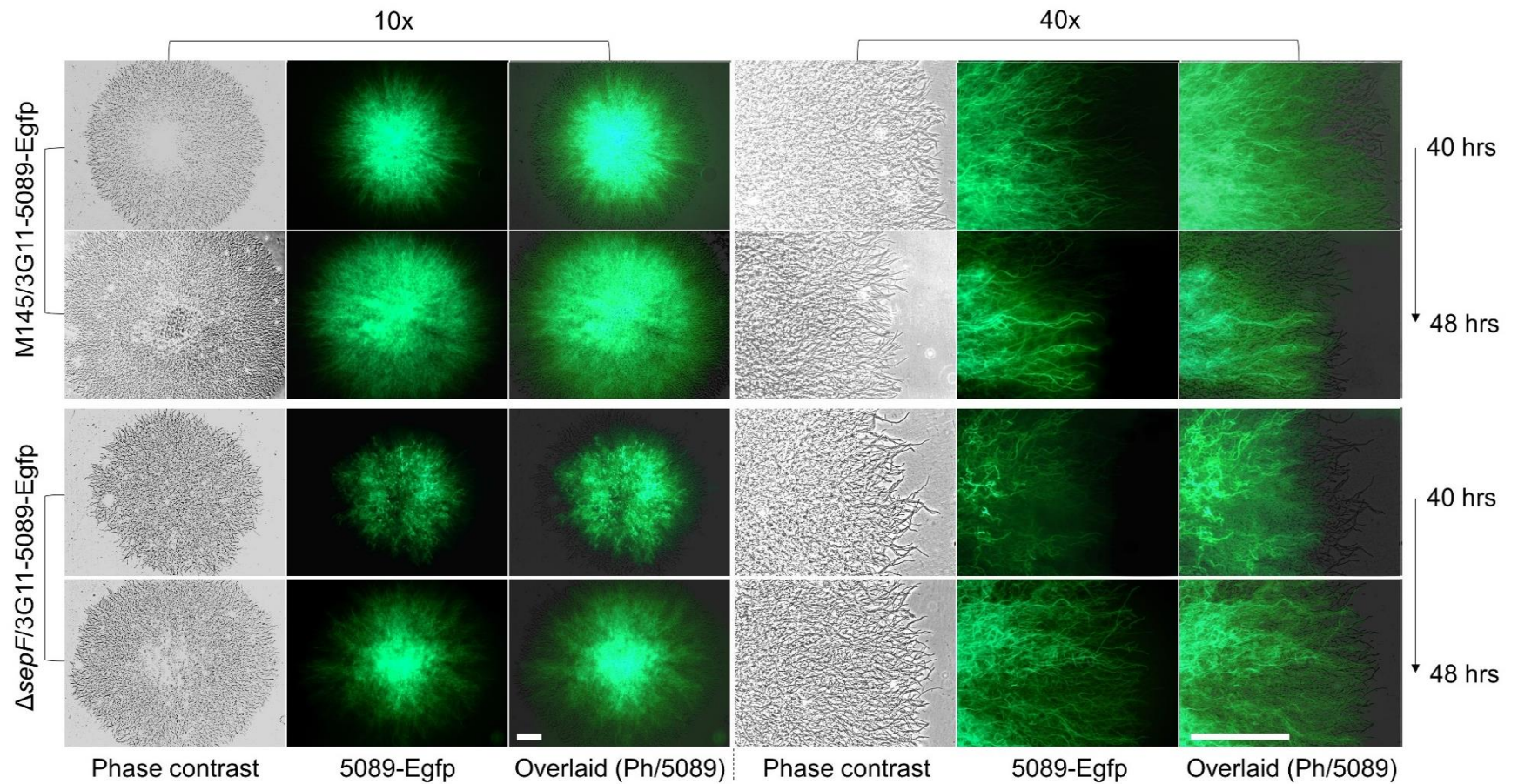


Figure 7.10 The localisation of 5089-Egfp in the maturing colonies of *M145/3G11-5089-Egfp* and Δ *sepF/3G11-5089-Egfp*. Colonies were visualised, at the stated timepoints, under 10x and 40x magnification. For each panel the phase contrast image (left) is shown alongside the fluorescent image, taken with 200 ms exposure (middle) then both images were overlaid (right). The scale bars represent 50 μ m.

The early fluorescent signal within the individual hyphae of M145/3G11-5089-Egfp and $\Delta sepF/3G11-5089-Egfp$, raised the question of how 5089-Egfp localises within these hyphae (Figure 7.8). To visualise the localisation of 5089-Egfp at a hyphae level, the M145/3G11-5089-Egfp and $\Delta sepF/3G11-5089-Egfp$ strains were grown alongside a sterile coverslip until the stated timepoints, covering both vegetative and aerial growth, then viewed using epi-fluorescent microscopy.

After 24 hrs of growth, the vegetative network of M145/3G11-5089-Egfp had readily detectable fluorescent segments (Figure 7.11). The segments of fluorescence suggests *SCO5089* is not uniformly expressed and there are areas of the hyphae where 5089-Egfp expression is first upregulated. Compartments next to those containing fluorescence were often bright on the phase contrast image compared to the dark actively growing hyphae. Brightness on the phase contrast might be an indication of hyphal ageing or the beginning of hyphal lysis. Hence production of 5089-Egfp is suggested to be affected by cell lysis. In areas where lysed hyphae were less common, hyphae often contained adjoining fluorescent compartments with varying intensities, suggesting that the production of 5089-Egfp in neighbouring compartments could be controlled by signalling, perhaps even signalling by actinorhodin itself.

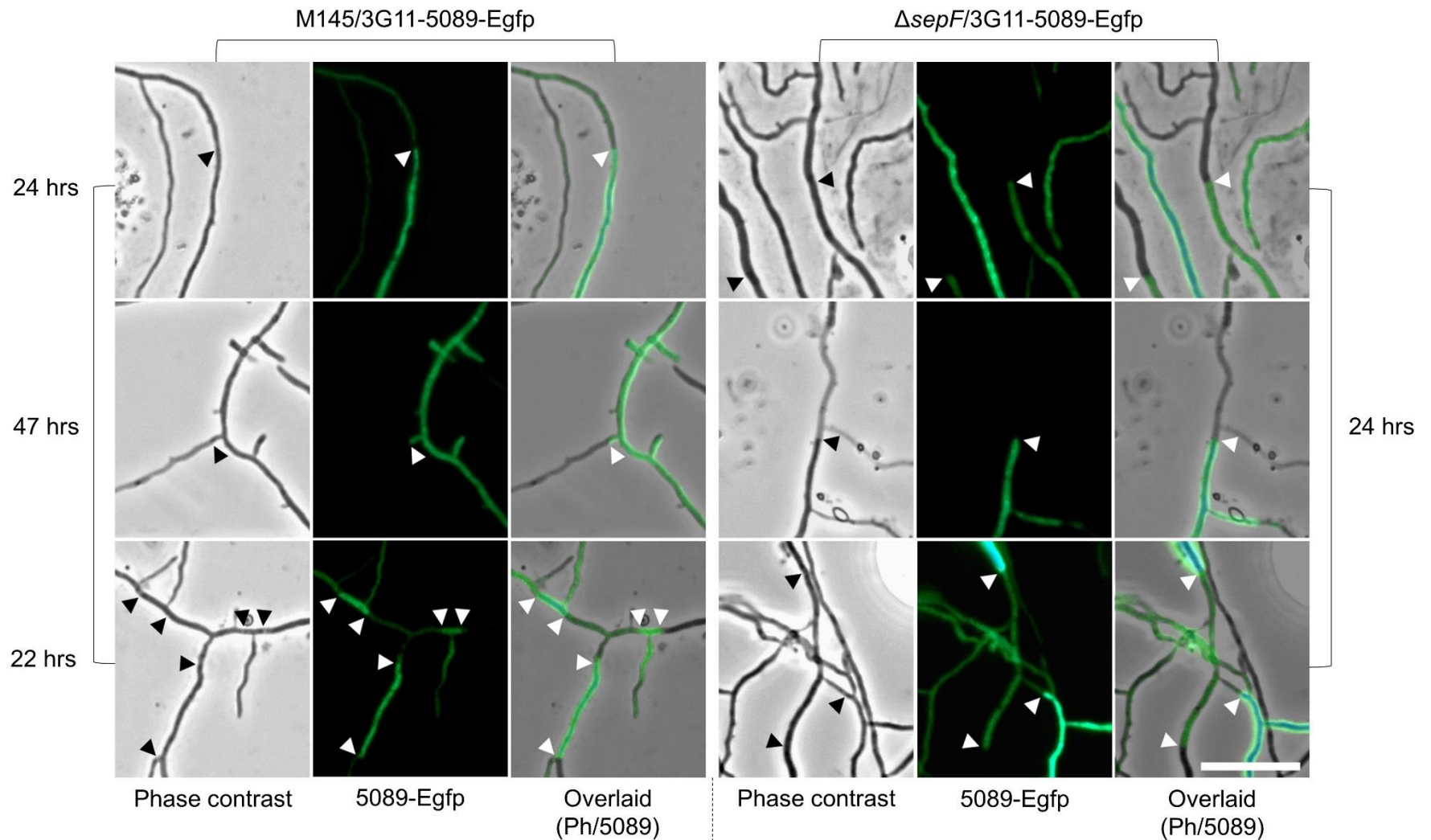


Figure 7.11 Compartmentalisation in the hyphae of M145/3G11-5089-Egfp and Δ sepF/3G11-5089-Egfp. For each panel the phase contrast image (left) is shown alongside the fluorescent image (middle) then both images were overlaid (right). Lysis was identified by a blotchy or inverted appearance on the phase contrast image. The arrows mark a sudden change in fluorescence. Images were taken under 100x magnification with 100 ms exposure. The scale bar represents 10 μ m.

Further investigation into the compartmentalised expression pattern of 5089-Egfp in the vegetative hyphae of M145/3G11-5089-Egfp and $\Delta sepF/3G11-5089-Egfp$ indicated the repeated presence of longer fluorescent compartments in $\Delta sepF/3G11-5089-Egfp$ than those in M145/3G11-5089-Egfp at the same timepoint (Figure 7.12). Unfortunately staining attempts using WGA-Alexa647 conjugate to stain cross-walls adjacent to the fluorescent compartments in the wild-type M145 and the $\Delta sepF$ strains were unsuccessful. Therefore the details and mechanisms of the segments remain to be confirmed.

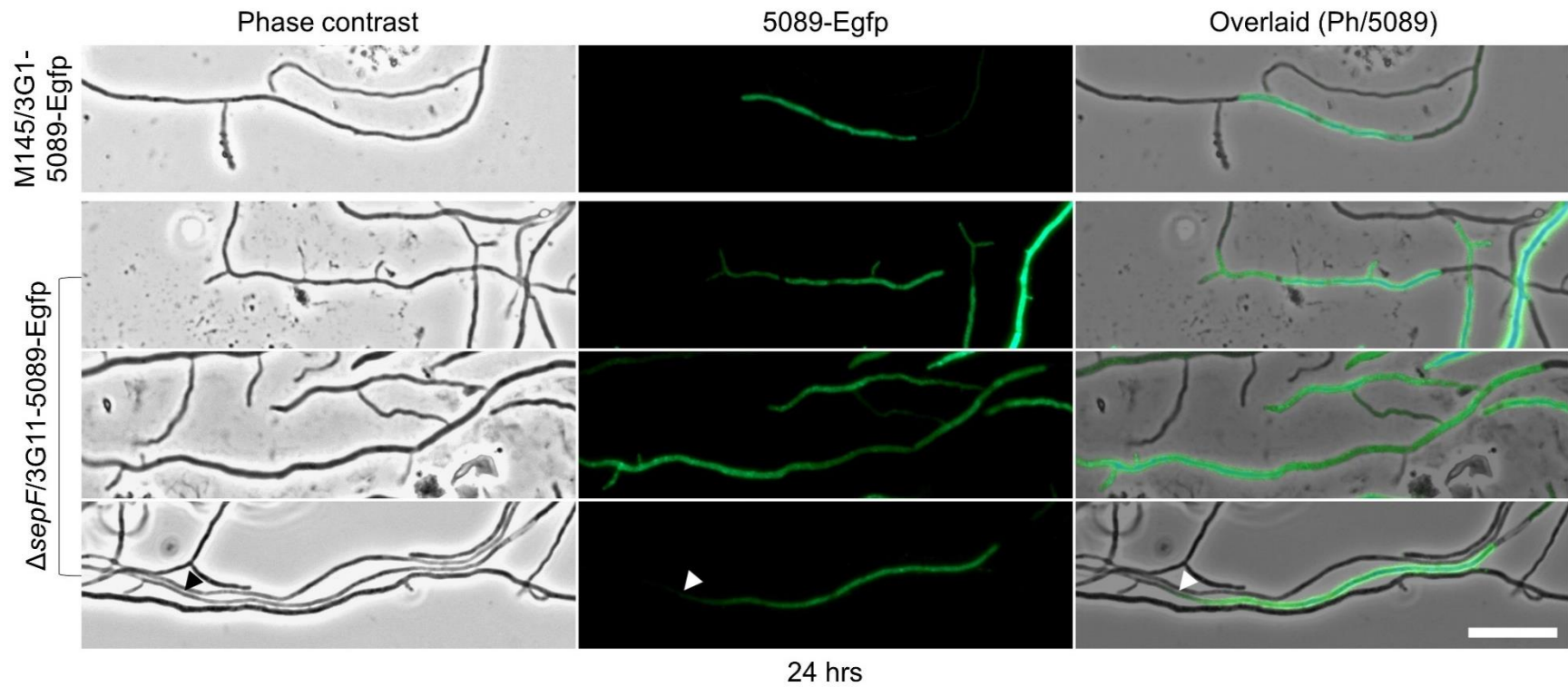


Figure 7.12 Fluorescent compartments in the hyphae of M145/3G11-5089-Egfp and $\Delta sepF/3G11-5089-Egfp$. The phase contrast image (left) is shown alongside the fluorescent image, (middle) then both images are overlaid (right). The arrows indicate a rare gradient in fluorescence. Images were taken under 100x magnification with 100 ms exposure. The scale bar represents 10 μ m.

The compartmentalised expression of 5089-Egfp in the M145/3G11-5089-Egfp strain is likely to be restricted by vegetative cross-walls. Surprisingly in the $\Delta sepF/3G11-5089-Egfp$ strain, which is derived from $\Delta sepF$ and is not expected to undergo any cross-wall formation, the expression pattern of 5089-Egfp was also compartmentalised. Potentially compartmentalisation of 5089-Egfp expression could occur due to the presence of the proposed cross-membranes that can form across the vegetative hyphae even in the absence of cross-walls (Celler *et al.*, 2016; Yagüe *et al.*, 2016). Interestingly >5% of fluorescent compartments in $\Delta sepF/3G11-5089-Egfp$ showed signs of diffusion at one or both ends (Figure 7.12 bottom row). In the future, fluorescent cell membrane stains could be used to test whether the compartments are separated by membranes rather than cell walls. Hence the structure or mechanism which defines the fluorescent compartments in the hyphae of M145/3G11-5089-Egfp and $\Delta sepF/3G11-5089-Egfp$ remains unclear.

The most striking difference between the fluorescence patterns of M145/3G11-5089-Egfp and $\Delta sepF/3G11-5089-Egfp$ occurred in the aerial hyphae. The aerial hyphae of M145/3G11-5089-Egfp did not contain detectable fluorescence (Figure 7.13). The absence of fluorescence in the aerial hyphae of M145/3G11-5089-Egfp is consistent with the observation that the surface of the wild-type M145 strain does not become blue even when copious amounts of secreted actinorhodin is visible in the surrounding solid medium. However, in the young aerial hyphae of $\Delta sepF/3G11-5089-Egfp$ fluorescence was detectable right to the hyphal tip (Figure 7.13). The localisation of 5089-Egfp to the aerial hyphae of $\Delta sepF/3G11-5089-Egfp$ was present only in aerial hyphae which were not undergoing septation. Hyphae with irregular septation primarily lacked any fluorescence.

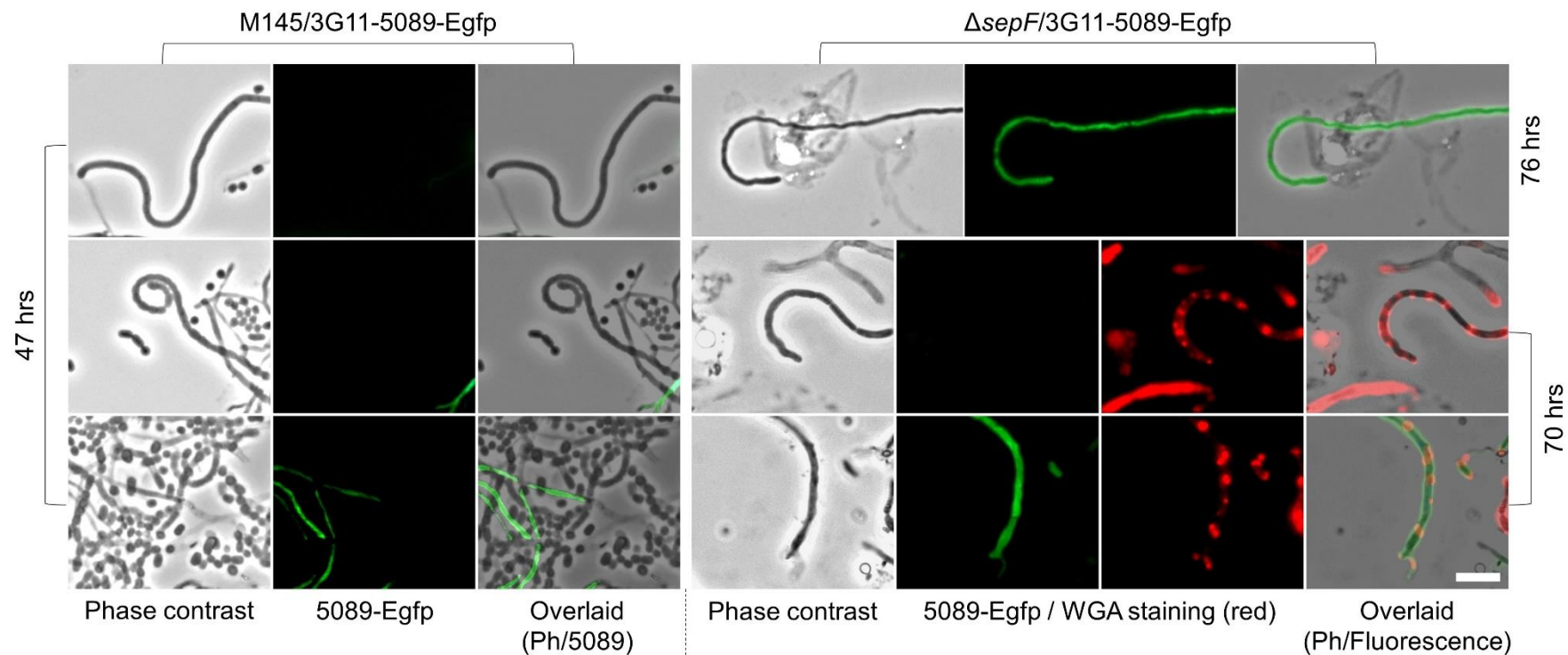


Figure 7.13 The localisation of 5089-Egfp in the aerial hyphae of *M145/3G11-5089-Egfp* and $\Delta sepF/3G11-5089-Egfp$. From top to bottom the aerial hyphae from both strains mature. The phase contrast image (left) is shown alongside the fluorescent image or images (middle) then all images are overlaid (right). Images were taken under 100x magnification with 100 ms exposure. The scale bar represents 5 μm .

Intriguingly, a few mature aerial hyphae of $\Delta sepF/3G11-5089-Egfp$ had detectable fluorescence from both 5089-Egfp and the red cell wall stain, WGA-Alexa647 conjugate (Figure 7.13). In these hyphae the fluorescence from 5089-Egfp was not compartmentalised suggesting that the partially developed septa, marked by the cell wall stain, were insufficient to affect the localisation of 5089-Egfp, leading to the deregulation of the localisation of 5089-Egfp.

7.3 Summary

Both of the cell division knock-out strains discussed in Chapter 3 and Chapter 6 had a distinctive blue pigmentation on the surface and in the surrounding media. The blue pigmentation on the surface of the colonies from the $\Delta sepF$ mutant exhibited the litmus-like transition from blue to pink, characteristic of the model antibiotic, actinorhodin (Abbas and Edwards, 1990). Using the absorbance of the medium, used to grow either wild-type M145 or $\Delta sepF$, we showed the $\Delta sepF$ mutant secreted 2-fold higher levels of actinorhodins into the media than the wild-type strain (Figure 7.3). This finding is consistent with the observation of an enlarged pigmented halo around the colonies of the $\Delta sepF$ mutant and suggests the $\Delta sepF$ mutant produces elevated levels of the actinorhodins (Figure 7.1 and Figure 7.5).

The reason for the production of antibiotics including actinorhodin by bacteria remains unknown. The classical theory for antibiotic production suggests antibiotics are produced as anti-microbial weapons originating from the periphery of the colony (Romero *et al.*, 2012; Wang *et al.*, 2010). However antibiotics at sub-inhibitory concentrations away from the human control clinical environment can coordinate a range of social behaviours potentially from the centre of the colony, such as quorum-sensing, expression of virulence genes and biofilm formation. Hence we investigated the localisation of actinorhodin production in the colonies of the wild-type M145 and $\Delta sepF$ strains using a Egfp translational fusion of the specific ACP involved in the formation of the octaketide backbone.

Single homologous cross-over events introducing the 3G11-5089-Egfp cosmid into the wild-type M145 and $\Delta sepF$ strains resulted in M145/3G11-5089-Egfp and $\Delta sepF/3G11-5089-Egfp$ strains, which exhibited elevated levels of the secreted actinorhodins and enlarged the pigmented halos in the surrounding solid medium (Figure 7.5 and Figure 7.6). Epi-fluorescent microscopy revealed 5089-Egfp was initially detected in the middle of the colonies then extended as a dense

fluorescent core, to the periphery (Figure 7.8 to Figure 7.10 and 7.14). At the periphery the younger exploring hyphae suspected to undergoing active growth are thought not to contain fluorescence right to the tip.

In the early vegetative hyphae fluorescence was detectable as well-defined segments, suggesting that expression of 5089-Egfp was compartmentalised (Figure 7.11 to Figure 7.13). The compartments which were expressing 5089-Egfp are not thought to be separated by septa as cell wall staining did not detect structures proximal to the fluorescent compartments. However cell wall staining detects current cell wall incorporation and not fully crosslinked cell walls so the possibility of cross-walls separating these compartments cannot be excluded. Alternatively, a secondary structure such as the proposed cross-membranes detected by Celler *et al.*, 2016; Yagüe *et al.*, 2016 in *S. coelicolor* and *S. albus* could be responsible for the restriction of 5089-Egfp expression to compartments. In support of the latter hypothesis, compartmentalised expression of 5089-Egfp was observed in the derivative of the $\Delta sepF$ mutant, which lacks cross-wall formation.

The lack of cross-wall formation in the $\Delta sepF$ mutant is thought to affect the localisation of SCO5089 to the aerial hyphae as fluorescence was restricted to the vegetative hyphae in the M145/3G11-5089-Egfp strain but not in the $\Delta sepF/3G11$ -5089-Egfp strain (Figure 7.14). The latter observation is thought to explain the intense blue pigmentation on the surface of the $\Delta sepF$ colonies, when grown on solid medium.

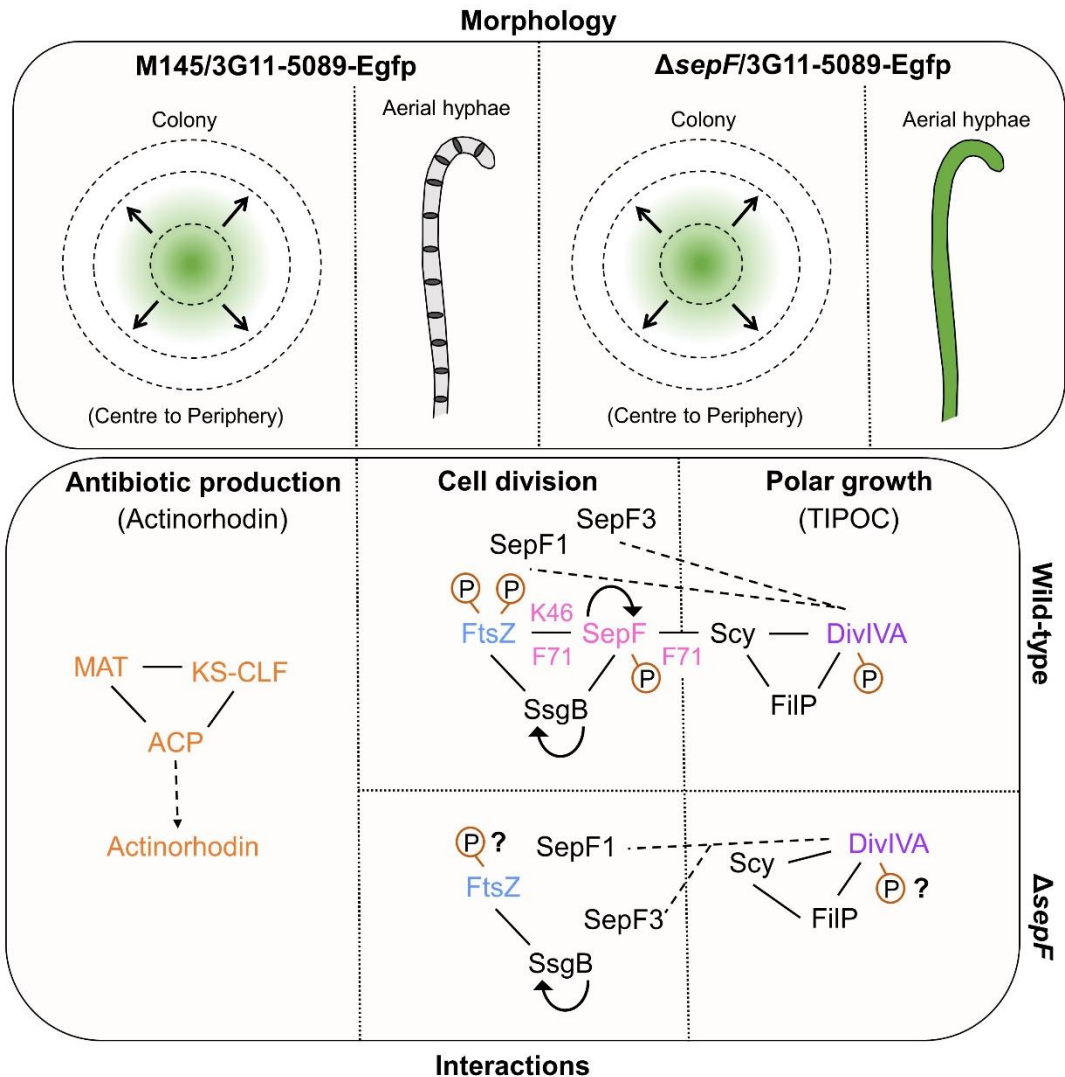


Figure 7.14 Summary of the 5089-Egfp localisation in M145/3G11-5089-Egfp and $\Delta sepF/3G11-5089-Egfp$ and protein-protein interactions in M145 and $\Delta sepF$ during development. 'Morphology' (top) shows the localisation of 5089-Egfp (green) at a colony and hyphae level during the development of M145/3G11-5089-Egfp and $\Delta sepF/3G11-5089-Egfp$. 'Interactions' (bottom) shows the known (solid line) and hypothesis (dashed line) interactions, relevant to Chapter 7, during cell division and polar growth in wild-type M145 and $\Delta sepF$. The cell division components, SepF and SsgB, self-interact and interact with FtsZ (Schlimpert *et al.*, 2017; Willemse *et al.*, 2011). In addition in Chapter 4 we showed using a bacterial two-hybrid SepF interacts with SsgB and Scy. To our knowledge the SepF-Scy interaction, identified is the first evidence of a direct link between cell division and polar growth. Residues K46 and F71 of the SepF C-terminal affected the SepF-FtsZ interaction and residue F71 affected the SepF-Scy interaction. Scy is known to interact with the TIPOC components DivIVA and FilP (Fuchino *et al.*, 2013; Holmes *et al.*, 2013; Kelemen, 2017). . DivIVA localises to sites of cell division independently of SepF so we hypothesise it could interact with other components of the divisome or SepF1 and SepF3. No direct link between actinorhodin production and cell division or polar growth was identified. Phosphorylation identified by Manteca *et al.*, 2011 and Rioseras *et al.*, 2018 is shown by a circled 'P'. Speculated alterations to the phosphorylated state of protein are shown by a question mark.

Based on the progression of 5089-Egfp expression within the *Streptomyces* colonies the production of actinorhodin is proposed to be used as a self-regulatory mechanism during the development of the colony. Further work is needed to characterise this mechanism in detail. Heterogenous gene expression in different parts of the population has previously been noted for SpoOA, a regulatory protein which allows activated cells in *B. subtilis* to undergo cannibalism during periods of nutrient depletion to delay commitment to sporulation (González-Pastor *et al.*, 2003). Also, in *Streptococcus pneumoniae* heterogeneity in the population allows the autolysis of non-competent cells for the advantageous DNA exchange to competent cells (Guiral *et al.*, 2005; Steinmoen *et al.*, 2003). Hence *Streptomyces* colonies could represent a complex, multi-cellular “population” with differential gene expression in different parts.

7.4 Acknowledgements

The microscopy in the current chapter utilised the 3G11-5089-Egfp cosmid, generated with the aid of the laboratory technician, Alan Lau, prior to the start of the study.

8.0 Discussion

Bacterial septa formation requires the polymerisation of the tubulin homologue, FtsZ, into Z-rings (McCormick *et al.*, 1994; Nogales *et al.*, 1998). In *B. subtilis* polymerisation of FtsZ utilises the FtsZ associated proteins, EzrA, FtsA and SepF (Duman *et al.*, 2013). The $\Delta sepF$ strain of *B. subtilis* is viable with slightly longer cells and irregular thick cell septa but the double knock-out strain, including *sepF* are synthetically lethal (Hamoen *et al.*, 2006; Ishikawa *et al.*, 2006). In the actinomycetes, *Mycobacterium* and *Streptomyces*, there are no known homologues of FtsA but there are homologues of SepF. Hence SepF is expected to have a central role in the cell division of *Streptomyces* species.

More specifically in *S. coelicolor* there are three SepF homologues. The three homologues are distributed throughout the linear chromosome of *S. coelicolor* with SepF1, also known as SflA, and SepF in the core region then SepF3, also known as SflB, in the right flanking arm. All three homologues have the conserved C-terminal domain containing the FtsZ binding site and only SepF3 lacks the N-terminal domain thought to be involved with lipid binding (Current Study; Duman *et al.*, 2013, Tan, 2018). However Zhang *et al.*, 2020 found the three homologues rarely localised together.

Knocking out each of the *sepFs* results in viable *S. coelicolor* colonies: Knocking-out SepF1 and SepF3 using the Redirect[®] PCR-directed mutagenesis approach resulting in sporulating colonies with a fluffier colony edge and branching aerial hyphae (Zhang *et al.*, 2020). Knocking-out SepF, encoded within the DCW gene cluster, was previously only achieved using CRISPRi (Zhang *et al.*, 2020). The CRISPRi knock-out did not produce vegetative cross-walls and visually overproduced actinorhodin.

To allow direct comparison between the three knock-out strains we generated a *sepF* knock-out strain using the Redirect[®] PCR-directed mutagenesis approach. The knock-out strain of the current study resulted in viable but severely developmental affected colonies (Chapter 3; Figure 3.5 to Figure 3.8). The lack of the grey sporulation pigment on the surface of the $\Delta sepF$ colonies corresponded to an inability to form both regular vegetative cross-walls and sporulation septa. Hence the cell division defect was more severe than previously reported for the CRISPRi knock-out. The lack of regular septa in the current $\Delta sepF$ strain is due to the

absence of correctly formed Z-rings. Irregularly spaced often partial septa, characterised by a tilted or cross shape, were formed potentially in straight aerial hyphae after prolonged incubation. These irregular septa lead to the formation of uneven spore compartments and the non-uniform segregation of chromosomes. Hence knocking-out *sepF* had a severe cell division defect.

Complementation of the $\Delta sepF$ mutant was previously attempted by Tan 2018, who highlighted the importance of two promoters upstream of *sepF*. To confirm these promoters and not the upstream SCO2080 is required for complementation, we complemented the $\Delta sepF$ mutant with the smallest DNA fragment carrying both promoters and the *sepF* gene (Chapter 3; Figure 3.12 and Figure 3.13). Colonies of the complemented $\Delta sepF/pMS82$ -SepF strain produced the grey sporulation pigment and the aerial hyphae underwent sporulation, forming regular septa and spores. Successful full complementation of the $\Delta sepF$ mutant shows the two upstream promoters were sufficient for complementation and the $\Delta sepF$ phenotype is due to the lack of *sepF* and not polar effects.

The localisation of FtsZ-Egfp in the aerial hyphae of *S. coelicolor* has been previously investigated by Grantcharova *et al.*, 2005 and Willemse and van Wezel, 2009. They found in the maturing aerial hyphae diffuse FtsZ-Egfp forms irregular or spiral-like filaments before rings at regular intervals, position perpendicular to the hyphae wall, which are thought to mark the site of the divisome. We show SepF-Egfp has a very similar localisation pattern in the aerial hyphae of *S. coelicolor*. Aerial hyphae of M145 containing SepF-Egfp or FtsZ-Egfp developed a curly morphology and both Egfp fusions localised diffusely before forming regularly spaced rings in a step-wise manner. Both SepF and FtsZ rings formed the 'rungs' of a ladder-like structure before septum formation, suggesting that SepF and FtsZ are co-localised. Interestingly in *E. coli* and *B. subtilis* FtsZ is not expected to stay once the septum is formed (Duman *et al.*, 2013; Söderström *et al.*, 2014). But in *S. coelicolor* FtsZ-Egfp and SepF-Egfp were detected after septum formation and spore maturation predominately at the poles of spores as foci or lines (Chapter 4; Figure 4.1 and Figure 4.2). Hence, there could be a difference in FtsZ and SepF turnover at the developing septum of *Streptomyces* compared to *E. coli* and *B. subtilis*.

In the $\Delta sepF$ mutant, FtsZ-Egfp has been shown to not regularly polymerise into filaments or rings (Kelemen, personal communication; Tan, 2018). Instead, in the absence of *sepF*, foci of FtsZ-Egfp were scattered throughout the aerial hyphae,

suggesting that FtsZ polymerisation is dependent on SepF. Reversely, we showed SepF-Egfp in the $\Delta ftsZ$ mutant did not regularly polymerise into rings either (Chapter 6; Figure 6.16). In the absence of *ftsZ*, foci of SepF-Egfp were often found at the hyphae tips, unlike in wild-type hyphae, and subapically. These findings suggest FtsZ and SepF are dependent on each other for the formation of and both constitute the cytokinetic ring. Therefore, unlike in *B. subtilis* where SepF is slightly redundant due to the overlapping activities of FtsA and ErzA, in *Streptomyces*, just as in the other actinomycetes, *Corynebacterium* and *Mycobacterium*, SepF has a key role in the formation of the cytokinetic ring (Gola *et al.*, 2015; Sogues *et al.*, 2020).

Intriguingly ~5% of hyphal tips from the $\Delta sepF$ mutant were prone to a fork-like morphology which shared some similarity to the morphology of the hyphal tips from the polar growth mutant, Δscy , lacking apical dominance and exhibiting increased branching (Holmes *et al.*, 2013). To investigate this observation and the potential binding partners of the C-terminal domain of SepF, SepFC, was introduced into a bacterial two-hybrid assay (Chapter 4; Figure 4.4 and Figure 4.5). The C-terminal domains of SepF from *B. subtilis* and *S. coelicolor* are known to contain the FtsZ binding site and are able to polymerise, under native conditions, into rings or tubular structures, potentially representing long continuous helical polymers (Duman, *et al.*, 2013; Kelemen, personal communication).

In addition to the expected SepF-FtsZ interaction and the SepF self-interaction we detected the known interaction between FtsZ and the sporulation specific positive regulator, SsgB, previously identified by Willemse *et al.* (2011). Excitingly the diameter of the SepF ring, determined by the C-terminal domain, was shown to correlate with the thickness of the septa in several Gram-positive bacterium including *B. subtilis*, *Clostridium perfringens*, *M. tuberculosis* and *Streptococcus pneumoniae* (Wenzel *et al.*, 2021). Therefore the interaction between SsgB and SepF in *S. coelicolor* could be an important distinctive feature of the sporulation septa with each sporulation divisome consisting of complex protein interactions between SepF, FtsZ and SsgB either in multi-protein assemblies or with dynamic partner switching. Furthermore a novel positive interaction was also detected between SepFC and Scy (Chapter 4; Figure 4.5: Figure 8.1). To our knowledge this is the first evidence for a direct molecular link between the processes of polar growth and cell division.

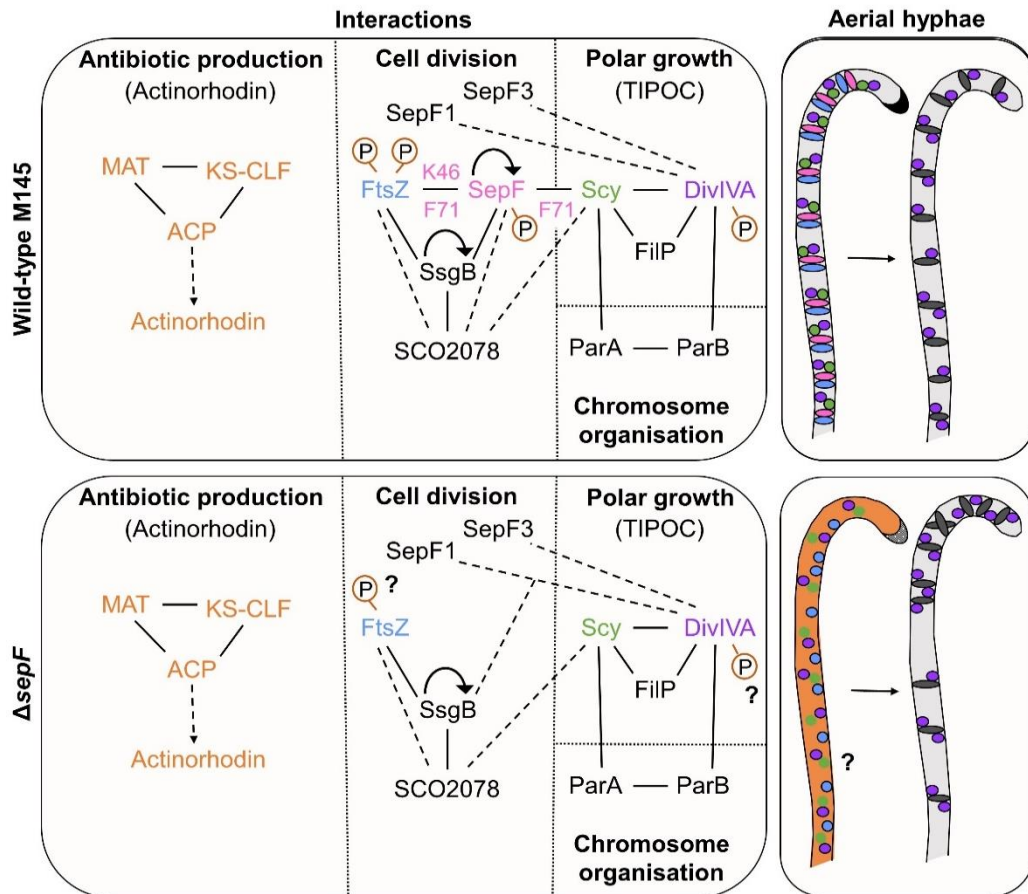


Figure 8.1 The protein-protein interactions and localisation of key cell division and polar growth proteins during the development of wild-type M145 (top) and $\Delta sepF$ (bottom). ‘Interactions’ (left) shows the potential links between the processes of actinorhodin production, cell division and polar growth. No direct links between actinorhodin production and cell division or polar growth were identified. Known interactions and interacts detected by our bacterial two-hybrid (Chapter 4; solid lines) are shown alongside speculated interactions (dashed lines). The cell division components, SepF and SsgB, both self-interaction and interact with FtsZ (Schlimpert *et al.*, 2017; Willemse *et al.*, 2011). SsgB also interacts with SCO2078 (Zhang *et al.*, 2016). In our bacterial two-hybrid direct interactions were detected between SepF and SsgB then SepF and the TIPOC component, Scy. To our knowledge this is the first link between the process of cell division and polar growth. Residues K46 and F71 of the SepF C-terminal affected the SepF-FtsZ interaction and residue F71 affected the SepF-Scy interaction. Scy interacts with TIPOC components DivIVA, FilP and the chromosomal organisation component, ParA (Ditkowski *et al.*, 2013; Fuchino *et al.*, 2013; Holmes *et al.*, 2013; Kelemen, 2017). Another chromosomal organisation component, ParB interacts with DivIVA (Donovan *et al.*, 2012). DivIVA localises to the sites of cell division independently of SepF so we hypothesise DivIVA could interact with other components of the divisome or SepF1 and SepF3. Phosphorylation identified by Manteca *et al.*, 2011 and Rioseras *et al.*, 2018 is shown by a circled ‘P’. Speculated alterations to the phosphorylated state of protein are shown by a question mark. ‘Aerial hyphae’ (right) shows the localisation of SepF (pink), FtsZ (blue), Scy (green), DivIVA (purple), the TIPOC (black) and actinorhodin production (orange) during early curled aerial development and septa (grey discs) forming aerial development. Known localisations have a solid black outline and speculated localisations have no outline. In $\Delta sepF$ the integrity of TIPOC is thought to be reduced (black dots) leading to fork-like tips in ~5% of vegetative hyphae.

STRING (2019) suggests the proteins which interact with SepF are encoded within the DCW gene cluster (Figure 8.2). Included in the SepF interaction network is DivIVA but not SsgB, Scy or FilP. The position of the suspected interacting partners genes within the DCW gene cluster suggests these genes could be co-expressed with *sepF*. However our study shows the two promoters upstream of SepF are sufficient for complementation, see above, therefore we suggest there is limited read-through along the DCW gene cluster. The independent transcription of genes in the DCW gene cluster does not appear to limit the amount of co-occurrence, suggestive of direct protein-protein interactions, even between the TIPOC member and Scy binding partner DivIVA and SepF despite the absence of a detectable positive interaction in our bacterial two-hybrid. The lack of experimentally determined protein-protein interactions within the SepF interact network, except for the SepF-FtsZ and FtsZ-FtsQ, highlights the importance of further work into the role of SepF during the development of *S. coelicolor*.

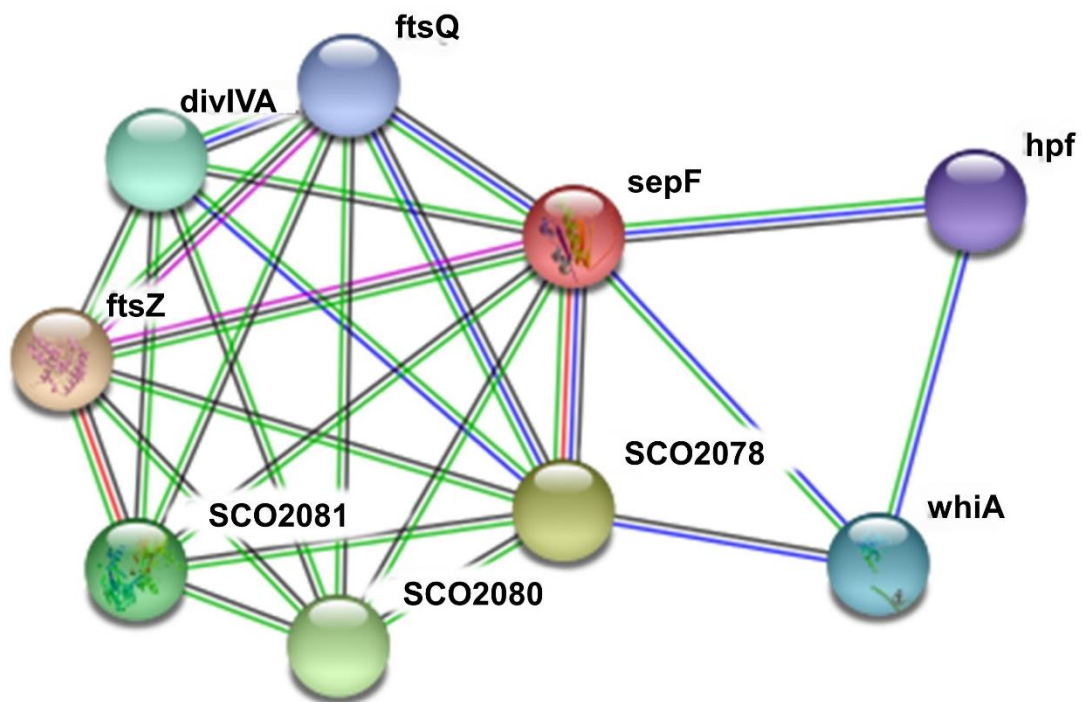


Figure 8.2 The SepF interaction network using STRING (2019). The protein represented by a node is showed in bold. Empty nodes indicate unknown 3D structures and filled nodes indicate some known or predicted 3D structure. Between the nodes the colours of the lines indicate: purple = interaction experimentally determined, green = gene neighbourhood, red = gene fusion, blue = gene co-occurrence and black = co-expression.

Previously it has been shown that a K190A mutation within *M. tuberculosis* SepF did not alter self-interaction but did abolish the interaction with FtsZ (Gupta *et al.*, 2005). Similarly we showed the corresponding mutation, K46A, in *S. coelicolor* did not alter self-interaction or the novel SepFC-Scy interaction but did abolish the SepFC-FtsZ interaction (Chapter 4; Figure 4.7). A second mutation, F215S, within *M. tuberculosis* SepF greatly reduced both SepF self-interaction and the SepF-FtsZ interaction (Gupta *et al.*, 2005). While the equivalent mutation, F126S, with *B. subtilis* SepF abolished the SepF-FtsZ interaction but did not affect self-interaction or interaction with wild-type SepF (Duman *et al.*, 2013). Interestingly, the corresponding mutation, F71A, in *S. coelicolor* showed greater similarity to the F126S mutation of *B. subtilis* as the F71A mutation did not affect self-interaction but did abolish the SepFC-FtsZC, the SepFC-SsgB and the SepFC-Scy interaction (Chapter 4; Figure 4.8). Based on the bacterial two-hybrid assay the F71 residue is thought to be involved in both the SepF-Scy interaction and the SepF-FtsZ interaction. The potential involvement of the F71 residue in both interactions indicates either Scy and FtsZ could compete to bind to SepF or the F71A mutation could influence the 3D folding of SepF (Figure 8.1). This latter is less likely though, as the self-interaction of SepFC F71A was not affected.

Although *sepF* and *ftsZ* are not thought to be part of the same transcription unit as both genes have at least two promoters each identified upstream, as a positive regulator of FtsZ, SepF is likely to be upregulated at the time of aerial hyphae formation (Flårdh *et al.*, 2002; Tan, 2018). Production of FtsZ is regulated by three upstream promoters, one constitutive promoter, one upregulated during vegetative growth and one upregulated in sporogenic aerial hyphae (Flårdh *et al.*, 2002). The latter promoter upregulates the production of FtsZ during a time period where potentially 100s of FtsZ rings are formed leading to successful sporulation.

Visualisation of SepF-Egfp and FtsZ-Egfp during vegetative, early aerial and late aerial growth revealed increased detected of both proteins at the latter stages of the *S. coelicolor* lifecycle (Figure 4.9). Whether these bands represent different oligomerised forms or different phosphorylate states remains unclear. The former would support the presence of complex partner switching or competition within the divisome as suggested by the bacterial two-hybrid (Figure 8.1). Partner-switching could be an important way the vegetative cross-walls and sporulation septa, including the sporulation specific SsgB, are differentiated. Alternatively, Rioseras *et al.*, 2018 showed FtsZ, SepF and DivIVA were phosphorylated in the aerial hyphae of *S. coelicolor* (Figure 8.1). Phosphorylation sites have been identified at Ser 319

and Ser 387 of FtsZ (Manteca *et al.*, 2011; Rioseas *et al.*, 2018). In addition, as mentioned in Section 1.3.2, phosphorylation of DivIVA by AfsK is strongly activated when, as part of a stress response, cell wall synthesis is arrested leading to the altered localisation of DivIVA and modified hyphal branching (Hempel *et al.*, 2012). Therefore the distinct bands on the native PAGE gel could represent the different phosphorylation sites of the cell division proteins, potentially leading to the formation of different polymerised structures. In this scenario the absence of *sepF* reduced the phosphorylation state of FtsZ and the absence of *scy* altered the phosphorylation state of Scy. These observations could support the direct links between the three proteins and raises the question of what is the importance of phosphorylation in maintaining the integrity of the divisome? Is the presence of irregular septa in the Δ sepF mutant linked to changes in the phosphorylation of associated proteins? In the future, along with sequencing of the bands, generation of strains containing a substitution at the identified phosphorylation sites would help to distinguish between the two scenarios and highlight the importance of phosphorylation during cell division.

If the SepF-Scy interaction identified by the bacterial two-hybrid assays is significant, we expected the localisation patterns of SepF or Scy to be dependant on the presence of Scy or SepF, respectively. Previously it was shown that FtsZ mis-localised in the *scy* mutant, forming filaments that often run parallel to the hyphal wall leading to very uneven septation during sporulation and the suggestion that cell division was dependent on *scy* (Holmes *et al.*, 2013). We showed in ~85% of the aerial hyphae of the Δ scy mutant, SepF-Egfp was persistently diffuse, which is consistent with the Δ scy mutant producing 10-fold less spores (Holmes *et al.*, 2012). In the 15% of aerial hyphae where SepF-Egfp condensed tilted rings or tilted helices were formed leading to variably sized spore-like compartments. Interestingly filaments running parallel to the hyphal wall, like those seen for FtsZ, have not been observed for SepF-Egfp, suggesting that the localisation of SepF and FtsZ can be de-coupled from each other (Holmes *et al.*, 2013). The fact that the localisation of SepF was severely altered in the Δ scy mutant, supports the SepF-Scy interaction. Furthermore, the lack of SepF polymers in 85% of the Δ scy aerial hyphae supports the hypothesis that Scy might be important for nucleation of the cytokinetic ring. However, this raised an important question: How can Scy affect SepF or FtsZ polymerisation at regularly spaced loci, when Scy only has been shown to localise to hyphal tips?

To address this, the localisation of the previously mentioned Scy binding partner and TIPOC component, DivIVA was investigated as a well-functioning Egfp-Scy construct was not available at the time of this investigation (Holmes *et al.*, 2013). As part of the TIPOC DivIVA is thought to organise the PG synthesis machinery during active polar growth (Flårdh, 2003a; Mukherjee *et al.*, 2009; Holmes *et al.*, 2012; Kelemen, 2017). DivIVA and Scy were previously shown to co-localise at the hyphal tips and *de novo* branching points (Holmes *et al.*, 2013; Flårdh, 2003a). However, both DivIVA and Scy were only monitored during early growth, including spore germination and early active vegetative growth. To investigate the localisation of DivIVA-Egfp in the aerial hyphae, where septa formation is most abundant, two novel DivIVA-Egfp constructs were made and introduced *in trans* to the wild-type strain. Unlike the existing Flårdh, 2003a strain carrying DivIVA-Egfp *in cis*, the introduction of DivIVA-Egfp *in trans* did not hinder the abilities of the colonies to undergo sporulation under any of the tested conditions.

We showed young vegetative hyphae produced sub-apical foci (Figure 5.6 and Figure 5.7). Individual sub-apical foci could mark *de novo* branching sites as stated by Flårdh, 2003a. In addition we also identified multiple regularly spaced sub-apical foci in the young vegetative hyphae, in mature vegetative hyphae prior to aerial hyphae formation and in the young aerial hyphae, which suggests these foci do not mark future branching points and that DivIVA is not restricted to the hyphal tips (Figure 5.8 and Figure 5.9; Figure 8.1).

In maturing aerial hyphae we clearly showed diffuse DivIVA-Egfp condensing into distinct foci at sporulation septa and the foci are present after the pre-spores transform into ovoid spores (Figure 5.8 and Figure 5.9; Figure 8.3). Previously, weak DivIVA-Egfp lines at potential subapical cross-wall positions were shown by Flårdh, 2003a but this is the first clear evidence to our knowledge of a TIPOC component localising to the sites of cell division. Future co-localisation studies could help to establish the localisation of TIPOC components to septum sites during the formation of the divisome. SepF is not expected to be required for the localisation of DivIVA to the future divisome or septa as in the absence of *sepF* DivIVA-Egfp continued to localise as foci along the hyphae, at the hyphal tips and at the irregular, often partial septa (Chapter 5; Figure 5.11 to Figure 5.13). Since the end of the current study, Scy-Egfp has been shown to localise at regular intervals away from the hyphal tip similarly to DivIVA (Kelemen, personal communication).

The localisation pattern is consistent with the proposed hypothesis that Scy and DivIVA are involved in the nucleation of the cytokinetic ring.

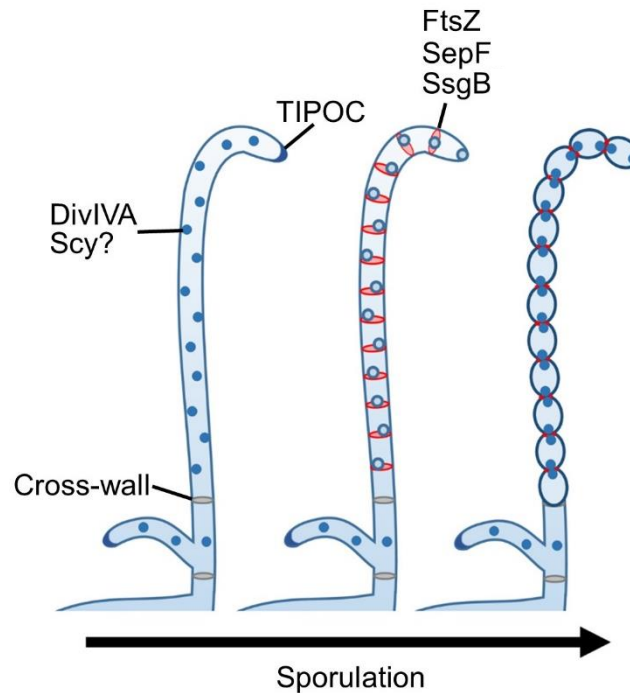


Figure 8.3 The transition from polar growth to cell division in the sporogenic aerial hyphae of *Streptomyces*. Actively growing aerial hyphae grow by polar growth at the hyphal tip (left). Polar growth is governed by the TIPOC which includes DivIVA, Scy and FilP. After the cessation of growth and chromosome organisation, cell division is initiated by the activity of FtsZ, SepF and SsgB. At this stage TIPOC and cell division proteins are expected to co-localise (middle). Then as the hyphae cell wall pinches we established DivIVA-Egfp localised to the sporulation septum as two foci per spore compartment (right).

Large scale RNA data by Jeong *et al.*, 2016 identified two promoters for *divIVA*, positioned at 184 bp and 475 bp upstream, the latter of which is located within *SCO2078*, also known as SepG. Hence The pMS82-2078-DivIVA-Egfp construct used to monitor DivIVA-Egfp could be affected by the presence of *SCO2078* in the upstream region. Homologues of *SCO2078* are widespread in bacteria and in the chloroplasts of photosynthetic eukaryotes (Kabeya *et al.*, 2010). In DCW gene clusters of actinomycetes the position of *SCO2078* homologues between homologues of *sepF* and *divIVA* is well conserved but the function of *SCO2078* remains unclear (data not shown).

The presence of at least two transmembrane domains, positioned at either termini of *SCO2078* suggests *SCO2078* might act as a membrane binding protein (data not shown; Zhang *et al.*, 2016). Recently, the central cytoplasmic region was suggested to enable *SCO2078* to localise SsgB to future cell division sites (Zhang

et al., 2016). Therefore SCO2078 could potentially be part of the divisome aiding the correct positioning of the Z-ring, with SsgB acting as a linker, due to the absence a transmembrane binding domain in FtsZ. Similarity in *Caulobacter crescentus* the Z-ring has been shown to be positioned 13 nm below the inner membrane at the site of midcell constriction (McQuillen and Xiao, 2020). Does a more complex positive regulatory system for divisome formation in *S. coelicolor* counter the absence of a known negative regulatory system?

Interestingly the two previous attempts to knock-out SCO2078 in *S. coelicolor* resulted in different phenotypes: colonies of the Zhang *et al.*, 2016 Δ SCO2078 strain were slow to develop and produced a low number of variable spores, characterised by thinner cell walls, unusual toroidal or doughnut shaped chromosomes and increased sensitivity to heat stress. On the other hand, colonies of the Kaur, 2018 Δ SCO2078 strain, produced in our laboratory, were only distinguishable from colonies of wild-type M145 due to a decrease in the distance between sporulation septa. The differences between the studies could reflect the different methodologies used to generate the two different strains. Both Δ SCO2078 strains have a cell division defect potentially due to the gene fusion of SepF and SCO2078 suggested by StringDB (2019) in Figure 8.2. The additional characteristics of the Zhang *et al.*, 2016 strain suggests SCO2078 could have a role in cell wall formation (Figure 8.1). By combining the SCO2078-SsgB interaction with the novel interactions, detected by the current study, between SsgB and SepF then SepF and Scy, there could also be an indirect mechanism for SCO2078 to affect both polar growth and cell division in *S. coelicolor* (SCO2078 – SsgB – SepF – Scy – DivIVA; Figure 8.1).

As previously mentioned, we showed in the Δ *ftsZ* mutant SepF-Egfp did not regularly polymerise into rings (Chapter 6; Figure 6.16). To test the localisation of SepF-Egfp, an accessible *ftsZ* knock-out strain was required. The first and only published attempt for an *ftsZ* knockout in *S. coelicolor* replaced the first 277 amino acids of the 400 long FtsZ by a neomycin resistance cassette (McCormick *et al.*, 1994). The knocking out of the first 277 amino acids of *ftsZ* resulted in the absence of vegetative cross-walls and sporulation septa despite the production of the sporulation pigment. Here, we used the Redirect[®] PCR-directed mutagenesis approach to create a complete *ftsZ* knockout strain (Gust *et al.*, 2002). In contrast to the McCormick *et al.*, 1994 strain, the current studies Δ *ftsZ* strain was unable to form septa and the grey sporulation pigment (Figure 6.4, Figure 6.5, Figure 6.9 and Figure 6.10; Figure 8.4). In addition, the current studies of Δ *ftsZ* strain did not form

fork-like tips like the $\Delta sepF$ mutant and showed signs of genetic instability with the formation of segments and secondary colony morphologies (Figure 6.5, Figure 6.6, Figure 6.8 and Figure 8.4).

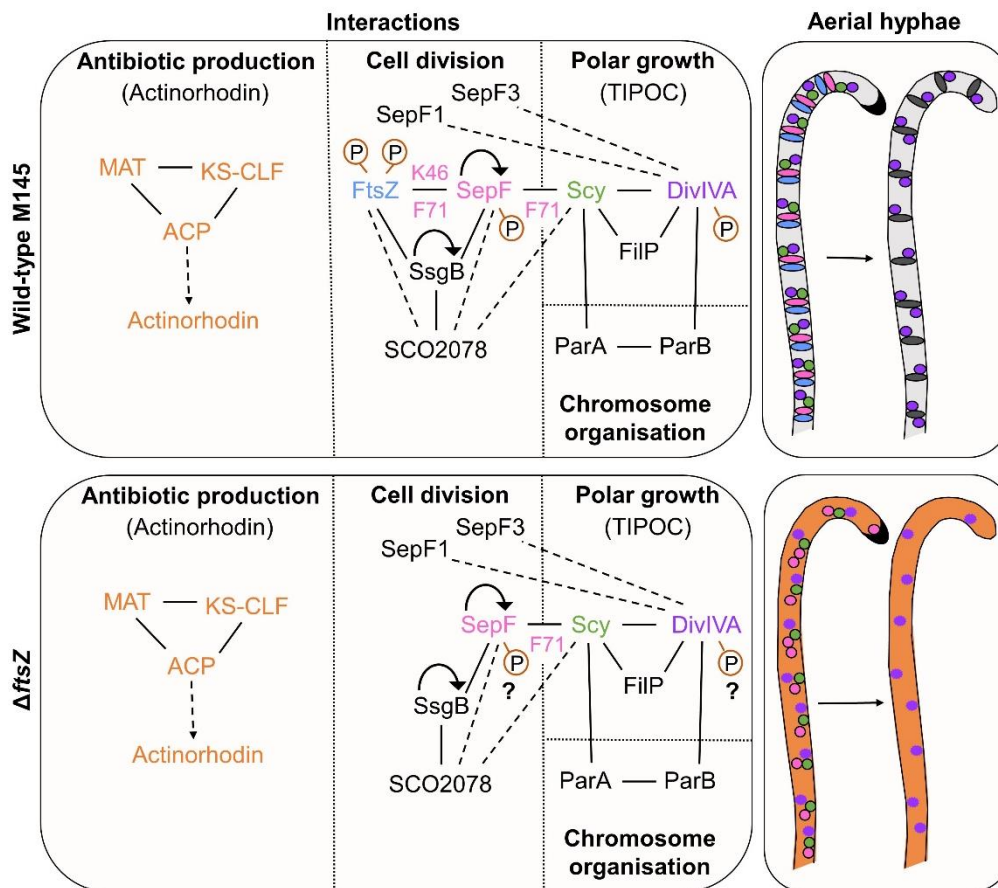


Figure 8.4 The protein-protein interactions and localisation of key cell division and polar growth proteins during the development of wild-type M145 (top) and Δ ftsZ (bottom). ‘Interactions’ (left) shows the potential links between the processes of actinorhodin production, cell division and polar growth. No direct links between actinorhodin production and cell division or polar growth were identified. Known interactions and interacts detected by our bacterial two-hybrid (Chapter 4; solid lines) are shown alongside speculated interactions (dashed lines). The cell division components, SepF and SsgB, both self-interaction and interact with FtsZ (Schlimpert *et al.*, 2017; Willemse *et al.*, 2011). SsgB also interacts with SCO2078 (Zhang *et al.*, 2016). In our bacterial two-hybrid direct interactions were detected between SepF and SsgB then SepF and the TIPOC component, Scy. To our knowledge this is the first link between the process of cell division and polar growth. Residues K46 and F71 of the SepF C-terminal affected the SepF-FtsZ interaction and residue F71 affected the SepF-Scy interaction. Scy interacts with TIPOC components DivIVA, FilP and the chromosomal organisation component, ParA (Ditkowski *et al.*, 2013; Fuchino *et al.*, 2013; Holmes *et al.*, 2013; Kelemen, 2017). Another chromosomal organisation component, ParB interacts with DivIVA (Donovan *et al.*, 2012). DivIVA localises to sites of cell division independently of SepF so we hypothesis DivIVA could interact with other components of the divisome or SepF1 and SepF3. Phosphorylation identified by Manteca *et al.*, 2011 and Rioeras *et al.*, 2018 is shown by a circled ‘P’. Speculated alterations to the phosphorylated state of protein are shown by a question mark. ‘Aerial hyphae’ (right) shows the localisation of SepF (pink), FtsZ (blue), Scy (green), DivIVA (purple), the TIPOC (black) and actinorhodin production (orange) during early curled aerial development and septa (grey discs) forming aerial development. Known localisations have a solid black outline and speculated localisations have no outline.

Instability was not previously reported for the \DeltaftsZ strain in *S. coelicolor* (McCormick *et al.*, 1994). However generation of the previous \DeltaftsZ strains was not straightforward. In *S. venezuelae* a single crossover strain was repeatedly re-streaked and screened until a double crossover strain was identified (Santos-Beneit *et al.*, 2017). Recently Szafran *et al.*, 2021 showed the linear chromosome of *S. venezuelae* alters in shape with the arms of the chromosome in an open form at the entry to sporulation to the arm being closely aligned to the core region in a close form during sporulation. We suspect a similar chromosome organisation will occur in *S. coelicolor*, although in this work, \DeltaftsZ double knock-out colonies were readily detectable and showed clear signs of a tendency to undergo secondary mutations (Chapter 6; Figure 6.5 and Figure 6.6). The prevalence of colony heterogeneity after sonication, designed to increase the colony forming units, indicated the presence of 'hidden' secondary mutations with the multi genomic, complex, hyphal networks. Hence genome sequencing of the \DeltaftsZ strains will be important to identify any secondary mutation, assumed to be required for viability.

The lack of septa in the novel \DeltaftsZ mutant and the \DeltasepF mutant coincided with the tendency towards hyphal lysis. Lysis in *S. coelicolor* is thought to be restricted to compartments of the vegetative hyphae by vegetative cross-walls during aerial hyphae formation. Hence in the absence of septa, lysis can spread more easily through the tube-like colonies of \DeltaftsZ and \DeltasepF . The successful passaging of the tube-like colonies is thought to be governed by the sealing and regrowth of hyphae fragments bound by a tip and branching point, as described in the \DeltaftsZ strain of *S. venezuelae* (Santos-Beneit *et al.*, 2017). We argue sonication prior to plating is likely to aid the formation of these hyphal fragments leading to successful passaging of non-sporulating strains in *S. coelicolor*.

In addition to cell division defects, the colonies of both the \DeltasepF and \DeltaftsZ strains were characterised by the distinctive blue pigmentation of actinorhodin on the colony surface and in the surrounding media. Interestingly overproduction of actinorhodin was also noted as a characteristic of the CRISPRi \DeltasepF knock-out strain suggesting altering SepF affect actinorhodin production directly or indirectly (Zhang *et al.*, 2020).

Our investigations into the actinorhodins production focused on the ACP from the minimal PKS, SCO5089, which is key for synthesizing the actinorhodin backbone. Initially 5089-Egfp was detected only after ~24 hrs of growth and localised to the centre of the colonies (Chapter 7; Figure 7.8 to Figure 7.10).

Fluorescence from 5089-Egfp spread rapidly outwards, toward the periphery prior to the timeframe for sporulation. Once at the periphery 5089-Egfp remained present throughout the whole colony. The spread of 5089-Egfp from the centre of the colony to the periphery suggests actinorhodin production is initiated by an internal stimulus well before the production of aerial hyphae. Could the production of actinorhodin induce the lysis at the centre of the colony associated with aerial hyphae formation? Could colony density induce actinorhodin production allowing actinorhodin to act as a signalling molecule and regulate the size of the colony?

Higher resolution microscopy studies established the remarkable observation that after ~24 hrs growth 5089-Egfp expression was restricted to selected segments of the hyphae even in the absence of cross-walls in the $\Delta sepF/3G11$ -5089-Egfp strain (Chapter 7; Figure 7.11, Figure 7.12, Figure 8.1 and Figure 8.4). The segments expressing 5089-Egfp were often next to segments showing signs of lysis, suggesting that either actinorhodin produced in one segment initiates cell lysis in the neighbouring, non-producer segment or that cell lysis promotes actinorhodin production. Heterogenous gene expression in different parts of a bacterial population has previously been noted. In a population of the bacterium *B. subtilis* entry of cells into the sporulation pathway is governed by the regulatory protein, Spo0A (González-Pastor *et al.*, 2003). Cells in the sporulation pathway export a killing factor, Skf, and an intercellular signalling protein, Sdp, that act cooperatively to induce cell lysis in non-producing sister cells allowing the uptake of nutrients and the delay of sporulation. In addition in a population of *Streptococcus pneumoniae* cell-to-cell contacts between competent cells, expressing CibAB, and non-competent cells trigger the lysis of non-competent cells and advantageous DNA exchange to competent cells (Guiral *et al.*, 2005). Therefore it would not be unreasonable to speculation that the colonies of *Streptomyces* could represent a complex, multi-cellular “population” with differential gene expression in different segments.

The observation of compartmentalised 5089-Egfp raises the question of what creates compartments in the *sepF* mutant? Recently, membranes forming small assemblies between the cell wall and cytoplasmic membrane were found in the vegetative hyphae of *S. coelicolor* and in *S. albus* (Celler *et al.*, 2016; Yagüe *et al.*, 2016). These cross-membrane large protein-impermeable structures were detected independently and more frequently, at up to every 1 μm , than cross-walls in the vegetative hyphae of the wild-type M145 strain (Celler *et al.*, 2016). Therefore

use of a cell membrane dye in the future could help to establish a potential link between cell lysis and antibiotic production.

Strikingly 5089-Egfp was detected in the young aerial hyphae of the $\Delta sepF$ mutant (Chapter 7; Figure 7.13). Fluorescence was only detected in aerial hyphae that did not develop any septation. Although 5089-Egfp was not detected in the aerial hyphae of the wild-type strain, actinorhodins were previously detected in the washed spores and the cell-free supernatant of *S. coelicolor* after germination, which is not consistent with our findings (Čihák *et al.*, 2017). Potentially the location of the initiation of actinorhodin production could be distinct from the location of the final actinorhodin export site. This raises the question as to how actinorhodin moves about the hyphae. Sexton and Tocheva, 2020 used cryo-electron tomography to show the vegetative cross-walls of *S. albus* have 12 nm wide septal junctions with a 9 nm wide lumen. Of the vegetative cross-walls visualised only half contained septal junctions but multiple septal junctions were identified in the vegetative cross-walls that did. Channels could allow the polar actinorhodin to move between segments defined by vegetative cross-walls and affect the neighbouring segments as speculated above. Alternatively actinorhodin could be exported from the vegetative segment after production, diffuse into the surrounding media and externally stimulate the production of actinorhodin in the neighbouring vegetative segments or spores, allowing spores to benefit from the anti-microbial activity of actinorhodin prior to germination.

Recently Santos-Beneit and Errington, 2017 monitored the localisation of an export pump, SCO5083 and early tailoring enzyme, SCO5086 encoded by the actinorhodin gene cluster, during the growth of *S. coelicolor* in liquid cultures. They suggested the export pump was localised at the membrane whilst SCO5086 was cytoplasmic in all hyphal fragments (Santos-Beneit and Errington 2017; Sun *et al.*, 1999). Although these findings support ours, antibiotic production in liquid cultures is potentially very different from production on solid medium. Combined with the different methodologies used to deliver the Egfp fusions and the extremely high maximum excitation period used by Santos-Beneit and Errington, 2017 (at 3000 m/s vs 200 m/s in the current study) we suggest our study into the localisation of an actinorhodin specific protein in *S. coelicolor* represents a more reliable methodology for further investigations.

8.1 List of Conclusions

The study aimed to investigate the potential links between cell division and polar growth then between cell division and actinorhodin production in *S. coelicolor* by investigating the five objectives outlined in Section 1.5. Based on these objectives the study concludes:

- SepF has a more important role in the development of *S. coelicolor* than in the development of *B. subtilis*. Knocking-out *sepF* in *S. coelicolor* causes a severe cell division defect, limiting vegetative cross-wall and sporulation septa formation. In addition knocking-out *sepF* has a mild effect on the integrity of the TIPOC, which governs polar growth. The phenotype of the $\Delta sepF$ mutant can be complemented back to wild-type by the introduction of *sepF* with two upstream promoters.
- The TIPOC component, Scy was identified as a novel binding partner for SepF. In the absence of *scy*, SepF was unable to form regular rings in aerial hyphae attempting to undergo sporulation. The SepF-Scy interaction could involve residues also involved in the SepF-FtsZ interaction suggesting FtsZ and Scy could compete to bind to SepF.
- Investigation into the localisation of another TIPOC component and Scy binding partner, DivIVA, in the aerial hyphae required two upstream promoters. In the aerial hyphae the localisation of DivIVA is dynamic. Most intriguingly DivIVA localises to the sites of septa formation in the sporulating aerial hyphae, independently of *sepF*.
- Knocking-out *ftsZ* in *S. coelicolor*, using the Redirect[®] PCR-directed mutagenesis approach, causes a highly severe cell division defect, preventing the formation of vegetative cross-walls and sporulation septa. The non-sporulating blue pigmented $\Delta ftsZ$ mutant exhibited signs of genetic instability which has not been previously noted and was fully complemented by the introduction of an untagged *ftsZ* fragment.
- Actinorhodin production commences in the centre of the colony and expands outside to the periphery by the expected timeframe for sporulation. Vegetative cross-walls have a limited effect on the compartmentalisation of actinorhodin production but septa do prevent the localisation of the actinorhodin biosynthesis protein, ACP, to the aerial hyphae.

8.2 Future Outlook

Building on the conclusions above, the current study proposes the elevated levels of SepF in the aerial hyphae alters the TIPOC dynamic, repressing *de novo* branching. In this model the ability of FtsZ and Scy to bind, and possibility compete for SepF, could enable SepF to aid the differentiation of vegetative and aerial septation events.

In the future, further investigation into the role of SepF in the development of *S. coelicolor* is required. Firstly it will be important to confirm the SepF-Scy interaction at a protein level via methodologies such as pull-down assays. Secondly, it will be important to clarify the expression and phosphorylation states of the cell division and TIPOC proteins in both wild-type and mutant strains. We had previously aimed to use MALDI-TOF to identify the proteins forming the banding on our native PAGE gels but were halted due to Covid-19. It would also be of interest to generate strains containing a substitution at the identified phosphorylation sites to see how these mutations affect the formation and integrity of the divisome.

Thirdly, it will be important to ascertain the cause of the suspected genetic instability of the $\Delta ftsZ$ mutant. Are these secondary mutations predominately positioned in certain genes known to be involved with cell division or novel gene/s? Especially now that we have shown sonication could be an effective way of propagating non-sporulating *S. coelicolor* strains, including the $\Delta ftsZ$ mutant, in the future.

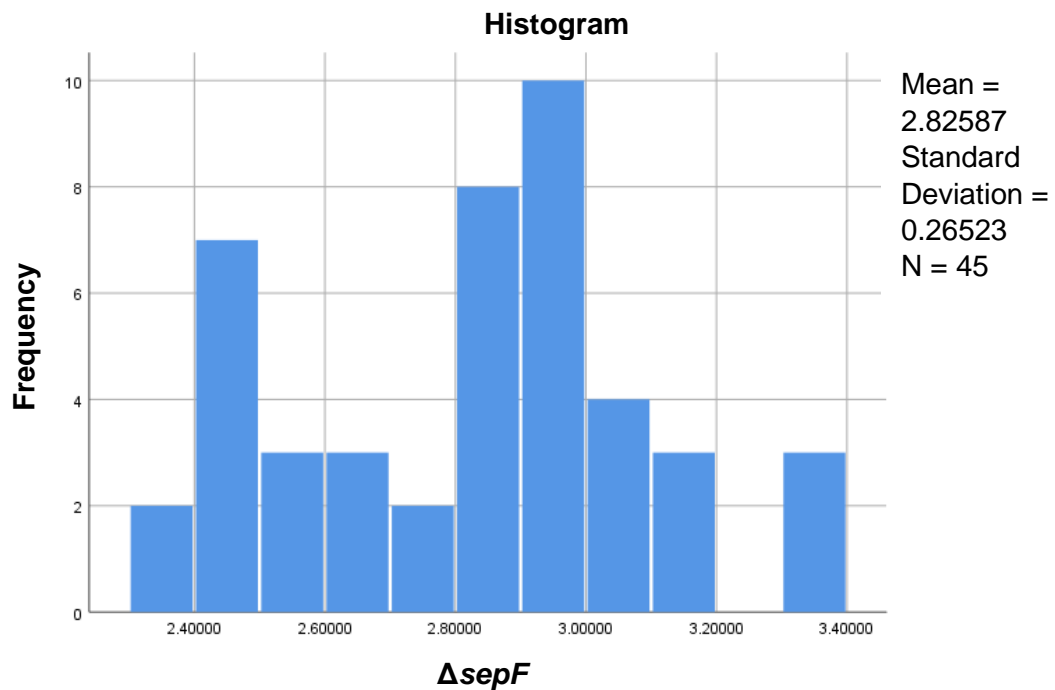
Fourthly, it will be important to determine the role of the cell-membranes in the compartmentalisation of actinorhodin production via specific membrane dyes. Key to this will be generation of an Egfp-tagged strain containing only one copy of the actinorhodin gene cluster by removal of 3G11 backbone from the existing single cross-over strains as these strains have more consistently detectable fluorescence than the previously published Egfp tagged strains. Furthermore although a link between cell division and actinorhodin production has not been directly established the localisation of proteins involved in the latter stages of actinorhodin production should be investigated at a colony level to determine the spatial localisation of actinorhodin excretion.

Finally now that individual knock-outs have been generated for all of the SepF homologues in *S. coelicolor* double and triple knock-outs can be generated to attempt to answer why *S. coelicolor* has multiple homologues distributed along the chromosome unlike in *B. subtilis*. The link between cell division and polar growth via

the SepF-Scy interaction in *S. coelicolor* raises the possibility that not only other polar growth proteins could be involved in cell division but that in other organisms such as *M. tuberculosis* SepF could have a much larger role in the lifecycle than previously thought.

9.0 Appendices

Appendix 1 Statistical outputs from IBM SPSS Statistics 25. For each of the statistics presented in the current study, the chosen statistical tests were underpinned by a histogram, a Kolmogorov-Smirnov test, a Shapiro-Wilk test and a Levene's test for each data set. The output of the histograms and all of the tests, mentioned above, are shown prior to the outputs for the respective independent sample *t* tests, mentioned in Chapter 3.



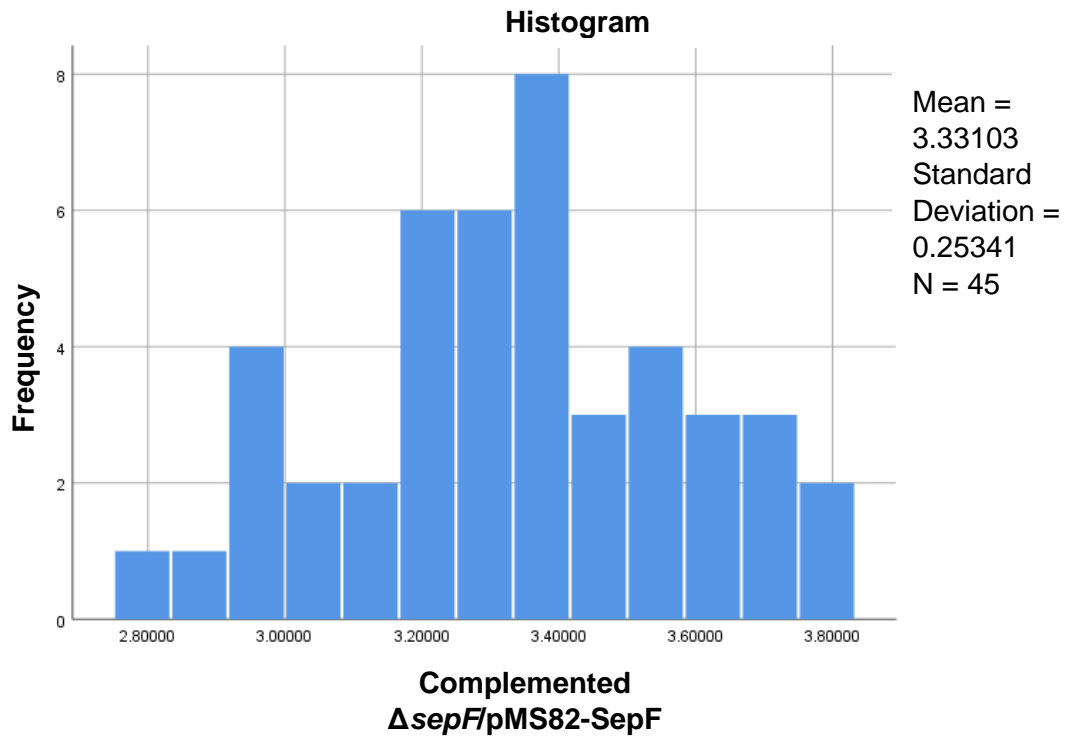
Tests of Normality

	Kolmogorov-Smirnov ^a			Shapiro-Wilk		
	Statistic	df	Sig.	Statistic	df	Sig.
<i>ΔsepF</i>	.109	45	.200*	.955	45	.079

*. This is a lower bound of the true significance.

a. Lilliefors Significance Correction

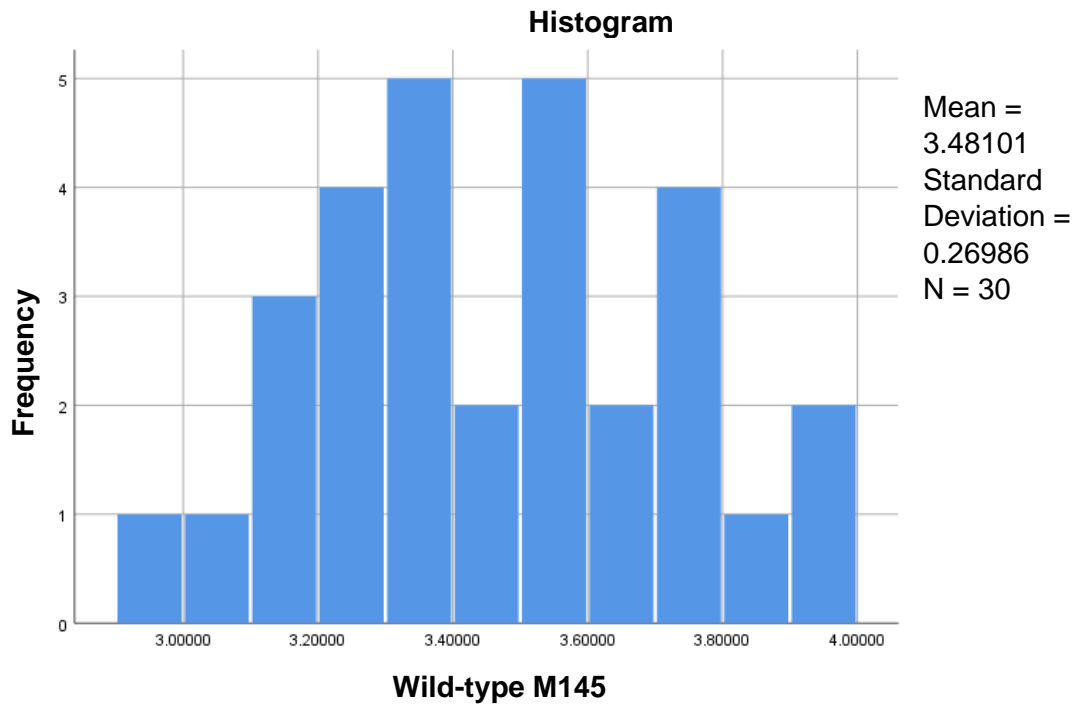
Appendix 1.1 The histogram (top panel) and tests of normality (bottom panel) for the colony size measurements of the *ΔsepF* strain in Chapter 3. Statistical analysis was undertaken using IBM SPSS Statistics 25



Tests of Normality

	Kolmogorov-Smirnov ^a			Shapiro-Wilk		
	Statistic	df	Sig.	Statistic	df	Sig.
Δ sepF/pMS82-SepF	.079	45	.200 [*]	.980	45	.604

Appendix 1.2 The histogram (top panel) and tests of normality (bottom panel) for the colony size measurements of the Δ sepF/pMS82-SepF strain in Chapter 3. Statal analysis was undertaken using IBM SPSS Statistics 25



Tests of Normality

	Kolmogorov-Smirnov ^a			Shapiro-Wilk		
	Statistic	df	Sig.	Statistic	df	Sig.
M145	.089	30	.200*	.983	30	.892

*. This is a lower bound of the true significance.

a. Lilliefors Significance Correction

Appendix 1.3 The histogram (top panel) and tests of normality (bottom panel) for the colony size measurements of the wild-type M145 strain in Chapter 3. Statal analysis was undertaken using IBM SPSS Statistics 25

T-Test

Group Statistics

	group	N	Mean	Std. Deviation	Std. Error Mean
M145sepF	1.00	30	3.4810	.26986	.04927
	2.00	45	2.8259	.26523	.03954

Independent Samples Test

		Levene's Test for Equality of Variances		t-test for Equality of Means						
		F	Sig.	t	df	Sig. (2-tailed)	Mean Difference	Std. Error Difference	95% Confidence Interval of the Difference	
									Lower	Upper
M145sepF	Equal variances assumed	.061	.805	10.407	73	.000	.65514	.06295	.52968	.78061
	Equal variances not assumed			10.371	61.555	.000	.65514	.06317	.52885	.78144

Appendix 1.4 Output from the Levene's test and independent sample *t* test comparing the colony sizes of wild-type M145 and Δ sepF in Chapter 3. Statal analysis was undertaken using IBM SPSS Statistics 25

T-Test

Group Statistics

	group2	N	Mean	Std. Deviation	Std. Error Mean
M145com	1.00	30	3.4810	.26986	.04927
	2.00	45	3.3310	.25341	.03778

Independent Samples Test

		Levene's Test for Equality of Variances		t-test for Equality of Means						
		F	Sig.	t	df	Sig. (2-tailed)	Mean Difference	Std. Error Difference	95% Confidence Interval of the Difference	
									Lower	Upper
M145com	Equal variances assumed	.495	.484	2.447	73	.017	.14998	.06130	.02781	.27215
	Equal variances not assumed			2.416	59.554	.019	.14998	.06208	.02578	.27419

Appendix 1.5 Output from the Levene's test and independent sample *t* test comparing the colony sizes of wild-type M145 and Δ sepF/pMS82-SepF in Chapter 3. Statical analysis was undertaken using IBM SPSS Statistics 25

Appendix 2 The pairwise protein-protein interactions of SepFC and SepFC point mutation using the bacterial two-hybrid assay. The combinations (described in Interaction partner and shorten as seen in the graphs) were quantified as described in the materials and methods. For each combination three streaks (at position A, B or C) had the median signal intensity of the blue pigment generated by Xgal hydrolysis randomly measured in triplet. The mean of the replicates generated the streak mean and from the streak means the interaction mean was generated. The interaction means classified the interactions into the three categories: negative (>1500), weak positives (1501 to 8000) and strong positive (<8000). For visual representation these categories were given the arbitrary values of 0.01, 0.5 and 1 respectively. Visual assessment (Visual) of the streaks into the same three categories was recorded (- are negative, ++ are weak positives and ++++ are strong positive) and was consistent with the quantitative data.

Interaction partners	Position	Streak mean	Interaction mean	Visual	Figure value
T18-SepFC + T25-SepFC (T18-S+T25-S)	A	17274	17637	++++	1
	B	16911			
	C	18726			
SepFC-T18 + SepFC-T25 (S-T18-S-T25)	A	21086	21992	++++	1
	B	22718			
	C	22173			
T18-SepFC + SepFC-T25 (T18-S+S-T25)	A	22717	24048	++++	1
	B	25621			
	C	23806			
SepFC-T18 + T25-SepFC (S-18+T25-S)	A	24533	24835	++++	1
	B	23988			
	C	25985			
T18-SsgB + T25-SsgB (T18-B+T25-B)	A	11457	11644	++++	1
	B	11831			
SsgB-T18 + SsgB-T25 (B-T18+B-T25)	A	14827	15763	++++	1
	B	16700			
	C	11457			
T18-SsgB + SsgB-T25 (T18-B+B-T25)	A	43690	41090	++++	1
	B	39009			
	C	40570			
SsgB-T18 + T25-SsgB (B-T18+T25-B)	A	15701	14266	++++	1
	B	12830			
	C	11706			
T18-SsgB + T25-FtsZC (T18-B+T25-F)	A	4935	5392	++	0.5
	B	5758			
	C	5484			
SsgB-T18 + FtsZC-T25 (B-T18+F-T25)	A	8875	10815	++++	1
	B	12885			
	C	10686			
T18-FtsZC + T25-SsgB (T18-F+T25-B)	A	4535	4180	++	0.5
	B	6375			
	C	1630			
FtsZC-T18 + SsgB-T25 (F-T18+B-T25)	A	1727	4567	++	0.5
	B	3760			
	C	8215			

Appendix 3 The pairwise protein-protein interactions of SepFC and TIPOC components using the bacterial two-hybrid assay. The combinations (described in Interaction partner and shorten as seen in the graphs) were quantified as described in the materials and methods. For each combination three streaks (at position A, B or C) had the median signal intensity of the blue pigment generated by Xgal hydrolysis randomly measured in triplet. The mean of the replicates generated the streak mean and from the streak means the interaction mean was generated. The interaction means classified the interactions into the three categories: negative (>1500), weak positive (1501 to 8000) and strong positive (<8000). For visual representation these categories were given the arbitrary values of 0.01, 0.5 and 1 respectively. Visual assessment (Visual) of the streaks into the same three categories was recorded (- are negative, ++ are weak positive and ++++ are strong positive) and was consistent with the quantitative data.

Interaction partners	Position	Streak mean	Interaction mean	Visual	Figure value
T18-Scy + T25-SepFC (T18-Y+T25-S)	A	8162	10154	++++	1
	B	12943			
	C	9358			
T18-SepFC + T25-Scy (T18-S+T25-Y)	A	16017	15220	++++	1
	B	13285			
	C	16359			
T18-Scy + SepFC-T25 (T18-Y+S-T25)	A	12944	9927	++++	1
	B	6113			
	C	10723			
SepFC-T18 + T25-Scy (S-T18+T25-Y)	A	9529	13798	++++	1
	B	16700			
	C	15163			
T18-Scy + T25-FtsZC (T18-Y+T25-F)	A	0	0	-	0.01
	B	0			
	C	0			
T18-FtsZC + T25-Scy (T18-F+T25-Y)	A	0	0	-	0.01
	B	0			
	C	0			
T18-Scy + FtsZC-T25 (T18-Y+F-T25)	A	1248	520	-	0.01
	B	312			
	C	0			
FtsZC-T18 + T25-Scy (F-T18+T25-Y)	A	0	0	-	0.01
	B	0			
	C	0			
T18-Scy + T25-SsgB (T18-Y+T25-B)	A	0	0	-	0.01
	B	0			
	C	0			
T18-SsgB + T25-Scy (T18-B+T25-Y)	A	0	0	-	0.01
	B	0			
	C	0			
T18-Scy + SsgB-T25 (T18-Y+B-T25)	A	0	0	-	0.01
	B	0			
	C	0			
SsgB-T18 + T25-Scy (B-T18+T25-Y)	A	0	0	-	0.01
	B	0			
	C	0			

Appendix 4 The pairwise protein-protein interactions of SepFC and SepFC-K46A using the bacterial two-hybrid assay. The combinations (described in Interaction partner and shorten as seen in the graphs) were quantified as described in the materials and methods. For each combination three streaks (at position A, B or C) had the median signal intensity of the blue pigment generated by Xgal hydrolysis randomly measured in triplet. The mean of the replicates generated the streak mean and from the streak means the interaction mean was generated. The interaction means classified the interactions into the three categories: negative (>1500), weak positive (1501 to 8000) and strong positive (<8000). For visual representation these categories were given the arbitrary values of 0.01, 0.5 and 1 respectively. Visual assessment (Visual) of the streaks into the same three categories was recorded (- are negative, ++ are weak positive and ++++ are strong positive) and was consistent with the quantitative data.

Interaction partners	Position	Streak mean	Interaction mean	Visual	Figure value
T18-SepFC + T25-SepFC (T18-S+T25-S)	A	17274	17637	++++	1
	B	16911			
	C	18726			
SepFC-T18 + SepFC-T25 (S-T18-S-T25)	A	21086	21992	++++	1
	B	22718			
	C	22173			
T18-SepFC + SepFC-T25 (T18-S+S-T25)	A	22717	24048	++++	1
	B	25621			
	C	23806			
SepFC-T18 + T25-SepFC (S-18+T25-S)	A	24533	24835	++++	1
	B	23988			
	C	25985			
T18-SepFC + T25-FtsZC (T18-S+T25-F)	A	5885	6284	++	0.5
	B	8179			
	C	4788			
SepFC-T18 + FtsZC-T25 (S-T18+F-T25)	A	14408	14505	++++	1
	B	17329			
	C	11778			
T18-FtsZC + T25-SepFC (T18-F+T25-S)	A	8857	9782	++++	1
	B	10902			
	C	9588			
FtsZC-T18 + SepFC-T25 (F-T18+S-T25)	A	19083	18450	++++	1
	B	19083			
	C	17184			
T18-SepFC + FtsZC-T25 (T18-S+F-T25)	A	9587	11340	++++	1
	B	11487			
	C	12947			
SepFC-T18 + T25-FtsZC (S-T18+T25-F)	A	8379	10008	++++	1
	B	10573			
	C	11072			
T18-FtsZC + SepFC-T25 (T18-F+S-T25)	A	18937	19375	++++	1
	B	18060			
	C	21128			
FtsZC-T18 + T25-SepFC (F-T18+T25-S)	A	0	0	-	0.01
	B	0			
T18-SsgB + T25-SepFC (T18-B+T25-S)	A	7289	8423	++++	1
	B	9891			
	C	8090			

SsgB-T18 + SepFC-T25 (B-T18+S-T25)	A	15696	18098	++++	1
	B	20099			
	C	18498			
T18-SepFC + T25-SsgB (T18-S+T25-B)	A	2397	5006	++	0.5
	B	6584			
	C	6038			
SepFC-T18 + SsgB-T25 (S-T18+B-T25)	A	14895	17097	++++	1
	B	19299			
T18-SsgB + SepFC-T25 (T18-B+S-T25)	A	11693	12160	++++	1
	B	13694			
	C	11092			
SsgB-T18 + T25-SepFC (B-T18+T25-S)	A	5536	4206	++	0.5
	B	3342			
	C	3741			
T18-SepFC + SsgB-T25 (T18-S+B-T25)	A	13294	13094	++++	1
	B	12694			
	C	13294			
SepFC-T18 + T25-SsgB (S-T18+T25-B)	A	12293	12994	++++	1
	B	13695			
T18-Scy + T25-SepFC (T18-Y+T25-S)	A	8162	10154	++++	1
	B	12943			
	C	9358			
T18-SepFC + T25-Scy (T18-S+T25-Y)	A	16017	15220	++++	1
	B	13285			
	C	16359			
T18-Scy + SepFC-T25 (T18-Y+S-T25)	A	12944	9927	++++	1
	B	6113			
	C	10723			
SepFC-T18 + T25-Scy (S-T18+T25-Y)	A	9529	13798	++++	1
	B	16700			
	C	15163			
T18-SepFC K46A + T25- SepFC K46A (T18-SK46+T25-SK46)	A	11063	11664	++++	1
	B	11321			
	C	12607			
SepFC K46A-T18 + SepFC K46A-T25 (SK46-T18+SK46-T25)	A	13894	15009	++++	1
	B	16467			
	C	14666			
T18-SepFC K46A + SepFC K46A-T25 (T18-SK46+SK46-T25)	A	11578	12865	++++	1
	B	11835			
	C	15181			
SepFC K46A-T18 + T25- SepFC K46A (SK46-T18+T25-SK46)	A	18269	16982	++++	1
	B	14409			
	C	18269			
T18-SepFC K46A + T25- FtsZC (T18-SK46+T25-F)	A	0	0	-	0.01
	B	0			
	C	0			
SepFC K46A-T18 + FtsZC-T25 (SK46-T18+F-T25)	A	0	322	-	0.01
	B	0			
	C	965			
T18-FtsZC + T25-SepFC K46A (T18-F+T25-SK46)	A	0	0	-	0.01
	B	0			
	C	0			

FtsZC-T18 + SepFC K46A-T25 (F-T18+SK46-T25)	A	0	0	-	0.01
	B	0			
	C	0			
T18-SepFC K46A + FtsZC-T25 (T18-SK46+F-T25)	A	1569	644	-	0.01
	B	362			
	C	0			
SepFC K46A-T18 + T25- FtsZC (SK46-T18+T25-F)	A	0	0	-	0.01
	B	0			
	C	0			
T18-FtsZC + SepFC K46A-T25 (T18-F+SK46-T25)	A	2282	2737	++	0.5
	B	2054			
	C	3875			
FtsZC-T18 + T25-SepFC K46A (F-T18+T25-SK46)	A	724	241	-	0.01
	B	0			
	C	0			
T18-SepFC K46A + T25- SsgB (T18-SK46A+T25-B)	A	0	1730	++	0.5
	B	4383			
	C	806			
SepFC K46A-T18 + SsgB- T25 (SK46A-T18+B-T25)	A	12582	12494	++++	1
	B	15491			
	C	9408			
T18-SsgB + T25-SepFC K46A (T18-B+T25-SK46A)	A	2002	1246	-	0.01
	B	1737			
	C	0			
SsgB-T18 + SepFC K46A- T25 (B-T18+SK46A-T25)	A	5303	9098	++++	1
	B	15491			
	C	6499			
T18-SepFC K46A + SsgB- T25 (T18-SK46A+B-T25)	A	9143	10907	++++	1
	B	9672			
	C	13905			
SepFC K46A-T18 + T25- SsgB (SK46A-T18+T25-B)	A	8879	10114	++++	1
	B	10202			
	C	11260			
T18-SsgB + SepFC K46A- T25 (T18-B+SK46A-T25)	A	13112	13905	++++	1
	B	13376			
	C	15227			
SsgB-T18 + T25-SepFC K46A (B-T18+T25-SK46A)	A	0	0	-	0.01
	B	0			
	C	0			
T18-SepFC K46A + T25- Scy (T18-SK46A+T25-Y)	A	14467	14092	++++	1
	B	12402			
	C	15406			
T18-Scy + T25-SepFC K46A (T18-Y+T25-SK46A)	A	9209	11525	++++	1
	B	13340			
	C	12026			
SepFC K46A-T18 + T25- Scy (SK46A-T18+T25-Y)	A	14843	16157	++++	1
	B	16720			
	C	16908			
T18-Scy + SepFC K46A- T25 (T18-Y+SK46A-T25)	A	13340	12965	++++	1
	B	12777			
	C	12777			

Appendix 5 The pairwise protein-protein interactions of SepFC and SepFC-F71A using the bacterial two-hybrid assay. The combinations (described in Interaction partner and shorten as seen in the graphs) were quantified as described in the materials and methods. For each combination three streaks (at position A, B or C) had the median signal intensity of the blue pigment generated by Xgal hydrolysis randomly measured in triplet. The mean of the replicates generated the streak mean and from the streak means the interaction mean was generated. The interaction means classified the interactions into the three categories: negative (>1500), weak positive (1501 to 8000) and strong positive (<8000). For visual representation these categories were given the arbitrary values of 0.01, 0.5 and 1 respectively. Visual assessment (Visual) of the streaks into the same three categories was recorded (- are negative, ++ are weak positive and ++++ are strong positive) and was consistent with the quantitative data.

Interaction partners	Position	Streak mean	Interaction mean	Visual	Figure value
T18-SepFC + T25-SepFC (T18-S+T25-S)	A	17274	17637	++++	1
	B	16911			
	C	18726			
SepFC-T18 + SepFC-T25 (S-T18-S-T25)	A	21086	21992	++++	1
	B	22718			
	C	22173			
T18-SepFC + SepFC-T25 (T18-S+S-T25)	A	22717	24048	++++	1
	B	25621			
	C	23806			
SepFC-T18 + T25-SepFC (S-18+T25-S)	A	24533	24835	++++	1
	B	23988			
	C	25985			
T18-SepFC + T25-FtsZC (T18-S+T25-F)	A	5885	6284	++	0.5
	B	8179			
	C	4788			
SepFC-T18 + FtsZC-T25 (S-T18+F-T25)	A	14408	14505	++++	1
	B	17329			
	C	11778			
T18-FtsZC + T25-SepFC (T18-F+T25-S)	A	8857	9782	++++	1
	B	10902			
	C	9588			
FtsZC-T18 + SepFC-T25 (F-T18+S-T25)	A	19083	18450	++++	1
	B	19083			
	C	17184			
T18-SepFC + FtsZC-T25 (T18-S+F-T25)	A	9587	11340	++++	1
	B	11487			
	C	12947			
SepFC-T18 + T25-FtsZC (S-T18+T25-F)	A	8379	10008	++++	1
	B	10573			
	C	11072			
T18-FtsZC + SepFC-T25 (T18-F+S-T25)	A	18937	19375	++++	1
	B	18060			
	C	21128			
FtsZC-T18 + T25-SepFC (F-T18+T25-S)	A	0	0	-	0.01
	B	0			
T18-SsgB + T25-SepFC (T18-B+T25-S)	A	7289	8423	++++	1
	B	9891			
	C	8090			

SsgB-T18 + SepFC-T25 (B-T18+S-T25)	A	15696	18098	++++	1
	B	20099			
	C	18498			
T18-SepFC + T25-SsgB (T18-S+T25-B)	A	2397	5006	++	0.5
	B	6584			
	C	6038			
SepFC-T18 + SsgB-T25 (S-T18+B-T25)	A	14895	17097	++++	1
	B	19299			
T18-SsgB + SepFC-T25 (T18-B+S-T25)	A	11693	12160	++++	1
	B	13694			
	C	11092			
SsgB-T18 + T25-SepFC (B-T18+T25-S)	A	5536	4206	++	0.5
	B	3342			
	C	3741			
T18-SepFC + SsgB-T25 (T18-S+B-T25)	A	13294	13094	++++	1
	B	12694			
	C	13294			
SepFC-T18 + T25-SsgB (S-T18+T25-B)	A	12293	12994	++++	1
	B	13695			
T18-Scy + T25-SepFC (T18-Y+T25-S)	A	8162	10154	++++	1
	B	12943			
	C	9358			
T18-SepFC + T25-Scy (T18-S+T25-Y)	A	16017	15220	++++	1
	B	13285			
	C	16359			
T18-Scy + SepFC-T25 (T18-Y+S-T25)	A	12944	9927	++++	1
	B	6113			
	C	10723			
SepFC-T18 + T25-Scy (S-T18+T25-Y)	A	9529	13798	++++	1
	B	16700			
	C	15163			
T18-SepFC F71A + T25- SepFC F71A (T18-SF71A+T25-SF71A)	A	2057	3343	++	0.5
	B	4373			
	C	3601			
SepFC F71A-T18 + SepFC F71A-T25 (SF71A-T18+SF71A-T25)	A	14409	12436	++++	1
	B	8490			
	C	14409			
T18-SepFC F71A + SepFC F71A-T25 (T18-SF71A+SF71A-T25)	A	17497	10892	++++	1
	B	12350			
	C	2829			
SepFC F71A-T18 + T25- SepFC F71A (SF71A-T18+T25-SF71A)	A	7718	9348	++++	1
	B	12865			
	C	7461			
T18-SepFC F71A + T25- FtsZC (T18-SF71A+T25-F)	A	0	0	-	0.01
	B	0			
	C	0			
SepFC F71A-T18 + FtsZC-T25 (SF71A-T18+F-T25)	A	0	0	-	0.01
	B	0			
	C	0			

T18-FtsZC + T25-SepFC F71A (T18-F+T25-SF71A)	A	0	0	-	0.01
	B	0			
	C	0			
FtsZC-T18 + SepFC F71A-T25 (F-T18+SF71A-T25)	A	0	0	-	0.01
	B	0			
	C	0			
T18-SepFC F71A + FtsZC-T25 (T18-SF71A+F-T25)	A	0	0	-	0.01
	B	0			
	C	0			
SepFC F71A-T18 + T25- FtsZC (SF71A-T18+T25-F)	A	0	0	-	0.01
	B	0			
	C	0			
T18-FtsZC + SepFC F71A-T25 (T18-F+SF71A-T25)	A	0	0	-	0.01
	B	0			
	C	0			
FtsZC-T18 + T25-SepFC F71A (F-T18+T25-SF71A)	A	0	0	-	0.01
	B	0			
	C	0			
T18-SepFC F71A + T25- SsgB (T18-SF71A+T25-B)	A	393	361	-	0.01
	B	393			
	C	295			
SepFC F71A-T18 + SsgB- T25 (SF71A-T18+B-T25)	A	0	0	-	0.01
	B	0			
	C	0			
T18-SsgB + T25-SepFC F71A (T18-B+T25-SF71A)	A	0	0	-	0.01
	B	0			
	C	0			
SsgB-T18 + SepFC F71A- T25 (B-T18+SF71A-T25)	A	10037	10233	++++	1
	B	9840			
	C	10824			
T18-SepFC F71A + SsgB- T25 (T18-SF71A+B-T25)	A	2755	1148	-	0.01
	B	295			
	C	393			
SepFC F71A-T18 + T25- SsgB (SF71A-T18+T25-B)	A	0	0	-	0.01
	B	0			
	C	0			
T18-SsgB + SepFC F71A- T25 (T18-B+SF71A-T25)	A	12693	13415	++++	1
	B	13481			
	C	14071			
SsgB-T18 + T25-SepFC F71A (B-T18+T25-SF71A)	A	0	0	-	0.01
	B	0			
	C	0			
T18-SepFC F71A + T25- Scy (T18-SF71A+T25-Y)	A	0	0	-	0.01
	B	0			
	C	0			
T18-Scy + T25-SepFC F71A (T18-Y+T25-SF71A)	A	0	0	-	0.01
	B	0			
	C	0			
SepFC F71A-T18 + T25- Scy (SF71A-T18+T25-Y)	A	119	198	-	0.01
	B	237			
	C	237			

T18-Scy + SepFC F71A-T25 (T18-Y+SF71A-T25)	A	9998	10451	++++	1
	B	11016			
	C	10338			

10.0 Definitions

Abbreviations which were used throughout the current study stand for:

(S)-DNPA = 4-dihydro-9-hydroxy-1-methyl-10-oxo-3-H-naphtho-[2,3c]-pyran-3-(S)-acetic acid

ACP = Acyl carrier protein

CM = Cell membrane

DCW = Division and cell wall

DDHK = 6-deoxy-dihydrokalafungin

DHK = Dihydrokalafungin

Egfp = Enhanced green fluorescent protein

FRET = Förster resonance energy transfer

FtsZC = the C-terminal of the *S. coelicolor* FtsZ

GlcNAc = *N*-acetylglucosamine

int = Φ BT1 integrase

KS-CLF = ketosynthase-chain length factor

LB = Solid lysogeny broth

LB Δ glucose = Solid lysogeny broth Δ glucose

LB Δ NaCl = Solid lysogeny broth Δ NaCl

M145 = wild-type *S. coelicolor*

MAT = malonyl-CoA:ACP transacylase

MMM = Minimal media mannitol

NBS = Noc binding sites

Ori = Origin of replication

OriT = Origin of transfer

PBP = Penicillin-binding protein

PG = Peptidoglycan

PI = Propidium iodide

PKS = Polyketide synthase

SARP = *Streptomyces* antibiotic regulatory protein

SBS = SImA binding sites

SepFC = the C-terminal of the *S. coelicolor* SepF

SepFC-F71A = the C-terminal of the *S. coelicolor* SepF containing an F71A mutation

SepFC-K46A = the C-terminal of the *S. coelicolor* SepF containing an K46A mutation

SFM = Soya flour mannitol

TIPOC = Tip organising centre

WGA = Wheat germ agglutinin

X-Gal = 5-bromo-4-chloro-3-indolyl- β -D-galactopyranoside

11.0 References

- Abbas, A. and Edwards, C., (1990), 'Effects of metals on *Streptomyces coelicolor* growth and actinorhodin production', *Applied Environmental Microbiology*, 3:675–680.
- Adams, D.W. and Errington, J., (2009), 'Bacterial cell division: assembly, maintenance and disassembly of the Z-ring', *Nature Reviews Microbiology*, 7:642-653.
- Adams, D.W., Wu, L.J. and Errington, J., (2015), 'Nucleoid occlusion protein Noc recruits DNA to the bacterial cell membrane', *The EMBO Journal*, 34(4):491-501.
- Aínsa, J.A., Parry, H.D. and Chater, K.F., (1999), 'A response regulator-like protein that functions at the intermediate stage of sporulation in *Streptomyces coelicolor* A3(2)', *Molecular Microbiology*, 34(3):607-619.
- Akagawa, H., Okanish, M. and Umezawa, H., (1975), 'A plasmid involved in chloramphenicol production in *Streptomyces venezuelae*: evidence from genetic mapping', *Journal of General Microbiology*, 90(2):336-346.
- Akhmanova, A. and Steinmetz, M.O., (2008), 'Tracking the ends: a dynamic protein network controls the fate of microtubule tips', *Nature Reviews*, 9:309-320.
- Alcock, E., (2019), Conversations with Gemma Cassetari, 13 October.
- Angert, E.R., (2005), 'Alternatives to binary fission in bacteria', *Nature Reviews Microbiology*, 3:214-224.
- Arias, P., Fernández-Moreno, M. and Malpartida, F., (1999), 'Characterization of the Pathway-Specific Positive Transcriptional Regulator for Actinorhodin Biosynthesis in *Streptomyces coelicolor* A3(2) as a DNA-Binding Protein', *Journal of Bacteriology*, 181(22): 6958-6068.
- Baarle, S.V. and Bramkamp, M., (2010), 'The MinCDJ system in *Bacillus subtilis* Prevents Minicell Formation by Promoting Divisome Disassembly', *PLoS One*, 5(3):e9850.
- Bagchi, S., Tomenius, H., Belova, L.M. and Ausmees, N., (2008), 'Intermediate filament-like proteins in bacteria and a cytoskeletal function in *Streptomyces*', *Molecular Microbiology*, 70(4):1037-1050.
- Baum, E.Z., Crespo-Carbone, S.M., Klinger, A., Foleno, B.D., Turchi, I., Macielag, M. And Bush, K., (2007), 'A MurF inhibitor that disrupts cell wall biosynthesis in *Escherichia coli*. *Antimicrobial agents and chemotherapy*, 51(12):4420-4426.

Beltran-Alvarez, P., Cox, R., Crosby, J. and Simpson, T., (2007), 'Dissecting the Component Reactions Catalyzed by the Actinorhodin Minimal Polyketide Synthase', *Biochemistry*, 46(50):14672-14681.

Bennett, J.A., Aimino, R.M. and McCormick, J.R., (2007), '*Streptomyces coelicolor* gene *ftsL* and *divIC* play a role in cell division but are dispensable for colony formation', *Journal of Bacteriology*, 189(24):8982-8992.

Bentley, S., Chater, K., Cerdeño-Tárraga, A., Challis, G., Thomson, N., James, K., Harris, D., Quail, M., Kieser, H., Harper, D., Bateman, A., Brown, S., Chandra, G., Chen, C., Collins, M., Cronin, A., Fraser, A., Goble, A., Hidalgo, J., Hornsby, T., Howarth, S., Huang, C., Kieser, T., Larke, L., Murphy, L., Oliver, K., O'Neil, S., Rabbinowitsch, E., Rajandream, M., Rutherford, K., Rutter, S., Seeger, K., Saunders, D., Sharp, S., Squares, R., Squares, S., Taylor, K., Warren, T., Wietzorrek, A., Woodward, J., Barrell, B., Parkhill, J. and Hopwood, D., (2002), 'Complete genome sequence of the model actinomycete *Streptomyces coelicolor* A3(2)', *Nature*, 417(6885):141-147.

Bernhardt, T.G. and de Boer, P.A.J., (2005), 'SlmA, a Nucleoid-Associated, FtsZ Binding Protein Required for Blocking Septal Ring Assembly over Chromosomes in *E. coli*', *Molecular Cell*, 18(5):555-564.

Bhattacharya, D., Sinha, K. and Panda, D., (2018), 'Mutation of G51 in SepF impairs FtsZ assembly promoting ability of SepF and retards the division of *Mycobacterium smegmatis* cells', *Biochemical Journal*, 475:2473-2489.

Blattner, F.R., Plunkett 3rd, G., Bloch, C.A., Perna, N.T., Burland, V., Riley, M., Collado-Vides, J., Glasner, J.D., Rode, C.K., Mayhew, G.F., Gregor, J., Davis, N.W., Kirkpatrick, H.A., Goeden, M.A., Rose, D.J., Mau, B. and Shao, Y., (1997), 'The complete genome sequence of *Escherichia coli* K-12', *Science*, 277(5331):1452-1462.

Bobek, J., Šmídová, K. and Čihák, M., (2017), 'A waking review: old and novel insights into the spore germination in *Streptomyces*', *Frontiers in Microbiology*, 8:2205.

Borodina, I., Siebring, J., Zhang, J., Smith C.P., van Keulen, G., Dijkhuizen, L. and Nielsen, J., (2008), 'Antibiotic overproduction in *Streptomyces coelicolor* A3(2) mediated by phosphofructokinase deletion', *Metabolism and Bioenergetics*, 282(137):25186-25199.

Braña, A.F., Manzanal, M-B. and Hardisson, C., (1982), 'Model of cell wall growth of *Streptomyces antibioticus*', *FEMS Microbiology Letters*, 13:231-235.

Bratton, B.P., Shaevitz, J.W., Gitai, Z. and Morgenstein, R.M., (2018), 'MreB polymers and curvature localisation are enhanced by RodZ and predict *E. coli*'s cylindrical uniformity', *Nature communications*, 9:2797.

- Brian, P., (1992), 'A developmentally regulated spore pigment locus from *Streptomyces coelicolor* A3(2)', PhD thesis, University of East Anglia, Norwich.
- Bush, M.J., Chandra, G., Bibb, M.J., Findlay, K.C. and Buttner, M. J., (2016), 'Genome-Wide chromatin Immunoprecipitation sequencing analysis shows that WhiB is a transcription factor that cocontrols its regulon with WhiA to initiate developmental cell division in *Streptomyces*', *mBio*, 7(2):e00523-16.
- Bystrykh, L.V., Fernandez-Moreno, M.A., Herrema, J.K., Malpartida, F., Hopwood, D.A. and Dijkhuizen, L., (1996), 'Production of Actinorhodin-Related "Blue Pigments" by *Streptomyces coelicolor* A3(2)', *Journal of Bacteriology*, 178(8):2238-2244.
- Celler, K., Koning, R.I., Willemse, J., Koster, A.J. and van Wezel, G.P., (2016), 'Cross-membranes orchestrate compartmentalization and morphogenesis in *Streptomyces*', *Nature communications*, 7:11836.
- Chakraborty, R. and Bibb, M., (1997), 'The ppGpp synthetase gene (*relA*) of *Streptomyces coelicolor* A3(2) plays a conditional role in antibiotic production and morphological differentiation', *Journal of Bacteriology*, 179(18):5854-5861.
- Chater, K.F., (1972), 'A morphological and genetic mapping study of white colony mutants of *Streptomyces coelicolor*', *Journal of General Microbiology*, 72:9-28.
- Chater, K., Biró, S., Joon Lee, K., Palmer, T. and Schrempf, H., (2010), 'The complex extracellular biology of *Streptomyces*', *FEMs Microbiology Reviews*, 34(2):171-198.
- Chater, K.F, Bruton, C.J., Plaskitt, K.A., Buttner, M.J., Méndez, C. and Helemann, J.D., (1989), 'The developmental fate of *S. coelicolor* hyphae depends upon a gene product homologous with the motility sigma factor of *B. subtilis*', *Cell*, 59(1):P133-143.
- Chen, H. and Du, L., (2016), 'Iterative polyketide biosynthesis by modular polyketide synthases in bacteria', *Applied Microbiology and Biotechnology*, 100(2):541-557.
- Chen, J.C. and Beckwith, J., (2008), 'FtsQ, FtsL and FtsI require FtsK, but not FtsN, for co-localization of FtsZ during *Escherichia coli* cell division', *Molecular Microbiology*, 42(2):393-413.
- Cho, H., McManus, H.R., Dove, S.L. and Bernhardt, T.G., (2011), 'Nucleoid occlusion factor SlmA is a DNA-activated FtsZ polymerization antagonist', *PNAS*, 108(9):3773-3778.
- Čihák, M., Kamenik, Z., Šmidová, K., Bergman, N., Benada, O., Kofroňová, O., Petříčková, K. and Bobek, J., (2017), 'Secondary Metabolites Produced during the Germination of *Streptomyces coelicolor*', *Frontiers in Microbiology*, 8:2495.

Claessen, D., Rink, R., de Jong, W., Siebring, J., de Vreugd, P., Hidde Boersma, F.G., Dijkhuizen, L. and Wösten, H.A.B., (2003), 'A novel class of secreted hydrophobic proteins is involved in aerial hyphae formation in *Streptomyces coelicolor* by forming amyloid-like fibrils', *Genes and Development*, 17(14):1714-1726.

Claessen, D., Wösten, H.A.B., van Keulen, G., Faber, O.G., Alves, A.M.C.R., Meijer, W.G. and Dijkhuizen, L., (2002), 'Two novel homologous proteins of *Streptomyces coelicolor* and *Streptomyces lividans* are involved in the formation of the rodlet layer and mediate attachment to a hydrophobic surface', *Molecular Microbiology*, 44(6):1483-1492.

Conti, J., Viola, M.G. and Camberg, J.L., (2014), 'The bacterial cell division regulators MinD and MinC form polymers in the presence of nucleotide', *FEBS Letters*, 589(2):201-206.

Conti, J., Viola, M.G. and Camberg, J.L., (2018), 'FtsA reshapes membrane architecture and remodels the Z-ring in *Escherichia coli*', *Molecular Microbiology*, 107(4):558-576.

Cooper, G.M., (2000), '*The Cell: A Molecular Approach*', 2nd edition, Sinauer Associates: Sunderland (MA), Microtubules. (Available from: <https://www.ncbi.nlm.nih.gov/books/NBK9932/>).

Cosine, S., Béchet, M. and Blondeau, R., (1999), 'Actinorhodin production by *Streptomyces coelicolor* A3(2) in iron-restricted media', *Letters in Applied Microbiology*, 28(3):199-202.

Craney, A., Ahmed, S. and Nodwell, J., (2013), 'Towards a new science of secondary metabolism', *The Journal of Antibiotics*, 66:387-400.

Dalton, K.A., Thibessard, A., Hunter, J.I.B. and Kelemen, G.H., (2007), 'A novel compartment, the 'subapical stem' of the aerial hyphae, is the location of a *sigN*-dependent, developmentally distinct transcription in *Streptomyces coelicolor*', *Molecular Microbiology*, 64(3): 719-737.

den Hengst, C.D. and Buttner, M.J., (2008), 'Redox control in actinobacteria', *Biochimica et Biophysica Acta (BBA) – General Subjects*, 1780(11):1201-1216.

Ditkowski, B., Holmes, N., Rydzak, J., Donczew, M., Bezulska, M., Gind, K., Kędzierski, P., Zakrzewska-Czerwiń, J., Kelemen, G.H. and Jakimowicz, D., (2013), 'Dynamic interplay of ParA with the polarity protein, Scy coordinates the growth with chromosome segregation in *Streptomyces coelicolor*', *Open Biology*, 3(3):130006.

- Dokouhaki, M., Hung, A., Day, L. and Gras, S.L. (2017), 'The pH-dependent assembly of Chaplin E from *Streptomyces coelicolor*', *Journal of Structural Biology*, 198:82-91.
- Donczew, M., Mackiewicz, P., Wróbel, A., Flärdh, K., Zakrzewska-Czerwińska, J. and Jakimowicz, D., (2016), 'ParA and ParB coordinate chromosome segregation with cell elongation and division during *Streptomyces* sporulation', *Open Biology*, 6:150263.
- Donovan, C., Sieger, B., Krämer, R. and Bramkamp, M., (2012), 'A synthetic *Escherichia coli* system identifies a conserved origin tethering factor in Actinobacteria', *Molecular Microbiology*, 84(1):105-116.
- Dreier, J., Shah, A. and Khosla, C., (1999), 'Kinetic Analysis of the Actinorhodin Aromatic Polyketide Synthesis', *The Journal of Biological Chemistry*, 274(35):2508-25112.
- Du, S. and Lutkenhaus, J., (2017), 'Assembly and activation of the *Escherichia coli* divisome', *Molecular Microbiology*, 105(2):177-187.
- Duman, R., Ishikawa, S., Celik, I., Strahl, H., Ogasawara, N., Troc, P., Löwe, J. and Hamoen, L., (2013), 'Structural and genetic analyses reveal the protein SepF as a new membrane anchor for the Z ring', *PNAS*, 110:e4601-4610.
- Dyer, N., (2009), 'Tubulin and its prokaryotic homologues FtsZ: a structural and functional comparison', *Science Progress*, 92(Pt 2):113-137.
- Edwards, D.H. and Errington, J., (1997), 'The *Bacillus subtilis* DivIVA protein targets to the division septum and controls the site specificity of cell division', *Molecular Microbiology*, 24(5): 905-915.
- Elliot, M.A., Bibb, M.J., Buttner, M.J. and Laskiw, B.K., (2001), 'BldD is a direct regulator of key developmental genes in *Streptomyces coelicolor* A3(2)', *Molecular Microbiology*, 40(1):257-269.
- Elliot, M.A., Karoonuthaisiri, N., Huang, J., Bibb, M.J., Cohen, S.N., Kao, C.M. and Buttner, M.J., (2003), 'The chaplins: a family of hydrophobic cell-surface proteins involved in aerial mycelium formation in *Streptomyces coelicolor*', *Genes and Development*, 17(14):1727-1740.
- Erickson, H.P., (1995), 'FtsZ, a prokaryotic homolog of tubulin?', *Cell*, 80(3):267-70.
- Fenton, A. and Gerdes, K., (2013), 'Direct interaction of FtsZ and MreB is required for septum synthesis and cell division in *Escherichia coli*', *The EMBO Journal*, 32(13):1953-1965.
- Fernández-Moreno, M., Martínez, E., Boto, L., Hopwood, D. and Malpartida, F., (1992), 'Nucleotide sequence and deduced functions of a set of cotranscribed

genes of *Streptomyces coelicolor* A3(2) including of polyketide synthase for the antibiotic actinorhodin', *The Journal of Biological Chemistry*, 267(27):19278-19290.

Flärdh, K., (2003a), 'Essential role of DivIVA in polar growth and morphogenesis in *Streptomyces coelicolor* A3(2)', *Molecular Microbiology*, 49(6):1523-1536.

Flärdh, K., (2003b), 'Growth polarity and cell division in *Streptomyces*', *Current Opinion in Microbiology*, 6(6):564-571.

Flärdh, K., (2010), 'Cell polarity and the control of apical growth in *Streptomyces*', *Current Opinion in Microbiology*, 13(6):758-768.

Flärdh, K. and Buttner, M.J., (2009), '*Streptomyces* morphogenetics: dissecting differentiation in a filamentous bacterium', *Nature Reviews Microbiology*, 7:36-49.

Flärdh, K., Findlay, K.C. and Chater, K.F., (1999), 'Association of early sporulation genes with suggested developmental decision points in *Streptomyces coelicolor* A3(2)', *Microbiology*, 145:2229-2243.

Flärdh, K., Leibovitz, E., Buttner, M.J. and Chater, K.F., (2002), 'Generation of the non-sporulating strain of *Streptomyces coelicolor* A3(2) by the manipulation of a developmentally controlled *ftsZ* promoter', *Molecular Microbiology*, 38(4):737-749.

Fröjd, M.J. and Flärdh, K., (2019), 'Apical assemblies of intermediate filament-like protein FilP are highly dynamic and affect polar growth determinant DivIVA in *Streptomyces venezuelae*', *Molecular Microbiology*, 112(1):47-61.

Fu, J., Zong, G., Zhang, P., Zhao, Z., Ma, J., Pang, X. and Cao, G., (2017), 'XdhR negatively regulates actinorhodin biosynthesis in *Streptomyces coelicolor* M145', *FEMS Microbiology Letters*, 364(22):fnx226.

Fuchino, K., Bagchi, S., Cantlay, S., Sandblad, L., Wu, D., Bergman, J., Kamali-Moghaddam, M., Flärdh, K. and Ausmees, N., (2013), 'Dynamic gradients of an intermediate filament-like cytoskeleton are recruited by a polarity landmark during apical growth', *PNAS*, 110(21):E1889-E1897.

Gao, Y., Wenzel, M., Jonker, M.J. and Hamoen, L.W., (2017), 'Free SepF interferes with recruitment of late cell division proteins', *Scientific Reports*, 7:16928.

Gardner, M.K., Zanic, M. and Howard, J., (2014), 'Microtubule Catastrophe and Rescue', *Current Opinion in Cell Biology*, 25(1):14-22.

Ghosal, D., Trambaiolo, D., Amos, L.A. and Löwe, J., (2014), 'MinCD cell division proteins form alternating copolymeric cytomotive filaments', *Nature Communications*, 5:5341.

- Gola, S., Munder, T., Casonato, S., Manganeli, R. and Vicente, M., (2015), 'The essential role of SepF in mycobacterial division', *Molecular Microbiology*, 97(3):560-576.
- González-Pastor, J., Hobbs, E. and Losick, R., (2003), 'Cannibalism by Sporulating Bacteria', *Science*, 301:510-513.
- Gordon, E., Flouret, B., Chantalat, L., van Heijenoort, J., Mengin-Lecreulx, D. and Dideberg, O., (2001), 'Crystal structure of UDP-*N*-acetylmuramoyl-l-alanyl-d-glutamate:*meso*-Diaminopimelate ligase from *Escherichia Coli*', *Protein Structure and Folding*, 276(14):10999-11006.
- Grantcharova, N., Lustig, U. and Flärdh, K., (2005), 'Dynamics of FtsZ assembly during sporulation in *Streptomyces coelicolor* A3(2)', *Journal of Bacteriology*, 187(9):3227-3237.
- Gray, D.I., Gooday, G.W. and Prosser, J.I., (1990), 'Apical hyphal extension in *Streptomyces coelicolor* A3(2)', *Journal of General Microbiology*, 136(6):1077-1084.
- Gregory, M.A., Till, R. and Smith, M.C.M., (2003), 'Integration Site for *Streptomyces* Phage ϕ BT1 and Development of Site-Specific Integrating Vectors', *Journal of Bacteriology*, 185(17):5320-5323.
- Guan, F., Yu, J., Yu, J., Liu, Y., Li, Y., Feng, X-H., Huang, K.C., Chang, Z. and Ye, S., (2018), 'Lateral interaction between protofilaments of the bacterial tubulin homolog FtsZ are essential for cell division', *eLife*, 7:e35578.
- Guiral, S., Mitchell, T., Martin, B. and Claverys, J., (2005), 'Competence-programmed predation of noncompetent cells in the human pathogen *Streptococcus pneumoniae*: Genetic requirements', *PNAS*, 102(24):8710-8715.
- Gündoğdu, M., Kawai, Y., Pavlendova, N., Ogasawara, N., Errington, J., Scheffers, D. and Hamoen, L., (2011), 'Large ring polymers align FtsZ polymers for normal septum formation', *The EMBO Journal*, 30(3):617-26.
- Gupta, R.S., Lo, B. and Son, J., (2018), 'Phylogenomics and Comparative Genomic Robustly Support Division of the Genus *Mycobacterium* into an Emended Genus *Mycobacterium* and Four Novel Genera', *Frontiers in Microbiology*, 9:67.
- Gupta, S., Banerjee, S.K., Chatterjee, A., Sharma, A.K., Kundu, M. and Basu, J., (2015), 'Essential protein SepF of mycobacteria interacts with FtsZ and MurG to regulate cell growth and division', *Microbiology*, 161(8):1627-1638.
- Gust, B., Challis, G.L., Fowler, K., Kieser, T. and Chater, K.F., (2003), 'PCR-targeted *Streptomyces* gene replacement identifies a protein domain needed for biosynthesis of the sesquiterpene soil odour geosmin', *PNAS*, 100(4):1541-1546.
- Gust, B., Kieser, T. and Chater, K., (2002), 'PCR targeting system in *Streptomyces coelicolor* A3(2)', *The John Innes Foundation, Norwich*.

- Hadfield, A., Limpkin, C., Teartasin, W., Simpson, T., Crosby, J. and Crump, M., (2004), 'The Crystal Structure of the actIII Actinorhodin Polyketide Reductase: Proposed Mechanism of ACP and polyketide Binding', *Structure*, 12:1865-1875.
- Hamoen, L.W., Meile, J-C., De Jong, W., Noirot, P. and Errington, J., (2006), 'SepF, a novel FtsZ-interacting protein required for a late step in cell division', *Molecular Microbiology*, 59(3):989-999.
- Hale, C.A. and de Boer, P.A.J., (1997), 'Direct Binding to FtsZ to ZipA, an Essential component of the Septal Ring Structure That Mediates Cell Division in *E. coli*', *Cell*, 88:175-185.
- Hale, C.A., Meinhardt, H. and de Boer, P.A.J., (2001), 'Dynamic localization cycle of the cell division regulator MinE in *Escherichia coli*', *The EMBO Journal*, 20:1563-1572.
- Hardisson, C., Manzanal, M-B., Salas, J-A. and Suárez, J-E., (1978), 'Fine Structure, Physiology and Biochemistry of Arthrospore Germination in *Streptomyces antibioticus*', *Journal of General Microbiology*, 105(2):203-214.
- Harvey, J., (2019), 'The Characterisation of Germination in a *sigF* Null Mutant of *Streptomyces coelicolor*', Degree project, University of East Anglia, Norwich.
- Hempel, A.M., Cantlay, S., Molle, V., Wang, S-B., Naldrett, M.J., Parker, J.L., Richards, D.M., Jung, Y-G., Buttner, M.J. and Flärdh, K., (2012), 'The Ser/Thr protein kinase AfsK regulates polar growth and hyphal branching in the filamentous bacteria *Streptomyces*', *PNAS*, 109(3):E2371-E2379.
- Hempel, A.M., Wang, S-b, Letek, M., Gil, J.A. and Flärdh, K., (2008), 'Assemblies of DivIVA Mark Sites of Hyphal Branching and Can Establish New Zones of Cell Wall Growth in *Streptomyces coelicolor*', *Journal of Bacteriology*, 190(22):7579-7583.
- Hesketh, A. and Chater, K., (2003), 'Evidence from proteomics that some of the enzymes of actinorhodin biosynthesis have more than one form and may occupy distinctive cellular locations', *Journal of Industrialised Microbiology Biotechnology*, 30:523-529.
- Hollingshead, S. and Vapnek, D., (1985), 'Nucleotide sequence analysis of a gene encoding a streptomycin/spectinomycin adenylyltransferase', *Plasmid*, 13(1):17-30.
- Holmes, N.A., Walshaw, J., Leggett, R.M., Thibessard, A., Dalton, K.A., Gillespie, M.D., Hemming, A.M., Gust, B. and Kelemen, G.H., (2013), 'Coiled-coil protein Scy is a key component of a multiprotein assembly controlling polarized growth in *Streptomyces*', *PNAS*, 110(5):E397-E406.

- Höltje, J.-V., (1998), 'Growth of the Stress-Bearing and Shape-Maintaining Murein Sacculus of *Escherichia coli*', *Microbiology and Molecular Biology Reviews*, 62(1):181-203.
- Hopwood, D.A., Wildermuth, H. and Palmer, H.M., (1970), 'Mutants of *Streptomyces coelicolor* defective in sporulation', *Journal of General Microbiology*, 61(3):397-408.
- Horio, T. and Murata, T., (2014), 'The role of dynamic instability in microtubule organization', *Frontiers in Plant Science*, 5:511.
- Hu, Z., Gogol, E.P. and Lutkenhaus, J., (2002), 'Dynamic assembly of MinD on phospholipid vesicles regulated by ATP and MinE', *PNAS*, 99(10):6761-6766.
- Huang, K.C., Meir, Y. and Wingreen, N.S., (2003), 'Dynamic structures in *Escherichia coli*: Spontaneous formation of MinE rings and MinD polar zones', *PNAS*, 100(22):12724-12728.
- Ishikawa, S., Kawai, Y., Hiramatsu, K., Kuwano, M. and Ogasawara, N., (2006), 'A new FtsZ-interacting protein, YlmF, complements the activity of FtsA during progression of cell division in *Bacillus subtilis*', *Molecular Microbiology*, 60(6):1364-80.
- Jakimowicz, D., Chater, K. and Zakrzewska-Czerwi, J., (2002), 'The ParB protein of *Streptomyces coelicolor* A3(2) recognizes a cluster of *ParS* sequences within the origin-proximal region of the linear chromosome', *Molecular Microbiology*, 45(5):1365-1377.
- Jakimowicz, D. and van Wezel, G.P., (2012), 'Cell division and DNA segregation in *Streptomyces*: how to build a septum in the middle of nowhere?', *Molecular Microbiology*, 85(3):393-404.
- Jakimowicz, D., Źydek, P., Kois, A., Zakrzewska-Czerwi, J. and Chater, K.F., (2007), 'Alignment of multiple chromosomes along helical ParA scaffolding in sporulating *Streptomyces* hyphae', *Molecular Microbiology*, 65(3):625-641.
- Jamroškovič, J., Pavlendová, N., Muchová, K., Wilkinson, A.J. and Barák, I., (2012), 'An Oscillating Min system in *Bacillus subtilis* influences asymmetrical septation during sporulation', *Microbiology*, 158(Pt 8):1972-1981.
- Javadi, A., Söderholm, N., Olofsson, A., Flärdh, K. and Sandblad, L., (2019), 'Assembly mechanisms of the bacterial cytoskeletal protein FilP', *Life Science Alliance*, 2(3):e201800290.
- Jeong, Y., Kim, J.-N., Kim, M.W., Bucca, G., Cho, S., Yoon, Y.J., Kim, B.-G., Roe, J.-H., Kim, S.C., Smith, C.P. and Cho, B.-K., (2016), 'The dynamic transcriptional and translational landscape of the model antibiotic producer *Streptomyces coelicolor* A3(2)', *Nature communications*, 7:11605.

Jones, S. and Elliot, M.A., (2018), 'Exploring' the regulation of *Streptomyces* growth and development', *Current Opinion in Microbiology*, 42:25-30.

Jyothikumar, V., Tilley, E.J., Wali, R. and Herron, P.R., (2008), 'Time-lapse Microscopy of *Streptomyces coelicolor* Growth and sporulation', *Applied and Environmental Microbiology*, 74(21):6774-6781.

Kabeya, Y., Nakanishi, H., Suzuki, K., Ichikawa, T., Kondou, Y., Matsui, M. and Miyagishima, S-Y., (2010), 'The YlmG protein has a conserved function related to the distribution of nucleoids in chloroplasts and cyanobacteria', *BMC Plant Biology*, 10:57.

Kaiser, B.K. and Stoddard, B.L., (2011), 'DNA recognition and transcriptional regulation by the WhiA sporulation factor', *Scientific Reports*, 1:156.

Karimova, G., Pidoux, J., Ullmann, A. and Ladant, D., (1998), 'A bacterial two-hybrid system based on a reconstituted signal transduction pathway', *PNAS*, 95(10):5752-5756.

Kaur, S., (2018), 'Study of Cell Division Genes *sepF*, *SCO2078* and *divIVA* in *Streptomyces coelicolor*', PhD thesis, University of East Anglia, Norwich.

Keatinge-Clay, A., Maltby, D., Medzihradzsky, K., Khosla, C. and Stroud, R., (2004), 'An Antibiotic factory caught in action', *Nature Structural & Molecular biology*, 11(9): 888-893.

Keatinge-Clay, A., Shelat, A., Savage, D., Tsai, S-C., Miercke, L., O'Connell III, J., Khosla, C. and Stroud, R., (2003), 'Catalysis, Specificity and ACP Docking site of *Streptomyces coelicolor* Malonyl-CoA:ACP transacylase', *Structure*, 11:147-154.

Keijsers, A.J.F., Noens, E.E.E., Kraal, B., Koerten, H.K. and van Wezel, G.P., (2003), 'The *Streptomyces coelicolor* *ssgB* gene is required for early stages of sporulation', *FEMS Microbiology Letters*, 225(1):59-67.

Kelemen, G.H., Brian, P., Flärdh, K., Chamberlin, L., Chater, K.F. and Buttner, M.J., (1998), 'Developmental regulation of transcription of *WhiE*, a locus specifying the polyketide spore pigment in *Streptomyces coelicolor* A3(2)', *Journal of Bacteriology*, 180(9):2515-2521.

Kelemen, G.H., Brown, G.L., Kormanec, J., Potůčková, L., Chater, K.F. and Buttner, M.J., (1996), 'The positions of the sigma-factor genes, *whiG* and *sigF*, in the hierarchy controlling the development of spore chains in the aerial hyphae of *Streptomyces coelicolor* A3(2)', *Molecular Microbiology*, 21(3):593-603.

Kelemen, G.H., (2017), 'Intermediate Filaments Supporting Cell Shape and Growth in Bacteria', *Sub-cellular Biochemistry*, 84:161-211.

Kelemen, G.H., Personal Communication with Gemma Cassettari, 13th October 2018 and 9th Oct 2020.

Kieser, T., Bibb, M. J., Buttner, M. J., Chater, K. F. and Hopwood, D. A., (2000), 'Growth and preservation of *Streptomyces*' in *Practical Streptomyces Genetics*, Norwich, The John Innes Foundation: Norwich, p53.

Kim, H-J., Calcutt, M.J., Schmidt, F.J. and Chater, K.F., (2000), 'Partitioning of the Linear Chromosome during Sporulation of *Streptomyces coelicolor* A3(2) Involves an *OriC*-Linked *parAB* locus', *Journal of Bacteriology*, 182(5):1313-1320.

Król, E., van Kessel, S., Bezouwen, L., Kumar, N., Boekema, E. and Scheffers, D., (2012), '*Bacillus subtilis* SepF binds to the C-terminus of FtsZ', *PloS One*, 7(8):e43293.

Krupka, M., Rowlett, V.W., Morado, D., Vitrac, H., Schoenemann, K., Liu, J. and Margolin, W., (2017), '*Escherichia coli* FtsA forms lipid-bound minirings that antagonize lateral interactions between FtsZ protofilaments', *Nature communications*, 8:15957.

Krupka, M., Sobrinos-Suguino, M., Jiménez, M., Rivas, G. and Margolin, W., (2018), '*Escherichia coli* ZipA Organizes FtsZ Polymers into Dynamic Ring-Like Protofilament Structures', *American society of microbiology*, 9(3):e01008-18.

Kruse, K., (2002), 'A dynamic Model for Determining the Middle of *Escherichia coli*', *Biophysical Journal*, 83(2):618-627.

Kunst, F., Ogasawara, N., *et al.*, (1997), 'The complete genome sequence of the Gram-positive bacterium *Bacillus subtilis*', *Nature*, 390(6657):249-256.

Kwak, J., Dharmatilake, A.J., Jiang, H. and Kendrick, K.E., (2001), 'Differential Regulation of FtsZ Transcription during Septation of *Streptomyces griseus*', *Journal of Bacteriology*, 183(17):5092-5101.

LaBreck, C.J., Conti, J., Viola, M.G. and Camberg, J.L., (2019), 'MinC N- and C-domain interactions modulate FtsZ assembly, division site selection, and MinD-dependent oscillation in *Escherichia coli*', *Journal of Bacteriology*, 201(4):e00374-18.

Lawlor, E., Baylis, H. and Chater, K., (1987), 'Pleiotropic morphological and antibiotic deficiencies result from mutations in a gene encoding a tRNA-like product in *Streptomyces coelicolor* A3(2)', *Genes & Development*, 1:1305-1310.

Lebkowski, T., Wolański, M., Ołdziej, S., Flärdh, K. and Zakrzewska-Czerwińska, J., (2020), 'AfsK-Mediate Site-specific Phosphorylation Regulates DnaA Initiator Protein Activity in *Streptomyces coelicolor*', *Journal of Bacteriology*, 202(3):e00597-19.

- Lee, N., Kim, W., Chung, J., Lee, Y., Cho, S., Jang, K-S., Kim, S.C., Palsson, B. and Cho, B-K., (2020), 'Iron competition triggers antibiotic biosynthesis in *Streptomyces coelicolor* during coculture with *Myxococcus xanthus*', *The ISME Journal*, 14:1111-1124.
- Lenarcic, R., Halbedel, S., Visser, L., Shaw, M., Wu, L.J., Errington, J., Marenduzzo, D. and Hamoen, L.W., (2009), 'Localisation of DivIVA by targeting to negatively curved membranes', *The EMBO Journal*, 28(15):2272-2282.
- Levin, P.A., Margolis, P.S., Setlow, P., Losick, R. and Sun, D., (1992), 'Identification of *Bacillus subtilis* genes for septum placement and shape determination', *Journal of Bacteriology*, 174(21):6717-6728.
- Li, C., Li, L., Huang, L. And Li, A., (2021), 'Pleiotropic effects of ActVI-ORFA as an unusual regulatory factor identified in the biosynthetic pathway of actinorhodin in *Streptomyces coelicolor*', *Microbiological Research*, 250:126792.
- Li, W., Wu, J., Tao, W., Zhao, C., Wang, Y., He, X., Chandra, G., Zhou, X., Deng, Z., Chater, K.F. and Tao, M., (2007), 'A genetic and bioinformatic analysis of *Streptomyces coelicolor* genes containing TTA codons, possible targets for regulation by a developmentally significant tRNA', *FEMS Microbiology Letters*, 266(1):20-28.
- Lim, J-H., Lee, C-R., Dhakshnamoorthy, V., Park, J.S. and Hong, S-K., (2016), 'Molecular characterization of *Streptomyces coelicolor* A(3) SCO6548 as a cellulose 1,4- β -cellobiosidase', *FEMS Microbiology Letters*, 363(3):fnv245.
- Liman, R., Facey, P.D., van Keulen, G., Dyson, P.J. and Del Sol, R., (2013), 'A laterally acquired galactose oxidase-like gene is required for aerial development during osmotic stress in *Streptomyces coelicolor*', *PloS One*, 8(1):e54112.
- Loose, M., Fischer-Friedrich, E., Herold, C., Kruse, K. and Schwille, P., (2011), 'Min protein patterns emerge from rapid rebinding and membrane interaction of MinE', *Nature Structural & Molecular Biology*, 18(5):577-583.
- Löwe, J. and Amos, L.A., (1998), 'Crystal structure of the bacterial cell-division protein FtsZ', *Nature*, 391(6663):203-6.
- Lu, T., Cao, Q., Pang, X., Xia, Y., Xun, L. and Liu, H., (2020), 'Sulfane sulfur-activated actinorhodin production and sporulation is maintained by a natural gene circuit in *Streptomyces coelicolor*', *Microbial Biotechnology*, 13(6):1917-1932.
- Lutkenhaus, J., (2012), 'The ParA/MinD family puts things in their place', *Trends in Microbiology*, 20(9):411-418.
- Ma, X., Ehrhardt, D.W. and Margolin, W., (1996), 'Colocalization of cell division proteins FtsZ and FtsA to cytoskeletal structures in living *Escherichia Coli* cells by using green fluorescent protein', *PNAS USA*, 93(23):12998-13003.

Mak, S. and Nodwell, J.R. (2017), 'Actinorhodin is a redox-active antibiotic with a complex mode of action against Gram-positive cells', *Molecular Microbiology*, 106(4):597-613.

Marbouty, M., Saguez, C., Cassier-Chauvat, C. and Chauvat, F., (2009), 'Characterization of the FtsZ-Interacting Septal Proteins SepF and Ftn6 in the Spherical-Celled Cyanobacterium *Synechocystis* PCC 6803', *Journal of Bacteriology*, 191(19):6178-6185.

Manikprabhu, D. and Lingappa, K., (2013), 'γ Actinorhodin a natural and attorney source for synthetic dye to detect acid production of fungi', *Saudi Journal of Biological Sciences*, 20(2):163-168.

Manteca, A., Ye, J., Sánchez, J. And Jensen, O.N., (2011), 'Phosphoproteome analysis of *Streptomyces* development reveals extensive protein phosphorylation accompanying bacterial differentiation', *Journal of Proteome Research*, 10:5481-5492.

McCormick, J.R. (2009), 'Cell division is dispensable but not irrelevant in *Streptomyces*', *Current Opinion in Microbiology*, 12(6):689-698.

McCormick, J.R., Su, E.P., Drinkes, A. and Losick, R., (1994), 'Growth and viability of *Streptomyces coelicolor* mutant for the cell division gene *ftsZ*', *Molecular Microbiology*, 14(2):243-254.

McCormick, J.R. and Flärdh, K., (2012), 'Signal and regulators that govern *Streptomyces* development', *FEMs Microbiology Reviews*, 36(1):206-231.

McQuillen, R. and Xiao, J., (2020), 'Insights into the structure, function, and dynamics of the bacterial cytokinetic FtsZ-Ring', *Annual Review of Biophysics*, 49:309-341.

Meiring, J.C.M., Shneyer, B.I. and Akhmanova, A., (2020), 'Generation and regulation of microtubule network asymmetry to drive cell polarity', *Current Opinion in Cell Biology*, 62:86-95.

Mierzejewska, J. and Jagura-Burdzy, G., (2012), 'Prokaryotic ParA-ParB-*parS* system links bacterial chromosome segregation with the cell cycle', *Plasmid*, 67(1):1-14.

Miguélez, E.M., Hardisson, C. and Manzanal, M.B., (1999), 'Hyphal Death during Colony Development in *Streptomyces antibioticus*: Morphological Evidence for the Existence of a Process of Cell Deletion in a Multicellular Prokaryote', *Journal of Cell Biology*, 145(3):515-525.

- Mistry, B.V., Del Sol, R., Wright, C., Findlay, K. and Dyson, P., (2008), 'FtsW is a dispensable cell division protein required for Z-ring stabilization during sporulation septation in *Streptomyces coelicolor*', *Journal of Bacteriology*, 190(6):5555-5566.
- Monier, J-M., Demanèche, S., Delmont, T., Mathieu, A., Vogel, T. and Simonet, P., (2011), 'Metagenomic exploration of antibiotic resistance in soil', *Current Opinion in Microbiology*, 14:229–235.
- Moore, J.M., Bradshaw, E., Seipke, R.F., Hutchings, M.I. and McArthur, M., (2012), 'Use and Discovery of Chemical Elicitors That Stimulate Biosynthetic Gene Clusters in *Streptomyces* Bacteria' in Hopwood, D.A. (ed.) *Methods in enzymology: Natural Product Biosynthesis by Microorganisms in Plants Part C*, London: Elsevier Inc, p377.
- Morgenstein, R.M., Bratton, B.P., Nguyen, J.P., Ouzounov, N., Shaevitz, J.W. and Gitai, Z., (2015), 'RodZ links MreB to cell wall synthesis to mediate MreB rotation and robust morphogenesis', *PNAS*, 112(40):12510-12515.
- Mukherjee, P., Sureka, K., Datta, P., Hassain, T., Barik, S., Das, K.P., Kundu, M. and Basu, J., (2009), 'Novel role of Wag31 in protection of mycobacteria under oxidative stress', *Molecular Microbiology*, 73(1):103-119.
- Muok, A.R., Claessen, D. and Briegel, A., (2021), 'Microbial hitchhiking: how *Streptomyces* spores are transported by motile soil bacteria', *The ISME Journal*, 15:2591-2600.
- Nass, N.M., Forooque, S., Hind, C., Wand, M.E., Randall, C.P., Sutton, J.M., Seipke, R.F., Rayner, C.M. and O'Neil, A.J., (2017), 'Revisiting unexploited antibiotics in search of new antibacterial drug candidates: the case of γ -actinorhodin', *Scientific Reports*, 7:17419.
- Neumeyer, M. and Brückner, R., (2017), 'First Stereoselective Total Synthesis of a Dimeric Naphthoquinonopyrano- γ -lactone:(+)- γ -Actinorhodin', *Angewandte Chemie*, 56(12):3383-3388.
- Ninomiya, M., Ando, Y., Kudo, F., Ohmori, K. and Suzuki, K., (2019), 'Total synthesis of Actinorhodin', *Angewandte Chemie*, 131(13):4308-4314.
- Noens, E.E., Mersinias, V., Willemse, J., Traag, B.A., Laing, E., Chater, K.F., Smith, C.P. Koerten, H.K. and van Wezel, G.P., (2007), 'Loss of the controlled localisation of growth stage-specific cell-wall synthesis pleiotropically affects developmental gene expression in an *ssgA* mutant of *Streptomyces coelicolor*', *Molecular Microbiology*, 64(5):1244-1259.
- Nogales, E., Downing, K.H., Amos, L.A. and Löwe, J., (1998), 'Tubulin and FtsZ form a distinct family of GTPases', *Nature Structural Biology*, 5:451-458.

- Nurse, P. and Mariani, K.J., (2013), 'Purification and Characterisation of *Escherichia coli* MreB protein', *Journal of Biological Chemistry*, 288(5):2469-3475.
- Ojeda-Lopez, M.A., Needleman, D.J., Song, C., Ginsburg, A., Kohl, P.A., Li, Y., Miller, H.P., Wilson, L., Raviv, U., Chul Choi, M. and Safinya, C.R., (2014), 'Transformation of taxol-stabilized microtubules into inverted tubulin tubules triggered by a tubulin conformation switch', *Nature Materials*, 13(2):195-203.
- Okamoto, A., Taguchi, T., Ochi, K. and Ichinose, K., (2009), 'Biosynthesis of Actinorhodin and Related Antibiotics: Discovery of Alternative Routes for Quinone Formation Encoded in the act Gene Cluster', *Chemistry & Biology*, 16(2): 226-236.
- Oliva, M.A., Halbedel, S., Freund, S.M., Dutow, P., Leonard, T.A., Veprintsev, D.B., Hamoen, L.W. and Löwe, J., (2010), 'Features critical for membrane binding revealed by DivIVA crystal structure', *The EMBO Journal*, 29(12):1988-2001.
- Oliveira Jr, A.F., Folador, E.L., Gomide, A.C.P., Goes-Neto, A., Azevedo, V.A.C. and Wattam, A.R., (2018), 'Cell Division in genus *Corynebacterium*: protein-protein interaction and molecular docking of SepF and FtsZ in understanding of cytokinesis in pathogenic species', *Anais de Academia Brasileira de Ciências*, 90(2 Suppl. 1):2179-2188.
- Ômura, S., Ikeda, H., Ishikawa, J., Hanamoto, A., Takahashi, C., Shinose, M., Takahashi, Y., Horikawa, H., Nakazawa, H., Osonow, T., Kikuchi, H., Shibata, T., Sakaki, Y. and Hattori, M., (2001), 'Genome sequence of an industrial microorganism *Streptomyces avermitilis*: Deducing the ability of producing secondary metabolites', *PNAS*, 98(21):12215-12220.
- Osawa, M. and Erickson, H.P., (2011), 'Inside-out Z rings – constriction with and without GTP hydrolysis', *Molecular Microbiology*, 81(2):571-579.
- Ouzounov, N., Nguyen, J.P., Bratton, B.P., Jacobowitz, D., Gitai, Z. and Shaevitz, J.W., (2016), 'MreB Orientation correlates with Cell Diameter in *Escherichia coli*', *Biophysical Journal*, 111(5):1035-1043.
- Passot, F.M., Cantley, S. and Flärdh, K., (2021), 'Protein phosphatase SppA regulates apical growth and dephosphorylates cell polarity determinant DivIVA in *S. coelicolor*', *BioRxiv*, 433328: doi: <https://doi.org/10.1101/2021.03.01.433328>.
- Patrick, J.E. and Kearns, D.B., (2008), 'MinJ (YvjD) is a topological determinant of cell division in *Bacillus subtilis*', *Molecular Microbiology*, 70(5):1166-1179.
- Pende, N., Sogues, A., Megrian, D., Sartori-Rupp, A., England, P., Palabikyan, H., Rittmann, S. K-M.R., Graña, M., Wehenkel, A.M., Alzari, P.M. and Gribaldo, S., (2021), 'SepF is the FtsZ anchor in archaea, with features of an ancestral cell division system', *Nature Communication*, 12:3214.

Pichoff, S. and Lutkenhaus, J., (2002), 'Unique and overlapping roles of ZipA and FtsA in septal ring assembly in *Escherichia coli*', *The EMBO Journal*, 21(4):685-693.

Pichoff, S. and Lutkenhaus, J., (2005), 'Tethering the Z-ring to the membrane through a conserved membrane targeting sequence in FtsA', *Molecular Microbiology*, 55(6):1722-1734.

Pióro, M. and Jakimowicz, D., (2020), 'Chromosome Segregation Proteins as Coordinators of Cell Cycle in Response to Environmental Conditions', *Frontiers in Microbiology*, 11:588.

Potůčková, L., Kelemen, G.H., Findlay, K.C., Lonetto, M.A., Buttner, M.J. and Kormanec, J., (1995), 'A new RNA polymerase sigma factor, σ^F , is required for the late stages of morphological differentiation in *Streptomyces* spp.', *Molecular Microbiology*, 17(1):37-48.

Powell, J.F. and Strange, R.E., (1953), 'Biochemical Changes Occurring During the Germination of Bacterial Spores', *Biochemical Journal*, 54(2):205-209.

Prudence, S.M.M., Addington, E., Castaño-Espriu, L., Mark, D.R., Pintor-Escobar, L., Russell, A.H. and McLean, T.C., (2020), 'Advances in actinomycete research: an ActinoBase review of 2019', *Microbiology*, 166(8):683-694.

Raaijmakers, J. and Mazzola, M., (2012), 'Diversity and Natural Functions of Antibiotics Produced by Beneficial and Plant Pathogenic Bacteria', *Annual Review of Phytopathology*, 50:403-424.

Ramirez-Diaz, D.A., Garcia-Soriano, D.A., Raso, A., Mücksch, J., Feingold, M., Rivas, G. and Schwille, P., (2018), 'Treadmilling analysis reveals new insights into dynamic FtsZ ring architecture', *PLOS Biology*, 16(5):e2004845.

Ramm, B., Heermann T. and Schwille, P., (2019), 'The *E. coli* MinCDE system in the regulation of protein patterns and gradients', *Cellular and Molecular Life Sciences*, 76:4245-4273.

Reuther, J., Gekeler, C., Tiffert, Y., Wohlleben, W. and Muth, G., (2006), 'Unique conjugation mechanism in mycelial *Streptomyces*: a DNA-binding ATPase translocates unprocessed plasmid DNA at the hyphal tip', *Molecular Microbiology*, 61(2):436-446.

Rigali, S., Titgemeyer, F., Barends, S., Mulder, S., Thomae, A.W., Hopwood, D.A. and van Wezel, G.P., (2008), 'Feast or famine: the global regulator DasR links nutrient stress to antibiotic production by *Streptomyces*', *EMBO reports*, 9(7):670-675.

Rigali, S., Nothhaft, H., Noens, E.E.E., Schlicht, M., Colson, S., Müller, M., Joris, B., Koerten, H.K., Hopwood, D.A., Titgemeyer, F. and van Wezel, G.P., (2006), 'The sugar phosphotransferase system of *Streptomyces coelicolor* is regulated by the

GnR-family regulator DasR and links *N*-acetylglucosamine metabolism to the control of development', *Molecular Microbiology*, 61(5):1237-1251.

Rioseras, B., Shliahas, P.V., Gorshkov, V., Yagüe, P., López-García, M.T., Gonzalez-Quiñonez, N., Kovalchuk, S., Rogowska-Wrzesinska, A., Jensen, O.N. and Manteca, A., (2018), 'Quantitative proteome and phosphoproteome analyses of *Streptomyces coelicolor* reveal proteins and phosphoproteins modulating differentiation and secondary metabolism', *Molecular & Cellular Proteomics*, 17:1591-1611.

Romero, D.A., Hasan, A.H., Lin, Y-f., Kime, L., Ruiz-Iarrabeiti, O., Urem, M., Bucca, G., Mamanova, L., Laing, E.E., van Wezel, G.P., Smith, C.P., Karberdin, V.R. and McDowall, K.J., (2014), 'A comparison off key aspects of gene regulation in *Streptomyces coelicolor* and *Escherichia coli* using nucleotide-resolution transcription maps produced in parallel by global and differential RNA sequencing', *Molecular Microbiology*, 94(5):963-987.

Romero, D., Traxler, M., López, D. and Kolter, R., (2012), 'Antibiotics as Signal Molecules', *Chemical Reviews*, 111(9):5492-5505.

Ross, W., Vrentas, C.E., Sanchez-Vazquez, P., Gaal, T. and Gourse, R.L., (2013), 'The magic spot: a ppGpp binding site on *E. coli* RNA polymerase responsible for regulation of transcription initiation', *Molecular Cell*, 50(3):420-429.

Rowlett, V.W. and Margolin, W., (2013), 'The bacterial Min system', *Current Biology*, 23(13):R553-R556.

Rowlett, V.W. and Margolin, W., (2015), 'The Min system and other nucleoid independent regulators of Z-ring positioning', *Frontiers in Microbiology*, 6:478.

Rudd, B.A. and Hopwood, D.A., (1979), 'Genetics of actinorhodin biosynthesis by *Streptomyces coelicolor* A3(2)', *Journal of General Microbiology*, 114(1):35-43.

Rudd, B.A. and Hopwood, D.A., (1980), 'A pigmented mycelial antibiotic in *Streptomyces coelicolor*: control by a chromosomal gene cluster', *Journal of General Microbiology*, 119(2):333-340.

Ryding, N.J., Kelemen, G.H., Whatling, C.A., Flärdh, K., Buttner, M.J. and Chater, K.F., (1998), 'A developmentally regulated gene encoding a repressor-like protein is essential for sporulation in *Streptomyces coelicolor* A3(2)', *Molecular Microbiology*, 29(1):343-357.

Sanchez-Vazquez, P., Dewery, C.N., Kitten, N., Ross, W. and Gourse, R.L., (2019), 'Genome-wide effects on *Escherichia coli* transcription from ppGpp binding to its two sites on RNA polymerase', *PNAS*, 116(17):8310-8319.

Salje, J., van den Ent, F., de Boer, P. and Löwe, J., (2011), 'Direct Membrane Binding by Bacterial Actin MreB', *Molecular cell*, 43(3-6):478-487.

Santos-Beneit, F. and Errington, J., (2017), 'Green fluorescent protein as a reporter for the spatial and temporal expression of *actIII* in *Streptomyces coelicolor*', *Archives of Microbiology*, 199:865-880.

Santos-Beneit, F., Roberts, D.M., Cantlay, S., McCormick, J.R. and Errington, J., (2017), 'A mechanism for FtsZ-independent proliferation in *Streptomyces*', *Nature communications*, 8:1378.

Schindelin, J., Arganda-Carreras, I., Frise, E., Kaynig, V., Longair, M., Pietzsch, T., Preibisch, S., Rueden, C., Saalfeld, S., Schmid, B., Tinevez, J-Y., White, D.J., Hartenstein, V., Eliceiri, K., Tomancak, P. and Cardona, A., (2012), 'Fiji: an open-source platform for biological-image analysis', *Nature methods*, 9(7): 676-682.

Schwedock, J., McCormick, J.R., Angert, E.R., Nodwell, J.R. and Losick, R., (1997), 'Assembly of the cell division protein FtsZ into ladder-like structures in the aerial hyphae of *Streptomyces coelicolor*', *Molecular Microbiology*, 25(5):847-858.

Schlimpert, S., Wasserstorm, S., Chandra, G., Bibb, M.J., Findlay, K.C., Flärdh, K. and Buttner, M.J., (2017), 'Two dynamin-like proteins stabilize FtsZ rings during *Streptomyces* sporulation', *PNAS*, E6176-E6183.

Schumacher, M.A. and Zeng, W., (2016), 'Structures of nucleoid occlusion protein SlmA bound to DNA and the C-terminal domain of the cytoskeletal protein FtsZ', *PNAS*, 113(18):4988-4993.

Sexton, D.L., St-Onge, R.J., Haiser, H.J., Yousef, M.R., Brady, L., Gao, C., Leonard, J. and Elliot, M.A., (2015), 'Resuscitation-promoting factors are cell wall-lytic enzymes with important roles in the germination and growth of *Streptomyces coelicolor*', *Journal of Bacteriology*, 197(5):848-860.

Sexton, D.L. and Tocheva, E.I., (2020), 'Ultrastructure of exospore formation in *Streptomyces* revealed by cryo-electron tomography', *Frontiers in Microbiology*, 11:581135.

Shen, B., (2003), 'Polyketide biosynthesis beyond the type I, II and III polyketide synthase paradigms', *Current Opinion in Chemical Biology*, 7(2):285-295.

Shen, J-P., Chang, Y-R. and Chou, C-F., (2020), 'Frequency modulation of the Min-protein oscillator by nucleoid-associated factors in *Escherichia coli*', *Biochemical and Biophysical Research Communications*, 535(4):857-862.

Singh, J., Makde, R., Kumar, V. and Panda, D., (2008), 'SepF Increases the Assembly and Bundling of FtsZ Polymers and Stabilizes FtsZ Protofilaments by Binding along Its Length', *Journal of Biological Chemistry*, 283(45):31116-31124.

Snapgene, (2020), SnapGene Viewer, *Free software for plasmid mapping, primer design, and restriction site analysis*. [online] Available at: http://www.snapgene.com/products/snapgene_viewer/ [Accessed on 8th June 2020].

Söderström, B., Mizadeh, K., Toddo, S., von Hejine, G., Skoglund, U. and Daley, D. O., (2014), 'Coordinated disassembly of the divisome complex in *Escherichia coli*', *Molecular Microbiology*, 101(3):425-438.

Sogues, A., Martinez, M., Caday, Q., Assaya, M.B., Graña, M., Voegelé, A., VanNieuwenhze, M., England, P., Haouz, A., Chenal, A., Trépout, S., Duran, R., Wehenkel, A-M. and Alzari, P.M., (2020), 'Essential dynamic interdependence of FtsZ and SepF for Z-ring and septum formation in *Corynebacterium glutamicum*', *Nature communications*, 11:1641.

Strakova, E., Bobek, J., Zikova, A., Rehulka, P., Benada, O., Rehulkova, H., Kofronova, O. and Vohradsky, J., (2012), 'System Insight into the Spore Germination of *Streptomyces coelicolor*', *Journal of Proteome research*, 12(1):525-536.

Steinmoen, H., Teigen, A. and Havarstein, L. S., (2003), 'Competence-induced cells of *Streptococcus pneumoniae* lyse competence- deficient cells of the same strain during cocultivation', *Journal of Bacteriology*, 185:7176-7183.

StrepDB (2018), *StrepDB – The Streptomyces Annotation Server*, Available at: <http://strepdb.streptomyces.org.uk/> [Accessed on 12th May 2018].

StrepDB (2020), *StrepDB – The Streptomyces Annotation Server*, Available at: <http://strepdb.streptomyces.org.uk/> [Accessed on 5th February 2020].

Stothard, P., (2000), 'The Sequence Manipulation Suite: JavaScript programs for analyzing and formatting protein and DNA sequences', *Biotechniques*, 28:1102-1104.

Spyropoulos, I.C., Liakopoulos, T.D., Bagos, P.G. and Hamodrakas, S.J., (2004), 'TMRPres2D: high quality visual representation of transmembrane protein models', *Bioinformatics*, 20:3258–326.

Sun, J., Kelemen, G.H., Fernández-Abalos, J.M. and Bibb, M.J., (1999), 'Green Fluorescent Protein as a Reporter for Spatial and Temporal Gene Expression *Streptomyces Coelicolor* A3(2)', *Microbiology*, 145(Pt 9):2221-2227.

Sun, J., Hesketh, A. and Bibb, M., (2001), 'Functional analysis of relA and rshA, two relA/spot homologues of *Streptomyces coelicolor* A3(2)', *Journal of Bacteriology*, 183(11):3488-3498.

Sun, Q. and Margolin, W., (1998), 'FtsZ Dynamics during Division Cycle of Live *Escherichia coli* Cells', *Journal of Bacteriology*, 180(8):2050-2056.

Świątek, M.A., Tenoconi, E., Rigali, S. and van Wezel, G.P., (2012), 'Functional analysis of the *N*-Acetylglycosamine Metabolic Genes of *Streptomyces coelicolor* and Role in Control of Development and Antibiotic Production', *Journal of Bacteriology*, 194(5):1136-1144.

Świątek-Połatyńska, M.A., Bucca, G., Laing, E., Gubbens, J., Titgemeyer, F., Smith, C.P., Rigali, S. and van Wezel, G.P., (2015), 'Genome-Wide Analysis of *In Vivo* Binding of the Master Regulator DasR in *Streptomyces coelicolor* Identifies Novel Non-Canonical Targets', *PLoS One*, 10(4):e122479.

Szafran, M.J., Jakimowicz, D. and Elliot, M.A., (2020), 'Compaction and control-the role of chromosome-organizing proteins in *Streptomyces*', *FEMS Microbiology Reviews*, 44(6):725-739.

Szafran, M.J., Malecki, T., Strzalka, A., Pawlikiewicz, K., Dulawa, J., Kois-Ostrowska, A., Findlay, K.C., Le, T.B.K. and Jakimowicz, D., (2021), 'Spatial rearrangement of the *Streptomyces venezuelae* linear chromosome during sporogenic development', *Nature Communications*, 12:5222.

Szklarczyk, D., Gable, A.L., Lyon, D., Junge, A., Wyder, S., Huerta_Cepas, J., Simonovic, M., Doncheva, N.T., Morris, J.H., Bork, P., Jensen, L.J. and Mering, C.V., (2019), 'STRING v11: protein association networks with increased coverage, supporting functional discovery in genome-wide experimental datasets', *Nucleic Acids Research*, 47(D1):D607-D613.

Taguchi, T., Itou, K., Ebizuka, Y., Malpartida, F., Hopwood, D.A., Surti, C.M., Booker-Milburn, K.I., Stephenson, G.R. and Ichinose, K., (2000), 'Chemical Characteristic of disruptants of the *Streptomyces coelicolor* A3(2) actVI Genes Involved in Actinorhodin Biosynthesis', *The Journal of Antibiotics*, 53(2):144-152.

Tahlan, K., Kyun Ahn, S., Sing, A., Bodnaruk, T.D., Willems, A.R., Davidson, A.R. and Nodwell, J.R., (2007), 'Initiation of actinorhodin export in *Streptomyces coelicolor*', *Molecular Microbiology*, 63(4): 951-961.

Tan, X., (2018), 'Investigation of Cell Division Genes in *Streptomyces coelicolor*', PhD thesis, University of East Anglia, Norwich.

Thoma, L. and Muth, G., (2015), 'The conjugative DNA-transfer apparatus of *Streptomyces*', *International Journal of Medical Microbiology*, 305(2):224-229.

Thomaides, H.B., Freeman, M., Karoui, M.E. and Errington, J., (2001), 'Division site selection protein DivIVA of *Bacillus subtilis* has a second distinct function in chromosome segregation during sporulation', *Genes & Development*, 15(13):1662-1673.

Tonthat, N.K., Arold, S.T., Pickering, B.F., Van Dyke, M.W., Liang, S., Lu, Y., Beuria, T.K., Margolin, W. and Schumacher, M.A., (2011), 'Molecular mechanism by which the nucleoid occlusion factor, SlmA, keeps cytokinesis in check', *The EMBO Journal*, 30(1):154-164.

Tzanis, A., Dalton, K.A., Hesketh, A., den Hengst, C.D., Buttner, M.J., Thibessard, A. and Kelemen, G.H., (2014), 'A sporulation-specific, *sigF*-dependent protein,

- SspA, affects septum positioning in *Streptomyces coelicolor*', *Molecular Microbiology*, 91(2):363-380.
- van Baarle, S. and Bramkamp, M., (2010), 'The MinCDJ System in *Bacillus subtilis* Prevents Minicell Formation by promoting Divisome Disassembly', *PLoS One*, 5(3):e9850.
- van den Ent, F., Amos, L.A. and Löwe, J., (2001), 'Prokaryotic origin of the actin cytoskeleton', *Nature*, 413:39-44.
- van Keulen, G. and Dyson. P.J., (2014), 'Production of specialized metabolites by *Streptomyces coelicolor* A3(2)', *Advances in Applied Microbiology*, 89:217-266.
- van Wezel, G.P., van der Meulen, J., Kawamoto, S., Luiten, R.G.M., Koerten, H.K. and Kraal, B., (2000), 'ssgA is Essential for Sporulation of *Streptomyces coelicolor* A3(2) and Affects Hyphal Development by Stimulating Septum Formation', *Journal of Bacteriology*, 182(20):5653-5662.
- Varma, A. and Young, K.D., (2009), 'In *Escherichia Coli*, MreB and FtsZ Direct the Synthesis of Lateral Cell Wall via Independent Pathways That Require PBP2', *Journal of Bacteriology*, 191(11):3526-3533.
- Vaughan, S., Wickstead, B., Gull, K. and Addinall, S.G., (2004), 'Molecular Evolution of FtsZ Protein Sequences Encoded Within the Genomes of Archaea, Bacteria, and Eukaryota', *Journal of Molecular Evolution*, 58:19-29.
- Vega, D.E. and Margolin, W., (2019), 'Direct Interaction between the Two Z-ring Membrane Anchors FtsA and ZipA', *Journal of Bacteriology*, 201(4):e00579-18.
- Vrentas, C.E., Gaal, T., Ross, W., Ebright, R.H. and Gourse, R.L., (2005), 'Response of RNA polymerase to ppGpp: requirement of the ω subunit and relief of this requirement of DksA', *Genes & Development*, 19(19):2378-2387.
- Walshaw, J., Gillespie, M.D., Kelemen, G.H., (2010), 'A novel coiled-coil repeat variant in a class of bacterial cytoskeletal proteins', *Journal of Structural Biology*, 170(2):202-215.
- Wang, P., Zhang, X., Wang, L., Zhen, Z., Tang, M. and Li, J., (2010), 'Subinhibitory concentrations of ciprofloxacin induce SOS response and mutations of antibiotic resistance in bacteria', *Annals of Microbiology*, 60:511-517.
- Wang, X., Huang, J., Mukherjee, A., Cao, C. and Lutkenhaus, J., (1997), 'Analysis of the interaction of FtsZ with itself, GTP, and FtsA', *Journal of Bacteriology*, 179(17):5551-5559.
- Wehrens, M., Ershov, D., Rozendall, R., Walker, N., Shultz, D., Kishony, R., Leven, P.A. and Tans, S.J., (2018), 'Size laws and division ring dynamics in filamentous *Escherichia coli* cells', *Current Biology*, 28(6):972-979.

Wenzel, M., Gulsoy, I.N.C., Gao, Y., Teng, Z., Willemse, J., Middelkamp, M., van Rosmalen, M.G.M., Larsen, P.W.B., van der Wel, N.N., Wuite, G.J.L., Roos, W.H. and Hamoen, L.W., (2021), 'Controlling septum thickness by the curvature of SepF polymers', *PNAS*, 118(2):e2002635118.

Wildermuth, H. and Hopwood, D.A., (1970), 'Septation During Sporulation in *Streptomyces coelicolor*', *Journal of general microbiology*, 60(1):51-59.

Willemse, J. and van Wezel, G.P., (2009), 'Imaging of *Streptomyces Coelicolor* A3(2) with Reduced Autofluorescence reveals a novel stage of FtsZ localisation', *PLoS One*, 4(1):e4242.

Willemse, J., Mommaas, A.M. and van Wezel, G.P., (2012), 'Constitutive expression of *ftsZ* overrides the *whi* developmental gene to initiate sporulation of *Streptomyces coelicolor*', *Antonie van Leeuwenhoek*, 101:619-632.

Willemse, J., Willem Borse, J., de Waal, E., Bisseling, T. and van Wezel, G.P., (2011), 'Positive control of cell division: FtsZ is recruited by SsgB during sporulation of *Streptomyces*', *Genes & Development*, 25:89-99.

Willey, J., Santamaria, R., Gujjarro, J., Gelstich, M. and Losick, R., (1991), 'Extracellular Complementation of a Developmental Mutation Implicates a Small Sporulation Protein in Aerial Mycelium Formation by *S. coelicolor*', *Cell*, 85:641-650.

White, J. and Bibb, M., (1997), 'bldA dependence of undecylprodigiosin production in *Streptomyces coelicolor* A3(2) involves a pathway-specific regulatory cascade', *Journal of Bacteriology*, 179(3):627-633.

White, C.L. and Gober, J.W., (2012), 'MreB: pilot or passenger of cell wall synthesis?', *Trends in Microbiology*, 20(2):74-49.

Wright, L.F. and Hopwood, D.A., (1976), 'Actinorhodin Is a Chromosomally-determined Antibiotic in *Streptomyces coelicolor* A3(2)', *Journal of General Microbiology*, 96:289-297.

Wu, L.J. and Errington, J., (2004), 'Coordination of Cell Division and Chromosome Segregation by a Nucleoid Occlusion Protein in *Bacillus subtilis*', *Cell*, 117(7):915-925.

Wu, L.J. and Errington, J., (2011), 'Nucleoid occlusion and bacterial cell division', *Nature Reviews Microbiology*, 10(1):8-12.

Wu, L.J., Ishikawa, S., Kawai, Y., Oshima, T., Ogasawara, N. and Errington, J., (2009), 'Noc protein binds to specific DNA sequences to coordinate cell division with chromosome segregation', *The EMBO Journal*, 28(13):1940-1952.

- Xia, H., Zhan, X., Mao, X-H. and Li, Y-Q., (2020), 'The regulatory cascades of antibiotic production in *Streptomyces*', *World Journal of Microbiology and Biotechnology*, 36:13.
- Xiao, J., Jia, H., Pan, L., Li, Z., Lv, L., Du, B., Zhang, L., Du, F., Huang, Y., Cao, T., Sun, Q., Wei, R., Xing, A., Zhang, Z., (2019), 'Application of the CRISPRi system to repress *sepF* expression in *Mycobacterium smegmatis*', *Infection, Genetics and Evolution*, 72:183-190.
- Xiao, X., Willemse, J., Voskamp, P., Li, X., Prota, A.E., Lamers, M., Pannu, N., Abrahams, J.P. and van Wezel, G.P., (2021), 'Ectopic positioning of the cell division plane is associated with single amino acid substitutions in the FtsZ-recruiting SsgB in *Streptomyces*', *Open Biology*, 11:200409.
- Xu, H., Chater, K.F., Deng, Z. and Tao, M., (2008), 'A cellulose Synthase-Like Protein Involved in Hyphal Tip Growth and Morphological Differentiation in *Streptomyces*', *Journal of Bacteriology*, 190(14):4971-4978.
- Xu, Y., Williams, A., Au-yeung, C., Tahian, K. and Nodwell, J.R., (2012), 'A Two-step Mechanism for the Activation of Actinorhodin Export and Resistance in *Streptomyces coelicolor*', *The American Society for Microbiology*, 3(5):1-11.
- Xu, Z., Li, Y., Wang, Y., Deng, Z. and Tao, M., (2019), 'Genome-Wide Mutagenesis Links Multiple Metabolic Pathways with Actinorhodin Production in *Streptomyces coelicolor*', *Applied and Environmental Microbiology*, 85:e03005-18.
- Yadu, N., Namboothiri, A. and Arumugan, S., (2021), 'FtsZ: The Force Awakens', *Journal of the Indian Institute of Science*, 101(1):31-38.
- Yagüe, P., Willemse, J., Koning, R.I., Rioseras, B., López-García, M.T., Gonzalez-Quiñonez, N., Lopez-Iglesias, C., Shliaha, P.V., Rogowska-Wrzesinska, R., Koster, A.J., Jensen, O.N., van Wezel, G.P. and Manteca, A., (2016), 'Subcompartmentalization by cross-membranes during early growth of *Streptomyces hyphae*', *Nature communications*, 7:12467.
- Yang, W., Willemse, J., Sawyer, E.B., Lou, F., Gong, W., Zhang, H., Gras, S.L., Claessen, D. and Perrett, S., (2017a), 'The propensity of the bacterial rodlin protein RdlB to form amyloid fibrils determines its function in *Streptomyces coelicolor*', *Scientific Reports*, 7:42867.
- Yang, X., Lyu, Z., Miguel, A., McQuillen, R., Huang, K.C. and Xiao, J., (2017b), 'GTPase activity-coupled treadmilling of the bacterial tubulin FtsZ organizes septal cell wall synthesis', *Science*, 355(6326):744-747.
- Yin, H., Wang, W., Fan, K. and Li, Z., (2019), 'Regulatory perspective of antibiotic biosynthesis in *Streptomyces*', *Science China Life Sciences*, 62:698-700.

Yu, D., Xu, F., Zeng, J. and Zhan, J., (2012), 'Type III polyketide synthases in natural product biosynthesis', *IUPBMB Life*, 64(4):285-295.

Yu, Y., Zhou, J., Gueiros-Filho, F.J., Kearns, D.B. and Jacobson, S.C., (2021), 'Noc corrals migration of FtsZ protofilaments during cytokinesis in *Bacillus subtilis*', *mBio*, 12(1):e02964-20.

Zhang, H., Zhan, J., Su, K. and Zhang, Y., (2006), 'A kind of potential food additive produced by *Streptomyces coelicolor*. Characteristics of blue pigment and identification of a novel compound, λ -actinorhodin', *Food Chemistry*, 95(2):186-192.

Zhang, L., Ramijan, K., Carrión, V.J., van der Aart, L.T., Willemse, J., van Wezel, G.P. and Claessen, D., (2021), 'An alternative and conserved cell wall enzyme that can substitute for the lipid II synthase MurG', *mBio*, 12(2):e03381-20.

Zhang, L., Willemse, J., Classen, D. and van Wezel, G.P., (2016), 'SepG coordinates sporulation-specific cell division and nucleoid organization in *Streptomyces coelicolor*', *Open Biology*, 6:150164.

Zhang, L., Willemse, J., Yagüe, P., de Waal, E., Claessen, D. and van Wezel, G.P., (2020), 'Branching of sporogenic aerial hyphae *sflA* and *sflB* mutants of *Streptomyces coelicolor* correlates to ectopic localization of DivIVA and FtsZ in time and space', *BioRxiv*, 424426: doi: <https://doi.org/10.1101/2020.12.26.424426>.

Zhang, X., Hindra and Elliot, M.A., (2019), 'Unlocking the trove of metabolic treasures: activating silent biosynthetic gene clusters in bacteria and fungi', *Current Opinion in Microbiology*, 51:9-15.